A combined *in vitro* and *in silico* approach in the study of drug-induced mitochondrial dysfunction

Thesis Submitted for the Degree of Doctor of Philosophy (PhD)

By

Alicia Rosell Hidalgo

UNIVERSITY OF SUSSEX

Department of Biochemistry and Biomedicine

October 2020

Declaration of Originality

I (Alicia Rosell Hidalgo), hereby declare that the data and information contained within this thesis is, to the best of my knowledge, original and all work of others is adequately referenced. This thesis has not been and will not be submitted in whole or in part to another University for the award of any other degree.

_____

Acknowledgements

First and foremost, I would like to express my gratitude to God, for his wonderful provision and blessings that allowed me to conduct the research presented in this thesis.

I would like to say a very big thank you to my principal supervisor Dr Tara Ghafourian, who guided me so positively throughout my PhD studies. Her continuous support, encouragement and constructive suggestions have made working under her tutelage an enriching and delightful experience. A big thank you to my co-supervisor Prof Anthony Moore for his invaluable supervision. Without his guidance and extensive knowledge on mitochondria this PhD would not have been possible. I would also like to thank the rest of my thesis committee Prof Louise Serpell and Dr Nick Crickmore, for their insightful comments and feedback that encouraged me to think critically.

A huge thanks to the laboratory team: Dr Mary Albury, Dr Alice Copsey, Dr Mario Barsottini, Dr Luke Young and Dr James Misselbrook for stimulating discussions and invaluable help. Big thanks to the rest of the biochemistry department for their help throughout my PhD, especially to Mr Moji Nasiri, Dr Wided Souissi and Dr David Wood.

A special thank you to Cyprotex, particularly to Dr Paul Walker, Head of the Toxicology team, who provided me a wonderful opportunity to join their team, giving me access to the laboratory and research facilities. I will always be grateful for this experience and the positive impact it had on my research. A special thanks goes out to Senior Research Scientist Julie Eakins. Without her valuable support it would not have been possible to conduct this research. Thanks to the rest of the toxicology team Dr Andrea Lavado, Dr Lynsey Chatham, Dr Caroline Bauch, Dr Ahtasham Raza and Mr Lawrence Rhodes.

I am also thankful for the enriching opportunity of having been part of the Gordon Research Bioenergetics Conference 2019. I am grateful to Prof Wayne D. Frasch and Prof Gregory M. Cook for the funding. A special mention to Dr Ilse Mariel Zarco Zavala and Mrs Quynh van Duong who inspired me and reminded me of the key role women play in science.

Last but not the least, I would like to thank my dear parents Miguel Rosell Carrillo and Conchi Hidalgo Moreno. You are a true blessing to my life. Your love, encouragement and sacrifices have taken me where I am today. A big thanks also to my brother Miguel and sister Judit for their love and constant support.

Johan, my beloved husband, my rock and best friend. Thanks for always believing in me, for your kind patience and for always being there.

A combined *in vitro* and *in silico* approach in the study of drug-induced mitochondrial dysfunction

Summary

Mitochondria are the cellular organelles that generate 95% of the energy needed for a cell to remain viable. Due to their vital role in energy metabolism and homeostasis, mitochondria are increasingly viewed as important off-targets in the study of drug-induced organ toxicities. Indeed, a significant body of evidence has shown that drugs from diverse chemical and therapeutic classes are responsible for mitochondrial dysfunction, which has led in some cases to 'Black Box' warnings and drug withdrawals by regulatory bodies. In this research, multiple *in vitro* assays using different model systems and mitochondrial endpoints were used to gain understanding on the mechanisms involved in drug-induced mitochondrial toxicity (DIMT), specifically those relevant to the operation of the mitochondrial electron transport chain (ETC). Furthermore, *in silico* methods, such as Quantitative Structure Activity Relationships (QSAR) and molecular docking were used to investigate the chemical features associated with inhibition of the ETC.

The first objective was to investigate the interactions between the alternative oxidase (AOX), a crucial respiratory protein present in the ETC of some pathogenic parasites, and inhibitors through *in silico* studies such as QSAR and molecular docking to highlight key residues and molecular properties required for inhibition. Given the relative structural simplicity of the AOX, this investigation offered an opportunity to develop a methodology that could be later applied to other more complex protein targets, such as the cytochrome bc_1 complex.

The second objective was to study the *in vitro* effects of some well-known complex III and AOX inhibitors used as fungicides on both isolated mitochondria and whole cells. The aim was to gain a clearer understanding on the mechanisms of toxicity of this compound set, as well as to validate the techniques employed for future investigations on pharmaceutical drugs.

The third objective was to investigate the effects of a wide range of pharmaceutical drugs on various aspects of mitochondrial function using molecular docking and the *in vitro* techniques validated in previous chapters. This included the effects of drugs on oxygen consumption, mitochondrial membrane potential and reactive oxygen species using isolated mitochondria from rat liver, as well as cell viability and cell bioenergetics using intact and permeabilised HepG2 cells. The tested drugs covered a wide range of pharmacological classes including, but not limited to, antidiabetics, antihyperlipidemics, anti-inflammatories, antipsychotics and anticonvulsants. Many of the drugs tested showed an effect on various aspects of mitochondrial function, with the wealth of experimental results allowing an estimation of the mechanism of actions.

Some of these mechanisms included direct inhibition or uncoupling of the ETC and, in some cases, a dual activity was observed depending on drug concentration and mitochondrial state.

Finally, QSAR analysis using stepwise regression with half maximal inhibitory concentrations (IC_{50} values) generated in previous chapters as the response variable, and hundreds of computed molecular descriptors of compounds as independent variables, resulted in three regression models with good prediction accuracy for inhibition of the cytochrome bc_1 complex. These models highlighted several physicochemical and topological properties that could be responsible for the inhibitory effects of the compounds on the cytochrome bc_1 complex.

In summary, the findings within this thesis have shed light on the underlying mechanisms of toxicity of several pharmaceutical drugs currently clinically used and have highlighted the importance of obtaining a complete understanding of DIMT through multiple assays and mitochondrial endpoints in order to improve the safety of pharmaceutical drugs.

Table of Contents

List of Tables

List of Figures

List of Abbreviations

Abbreviation		Full name
5-ASA	-	5-aminosalicylic acid
AC_{50}	-	50% maximum effect is observed at this concentration
Acetyl-CoA	-	Acetyl coenzyme A
ACs	-	Anticonvulsants
ADP	-	Adenosine diphosphate
ADs	-	Antidepressants
AEFA	-	Acute extracellular flux assay
AF	-	Ascofuranone
AmR	-	Amplex Red
ANT	-	Adenosine nucleoside translocators
AOP	-	Adverse outcome pathway
AOX	-	Alternative oxidase
APs	-	Antipsychotics
ATP	-	Adenosine triphosphate
AU	-	Arbitrary units
BSA	-	Bovine serum albumin
BSF	-	Bloodstream form
CCCP	-	Carbonyl cyanide m-chlorophenyl hydrazine
CB	-	Colletochlorin B
CD		Colletochlorin D
Chl	-	Chlorpromazine
C_{max}	-	Maximum plasma concentration
CNS	-	Central nervous system
CO_2	-	Carbon dioxide
CoQ	-	Coenzyme Q
CYP450	-	Cytochrome P450
DAMPs	-	Damage-associated molecular pattern molecules
DCPIP	-	2,6-Dichlorophenolindophenol
DHAP	-	Dihydroxyacetone phosphate
DILI	-	Drug-induced liver injury
DIMT	-	Drug-induced mitochondrial toxicity
DMEM	-	Dulbecco's Modified Eagle's Medium
DMSO	-	Dimethyl sulfoxide
DNP	-	2,4-dinitrophenol
EC_{50}	-	Half maximal effective concentration
ECAR	-	Extracellular acidification rate
EGTA	-	Ethylene glycol-bis(β-aminoethyl ether)N,N,N′,N′-tetraacetic acid
ETC	-	Electron transport chain
FAD	-	Flavin adenine dinucleotide
$FADH_2$	-	Flavin adenine dinucleotide hydroquinone
FAO	-	Fatty acid β-oxidation
FBS	-	Fetal bovine serum
FCCP	-	p-triflouromethoxy-phenyl-hydrazone
FCS	-	Fetal calf serum

FDA	-	Food and Drug Administration
FET	-	Forward direction of electron transfer
G-3-PDH	-	Glycerol-3-phosphate dehydrogenases
GABA	-	Gamma aminobutylic acid
Gal	-	Galactose
Glu	-	Glucose
GPx	-	Glutathione peroxidase
GSH	-	Gluthathione
GTP	-	Guanosine-5'-triphosphate
H_2O_2	-	Hydrogen peroxide
HAT	-	Human African sleeping sickness or trypanosomiasis
Hlp	-	Haloperidol
HMG-CoA reductase	-	3-hydrohy-3-methyl-glutaryl-coenzyme A reductase
HRP	-	Horseradish peroxidase
HTS	-	High-throughput screening
IC_{50}	-	Half maximal inhibitory concentration
IDRs	-	Idiosyncratic drug reactions
IMM	-	Inner mitochondrial membrane
IMS	-	Intermembrane space
ISP	-	Iron-sulfur protein
KCN	-	Potassium cyanide
Ki	-	The inhibitor constant
LOO	-	Leave-one-out
LSO	-	Leave-some-out
MAE	-	Mean absolute error
MAO	-	Monoamine oxidase
MAS	-	Mannitol and sucrose
MDs	-	Molecular descriptors
MEC	-	Minimum effective concentration
MIE	-	Molecular initiating event
MMP	-	Mitochondrial membrane potential
MOE	-	Molecular operating environment
MOPS	-	3-(N-morpholino)propanesulfonic acid
MPC	-	Mitochondrial pyruvate carrier
MPP+	-	1-methyl-4-phenylpyridinium
MPTP	-	Membrane permeability transition pore
MRS	-	Magnetic resonance spectroscopy
mtDNA	-	Mitochondrial DNA
MTT	-	3-(4,5-dimethyl-2-thiazolyl)-2-diphenyl-2H-tetrazolium bromide
NAD+	-	Nicotinamide adenine dinucleotide oxidised
NADH	-	Nicotinamide adenine dinucleotide reduced
NAPQI	-	N-acetyl-*p*-benzoquinone imine
nDNA	-	Nuclear DNA
NEAA	-	Non-essential aminoacids
NMDA	-	N-methyl-D-aspartate
NMR	-	Nuclear magnetic resonance
NQNO	-	2-n-nonyl-4-hydroxyquinoline N-oxide
NRTIs	-	Nucleoside reverse transcriptase inhibitors
NSAIDs	-	Non-steroidal anti-inflammatory drugs

OCR	-	Oxygen consumption rate
Olz	-	Olanzapine
OMM	-	Outer mitochondrial membrane
OXPHOS	-	Oxidative phosphorylation
PBS	-	Phosphate buffered saline
PCA	-	Principal component analysis
PDB	-	Protein data bank
PDH	-	Pyruvate dehydrogenase
PEOE	-	Partial equalization of orbital electronegativities
PET	-	Positron emission tomography
PLIF	-	Protein-ligand interaction fingerprinting
PPAR	-	Peroxisome proliferator-activated receptors
Q^2	-	Cross-validated R^2
QH	-	Ubisemiquinone
QSAR	-	Quantitative structure activity relationship
RCR	-	Respiratory control ratio
RET	-	Reverse electron transfer
RLM	-	Rat liver mitochondria
RMSD	-	Root mean square deviation
RNA	-	Ribonucleic acid
ROS	-	Reactive oxygen species
rPFO	-	Recombinant perfringolysin O
rRNA	-	Ribosomal ribonucleic acid
SA	-	Salicylic acid
SCR	-	Succinate-cytochrome *c* reductase
SDH	-	Succinate dehydrogenase
SDS	-	Sodium dodecyl sulfate
SMILES	-	Simplified molecular input line entry system
SOD	-	Superoxide dismutase
SQR	-	Succinate-ubiquinone oxidoreductase
SSRIs	-	Selective serotonin reuptake inhibitors
TAO	-	Trypanosome alternative oxidase
TCA	-	Tricarboxylic acid cycle
TGK	-	Trypanosomal glycerol kinase
TMPD	-	Tetramethyl-p-phenylene diamine
tRNA	-	Transfer ribonucleic acid
TZDs	-	Thiazolidinediones
UQ	-	Ubiquinone
UQH_2	-	Ubiquinol
VPA	-	Valproic acid
WGA	-	Wheat germ agglutinin
WHO	-	World Health Organisation
$\Delta G°$	-	Gibbs free energy
ΔH	-	Change in enthalpy
ΔS	-	Change in entropy
$\Delta\mu H+$	-	Proton electrochemical gradient
$\Delta\Psi$	-	Membrane potential

¿No te he dicho que si crees verás la gloria de Dios?

1. General Introduction

1.1. Introduction to Mitochondria

Mitochondrion, from the Greek *mito* (thread) and *chondros* ("granule" or "grain like"), are organelles present in all human cell types except for anucleate red blood cells. They host numerous and diverse metabolic functions such as the tricarboxylic acid cycle (TCA), fatty acid and amino acid metabolism, production of heat, reactive oxygen species (ROS) signalling and cellular stress responses such as autophagy and apoptosis. However, a dominant role for the mitochondria is the generation of energy in the form of adenosine triphosphate (ATP).

The discovery of mitochondria goes back to the late 19th century, when Robert Altmann was the first to recognize the ubiquitous presence of these structures. He called them "bio-blasts" and concluded that they were "elementary organisms" living inside the cells carrying out vital functions[1]. In 1900, Leonor Michaelis found that the redox dye Janus Green B served as a specific stain of mitochondria. He recognised that these filamentous structures were similar to the "elementary filaments" described by Altmann in 1890. However, it took 50 years until Lazarow and Cooperstein associated this specific staining with the capacity of the mitochondria to reoxidise the reduced dye via cytochrome oxidase[2]. In 1913, Otto Warburg found oxygen consumption by a particulate fraction obtained from tissue dispersions, a key discovery that represented an early indication that mitochondria were sites of intracellular redox processes, and for this discovery he was awarded a Nobel Prize in 1931. It was not until 1940 when Albert Claude isolated relatively pure mitochondria by differential centrifugation for the first time, and in 1952 the first images of mitochondria obtained by electron microscopy were published by Palade, which allowed detailed studies of the mitochondrial ultrastructure[3]. The following decades in mitochondrial research were dedicated to understanding the role of mitochondria in cellular respiration, the mechanism of electron transport and oxidative phosphorylation (OXPHOS). Of significant importance was the chemiosmotic hypothesis of ATP synthesis proposed by Peter D. Mitchell, who was awarded the Nobel Prize in 1978[4].

1.2. Structure and Compartmentation of Mitochondria

Mitochondria are widely acknowledged to be highly dynamic organelles, whose location, size and distribution show great variation due to constant fission and fusion processes[5]. Mitochondria are between 0.75 to 3 μm in diameter, meaning they can only be visualised in detail using an electron microscope. The range of possible morphologies is wide and dependent on cell-type, but they most commonly adopt elongated or ovoid shapes[6].

Mitochondria possess two distinct phospholipid membranes, the outer mitochondrial membrane (OMM) that forms the boundary with the cytoplasm, and the inner mitochondrial membrane (IMM) that encapsulates the matrix compartment. In between these two membranes there is the intermembrane space (IMS). The inner membrane forms multiple invaginations into the matrix compartment, the cristae, which greatly increases its total surface area for maximal ATP production (Figure 1.1). Depending on the tissue, the density of cristae varies from quite scarce to tightly packed, which usually correlates with the roles played by the mitochondria in that specific tissue. The OMM is permeable to all ions and solutes up to 14 kDa due to their many aqueous pores. In contrast, the IMM is not freely permeable to ions or metabolites, however it contains many specific transporters. These include transporters for anionic metabolites, respiratory substrates, inorganic phosphate, ADP and ATP (the adenosine nucleoside translocators or ANT). Nonetheless, perhaps the most remarkable characteristic of the IMM is that it contains the entire mitochondrial respiratory chain plus the ATP synthase complex[7].

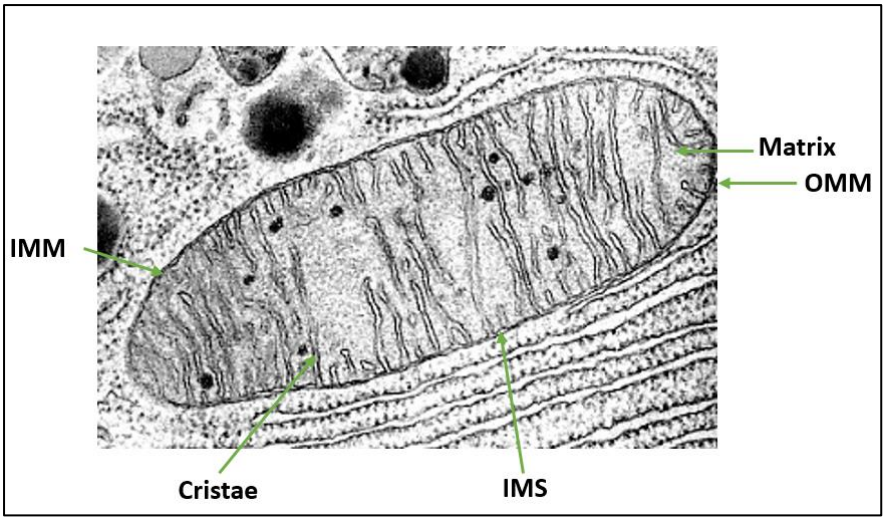

Figure 1.1. Electron micrograph of mitochondria using electron microscopy of cells by Keith R. Porter, a pioneer biology researcher. Arrows show the key structural regions of the mitochondria, the outer mitochondrial membrane (OMM), the inner mitochondrial membrane (IMM), the intermembrane space (IMS), the matrix and the cristae.

The mitochondrial matrix is densely packed with enzymatic proteins, coenzymes, metabolites and inorganic ions. It is where the tricarboxylic acid (TCA) cycle takes place, a series of enzymatic reactions that provide the reduced electron carriers, which are further oxidized by the mitochondrial respiratory chain. Mitochondria are unique among the cellular organelles because they harbour part of their own genetic information: the mitochondrial DNA or mtDNA. The mtDNA can present between 100 and 10000 copies within the cells and it is only maternally inherited[8]. In most eukaryotic cells, mtDNA is circular in shape and organised in a double-stranded DNA molecule. It contains 37 genes that are distributed in a guanine-rich heavy strand (H-strand) and a cytosine-rich light strand (L-strand)[9]. These include genes for 22 tRNAs, 2 rRNAs and 13 structural OXPHOS subunit genes. Unlike the nuclear DNA (nDNA), mtDNA is extremely efficient with approximately 93% representing a coding region, since mtDNA genes lack intronic regions. However, unlike nDNA, mtDNA is not protected by histone proteins and is located close in proximity to sites where reactive oxygen species (ROS) are routinely generated[10]. These free radicals can increase the susceptibility of mtDNA to oxidative damage and cause permanent mutations[11]. In addition, the DNA repair machinery for mtDNA is less efficient compared with nDNA, causing the mtDNA mutation rates to be significantly higher[12]. As it can be expected, ROS-induced oxidative damage is probably a major source of mitochondrial genomic instability, and defects in the mtDNA are the basis for some serious

mitochondrial diseases. Some examples of mitochondrial diseases include Leber Hereditary Optic Neuropathy (LHON)[13], Mitochondrial Encephalomyopathy, Lactic Acidosis and Stroke-like episodes (MELAS)[14], Myoclonus Epilepsy with Ragged Red Fibres (MERRF)[15], Kearns–Sayre Syndrome (KSS)[16] and Pearson's syndrome[17]. Additionally, mtDNA instability is thought to be one of the most important factors affecting ageing[18].

1.3. Energy Generation

Mitochondria are often referred to as the *powerhouses* of the cell, as approximately 95% of ATP production in animal cells occurs via oxidative phosphorylation (OXPHOS). Glycolysis is the metabolic pathway that oxidises one molecule of glucose to convert it into two molecules of pyruvate, a process that takes place in the cytoplasm of the cell and that yields two molecules of nicotinamide adenine dinucleotide (NADH) and four molecules of ATP per molecule of glucose. However, since two molecules of ATP are used in the first half of the pathway, the net yield of glycolysis is only two molecules of ATP. Pyruvate is then transported into the mitochondrial matrix to be converted into acetyl coenzyme A (acetyl-CoA) by pyruvate dehydrogenase (PDH), a reaction that also yields two molecules of NADH[19]. Acetyl-coA then enters into the TCA cycle, where it is oxidised through a series of enzyme-catalysed reactions that release CO_2 and water, along with six NADH and two guanosine-5'-triphosphate (GTP) molecules (per two molecules of acetyl-coA). Acetyl-CoA can derive not only from carbohydrates, but also from the catabolism of fats (via β-oxidation) and proteins. Therefore, the TCA cycle is key for the cellular metabolism as it is a convergence point for many catabolic pathways.

Ultimately, these processes provide substrates that act as electron donors to the electron transport chain (ETC) complexes, such as NADH or the succinate intermediate formed in the TCA cycle, which donate electrons to complex I and complex II, respectively[20]. Hence, the ETC derives energy through the oxidation of these metabolic products where the transfer of electrons from substrates to oxygen is coupled to the translocation of protons from the matrix to the intermembrane space, generating a proton electrochemical gradient ($\Delta\mu H+$). This gradient is used to drive the synthesis of ATP via the F_1-F_O-ATP synthase, in a process called oxidative phosphorylation (OXPHOS). Therefore, OXPHOS consists of two processes, the

oxidation of reduced substrates through aerobic respiration and the phosphorylation of ADP by inorganic phosphate via the ATP synthase, a reaction catalysed by the mitochondrial proton-motive force built up during respiration. This is where the efficient production of ATP occurs, since OXPHOS generates approximately 30 molecules of ATP per molecule of glucose[21].

1.3.1. Electron Transport Chain

The mammalian mitochondrial respiratory chain, located in the IMM, is comprised of four major respiratory chain complexes: NADH–ubiquinone oxidoreductase (complex I; EC 1.6.5.3), succinate dehydrogenase–ubiquinone oxidoreductase (complex II; EC 1.3.5.1), ubiquinone–cytochrome *c* oxidoreductase (complex III; EC 1.10.2.2), cytochrome *c* oxidase (complex IV; EC 1.9.3.1) and the ATP synthase (also called complex V, although it is not part of the ETC; EC 3.6.3.14). In addition to the enzyme complexes, the respiratory chain also requires two small mobile electron carriers: ubiquinone (coenzyme Q10) and cytochrome *c*, the latter being in the IMS. Figure 1.2 provides a depiction of the mammalian respiratory chain that includes the crystal structures of each complex.

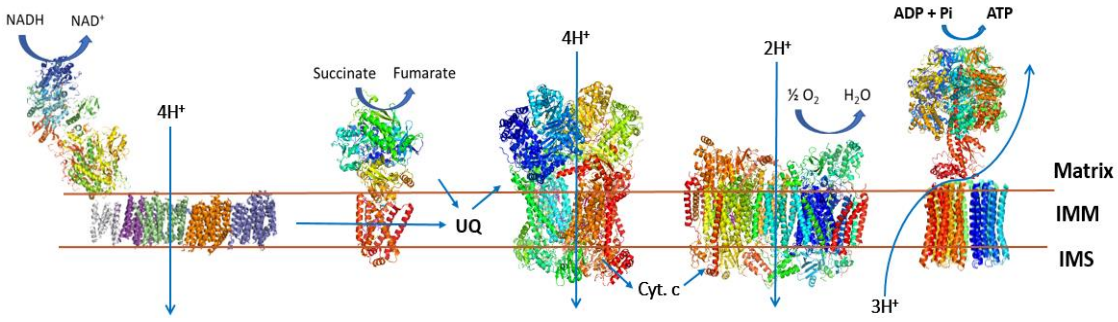

Figure 1.2. Overview of the mammalian respiratory chain and the ATP synthase. Displays the oxidation of NADH and succinate by complex I and II, respectively. The electrons are transferred to complex III and complex IV while protons are being pumped across the IMM generating the electrochemical gradient that drives the synthesis of ATP via the ATP synthase. Crystal structures of the components of the mitochondrial respiratory chain: Complex I (PDB: 4WZ7), complex II (PDB: 1YQ3), complex III (PDB: 1PPJ), complex IV (1OCO) and the ATP synthase (F_o (PDB: 1C17), F_i (PDB: 1E79)).

As mentioned before, NADH from glycolysis and the TCA cycle is oxidised by complex I (NADH-ubiquinone oxidoreductase), concomitantly with the reduction of ubiquinone (UQ) into ubiquinol (UQH_2). This reaction is coupled to the pumping of

four protons across the IMM to the IMS per pair of electrons donated by NADH. Complex II (succinate dehydrogenase–ubiquinone oxidoreductase), on the other hand, catalyses the oxidation of succinate to fumarate, with concomitant reduction of FAD into $FADH_2$, which is then reoxidised by UQ of the IMM. Complex II differs significantly from the other major complexes. Located in the internal side of the IMM, it represents a direct enzymatic component of the TCA cycle and is the only complex completely encoded by nDNA. Additionally, electron transfer by complex II is not coupled to proton translocation across the IMM[22, 23].

As an electron carrier that diffuses along the IMM, ubiquinone can then accept electrons from both complex I and complex II and transfer them to cytochrome *c*, in a reaction catalysed by complex III (ubiquinone–cytochrome *c* oxidoreductase). This reaction allows translocation of four protons, contributing to the generation of the proton electrochemical gradient (ΔμH+). Finally, complex IV (cytochrome *c* oxidase) catalyses the sequential transfer of four electrons from the reduced cytochrome *c*, a water-soluble carrier protein, to molecular oxygen (O_2) forming two molecules of water. This reaction further contributes to the generation of the ΔμH+ with the pumping of $2H^+$ across the IMM.

As described above, the sequential reduction/oxidation (redox) reactions that take place in the ETC, generate a ΔμH+ that is used by the ATP synthase to phosphorylate ADP to produce ATP. This is possible because of the large redox potential difference between the electron donors and the final electron acceptor (1.10 V in the case of NADH as electron donor), meaning that the electron transport along the respiratory chain is accompanied by a significant decrease in the Gibbs potential and a large release of free energy[24]. Consequently, this energy can be used to pump protons to the IMS to generate the ΔμH+, which basically consists of two components: a chemical potential due to the unequal distribution of protons (ΔpH) and an electrical component due to the unequal distribution of electrical charge (ΔΨ).

During OXPHOS, protons return to the matrix, which is negatively charged, through the proton channel formed by the F_o subunit of the ATPase. This is the chemiosmotic concept of energy coupling proposed by Peter D. Mitchell, that essentially explains the generation of ATP due to the generation of the ΔμH+[4]. In fully energized mitochondria, the membrane potential (ΔΨ) is typically in the range of 180 to 220 mV

with a ΔpH of 0.4-0.6. The matrix side of the IMM is often called the N-side (negative), whereas the IMS is often referred to as the P-side (positive) because of the presence of higher levels of protons (positive charges).

1.3.1.1. The Cytochrome *bc₁* Complex

The cytochrome *bc₁* complex (also known as ubiquinol-cytochrome *c* oxidoreductase complex or complex III) was one of the earliest discovered electron transport chain complexes. The first isolation procedure from bovine heart mitochondria was published in 1962[25], the first crystal structure of bovine mitochondria was published in 1997[26] and the first human *bc₁* crystallographic structure was published in 2017[27].

The crystal structures confirm that the functional form of complex III is a homodimer with each half composed of different subunits (Figure 1.3). The subunit composition varies between species, from only three subunits in bacteria to eleven subunits in vertebrates [28]. However, the protein always comprises three catalytic subunits: the cytochrome b subunit containing two b-type heme groups (b_H and b_L), cytochrome *c₁* and the iron-sulfur protein (ISP) that possesses a 2Fe-2S cluster[29]. Functional roles of these redox centres have been explained by Mitchell in the Q cycle hypothesis[30]. The Q cycle of *bc₁* complex takes place at two distinct reaction sites within cytochrome b: a site close to the positive side (P-side) of the membrane (Q_o or Q_P), where ubiquinol (UQH_2) gets oxidised, and a site near the negative side (N-side) of the membrane (Q_i or Q_N), where quinone (Q) reduction takes place.

As already mentioned, the cytochrome *bc₁* complex catalyses electron transfer from ubiquinol to cytochrome *c*, which is coupled to the translocation of protons across the IMM. The stoichiometry of the reaction is given in Equation 1.1, where UQH_2 and UQ represent reduced and oxidized ubiquinone, respectively, $cyt\ c^{3+}$ and $cyt\ c^{2+}$represent oxidized and reduced cyt *c*, and H^+_{matrix} and H^+_{IMS} represent protons at the negative and positive sides of the membrane[31].

Equation 1.1 $$\boldsymbol{UQH_2 + 2\ cyt\ c^{3+} + 2\ H^+_{matrix} \rightarrow UQ + 2\ cyt\ c^{2+} + 4H^+_{IMS}}$$

According to the Q cycle model, one electron from UQH_2 is transferred to the iron-sulfur center and subsequently to cytochrome c_1 and cytochrome *c*. Proton translocation is the result of the deprotonation of UQH_2 in this process. The generated reactive ubisemiquinone (QH) then transfers the second electron to cytochrome b_L, which subsequently reduces cytochrome b_H to finally reduce a quinone (Q) molecule bound within the Q_i site generating a QH. This process is then repeated with a second UQH_2 molecule, converting the QH bound at the Q_i site to a UQH_2 and generating a second equivalent of reduced cytochrome *c*[26]. In a complete Q cycle, two UQH_2 molecules are consumed at the Q_o site and one UQH_2 molecules is regenerated, while four protons are translocated across the IMM[32].

The general structure of complex III can be divided into three regions: a membrane spanning, an intermembrane space and the matrix region (Figure 1.3). The three catalytic subunits essential for electron transport function are all transmembraneous. A monomer of bovine cytochrome bc_1 complex has 13 transmembrane helices, 8 of which are part of the cytochrome *b* subunit. The other 5 come from cytochrome c_1, the ISP, subunits 7, 10 and 11[31]. Both Q_o and Q_i binding sites of bc_1 are located within the cytochrome *b* subunit and were revealed by crystallographic studies with bound inhibitors[26]. The eight membrane spanning helices of cyt *b* are named sequentially from A to H, with both N and C terminus located in the matrix (Figure 1.3). The eight helices are arranged in two helical bundles, the first one consisting of helices A-E and the second one consisting of helices F-H. The first group (A-E), incorporates the b_H and b_L hemes, where histidines serve as the axial ligands for both (His 83 and His 182 coordinate heme b_L, while His 97 and His 196 coordinate heme b_H)[29]. There are four loops connecting the helices: three located on the IMS (AC, CD, EF) and one (DE) located on the matrix side. These loops are important because they participate in the formation of the Q_o and Q_i binding sites, which are located at the P-side and the N-side, respectively, in close vicinity of hemes b_L and b_H[29]. The two bundles contact each other on the N-side of the membrane, but diverge towards the P-side to form the Q_o pocket, between the heme b_L and the 2Fe-2S cluster of ISP[29]. The Q_o pocket is a highly hydrophobic pocket, exceptionally rich in highly conserved residues. It displays six aromatic residues in addition to a number of aliphatic residues. The Q_o site was first visualised by the binding of the Q_o specific inhibitor myxothiazol, while the Q_i site was inferred from the antimycin-binding pocket of cyt *b*[31].

Historically, complex III inhibitors have been classified based on their site of action. Class I include those targeting the Q_o site, whereas class II include those binding to the Q_i site. Later on, all Q_o inhibitors were further divided into three subclasses (Ia, Ib and Ic) based on chemical characteristics of the compounds and spectroscopic effects of the b_L heme and the iron-sulfur cluster of ISP upon binding of inhibitors[29]. The three subclasses are outlined below:

- Class Ia: contain an E-β-methoxyacrylate (MOA) group, which resembles part of the structure of ubiquinone. These inhibitors block electron transfer from quinol to ISP and cause a red shift in the α- and β-bands of the reduced b_L heme spectrum (e.g. myxothiazol, strobilurins and oudemansins).
- Class Ib: contain a chromone ring system and are believed to block electron transfer from ISP to cyt c_1. They cause a red shift of the reduced b_L heme spectrum (e.g. stigmatellin A and B).
- Class Ic: contain a 6-hydroxyquinone fragment and block electron transfer in a similar way to the class Ib inhibitors, but cause a smaller positive redox potential shift of the ISP and have no effect on the spectrum of the b_L heme (e.g. 5-undecyl-6-hydroxy-4,7-dioxobenzothiazole (UHDBT)).

Class II is comprised of compounds that bind into the Q_i binding site and block electron transfer from heme to a quinone or semiquinone molecule. It includes only a few known compounds, such as the classic inhibitor antimycin A, cyazofamid, amisulbrom and funiculosin[33]. Dual site inhibitors have been found to bind into both Q_o and Q_i sites. This group includes 2-n-nonyl-4-hydroxyquinoline N-oxide (NQNO) and ascochlorin[34].

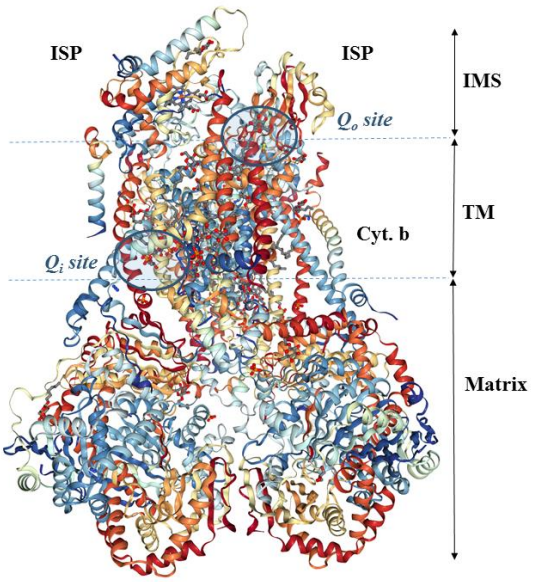

Figure 1.3. Crystal structure of the bovine cytochrome *bc₁* complex (PDB entry: 1PPJ). All subunits of the cytochrome *bc₁* complex are distributed in three regions: the matrix, the trans-membrane (TM) and the inter-membrane space (IMS) region. The two active sites of the cytochrome *bc₁* complex are labelled as the quinol oxidation site (Q_o) and the quinone reduction site (Q_i).

1.3.1.2. The Alternative Oxidase (AOX)

The alternative oxidase (AOX) is a non-protonmotive ubiquinol–oxygen oxidoreductase that couples the oxidation of ubiquinol with the complete reduction of oxygen to water in a manner insensitive to inhibitors of the cytochrome oxidase pathway[35, 36]. It offers an alternative route to the classical electron transport chain for respiration. In eukaryotes, AOXs are attached to the inner surface of the inner membrane of the mitochondria, on the substrate-side of the cytochrome *bc₁* complex[37]. Historically, the AOX was first identified in thermogenic plants, however the gene encoding this protein has been found in all higher plants and also throughout other kingdoms such as the fungal, protist and in prokaryotes[38]. Homologs have also been identified in α-proteobacteria, cyanobacteria and in some animals such as molluscs, nematodes and chordates, but not in mammals[39]. The physiological functions of AOXs vary between organisms, but typically include thermogenesis, stress tolerance and maintenance of mitochondrial and cellular homeostasis[36]. For instance, the role of the AOX in thermogenic plants, such as *Arum maculatum or Sauromatum guttatum*, is well described[40]. Since the AOX is non-protonmotive and is therefore not coupled to

the generation of ATP, the excess energy is released as heat within the thermogenic tissue[40].

The AOX is widespread among some important human pathogenic parasites such as *Blastocystis hominis*, the most common eukaryotic microbe found in the human gut[41], *Paracoccidioides brasiliensis*, the pathogenic fungus responsible for paracoccidioidomycosis in humans[42] or *Candida albicans*, an opportunistic human pathogen[43]. The AOX is also found in *Cryptosporidium parvum*, one of the most widespread intestinal parasites, responsible for diarrheal disease cryptosporidiosis, for which there is no effective treatment currently available. Cryptosporidiosis represents a potentially fatal disease especially in opportunistic infections in immunodeficient individuals[44, 45]. However, amongst all these, the AOX has been most intensely investigated for its crucial role in the energy metabolism of the African trypanosomes[46].

African trypanosomes of the genus *Trypanosoma*, classified as human (*Trypanosoma brucei gambiense* and *Trypanosoma brucei rhodesiense*) or animal (*T. b. brucei, T. congolense* and *T. vivax*) are the etiological agents of human African sleeping sickness or trypanosomiasis (HAT) and nagana in cattle, respectively. They are transmitted to man and animals by the bite of the *Glossina spp.* insect, commonly known as the tsetse fly. African trypanosomiasis is endemic to sub-Saharan Africa - with approximately 70 million people at different levels of risk of contracting HAT, it is considered one of the leading neglected tropical diseases[47]. Without prompt diagnosis and treatment, the disease is usually fatal: the parasites reside in the bloodstream, multiply in the body, cross the blood–brain barrier and invade the central nervous system[47]. Currently, there is no effective vaccine for its prevention and treatments are far from satisfactory due to the toxicity and complex administration of the available drugs. Only a few drugs are registered for the treatment of HAT: pentamidine, suramin, melarsoprol, eflornithine and, only under special authorisation, nifurtimox in combination with eflornithine. However, all these drugs are problematic due to associated severe adverse effects and toxicities, resistance and cross reaction with human targets[48]. For instance, eflortnithine is the only drug with a defined target, the ornithine decarboxylase, and still it has poor potency against *T. brucei*[48]. Clearly, new drugs with known mechanisms of action are urgently required.

Given the integral role that the AOX plays in respiration and its increasing occurrence in relevant pathogenic organisms, it has become an important drug target to consider. The trypanosome alternative oxidase (TAO) represents a unique and safe therapeutic target, not only because it is absent from mammals, but also because it plays a critical role in the survival of the parasite in its bloodstream form (BSF)[49]. While in the mammalian host energy is produced from multiple pathways (i.e. glycolysis, citric acid cycle and oxidative phosphorylation), the BSFs downregulate the cytochrome pathway, leaving ATP production dependent solely upon glycolysis[50]. In this scenario, TAO, which is localised in the mitochondrial inner membrane, is used to generate quinone, which in turn is utilised by the glycosomal and cytosolic glycerol-3-phosphate dehydrogenases (G-3-PDH) to convert glyceraldehyde 3-phosphate (G-3-P) to dihydroxyacetone phosphate (DHAP). This allows the regeneration of NAD^+ necessary for continued glycolysis and the transfer of four electrons to form ubiquinol, which is subsequently oxidized by TAO to convert dioxygen into water[46, 48]. Thus, under aerobic conditions, in the BSF a molecule of glucose produces a net yield of 2 ATP molecules. However, in the presence of a TAO inhibitor, only one ATP molecule per mole of glucose is produced, as G-3-P cannot be converted into DHAP[46]. Under these conditions, BSFs can survive for short periods due to the trypanosomal glycerol kinase (TGK), which catalyses the phosphorylation of ADP from G-3-P to form ATP and glycerol[46]. Hence, simultaneous inhibition of TAO and TGK seems an attractive approach to effectively treating trypanosomal infection[15].

The recent elucidation of the AOX crystal structure from TAO, with a resolution of 2.85 Å[51] (PDB: 3VV9) has provided revealing insights into its α-helical structure, its attachment to the membrane and structural details regarding the active site and nature of the substrate binding site. The TAO crystal structure shows that it is composed of a dimeric structure with each monomer consisting of six long and four short α-helices (Figure 1.4). The active site is composed of a diiron centre, four glutamates (Glu 123, Glu 162, Glu 213 and Glu 266) and two histidine residues (His 165 and His 269), all of which are fully conserved across the different species. In addition to this catalytic site, the AOX contains a binding site for its natural substrate ubiquinol. In fact, the AOX has also been successfully co-crystallised with a number of inhibitors including ascofuranone derivatives (PDB: 3VVA) and colletochlorin B (PDB: 3W54)[51], with a resolution of 2.59 and 2.3 Å, respectively. This has provided invaluable structural

information of the hydrophobic cavity and binding site of quinol, which has led to the generation of novel AOX inhibitors[52, 53].

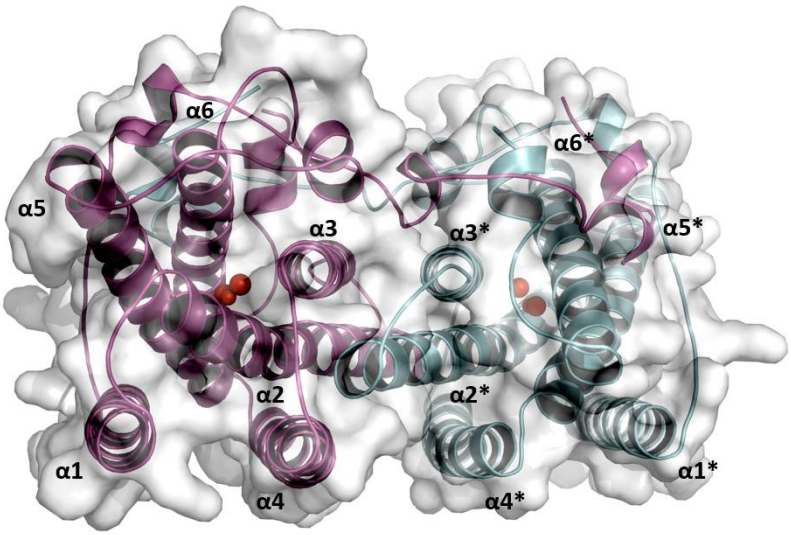

Figure 1.4. Crystal structure of TAO (PDB: 3W54). The structure is a dimer, helices are labelled α1-α6 and α1*-α6* on each monomer (depicted in magenta and cyan, respectively). Surface is shown in grey and the di-iron core is shown as orange spheres.

1.4. Drug-Induced Mitochondrial Toxicity (DIMT)

Mitochondrial dysfunction can be the result of drug-induced toxicities. Knowledge of compounds capable of poisoning mitochondria, such as oligomycin[54], 2,4-dinitrophenol[55] or carbon monoxide[56] goes back more than 60 years. Since then, the number of reports of chemicals affecting mitochondria began to expand and raise awareness of how common these mitochondrial toxicities were[57-59]. It is now known that chemicals can induce mitochondrial impairment through multiple mechanisms, which can be the underlying cause of many diseases and toxic effects.

During the last century, a good number of drugs have been withdrawn from the market due to safety concerns, and others have received Black Box warnings from the Food and Drug Administration (FDA). Interestingly, a high percentage of drugs with Black Box warnings cause mitochondrial liabilities in different target organs (Table 1.1). Perhaps two classic examples of this are the anti-diabetic drug troglitazone and the lipid-lowering agent cerivastatin. Both drugs were withdrawn from the market due to

high rates of hepatotoxicity and rhabdomyolisis, respectively, which was later linked to adverse effects on the mitochondria. However, this toxicity was not evident throughout pre-clinical and clinical trials. Another example is nefazodone, an antidepressant withdrawn from the market in 2004 after several reports of serious hepatotoxicity. It was later demonstrated that nefazodone was highly toxic to isolated liver mitochondria[60].

Table 1.1. Clinically used drugs with Black Box warnings from the FDA for hepatic, cardiovascular and renal toxicity. Drugs with mitochondrial liabilities are highlighted in red. Adapted from Dykens JA and Will Y, and Pereira C *et al.*[57, 61].

Hepatic toxicity		Cardiovascular toxicity			Renal toxicity
Antivirals	**CNS Depressants and Stimulants**	**NSAIDs**		**Anti-cancer**	**Antibiotics**
Abacavir	Dandrolene	Celecoxib	Naproxen	Arsenic trioxide	Gentamicin
Didanosine	Divalproex Sodium	Diclofenac	Nabumetone	Cetuximab	
Emtricitabine	Felbamate	Diflunisal	Oxaprozin	Denileukin diftitox	**Immunosuppressants**
Entecavir	Naltrexone	Etodolac	Piroxicam	Mitoxantrone	Cyclosporin A
Lamivudine	Nefazodone	Fenoprofen	Salsalate	Tamoxifen	
Nevirapine	Valproic acid	Ibuprofen	Sulindac		**Antivirals**
Telbivudine		Indomethacin	Thioridazine	**Antiarhythmic**	Tenofovir
Tenofovir		Ketoprofen	Tolmetin	Amiodarone	
Tipranavir		Mefenamic acid		Disopyramide	**Anti-cancer**
Stavudine		Meloxicam		Dofetilide	Doxorubicin
Zalcitabine				Ibutilide	Cisplatin
Zidovudine					Ifosfamide
Anti-cancer	**Antibiotics**	**Anthracyclines**	**Beta-blocker**	**CNS Depressants and Stimulants**	
Flutamide	Isoniazid	Daunorubicin	Atenolol	Amphetamines	
Dacarbazine	Ketoconazole	Doxorubicin		Atomoxetin	
Gemtuzumab	Streptozocin	Epirubicin	**Anti-diabetic**	Droperidol	
Methotrexate	Trovafloxacin	Idarubicin	Pioglitazone	Methamphetamine	
Pentostatin		**Anaesthetics**	Rosiglitazone	Pergolide	
Tamoxifen		Bupivacaine			

Drug withdrawals inevitably cause an enormous economic burden and decreases people's trust in how pharmaceutics safety is assessed. Therefore, identifying mitochondrial toxicity early in the drug development process must be taken seriously, as it can help reduce late stage attrition rates. If troglitazone, cerivastatin or nefazodone had been initially assessed for mitochondrial toxicity, it is very unlikely that they would have entered further clinical trials. According to the FDA, developing a new medicine takes at least 10 years and costs an average of $2.6 billion[62]. Furthermore, less than 12% of the candidates that make it into Phase I clinical trials are approved by the FDA. Nonetheless, despite the huge financial implications, testing for mitochondrial toxicity is still not required by the FDA or any other regulatory body responsible for drug approval.

The importance of drug-induced mitochondrial dysfunction was acknowledged for the first time when several nucleoside reverse transcriptase inhibitors (NRTIs) used as antiviral drugs were withdrawn from the market due to deleterious effects on mitochondrial function. Many of these antiviral drugs were found to inhibit the polymerase that replicates mtDNA, thereby preventing mitochondrial biogenesis[63]. The result was a gradual loss of mitochondrial biomass, and consequently, a reduced mitochondrial function in various tissues, resulting in many cases in muscle and liver toxicity[64, 65]. Another example is the high occurrence of a Reye-like syndrome observed in the early 1980s in some epileptic patients medicated with valproic acid (VPA)[66]. VPA, along with some salicylates (e.g. salicylic acid), acts as an inhibitor of fatty acid β-oxidation (FAO) by directly inhibiting one or several mitochondrial FAO enzymes[67]. The consequence of this is an accumulation of free fatty acids and tryglicerides (microsteatosis), reduced ATP synthesis and lower production of ketone bodies, which can ultimately induce microvesicular steatosis and profound hypoglycemia[68].

Moreover, because of the mitochondrial endosymbiotic origin from bacteria and consequent big similarity between them, some antibiotics designed to affect bacteria have also been shown to disrupt mitochondrial function. A clear example of this is chloramphenicol, which inhibits bacterial translation by binding to a specific region of the 23S ribosomal RNA, while it also inhibits mitochondrial translation by binding to another region in the human mitochondrial analog 16S rRNA[69]. Other antibiotics, such as the oxazolidines or aminoglycoside antibiotics including streptomycin, gentamicin or neomycin also inhibit both bacterial and mitochondrial translation[69].

Certainly, given the structural and functional complexity of mitochondria, it comes as no surprise that mitochondria can represent the unintended off-target of some pharmaceutical drugs, and responsible, at least in part, for some of the undesirable side effects. The mitochondrial membrane environment is unique because of the presence of specific phospholipids (such as cardiolipin), as well as the highly folded IMM structure characterized by its cristae protrusions, and the mitochondrial matrix is an overall negatively charged environment, as well as being slightly alkaline compared with the IMS and cytosol[70]. These characteristics allow certain molecules to accumulate within the mitochondria through specific transporters, or by passive diffusion driven by the charge and pH differences across the IMM[71].

There are multiple mechanisms whereby drugs can induce mitochondrial toxicity, and they can happen directly or indirectly. Direct mechanisms involve binding to specific mitochondrial targets and impacting directly a mitochondrial process. These mechanisms can include direct inhibition or uncoupling of the ETC, inhibition of the transport or oxidation of substrates or inhibition of mtDNA replication, transcription and translation, opening of the membrane permeability transition pore (MPTP) or inhibition of the import of proteins encoded by the nucleus (Figure 1.5)[59]. Indirect mechanisms involve alterations of cellular processes that ultimately affect mitochondrial function, such as inhibition of the 3-hydroxy-3-methyl-glutaryl-coenzyme A (HMG-CoA) reductase, an important enzyme in the biosynthesis of the mitochondrial electron carrier coenzyme Q. Eventually, all these mechanisms hamper OXPHOS and induce a failure in the generation of a functional ETC, leading to ATP depletion and bioenergetic insufficiency of the cell.

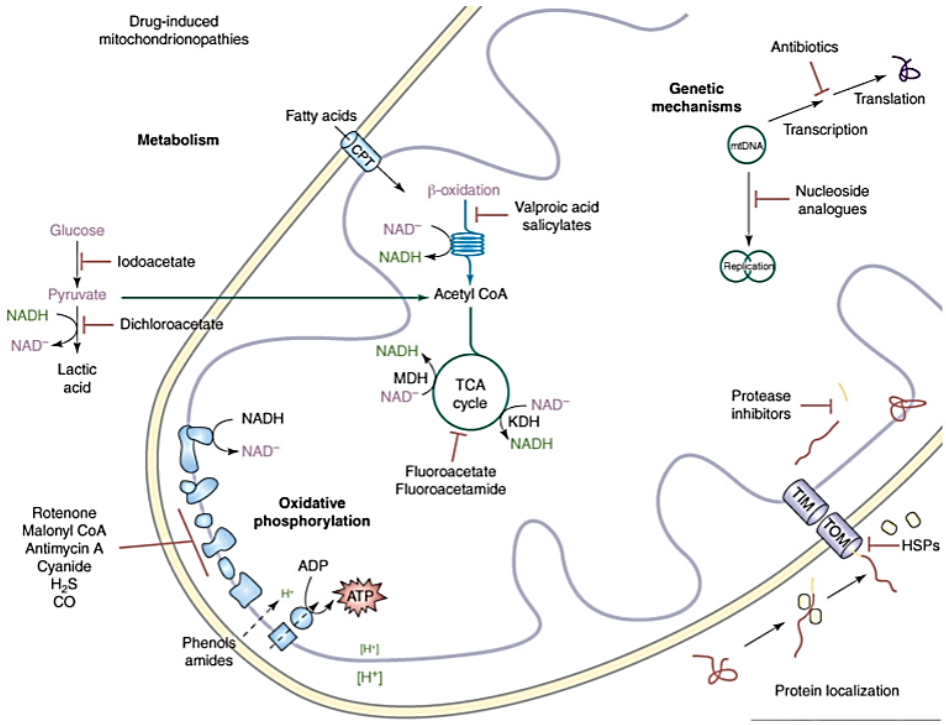

Figure 1.5. Mechanisms of drug-induced mitochondrial toxicity. Adapted from Wallace KB.[72]

The majority of the drugs that have been reported to impair mitochondrial function cause liver injury. The liver, as the primary detoxifying organ, is the major site for drug metabolism and bioactivation, and is the organ subjected to the highest levels of orally administered drugs. Hepatotoxicity is usually the result of an underlying mitochondrial liability, therefore drug-induced liver injury (DILI) is often undetected during the early stages of drug development[73]. DILI is a major issue for public health, and in the most severe cases it requires liver transplantation or can lead to the death of patients[73]. Individuals suffering from mitochondrial mutations, or with a compromised mitochondrial function due to age, may be at greater risk from exposure to mitochondrial toxicants.

Another important aspect of drug toxicity that should be considered is that when drugs require the action of transporters to access the cell, the distribution that those transporters display across the different tissues may provide a mechanism for tissue-specific accumulation of drugs, leading to tissue-specific toxicity[70]. Idiosyncratic drug reactions (IDRs) are adverse reactions that result from a combination of factors that is unique to the individual, and they are typically not detected until the drug in question has gained large exposure in a broad patient population. Risk factors for IDRs may include those that are specific to the drug (e.g. drug metabolism to reactive or toxic metabolites, impairment of cell processes) and those that are specific to the patient (e.g. underlying diseases, genetic deficiencies, physical activity, diet, age and co-medications). Hence, IDRs remain a serious issue for the pharmaceutical industry, as it is one of the least understood and most misrepresented complications in drug development[74]. Improving drug safety includes understanding risk factors for IDRs, which also entails obtaining knowledge of drug effects on mitochondrial function. Knowledge of this could help us make informed decisions in terms of risk-to-benefit considerations regarding treatments, which could lead to individualised therapies, where treatments would be tailored to fit specific populations or even individual patients. This strategy would be a significant advance in the field of targeted health care and would provide each patient the highest therapeutic efficacy with the lowest risk of side effects. For instance, if mitochondrial diseases or mutations may predispose an individual to toxicity with a drug, then avoiding the drug in question seems prudent, as otherwise it could exacerbate the pre-existing condition.

1.4.1.1. Direct inhibitors of the ETC

Among the multiple possible targets where toxicity can occur within mitochondria, one important site is the mitochondrial respiratory chain and the ATP synthase. Classically, mitochondrial respiration is evaluated *in vitro* by the analysis of different respiratory states. State 1 refers to oxygen consumption in mitochondria to which no substrates have been added. In well-coupled mitochondria, this is a very low oxygen consumption[75]. State 2 refers to increased oxygen consumption achieved by the addition of one or more substrates (glutamate/malate for complex I-linked respiration or succinate for complex II-linked respiration). State 3 is achieved by the addition of ADP, which activates the ATP synthase for the generation of ATP[75]. Finally, when all ADP is consumed, respiration drops to a value equivalent to state 2, and this is known as state 4. The ratio between state 3 and state 4 is known as the respiratory control ratio (RCR), and the amount of oxygen needed to phosphorylate the added ADP is known as the ADP/O ratio. Both are important parameters of the integrity of the OXPHOS process and the efficacy of the phosphorylative system[75].

Drugs that disrupt OXPHOS include both inhibitors of the individual ETC respiratory complexes and uncouplers, which cause the dissipation of the $\Delta\mu_H+$. Classic inhibitors of the individual respiratory complexes include rotenone (complex I), malonate (complex II), antimycin A (complex III) and cyanide (complex IV). On the other hand, oligomycin A is the classic inhibitor of the F_o subunit of the ATP synthase (also known as complex V). When the electron transport is blocked by any of these agents, both substrate oxidation and oxygen consumption is inhibited, which can ultimately lead to hyperlactic acidemia, microsteatosis (lipid accumulation) and hypoglycemia. Acute poisoning with specific ETC inhibitors classically presents symptoms that include muscle weakness, fatigue, hypotension, confusion and nausea, which is mainly attributed to the fact that inhibition of the ETC blocks oxygen consumption, causing cytotoxic hypoxia despite normal blood oxygen levels[76].

Compounds that inhibit substrate oxidation can cause a similar syndrome. This includes compounds that act as competitive inhibitors of the endogenous substrates, inhibitors of enzymes within the metabolic pathways as well as inhibitors of the transport proteins required to deliver the substrates into the mitochondrial matrix. Eventually, they all interfere with the supply of reducing equivalents for the

respiratory chain and, as a result, they can ultimately cause metabolic deficit similar to that of direct ETC inhibitors[72]. Classic examples of substrate inhibition include the inhibition of FAO by valproic acid and salicylic acid or the inhibition of the TCA cycle aconitase enzyme by fluorocitrate, a very toxic metabolite formed by the condensation of fluoroacetate and fluoroacetamide with oxaloacetate[77].

Many drugs or their electrophilic metabolites and xenobiotics inhibit the mitochondrial ETC increasing ROS formation, which can trigger MPTP opening and cell death[69]. A brief summary of specific inhibitors of each respiratory complex and the APT synthase is outlined below:

- **Complex I inhibitors (NADH ubiquinone oxidoreductase, EC 1.6.5.3).** It is the ETC complex with the highest number of medical drugs known to inhibit its activity. Complex I inhibitors include different types of natural and synthetic compounds, such as rotenoids, piericidins, capsaicins and pyridinium-type inhibitors, which act at or close to the ubiquinone reduction site[69]. The large diversity of complex I inhibitors has been reviewed before by Esposti MD[78].

Natural compounds. Rotenone is the most potent member of the rotenoids and is classified as a semiquinone antagonist. Found in *Leguminosae* plants, binds irreversibly to complex I at two sites, one buried in the hydrophobic part of the inner membrane and the other at an external site on the matrix surface. This binding blocks electron transport from the dehydrogenase iron-sulfur cluster to coenzyme Q (CoQ), resulting in high levels of ROS formation[69]. Piericidins are antibiotics produced by some *Streptomyces* strains. Particularly, due to the presence of a free pyridinol hydroxyl group that resembles closely the quinone ring, piericidin A is classified as quinone antagonist[69]. Capsaicin, the pungent active agent of hot peppers, acts as a competitive inhibitor for ubiquinone in complex I[79]. It is the most representative member of the vallinoids, which are widely used in neurobiology studies and have applications as topical analgesics[80].

Synthetic and commercial inhibitors. Whereas complex I is an important target for new pesticides in agrochemistry, its inhibition has also resulted in an increasing toxicological problem, since it constitutes an undesired off-target of several drugs used in medicine, which has led to some serious side effects. Barbiturates such as amytal were the first drugs found to inhibit complex I. Subsequently, more drugs were found

to inhibit complex I, which include tranquillizers such as meperidine (demerol), the anticonvulsant/antihistaminic cinnarizine, the antianginal ranolazine and the antiseptic dequalinium chloride[78]. Other important drug classes that have been reported to inhibit complex I are summarised below:

1) **Antipsychotic neuroleptic drugs.** Antipsychotic drugs are used primarily as D2 dopamine receptor antagonists for the treatment of schizophrenia and bipolar disorders. Nonetheless, it has been observed that long-term therapies result in some serious extrapyramidal side effects such as Parkinsonism and tardive dyskinesia, and they have long been suspected to do so by interfering with mitochondrial function[81]. Some of these compounds include haloperidol, chlorpromazine, fluphenazine, risperidone and clozapine.
2) **Local and volatile anaesthetics.** Highly lipophilic local anaesthetics, such as bupivacaine, have been reported to interfere with mitochondrial energy metabolism and are associated with cardiotoxicity and myotoxicity. Bupivacaine, for instance, has been proved to decrease ATP synthesis by directly inhibiting complex I[82]. Lidocaine is another local anaesthetic that has been associated with neurotoxicity initiated via inhibition of neuronal mitochondrial respiration[83]. The effects of the volatile anaesthetics halothane, isoflurane and sevoflurane on the ETC activity have also been studied, showing that they inhibit complex I in the mammalian heart in a dose-dependent fashion[84].
3) **Antihyperlipidemic drugs.** Fibrates are lipid lowering agents which are agonists of the peroxisome proliferator-activated receptors (PPARα), thereby reducing serum triglyceride levels. Some of their side effects include hepatotoxicity, hepatomegaly and myopathy. Clofibrate, fenofibrate, bezafibrate, ciprofibrate and gemfibrozil are some of the fibrates that have shown inhibition of complex I to different degrees[85]. Statins are another drug class used to reduce plasma lipid levels by inhibiting HMG-CoA reductase. One of the most widely prescribed drugs belonging to this group is simvastatin, which has also been observed to inhibit complex I[85].
4) **Antihyperglycemic drugs (Thiazolidinediones).** To this class belong the compounds troglitazone, darglitazone, rosiglitazone and pioglitazone, which are used in the treatment of non-insulin dependent diabetes mellitus by increasing insulin-stimulated glucose uptake by skeletal muscle. These drugs are known to

bind and activate the PPARγ, but they also inhibit complex I[85]. Troglitazone was introduced in 1997 but withdrawn from the market in 2000 after severe cases of hepatotoxicity. Whether such hepatotoxicity was a consequence of mitochondrial severe damage and oxidative stress is still a matter that requires more research.

- **Complex II inhibitors (succinate dehydrogenase, EC 1.3.5.1).** Complex II is less commonly studied in terms of its role in pharmacotoxicology. It is classically inhibited by the competitive inhibitor malonate, but also by the metabolic intermediate oxaloacetate[86]. Amongst the medical drugs that have been observed to inhibit complex II are cyclophosphamide, a medication used to suppress the immune system and isoniazid, an antitubercular agent. It is also inhibited by a number of fungicides including ketoconazole[87], aptenin A5 and aptenin A4[88].

- **Complex III inhibitors (ubiquinol cytochrome *c* oxidoreductase, EC 1.10.2.2).** The sensitivity of various species to complex III inhibition varies significantly, which has allowed application of inhibitors as antimalarials, anticancer drugs and, especially, fungicides. The list of fungicides that target complex III is long, and they can be categorised into two main groups: the quinone outside inhibitors (Q_oIs) and quinone inside inhibitors (Q_iIs)[89]. Antimycin A, a chemical produced by *Streptomyces spp.*, is a classic complex III inhibitor. It is known to bind to the Q_i site, blocking electron transport from the heme b_H center to ubiquinone, thereby increasing ROS production, which, along with ATP depletion, contributes to the subsequent cellular toxicity. Complex III has also been reported to be a common off-target of various pharmaceutical drugs clinically used. For instance, acetaminophen, a compound known for its acute harmful effects to the liver, is metabolised by CYP450 to a reactive metabolite, acetaminophen quinoneimine, which targets complex III[90]. Other studies have shown that local anaesthetics, such as isoflurane and sevoflurane, induce mitochondrial ROS formation as a result of inhibiting complex III, probably via ubisemiquinone autoxidation[91, 92]. Finally, some statins (simvastatin, lovastatin), fibrates (fenofibrate) and thiazolidinediones (ciglitazone, darglitazone, troglitazone) have been shown to also inhibit complex III activity[85].

- **Complex IV inhibitors (cytochrome c oxidase, EC 1.9.3.1).** Complex IV is a heme/copper terminal oxidase that uses cytochrome *c* as an electron donor. Classically, complex IV inhibitors have been classified into four different groups: 1) heme-binding inhibitors that are non-competitive with both oxygen and cytochrome *c* (e.g. azide, cyanide and sulphide), 2) non-competitive inhibitors which do not affect the heme groups (e.g. phosphate ions and alkaline pH), 3) inhibitors competitive with oxygen (e.g. carbon monoxide and nitric oxide) that are reversible and 4) inhibitors which are competitive with cytochrome *c* (e.g. polycations)[76]. Cyanide and azide are the most frequently used complex IV inhibitors and both react with heme a_3 noncompetitively with oxygen[93]. Hydrogen sulphide (H_2S) is a naturally occurring toxic compound that inhibits complex IV activity when inhaled at high concentrations[94]. Other inhibitors include local anaesthetics such as dibucaine, lidocaine and tetracaine, which are widely used in clinical practice. However, significant inhibition by these compounds has only been observed at millimolar concentrations[95]. Another example is tamoxifen, a nonsteroidal antiestrogenic drug widely used in the treatment of breast cancer, which acts both as an uncoupling agent and as an inhibitor of complex III and IV[96].

- **Complex V inhibitors (ATP synthase, EC 3.6.1.34).** The ATP synthase plays a key role in synthesising ATP from ADP and inorganic phosphate and it is highly evolutionarily conserved. Therefore, many of its inhibitors are of natural origin, mostly of fungal origin. For instance, oligomycins are produced in various strains of *Streptomyces* and include six different types: A, B, C, D, E and F. Oligomycin A is the classic inhibitor of the ATP synthase and it prevents protons from passing back into the mitochondria by binding to the F_o subunit. Some mycotoxins (naturally occurring toxins produced by certain fungi) are another example of compounds possessing significant ATPase inhibiting activity. These include aurovertins A-E, leucinostatins A and B, venturicidin and ossamycin, among others. Although mycotoxins are the most powerful inhibitors of mitochondrial ATP synthase, other compounds have also shown inhibitory activity. Examples include local anesthetics[97], the herbicide paraquat[98], the β-adrenergic receptor antagonist propranolol[99], several pyrethroid insecticides[100] and diethylstilbestrol, a nonsteroidal estrogen medication[101], amongst others.

1.4.2. Uncouplers of Oxidative Phosphorylation

Uncouplers of OXPHOS cause a dissipation of the $\Delta\mu_H+$ across the IMM by increasing the proton permeability, thereby stimulating substrate oxidation and inducing excessive oxygen consumption. Hence, in this case substrate oxidation is maintained and the electron transport continues to function, however, these compounds uncouple the phosphorylation of ADP from electron transfer. As a consequence, poisoning with these agents can lead to ATP deficits, as the free energy of substrate oxidation is released as heat (hyperpyrexia) causing fever in individuals poisoned with such agents[76].

Compounds that act as uncouplers are usually protonophores, i.e. molecules that are protonated in the mitochondrial intermembrane space. As cationic compounds, they can take advantage of the negative potential that is generated in the inside of energised mitochondria, allowing entrance of protons to the matrix independently of ATP synthesis[102]. Generally, such compounds are lipophilic weak acids, with a pKa in the range of 5-7. The weak acid group interacts with the phospholipids in the target membrane, making it permeable to protons. Other chemical structures required for potent uncouplers, apart from the presence of an acid-dissociable group, are bulky lipophilic groups and the presence of a strong electron-withdrawing moiety[102]. Examples of uncouplers in this group include carbonyl cyanide phenylhydrazones and salicylanilides. The most frequently used uncouplers include carbonyl cyanide p-triflouromethoxy-phenyl-hydrazone (FCCP) and cyanide meta-chlorophenylhydrazone (CCCP). Some of the medical drugs that show uncoupling activity are reviewed below:

1) **Non-steroidal anti-inflammatory drugs (NSAIDs).** Uncoupling activity is considered a common characteristic of some non-steroidal anti-inflammatory drugs (NSAIDs) including diclofenac, aspirin, nimesulide and indomethacin[103]. These anti-inflammatory agents contain a week acid group (carboxyl) that binds to the arachidonate binding site to inhibit the cyclooxygenases. However, presence of such group and their lipid nature also allows NSAIDs to interact with the mitochondrial IMM, acting as protonophores.

2) **Antipsychotics and antidepressant drugs.** Fluoxetine (Prozac) is an atypical, widely used antidepressant drug that inhibits neuronal serotonin reuptake. Its side effects include cardiovascular and extrapyramidal effects, which may be caused by an interference with the lipid bilayer of the IMM, particularly at high doses. Addition of fluoxetine or its active metabolite, norfluoxetine, to isolated rat brain mitochondrial uncoupled OXPHOS and inhibited the ATPase activity[104, 105].Other studies have shown that drugs such as the benzodiazepine diazepam or the antidepressant imipramine also increase the rate of oxygen consumption and display uncoupling properties[106].
3) **Anaesthetics.** Severe cardiotoxicity and myotoxicity of the anaesthetics bupivacaine and etidocaine limit their use, and studies have shown that these amphiphilic amines stimulate respiration by conducting protons across the mitochondrial membrane[107]. Other anaesthetics that are less lipophilic, such as ropivacaine or lidocaine, are also less potent uncouplers, hence they might represent a safer alternative[108, 109]. Another example is propofol, an intravenous anaesthetic that can induce metabolic lactic acidosis and hepatocellular damage. Impairment of mitochondrial energy metabolism has been attributed to its protonophore activity[110].
4) **Other drugs.** Tolcapone and entacapone are catechol-o-methyltransferase (COMT) inhibitors used as adjunct therapies to treat Parkinson's disease. Tolcapone has a longer life and penetrates the blood brain barrier better than entacapone, however, entacapone is less toxic for the liver. In fact, tolcapone was introduced in 1997, but within six months of use, death cases from fulminant hepatic failure led to its withdrawal in some countries, whereas some others limited its use[111]. Previously, it had been shown that 10 µM tolcapone uncoupled mitochondria to the same extent as 200 µM entacapone[112]. Later, the same laboratory showed that rat rectal body temperature was increased following administration of tolcapone (50 mg/kg), but not entacapone (400 mg/kg), which was attributed to mitochondrial uncoupling[113]. In the same way, 2,4-dinitrophenol (DNP) was introduced as diet pills in the 1930s and sold under different trade names, before testing for toxicity was required before marketing. Consequently, deaths cases from hyperthermia resulted in its ban a few years later. It is now known that DNP is a classic protonophoretic OXPHOS uncoupler that causes dramatic weight loss[114]. For this reason DNP

is still occasionally used as a fat burning agent by bodybuilders and numerous fatalities per year are still attributed to DNP poisoning, with signs and symptoms including hyperthermia, malaise, dyspnoea, respiratory failure and ultimately death[115].

1.4.3. Reactive Oxygen Species and Oxidative Stress

While they are the primary source of aerobic ATP, mitochondria are also the main producers of reactive oxygen species (ROS). Most of the electrons that enter the respiratory chain are used to reduce molecular oxygen (O_2) to form water (a reaction catalysed by complex IV that requires four electron transfers per molecule of oxygen to form two water molecules). However, a small proportion of electrons can prematurely leak from some redox sites of the respiratory chain. If they leak singly, they generate superoxide anion radical (O_2^-), a free radical that can be immediately converted into hydrogen peroxide (H_2O_2) in a reaction catalysed by mitochondrial superoxide dismutase (SOD). H_2O_2 is a strong oxidant and can react non-enzymatically with metal ions (Fe^{2+} or Cu^+) in the Fenton reaction, which yields extremely reactive hydroxyl radical (OH).

To date, at least 11 different sites of superoxide production and/or H_2O_2 have been identified in mammalian mitochondria, however, the ubiquinone-reducing site (I_Q) and flavin site (I_F) in complex I, the flavin site in complex II (II_F) and the ubiquinol-oxidising site in complex III (III_{Qo}) account for most of the mitochondrial ROS production[116]. In the forward direction of electron transfer (FET), coenzyme Q (CoQ) receives electrons from complexes I and II. During this process, most of the ROS is produced at the flavin site or NADH-binding site (I_F) of complex I during NADH oxidation, mainly in the form of superoxide. If rotenone is added under these conditions, it blocks the exit of the electrons from the Q-binding site (I_Q) of complex I, stopping electrons from being transferred, causing them to leak and produce higher amounts of superoxide[116]. Reverse electron transfer (RET) was initially discovered in 1961, when it was observed that isolated mitochondria could produce NADH from NAD^+ after supplying them with succinate[117]. Later, it was shown that when the pool of CoQ becomes highly reduced (high ratio of ubiquinol to ubiquinone) and in addition there is a high membrane potential, electrons can be transferred in a reverse direction to complex I[118].

Under physiological conditions, ROS are the by-products of aerobic metabolism. Under these conditions, ROS are produced in a tightly controlled process as mitochondria keep a very well-regulated balance between production and removal of ROS via antioxidant defenses. For instance, the mitochondrial glutathione peroxidase (GPx) detoxifies H_2O_2 into water, using reduced gluthathione (GSH) as a cofactor. Other antioxidant defence systems include peroxiredoxin and thioredoxin[18] or low molecular weight antioxidant scavengers, which are either endogenous, such as melatonin and histidine dipeptides, or exogenous (obtained through diet) such as ascorbic acid, tocopherols and carotenoids.

There is substantial literature regarding the physiological role that mitochondrial ROS play in several cell fate decisions and signal transduction pathways[119, 120]. Some examples of signalling pathways in which mitochondrial ROS are implicated include the response to hypoxia, apoptosis and cellular differentiation[121-123]. Hence, a dynamic balance between production and consumption of ROS levels allow to initiate the different cellular signalling pathways in a controlled manner. Inhibitors of the electron transport can either raise or lower the rate of ROS production at a given site, depending on whether they act predominantly downstream (leading to reduction of the site and increased electron leak) or upstream (leading to oxidation of the site and decreased electron leak)[116]. Nonetheless, in general an increase in $\Delta\mu H+$ is associated with an increased ROS production. Consequently, ROS production is higher in the resting state or state 4 (ADP limited), when the respiratory carriers are in a more reduced state and hence capable of donating electrons to oxygen. In this state the rate of electron flow in the respiratory chain is slow and this increases the probability of a free electron interacting with molecular oxygen. On the contrary, in the active state or state 3 (ADP-stimulated) when mitochondria are actively synthesizing ATP, $\Delta\mu H+$ is decreased to levels at which ROS production is very low[124, 125].

When ROS levels rise too much, they can react with cellular components such as proteins, lipids and mtDNA causing oxidative stress and irreversible damage. Such damage can contribute to the pathogenesis of several diseases (i.e. Parkinson's disease, Alzheimer's disease or Huntington's disease), mitochondrial drug-induced toxicities and even to the ageing process. A good example of this is the MPTP toxin, which itself is not toxic, but as a lipophilic compound it can cross the blood–brain barrier. Once inside the brain, MPTP is metabolized into the toxic cation MPP+ by the

enzyme monoamine oxidase B (MAO-B) of astrocytes. MPP+ gets accumulated by mitochondria, where it inhibits complex I, rising ROS production and leading to neuronal death, which causes symptoms of Parkinson's disease[69]. Another classic example is the role that ROS play in the injury response to ischaemia (when blood supply to an organ is disrupted) and reperfusion (when blood supply is restored). While reperfusion of ischaemic tissue is essential for survival, it also initiates oxidative damage through the burst ROS generation from mitochondria. During ischaemia, the respiratory chain becomes maximally reduced and there is large evidence that points to respiratory complex I as the main site of ROS production upon reperfusion[126]. Along with dysregulation of calcium levels, elevated ROS can also lead to cell death through induction of the mitochondrial permeability transition, and to the release of damage-associated molecular pattern molecules (DAMPs), such as mtDNA, which can initiate the inflammatory response[127, 128].

Therefore, ROS production exceeding physiological levels can lead to an overwhelmed antioxidant capacity, resulting in oxidative stress and cellular damage. The nature of the damage will depend on many factors, including the site of ROS production, reactivity of the target and the availability of metal ions[129]. A summary of the nature of ROS-induced damage on key cellular targets of oxidative stress can be found in Figure 1.6. Generally, the main targets of oxidative stress in cells include:

- DNA: mutations, rearrangements, transcriptional errors, damage to the DNA repair process, single and double strand breaks[130]. This leads to more oxidative stress and eventual cell death.
- Lipid membranes: via lipid peroxidation, which converts unsaturated lipids into polar lipid hydroperoxides[129]. This may impair normal cell function by increasing membrane fluidity, inactivating membrane-bound receptors or enzymes.
- Proteins: via metal-catalysed oxidation, oxidation-induced cleavage, amino acid oxidation and the conjugation of lipid peroxidation products[130]. This leads to changes in the tertiary structure, degradation and fragmentation leading to loss of enzymatic activity and altered cellular functions, such as energy production.

- Modulation of kinase signalling: key mediators of the biological effects of ROS include mitogen-activated protein kinases (MAPKs), which are activated by oxidative stress and to induce apoptosis via mitochondria-dependent mechanisms involving cytochrome *c* release.

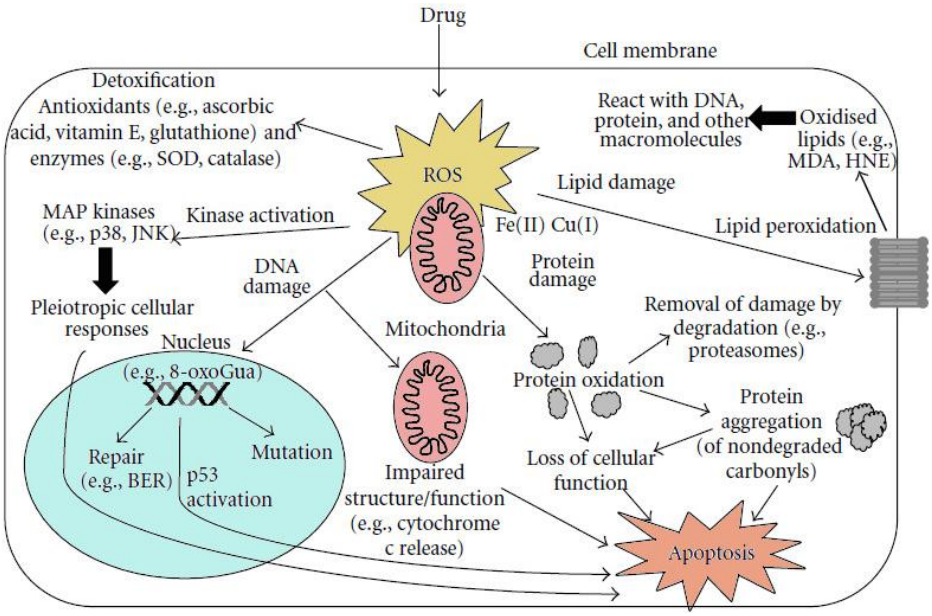

Figure 1.6. The main effects of drug-induced oxidative stress in cells. Adapted from Deavall DG *et al.*[129]. ROS: reactive oxygen species, BER: base excision repair, SOD: superoxide dismutase, JNK: c-Jun N-terminal kinases, MDA: malondialdehyde, HNE: 4-hydroxynonenal.

1.5. Methods of Detecting DIMT

Because drugs can induce mitochondrial impairment through multiple mechanisms, multiple assays may be required to understand DIMT. Such assays ought to cover multiple mitochondrial endpoints and consider the different means by which drugs can induce mitochondrial dysfunction. Classic methods include measurement of the activities of mitochondrial enzymes, membrane potential, respiration (oxygen consumption), metabolite production, ATP levels, calcium retention capacity, reactive oxygen species and morphological analysis.

Model systems that can be used for studying DIMT include animals (e.g. the nematode *Caenorhabditis elegans* or the zebrafish *Danio rerio*)[131-134], whole cells, isolated mitochondria, tissue sections and sub-mitochondrial particles. The model system of choice will depend on the assay being performed, and it is imperative to understand

the strengths and limitations of each when interpreting the findings. Important limitations of classic methods include specificity, throughput and extrapolability of *in vitro* to *in vivo* conditions. For instance, one of the major concerns related to most cell culture studies is the use of cancer cell lines and high-glucose media[58]. For ease of culturing, immortalised cell lines are commonly used for pre-clinical screening studies, however, they can be highly resistant to mitochondrial toxicants as they typically rely on glycolysis for ATP production over OXPHOS. Strategies to overcome this include the use of primary cell cultures[135], low-glucose media[134] or glucose-free medium supplemented with galactose[58]. While these approaches have been successful in some cases, false negative results have also been reported,[135] and consequently, combined approaches have been developed to reduce this[136].

With regard to the use of isolated mitochondrial fractions for the study of DIMT, there are also several limitations that ought to be considered: the high number of cells required to generate a sufficient yield of mitochondria, the limited time they remain functional post-isolation[137], compromised morphology and structural integrity following manual homogenisation of tissue, disintegration of mitochondrial–cytoskeletal networks and branching structure[138] or lack of cellular context, which gives the drugs unrestricted access to the mitochondria, which may provoke an exaggerated response in the absence of drug metabolism[139]. In reality, mitochondria are present in a complex physiological environment, not directly exposed to the full range of substrates and inhibitors and in constant interaction with the cytoplasm, plasma membrane and other organelles[139]. However, isolated mitochondrial fractions offer the advantage of pinpointing precise sites of action of the drug in question on mitochondria. When using mitochondrial preparations, it is important to determine their quality, which can be achieved by the respiratory control ratio (RCR). RCR is the ratio between state 3 and state 4 respiration, a parameter frequently used to evaluate the integrity of a mitochondrial preparation, as damaged mitochondrial preparations tend to show an increased proton leak. Values typically range from 3 to 15 in different preparations, and a ratio ≥6 is generally accepted as a highly intact and coupled preparation[24].

Advantages of using intact cells include undisturbed cellular environment, greater physiological relevance and no artefacts due to mitochondrial isolation. Additionally, whole cells allow tracking changes in mitochondrial localization, dynamics and

number. It should be noted that mitochondria are very dynamic organelles due to fission and fusion processes and that, in some cases, the effects of inhibitors can be overcome by increased fusion. In isolated mitochondria these protective mechanisms are lost, potentially resulting in artefactual toxicity[140]. However, there are also downsides to using isolated cells: they still lack the *in vivo* context, primary cells can be hard or impossible to isolate, many compounds are unable to permeate the cell membrane and the reagents, hormones, growth factors and other substrates often depend on the experimenter's choice, which may determine the outcome of the investigation[139].

In order to overcome the problem of compounds not being able to permeate the cell membrane, assays using permeabilised cells with recombinant perfringolysin O (rPFO) have been developed. rPFO is a cholesterol-dependent cytolysin derived from *Clostridium perfringens* that forms oligomeric pores in cholesterol-containing membranes, allowing the passage of solutes and proteins up to 200 kDa in size[141]. rPFO-mediated pore formation is highly specific towards cytoplasmic membrane, as it only occurs when cholesterol concentration exceeds a certain threshold[142-144], meaning intracellular organelles that do not possess enough cholesterol remain unaffected. In fact, concentrations 10-fold higher than those used to permeabilise the cell plasma membrane did not affect state 3 respiration, mitochondrial membrane potential or cytochrome *c* release from the intermembrane space[145]. Consequently, rPFO appears to have a much broader window for use in permeabilised cell experiments compared with other detergent-based options such as saponin or digitonin[145, 146]. In summary, rPFO-mediated cell permeabilisation allows analysing the effects of the test compounds on the different respiratory chain complexes without the need to isolate mitochondria. One of the advantages of this assay is an increase in throughput, while it uses less biological material than traditional isolated mitochondria assays. It also overcomes the disadvantages associated with mitochondrial isolation including damage, alterations in mitochondrial morphology and mitochondrial subpopulation selection bias.

Despite drug effects on mitochondrial function being frequently characterised *in vitro*, whether these findings are relevant pharmacologically or toxicologically is also frequently unclear. *In vitro* testing does not cover *in vivo* variables, which may play a very important role in drug-toxicity. These include distribution, metabolism, length of

exposure, target organ specificity, bioaccumulation, interaction with other drugs, etc. Additionally, one of the limitations is the challenging of extrapolating to chronic, developmental or latent/later-life effects of mitotoxicant exposures. To address this, *in vivo* assays have been used to help establish biological significance, including medium-throughput analysis of small animal models, such as *C. elegans*[133, 134].

Ideally, *in vivo* assays should be sensitive and organ specific, non-invasive and translatable from preclinical to clinical studies. Standard endpoints used for safety testing, such as clinical signs, histopathology, haematology and serum chemistry are very important filters for detecting compounds with unintended effects, but relatively imprecise and insensitive for detecting alterations in mitochondrial function[147]. Traditional preclinical toxicology studies using animals, for instance, have commonly employed ultrastructural morphology and blood lactate as endpoints of mitochondrial health, but these have strong limitations. On the one hand, obtaining tissue for ultrastructural examination is invasive and hence not suited for safety monitoring. On the other hand, blood lactate levels vary considerably in sensitivity and specificity (stress and exercises raise lactate, for instance), hence it would not necessarily ensure safety[148]. Therefore, specific *in vivo* endpoints are likely required in the future in order to help us understand DIMT. Some endpoints have already been proposed, including the development of specific biomarkers[149-152], imaging techniques such as positron emission tomography (PET), enhanced nuclear magnetic resonance (NMR) techniques, such as magnetic resonance spectroscopy (MRS) or breath testing[147]. All these techniques share characteristics that make them attractive to be used in the late phases of the drug development process, however further work is required to validate such endpoints and understand their strengths and limitations.

Ideally, the ultimate goal with regards to toxicological risk assessment would entail developing high quality large data sets integrating chemical structure and mechanistic toxicity that would allow us to perform predictive toxicology. Chemical databases of mitochondrial toxicants, where a certain mitochondrial toxic effect is attributed to common structural motives (toxicophores), could help researchers build predictive quantitative structure-activity relationship (QSAR) models and machine learning platforms capable of predicting mitochondrial toxicity. Consequently, predictive toxicology via *in silico* approaches would help us predict mitochondrial toxicity of

untested chemicals, with the potential of reducing *in vivo* experimentation and economic costs towards toxicity studies[153, 154].

1.6. Mitochondrial Toxicity Assessment in Industry

Early data that emerged from academia and industry started to indicate that off-target mitochondrial impairment was the underlying mechanism of drug-induced toxic effects. Traditionally, assessment of mitochondrial function was done using the Clark-type electrode to monitor oxygen consumption, which does not have enough throughput for an industrial setting. Mitochondrial toxicology has become an area of interest to the industry and, in response, high-throughput assays for testing DIMT have been developed to test compounds in a fast and relatively inexpensive way. High-throughput screening (HTS) methods have the potential to efficiently test large numbers of chemical compounds, and allow the production of robust and reliable data regarding effects on biological pathways[153]. For instance, Pfizer in collaboration with Luxcel developed the first HTS assay that entailed a 96-well plate (now 384-well) capable of measuring the effects of compounds on mitochondrial respiration using soluble oxygen sensors and time-resolved fluorescence[155, 156]. With this new technology, over 300 compounds could be analysed per day at a single dose or 56 compounds per day in a six-point dose-response curve. In 2007, the Seahorse metabolic flux analyser (24 or 96-well instrument) was launched, which allowed analysis of drug effects in any cell type by monitoring simultaneous oxygen consumption as a measure of mitochondrial respiration and extracellular acidification rate as an indirect measure of glycolysis. Furthermore, the XF96 analyser uses 20,000 cells per well, which, compared with isolated mitochondria experiments using Clark-type electrodes, decreases the cell number requirement by up to 10,000-fold (optimal yield and quality of isolated mitochondria requires 2–200 × 10^6 cells or more)[157].

HTS techniques that identify mitochondrial toxicants allow the creation of large chemical databases and help prioritise compounds with low toxicity risks for more expensive and exhaustive *in vivo* experimentation. However, *in vivo* experimentation has downsides too, in fact, idiosyncratic organ toxicity is one of the main problems that hinders toxicant identification. Animal models often fail to reveal such toxicities due to several reasons, such as presence of robust mitochondrial reserves, lack of genetic diversity, absence of environmental factors or co-medication. To address this,

animal models that better detect mitochondrial toxicity have been created, such as the MnSOD+/- mouse model, where mitochondrial superoxide dismutase is knocked out[158]. Nonetheless, the size and cost of whole organism rodent assays have been prohibited for translation to high-throughput platforms, and as a result, new assays that utilise *C. elegans* or zebrafish as alternative *in vivo* models have been developed.

Evaluating chemicals for mitochondrial toxicity is a priority for regulators because it is the mechanism of action of many compounds (i.e. pesticides, fungicides, etc.), and consequently most companies have now one or more preclinical mitochondrial assays in place[156]. For instance, of the 11 industry members who participated in the 'MIP-DILI' European project (Mechanism-Based Integrated Systems for the Prediction of Drug-Induced Liver Injury), 9 of them were conducting mitochondrial toxicity screening[159]. The MIP-DILI project was a 5-year project launched in 2012 with a total budget of €32.4 million and was comprised of 26 participants from the pharmaceutical industry, subject matter experts and academic institutions. As a matter of fact, industry-sponsored studies that investigate DIMT are becoming more numerous and cover a broad range of drug classes including anti-depressants[60], lipid-lowering agents or thiazolidinediones[85], among others.

1.7. Quantitative Structure-Activity Relationship (QSAR)

Quantitative-Structure Activity Relationship (QSAR) aims at the quantification of chemical information for the development of a mathematical relationship of the information with a response property or activity[160]. It is based on the notion that the activity or biological behaviour of a compound is conditioned by its chemical properties, therefore the biological activity of a newly designed or untested chemical can be inferred from the molecular structure of similar compounds whose activities have already been assessed[161]. A way to develop new, deeper scientific knowledge is by unravelling new relationships from information gathered by different scientific fields. In QSAR, several scientific fields are involved, as compounds' properties must be defined (chemistry and physics), mathematical models need to be developed (mathematics) and biological activities of compounds must be interpreted (biology)[161]. Hence, the developed models provide insight regarding the essential structural

requisites of the molecules for a given behaviour and may be used for the prediction of activities of unknown or new chemicals.

In more than 50 years of active development, QSAR modelling has significantly grown with respect to methodologies and applications[162]. Applications of QSAR are vast, since many types of drugs (e.g. pharmaceuticals, agrochemicals, etc.) may be subjected to QSAR modelling for the optimisation of their potency, receptor specificity and improved pharmacokinetic profile[160]. QSAR may be particularly helpful in savings costs in the drug development process (e.g. in the pharmaceutical, pesticide, personal products, etc. areas) and in the reduction (and even replacement in some cases) of animal tests[163]. Some specific applications of QSAR include the rational identification of new leads with pharmacological, biocidal or pesticidal activity or the identification of hazardous compounds at early stages of product development[163].

1.7.1. Model Development

Workflow of QSAR models involve four basic steps: data preparation, data processing, data prediction and validation and data interpretation. First, in order to build a reliable and robust QSAR method, it is necessary to have a good number of chemicals with a response activity based on which the model can be developed. The response activity represents the dependent variable in the QSAR models; examples may be the dose required for a fixed response, such as IC_{50} or EC_{50} values. In order to have a normal distribution, a logarithmic transformation is usually applied to the response data. Then, a series of molecular descriptors (further explained in section 1.7.2) for each chemical in the data set are calculated and represent the independent variables of the models. Data processing involves the division of the data into a training set and a test set. The former is used for the development of the model, whereas the latter is employed for model validation. This step is crucial as it may determine the quality of the model, therefore, a number of chemometric operations are used, such as cluster analysis, Kennard-Stone and sphere exclusion[160]. Once this division is done, the training set is used for model development using statistical tools, which can be broadly categorised into regression-based and classification-based approaches[164]:

- **Regression-based approaches.** Both response variable and independent variables are quantitative. Examples of popular methods that use this approach include multiple linear regression, partial least squares and principal component regression analysis.
- **Classification-based approaches.** Response variable is graded (like active-inactive or positive-negative), while independent variables are quantitative. Examples include decision trees, logistic regression, linear discriminant analysis and support vector machine.

1.7.2. Molecular Descriptors

Molecular descriptors (MDs) are quantitative parameters that encode information related to the molecular structure of a compound. MDs can be experimentally obtained or theoretically determined using computational algorithms: *"they are the final result of a logic and mathematical procedure which transforms chemical information encoded within a symbolic representation of a molecule into a useful number*"[161]. MDs may be physicochemical, structural, geometrical (based on a molecular surface area calculation), electronic (based on molecular orbital calculations) or topological. Up to today there are more than 3000 descriptors proposed derived from different theories and approaches, which reflects the increasing importance they have in different fields such as chemistry, toxicology, ecotoxicology and pharmaceutical sciences[161]. Some MDs are simple, like 1D descriptors, which are derived by counting some atom types or structural fragments in the molecule, whereas others, called topological or 2D descriptors, are derived from algorithms applied to a topological representation. 3D or geometrical descriptors are derived from the spatial (x, y, z) coordinates of the molecule, while 4D descriptors are derived from the interaction energies between the molecule, imbedded into a grid and some probe. Geometrical 3D/4D descriptors have higher information content than 1D/2D, which often show degeneracy. However, it is not always the best idea to use 3D/4D MDs in all modelling processes. This is because the best descriptors will always be those whose information content is comparable with the information content of the response for which the model is searched for[161]. There are several software that calculate theoretical descriptors from SMILES codes, 2D graphs or 3D x, y, z special coordinates, such as ADAPT, OASIS, CODESSA PRO or MOE. Examples of some commonly used MDs in QSAR studies include: partition coefficient or log P, acidic dissociation constant or

pK_a, molar refractivity (physicochemical descriptors), Wiener index, Zagreb group indices (topological descriptors), H-bond donor, H-bond acceptor, molecular weight, rotatable bonds (structural descriptors) and dipole moment (electronic descriptor).

Some features that make a MD ideal for a QSAR model are[165]:

1. It should be applicable to a broad class of compounds.
2. It should describe structural information and should have negligible correlation with other descriptors.
3. It should be simple, and it should have correlation with at least one property.
4. It should have reproducibility and should generate different values for different molecules, even if the structural differences are small (minimal degeneracy).
5. It should preferably discriminate among isomers.
6. It should not be trivially related to other descriptors.

1.7.3. Model Validation

QSAR models need to be validated to evaluate their quality and predictive power. There are two major QSAR validation approaches: internal validation, which uses the training set molecules, and external validation, which uses the test set molecules[166]. Validation metrics are the ultimate criteria to judge the quality of the models. There are different validation metrics for regression-based models and for classification-based models. Some commonly used metrics for regression-based models include:

- **Internal validation**: Leave-one-out (LOO) and Leave-some-out (LSO) cross-validation. By the LOO technique, one compound is removed from the set, model is rebuilt based on the remaining molecules of the training set using the descriptor combination originally selected, and finally, the activity of the deleted compound based on the resulting QSAR equation is predicted. This cycle is repeated until all the molecules of the training set have been deleted at least once. By the LSO technique, the data set is partitioned into *k* cross-validation groups (usually from 2 to 10). Finally, predictive power is calculated using the cross-validated R^2 (Q^2) for the model[161]. A model is considered acceptable if $Q^2 > 0.5$. A model can also be validated calculating the Mean Absolute Error (MAE).
- **External validation**: it is essential in the assessment of the predictive capability of the model. It ensures applicability of the model for the prediction

of untested molecules. Metrics proposed by Golbraikh and Tropsha[167] and Roy *et al.*[168] are some commonly used ones and are further explained in Materials and Methods 2.12.2.3.

1.7.4. Challenges in QSAR Modelling

The success of any QSAR model will strongly depend on the accuracy of the input data. It is essential to perform data set curation to mend any errors and redundancy. Biological activity should always come from a reliable source and standard error of data should be verified. Ideally, response data should be obtained under the same experimental conditions, otherwise it could potentially compromise the integrity of the model[162]. Care should also be taken with molecular structures of compounds, which should be manually checked to ensure correct calculation of molecular descriptors. Another important point is that, ideally, there should be a clear mechanistic interpretation for the MDs selected in the QSAR model. A predictive and interpretable model is always preferable than an equally predictive but non-interpretable one[162]. Furthermore, to minimise the risk of "over-fitting" the Topliss and Costello rule should be followed, which states that the ratio of observations: descriptors should be 5:1 when using simple linear regression methods[169]. This not only minimises chance correlations, but also makes interpretation of the model easier. Another challenge is that training and test data set should be well-distributed, otherwise poorly distributed chemicals will exert strong model leverage[170].

1.8. Molecular Docking

Molecular docking is a computer-based technique in structural molecular biology that predicts the energetically favourable binding conformations of a ligand in the binding site of a receptor of interest of known three-dimensional structure[171]. Since its beginnings in the 1960s, molecular docking has experienced a dramatic growth, and today it represents a very powerful tool in drug discovery, as thousands of compounds can be screened at a small cost, which is particularly beneficial in the long and costly drug development process[172]. Some of the uses of molecular docking in drug discovery include structure-activity studies, lead optimisation and finding potential leads by virtual screening[171]. Some common and well-established docking software packages include AutoDock[173], GOLD[174], DOCK[175] and FlexX[176].

Additionally, molecular docking has another important application: it can be used in the search for interactions of molecules with undesirable targets, categorised as "off-targets"[177]. Off-target binding refers to the interaction between a pharmacologically active molecule and a target protein other than its primary target, potentially leading to undesired and unexpected downstream effects. Nevertheless, not all off-target bindings are detrimental, as some beneficial effects have been observed that could potentially lead to drug repurposing[178]. It should be noted that one of the limitations of docking is that it cannot shed light on the agonist or antagonistic effect of a compound[172].

In summary, molecular docking involves computationally exploring a search space defined by the method (algorithm) and ranking candidate binding conformations. Therefore, docking requires both a search method and a scoring function[171].

1.8.1. Search Methods (Algorithms)

The search method or docking algorithm is responsible for searching through different ligand conformations and orientations (poses) within a given target protein[179]. In this process of conformational search, structural parameters of the ligand, like rotational degrees of freedom, are incrementally modified. Search methods fall into two major categories: systematic and stochastic. Systematic methods try to explore all degrees of freedom in a molecule, promoting slight variations in the structural parameters, gradually changing the conformation of the ligands[180]. Then, after probing the energy landscape, the algorithm converges to the minimum energy solution that corresponds to the most likely binding mode[181]. Stochastic methods perform random changes in the ligands' structural parameters until a user-defined termination criterion is met. This method overcomes the drawback of defining the final solution at a local energy minimum and increases the probability of finding a global minimum[181]. However, there is an important computational cost associated with this method as it involves broad coverage of the energy landscape. Some popular random approaches are Monte Carlo, Genetic Algorithms and Tabu Search[180]. Both systematic and stochastic methods are contemplated in several molecular docking programs.

Furthermore, there are two basic docking configurations: "flexible" docking or "rigid" docking[182]. Rigid docking refers to both the protein and ligand being fixed so that bond angles and lengths are not changeable[183]. This configuration allows very fast

calculations, because the size of the search space is much smaller, but it is not practical or realistic where substantial conformational changes occur during the formation of a ligand-protein complex. Flexible docking is more commonly used because it allows conformational shifts, however, more time and computational power is required[184]. Systematic search methods are commonly used in rigid docking, whereas stochastic methods are more suitable for flexible docking.

1.8.2. Scoring Functions

The driving forces that determine the protein-ligand complex include a number of interactions and energy exchange among the protein, ligand, water and buffer ions, which are explained by the laws of thermodynamics. Gibbs free energy (ΔG°) is a thermodynamic potential that measures the maximum of reversible work performed by a thermodynamic system at a constant temperature and pressure (Equation 1.2)[185].

Equation 1.2. Gibbs free energy (ΔG°)

$$\Delta G^\circ = \Delta H^\circ - T\,\Delta S^\circ$$

Essentially, ΔG° is a quantitative measure of the favourability of a given reaction at a constant temperature and pressure; in other words, it represents the amount of "free" or "useful" energy available to do the work. Therefore, spontaneous protein-ligand binding takes place when ΔG° is negative, and the extent to which that interaction is favourable will be determined by the magnitude of the negative ΔG°. ΔH and ΔS are change in enthalpy and entropy, respectively, and they will determine the sign and magnitude of the binding free energy. Enthalpy changes result from the formations of interactions like Van der Waals forces, ionic bonding and any other polar or non-polar interactions between the protein and ligand, ligand and solvent and solvent reorganization at the binding interface[186]. These components either give favourable or unfavourable contributions and the net enthalpy change is a result of combination of these contributions[187]. For instance, exothermic reactions (negative ΔH) involve formation of energetically favourable non-covalent interactions between atoms, whereas endothermic reactions (positive ΔH) involve disruption of the energetically favourable non-covalent interactions between atoms. Entropy measures the total energy of a thermodynamic system, i.e. it indicates the overall increase (positive sign) and decrease (negative sign) of the energy in the system[188].

In summary, binding energy is a reflection of the energy change of the system that takes place when a ligand binds to the protein, and negative binding energies indicate high stability of the complex. The scoring function is responsible for estimating the binding affinities of the generated poses, ranking them, and identifying the most favourable binding modes of the ligand to the given target[179]. Scoring functions are categorised into three different groups: empirical, force-field based or knowledge based functions[189] and are explained in more detailed below. Every scoring function has its advantages and limitations, therefore, the simultaneous use of different scoring methodologies has been increasingly employed as a way to obtain a consensus scoring[181].

- **Force-field-based scoring functions**:

Force-field-based scoring functions estimate the binding energy by summing two energies, the receptor–ligand interaction energy and internal ligand energy in a general master function[190]. The energies are normally computed with the contributions of the Van der Waals and electrostatic interactions. This type of scoring function applies an *ab initio* method to calculate the energy associated with each term of the function using the equations of classical mechanics[181]. Most force-field scoring functions only consider a single protein conformation, which makes it possible to omit the calculation of internal protein energy, which greatly simplifies scoring[190].

Disadvantages: these scoring functions were originally created to model enthalpic gas-phase contributions to structure and energetics, therefore they lack solvation and entropic terms[190].

- **Empirical scoring functions:**

Empirical scoring functions use a series of protein-ligand complexes with known binding affinities as a training set to perform a multiple linear regression analysis[181]. These scoring functions are based on the idea that binding energies can be approximated by a sum of individual uncorrelated terms[180], that is, the physical events involved in the formation of the ligand-receptor complex (hydrogen-bonding, ionic and apolar interactions, as well as desolvation and entropic effects)[181]. Therefore, binding affinities of a complex can be estimated by summing up these important energetic factors. Surflex and FlexX are broadly used molecular docking programs using empirical scoring functions[181].

Advantages: the terms of the equations are often simple to interpret and faster to compute at low cost. Disadvantages: these functions will depend on the accuracy of data used to develop the model.

- **Knowledge-based scoring functions:**

Knowledge-based scoring functions are designed to reproduce experimental structures rather than binding energies. They use very simple atomic interactions pair potentials extracted from known ligand-receptor complexes to obtain a general function[180]. These potentials are based on the frequency of occurrence of different atom-atom pair contacts, i.e. the frequency with which two different atoms are found within a given distance in the structural data set[189]. The different types of interactions are classified and weighted according to their frequency of occurrence; then final score is given as a sum of these individual interactions.

Advantages: They are relatively simple and allow screening of large compound databases. As they don't rely on reproducing binding affinities like empirical methods or *ab initio* calculations like force-field methods, they offer a proper balance between accuracy and speed[181]. Disadvantages: their derivation is essentially based on information implicitly encoded in limited sets of protein–ligand complex structures[180].

1.8.3. The Target Structures

The first step in docking is to select the target structure or protein of study. Crystal structures of proteins are increasingly more available due to development of techniques such as x-ray crystallography or nuclear magnetic resonance. If available, 3D structures of proteins can easily be retrieved from Protein Data Bank (PDB). If not available, the protein structures can be built using computational prediction methods such as homology modelling or *ab initio* prediction. However, quality of homology models can heavily influence the reliability of the docking results. Protein structures can be selected based on several factors, but resolution is often a critical one. High-resolution structures (resolution values close to 1 Å) show high-level of detail in their electron density map, so it is easy to see every atom, including information of amide bonds and the orientation of side chains. On the contrary, low-resolution structures (resolution values of 3 Å or higher) only represent the basic contour of the protein chain and the fine atomic structure must be inferred. Consequently, it is recommended to select protein structures with resolution values lower than 2 Å. Once selected, the

protein structure must undergo a series of preparatory steps that include addition of hydrogen ions and energy minimisation[182].

1.8.4. The Ligand

The structure of ligands to be docked can be manually drawn using ChemDraw software or downloaded from chemistry libraries as SMILES codes. These structures also need to be prepared before docking: some preparatory steps include washing, assignment of charges and energy minimisation. The overall size of the ligand impacts most docking algorithms, both in terms of computational cost and results accuracy. Molecules with a large number of rotatable bonds will increase the ligand's degree of freedom, increasing the number of possible conformations and complexity of the conformational space to explore. Hence, a correlation between the size of the ligand and its score has been observed, where molecules that can show more interactions, such as hydrogen bonds, usually obtain better docking scores[191].

1.8.5. Validation and Evaluation of Docking Results

Docking results can be validated by comparing the prediction of binding mode with known structural data. This can be done by re-docking any co-crystallised ligand within the binding pocket of the target protein and by comparing the root mean square deviation (RMSD) values between the docked and the crystallographic binding mode of the ligand[172]. RMSD values lower than 2 Å indicate acceptable accuracy for the docking procedure. Another option to assess the accuracy of the docking results in terms of ranking order is to correlate binding energies with existing experimental data (IC_{50} values or Ki values).

1.9. Thesis Rationale and Aims

Mitochondria are very important organelles not only because they generate over 95% of the cell energy, but also because they host many other key metabolic functions and participate in many important processes such as inflammation, metabolic signalling and cell death. Therefore, given the key role that mitochondria play in cell metabolism, they represent an attractive target for many antibiotics, fungicides and for many poorly treated common diseases.

An increasing body of evidence has shown that mitochondrial dysfunction can be the result of drug-induced toxicities and, during the last decades, mitochondria have been implicated in Black Box warnings and drug withdrawals by regulatory bodies. Therefore, improved methods of prediction and assessment of drug-induced mitochondrial toxicity (DIMT) and a better understanding of specific mechanisms will help in the identification and management of such toxicities. This is particularly important to guarantee a safe progression of candidate molecules in the long and costly drug-development process, but also in the design of compounds that deliberately target the mitochondria for agronomic or therapeutic purposes.

The rationale of this research lies in the lack of knowledge as to what structural and physicochemical features could be linked to DIMT. Such knowledge could help us recognise toxicities during the initial stages of drug development, as well as in marketed drugs. Furthermore, contradictory drug effects on mitochondria have been reported depending on the assay type and experimental model system of choice, while for some drugs there is little or no such data available. For example, effects which are reported on isolated mitochondria, where there is absence of drug metabolism and lack of cellular context, do not always necessarily correlate with what is observed in whole cells. Since drugs may induce mitochondrial impairment through different mechanisms, it seems reasonable that multiple assays may be required to completely understand the mechanisms of a toxicological event. Therefore, the overall goal was to compare multiple *in vitro* assays, using two different model systems (HepG2 cells and rat liver isolated mitochondria) and multiple mitochondrial endpoints, as well as to use *in silico* assays, such as molecular docking and QSAR to shed light on the mechanisms of toxicity. The overall aim of this research project was broken down into a series of objectives:

1. To develop a QSAR and molecular docking methodology to investigate the interactions between the AOX, a crucial respiratory protein present in the ETC of some pathogenic parasites, and inhibitors using experimental data (IC_{50} values) available in the literature, as well as data obtained in the laboratory. The rationale was to provide useful tools for future design and development of novel and specific AOX inhibitors, as well as to deliver a suitable methodology that could be applied to more structurally complex protein targets, such as the cytochrome bc_1 complex.

2. To isolate and characterise rat liver mitochondria to guarantee good quality of mitochondrial preparations. Then, to validate some of the *in vitro* methodology using high-resolution respirometry with control compounds.

3. To study the *in vitro* effects of some well-known complex III and AOX inhibitors, commonly used as fungicides, on both isolated mitochondria and whole cells. The rationale behind this was twofold, to gain a better understanding on the mechanisms of toxicity of this compound set, and to validate the techniques employed in this study for future investigations on pharmaceutical drugs.

4. To investigate the effects of some commonly prescribed drugs such as anticonvulsants, antidepressants, antidiabetic, antihyperlipidemic, anti-inflammatory, antipsychotic and anxiolytic drugs, as well as some other widely prescribed drugs, on mitochondrial bioenergetics by combining a series of *in vitro* techniques (previously validated) and molecular docking. The aim was to elucidate potential mechanisms of toxicity, as well as to provide some insight regarding toxicological risk posed by the members of these drug classes. Some of these drugs have shown a variety of negative pharmacological profiles in clinical use, therefore it is essential to understand if and how mitochondrial function could be affected. Gaining understanding into this will not only help with the design of safer drugs with reduced side effects linked to mitochondrial toxicity in the future but could also lead to drug repurposing.

5. To shed light on structural and physicochemical features associated with inhibition of the cytochrome *bc*$_1$ complex by generating QSAR models using the experimental data generated in previous chapters, as well as to perform molecular docking studies to obtain insight on the interactions occurring between the inhibitors and the binding site. The goal is to identify chemical motifs responsible for inhibition, which can be avoided in the design of new drugs to avoid toxicities resulting from interaction with the cytochrome *bc*$_1$ complex. The resulting models can also be used in the prediction of mitochondrial toxicity of new drug candidates and pre-existing compounds. The rationale behind this was that the Q_o site of the cytochrome *bc*$_1$ in particular has been reported to be a common off-target of various pharmaceutical drugs clinically used[69, 192]. Additionally, despite being powerful tools, very few QSAR models have been developed for mitochondrial toxicity, especially regarding ETC inhibition, probably due to limited experimental data. However, there is a need for the development of such predictive tools especially during the initial design of compounds, which can reduce the time and cost required for the development of new drugs.

2. Materials and Methods

2.1. Materials

All chemicals were purchased from Sigma-Aldrich (Dorset, UK) unless otherwise indicated and were of the highest purity available. Ascofuranone, ascochlorin and ferulenol were kindly provided by Prof Kiyoshi Kita (University of Nagasaki), whereas compounds ISSF31, ISSF33, colletochlorin B and colletochlorin D were synthesised in-house[193] (University of Sussex). Salicylic acid and acetaminophen were kindly provided by Prof Ali Nokhodchi (University of Sussex). HepG2 cells were provided by Dr Neil Crickmore (University of Sussex) and Cyprotex Ltd (Alderley Park, UK). The cell proliferation kit I (MTT) was purchased from Sigma-Aldrich. The XFp FluxPacks, calibration buffer, Seahorse XF base medium and XFp Cell Mito Stress Test Kit for the XFp Extracellular Flux Analyser were purchased from Agilent Technologies LDA UK Ltd. All cell culture media and supplements were from Fisher Scientific (Loughborough, UK). The rPFO was from Seahorse Bioscience as XF PMP.

2.2. Cell culture

HepG2 cells were cultured and maintained in Dulbecco's Modified Eagle's Medium (DMEM; Gibco, Life Technologies, Inc., NY, USA) high glucose media containing 1 mM sodium pyruvate and 25 mM glucose, supplemented with 10% fetal calf serum (FCS) (v/v) and 1% Penicillin-Streptomycin-Glutamine (100 U/mL penicillin, 100 μg/mL streptomycin and 2 mM glutamine). Cells were grown in 75 cm^2 flasks in a total volume of 25 mL in an incubator controlled at 37 ºC, 90% humidity and 5% CO_2. Culture medium was changed every two or three days and cells were used up to passage 25. At 70-80% confluence, cells were detached from the flasks using a solution of 0.05% trypsin / 0.54 mM EDTA (Gibco) and subcultured at an initial seeding density of 4.0 x 10^4 cells/mL (for a 3-day culture).

2.3. Isolation of Rat Liver Mitochondria

Mitochondria were isolated from adult Wistar rats that were euthanized via cervical dislocation or with an overdose of carbon dioxide depending on their weight. Organs were rapidly excised and immersed into ice-cold Milli-Q water and then transferred into isolation buffer containing 1 mM EGTA, 30 mM MOPS, 0.25 M sucrose, 3.5 mM L-cysteine and 0.1% (w/v) BSA, pH 7.4. The liver was homogenised with 10 passes

in a loose-fitting homogeniser, followed by 10 passes in a tight-fitting homogeniser and filtered through muslin. The resultant tissue homogenate was centrifuged at 1000 x g for 10 min at 4°C and the supernatants were kept and re-centrifuged at 10,000 x g for 10 min. This centrifugation step was repeated preserving the pellet. The final mitochondrial pellet was re-suspended to a protein concentration of 30-40 mg/mL with buffer solution and preserved on ice. Protein concentration was determined using the Bradford method (1976) with bovine serum albumin as the standard[194].

2.4. Measurement of Activities of Individual Respiratory Complexes

2.4.1. Succinate-Cytochrome *c* Reductase

The activity of succinate-cytochrome *c* reductase was measured in a 96-well plate by monitoring the increase in absorbance of cytochrome *c* at 550 nm in a Thermo Scientific™ Multiskan™ GO microplate spectrophotometer over a 4-min time-course at room temperature. Rat liver mitochondria (~3 μg/well) was added to an assay solution containing 200 mM sucrose, 25 mM KCl, 5 mM $MgCl_2$, 4 mM KH_2PO_4, 5 mM MOPS, 1 mM KCN, 1 mM ATP, 1 μM rotenone and 64 μM cytochrome *c* (Sigma C2506), pH 7.4. Reaction was started by the addition of 12.5 mM sodium succinate to each well. For drug treatments, compound stock solutions were added to the wells to give the indicated final concentrations. Values were normalised using a vehicle control containing 0.6% dimethyl sulfoxide (DMSO) (v/v) and a control with no mitochondria to establish 100% and 0% activity.

2.4.2. Succinate-Ubiquinone Oxidoreductase or Complex II

The activity of succinate-ubiquinone oxidoreductase (complex II) was measured by monitoring the decrease in absorbance of 2.6-dichlorophenolindophenol (DCPIP) at 600 nm at room temperature for 15 minutes. The assay media contained 200 mM sucrose, 25 mM KCl, 5 mM $MgCl_2$, 4 mM KH_2PO_4, 5 mM MOPS, 1 mM ATP, 1 μM rotenone, 1 μM antimycin A, 50 μM coenzyme Q_2 and 100 μM DCPIP, 12.5 mM sodium succinate, pH 7.4. Values were normalised using a vehicle control containing 0.6% dimethyl sulfoxide (DMSO) (v/v) and a control with 5 mM malonic acid, a specific complex II inhibitor, to establish 100% and 0% activity, respectively.

2.4.3. Ubiquinone–Cytochrome *c* Oxidoreductase or Complex III

The activity of ubiquinone–cytochrome *c* oxidoreductase (complex III) was assayed by monitoring the reduction of cytochrome *c* at 550 nm in the presence of 200 mM sucrose, 25 mM KCl, 5 mM $MgCl_2$, 4 mM KH_2PO_4, 5 mM MOPS, 1 μM rotenone, 5 mM malonic acid, 1 mM KCN, 50 μM coenzyme Q_2 and 64 μM cytochrome *c*, pH 7.4. Values were normalised using a vehicle control containing 0.6% dimethyl sulfoxide (DMSO) (v/v) and a control with 0.6 μM antimycin A, a specific complex III inhibitor, to establish 100% and 0% activity, respectively.

2.4.4. Data Analysis

Each assay was done in triplicate using a minimum of three different biological samples of rat liver mitochondria. Absorbance values obtained during all activity assays on the MultiskanTM GO plate reader were exported from SkanIt™ Software 4.1 to Excel and analysed using GraphPad Prism 7. For all wells a straight line from a non-linear regression was fitted to obtain the slope of the activity. IC_{50} values were obtained after having normalised the data, using the [inhibitor] vs. normalised response – variable slope model in GraphPad Prism 7. IC_{50} is the concentration of compound that gives a response halfway between bottom (0% activity) and top (100% activity). For establishment of significance, one-way ANOVA was performed followed by the Dunnet test to compare every mean to a control mean or the Tukey test to compare every mean with every other mean. The following statistical significance values were reported: * for $p<0.05$, ** for $p<0.01$ and *** for $p<0.001$.

2.5. High-Resolution Respirometry

2.5.1. *Escherichia coli* Membranes Expressing TAO

Respiratory activity of recombinant *Escherichia coli* (*E. coli*) membranes expressing the trypanosome alternative oxidase (TAO) were monitored with high-resolution respirometry to experimentally determine the IC_{50} values of several AOX inhibitors. Respiration was monitored using an Oroboros® Oxygraph-2K (Oroboros Instruments, Innsbruck, Austria[195]). Data acquisition and analysis were performed using DatLab® software, version 6.1 (Oroboros Instruments) and GraphPad Prism 7. Methods for E. *coli* membrane preparations have been presented before and were kindly provided by Dr Luke Young[193]. For the trypanosome alternative oxidase inhibition assay, the O2k

chambers were calibrated for 2 mL of 65 mM MOPS buffer adjusted to pH 7.4 and equilibrated with air at 37 °C at the beginning of each experiment. TAO membrane bounds (~600 µg total protein) were added to closed chambers containing respiration buffer with 1 mM KCN and supplemented with 1.25 mM NADH as substrate to assess basal respiration. Effects of increasing concentrations of inhibitor were determined using a single sample. Average values from 3 isolations ± standard deviation where applicable.

2.5.2. Rat Liver Mitochondria (RLM)

Mitochondria were isolated from rat liver using differential centrifugation as previously described in section 2.3. The final mitochondrial pellet was re-suspended to a protein concentration of 20-30 mg/mL with buffer solution (1 mM EGTA, 30 mM MOPS, 0.25 M sucrose, and 0.1% (w/v) BSA, pH 7.4) and preserved on ice. Mitochondrial respiration was measured using an Oroboros® Oxygraph-2K (Oroboros Instruments, Innsbruck, Austria[195]) at 37°C and room-air saturated oxygen tension, in the presence of 1 µM rotenone and 12.5 mM succinate. Mitochondrial protein concentrations in the chambers ranged between 100-300 µg. Respiratory control ratio (RCR), the ratio of state 3 to state 4 respiration, was determined to evaluate the mitochondrial coupling state. State 3 was obtained when increasing concentrations of ADP (100, 200, 400, 800, 1200, 2000 and 2750 µM) were added to isolated mitochondria in the presence of excess substrate (12.5 mM succinate) (state 3_{ADP}). State 3 was also obtained by the addition of increasing concentrations of ADP (100, 200, 400, 800, 1200 µM) followed by the addition of 1 µM CCCP (state 3_U). ADP/O ratio was also determined in the presence of excess substrate by the addition of a small quantity of ADP (140 nmol). ADP/O was calculated as the amount of ADP added divided by the amount of oxygen atoms (nmol) consumed during phosphorylation. The concentration of ADP in stock solutions was verified by spectrophotometry.

2.5.3. Mitochondrial Membrane Potential (MMP)

The mitochondrial membrane potential ($\Delta\Psi_{mt}$ or MMP) was investigated using safranin, a lipophilic cationic fluorescent probe that accumulates within the matrix of energized mitochondria. The Oroboros® Oxygraph-2K (Oroboros Instruments, Innsbruck, Austria[195]), which can incorporate fluorescence sensors equipped with a

filter set for safranin (excitation at 495 mm and emission at 587 nm), was used to simultaneously analyse high-resolution respirometry and MMP. At the beginning of each experiment, the O2k chambers were filled with 2 mL of reaction buffer (200 mM sucrose, 25 mM KCl, 5 mM $MgCl_2$, 4 mM KH_2PO_4, 5 mM MOPS, pH 7.4) and equilibrated with air at 37°C. During the experiments, the incubation chambers were kept at constant temperature by Peltier control (± 0.001°C) and the medium with sample was stirred using white PVDF-coated stirrers (750 rpm). For calibration, a 200 µM stock solution of safranin dissolved in distilled water was titrated in five steps into the O2k chamber, up to a final safranin concentration of 2 µM. A linear increase in the fluorescence signal was detected, reflecting the concentration of safranin in the chamber. Safranin cannot be used as an indicator of MMP at high concentrations, as it exerts a dose-dependent inhibitory effect on OXPHOS, particularly when CI-linked respiration is examined. To avoid this problem, the inhibitory effect of safranin was minimized using the complex I inhibitor rotenone and the CII-linked substrate succinate. The final concentration of safranin used in the experiments (2 µM) does not disturb mitochondrial respiration[196]. Upon calibration of the safranin signal, 100-300 µg of freshly isolated rat liver mitochondria (RLM) were injected into the 2-mL O2k chambers, followed by 1 µM rotenone and 12.5 mM succinate. This was followed by serial additions of the drug to assess its dose-dependent effect on the MMP. Injection of RLM results in an uptake of safranin and a corresponding decline in the fluorescence signal. Hence, the signal was normalised within a maximum fluorescence, which corresponded to the basal signal elicited upon addition of RLM, and a minimum, which corresponded to the fluorescence signal upon addition of succinate, which also corresponds to the membrane potential generated in the mitochondria.

2.5.4. Reactive Oxygen Species (ROS) production

Mitochondrial reactive oxygen species (ROS) production was assessed using Amplex® UltraRed (AmR) for combined high-resolution respirometry and fluorescence detection of hydrogen peroxide (H_2O_2) production. Complex III is considered one of the main producers of ROS, primarily in the form of superoxide anions (O_2^-)[116], which are immediately converted to H_2O_2 by the mitochondrial superoxide dismutase (SOD). H_2O_2 can freely pass biological membranes, and for this reason it represents a good method of choice for estimation of mitochondrial ROS

formation. The fluorescence-sensor green (525 nm) of the Oxygraph-2k (Oroboros Instruments, Innsbruck, Austria[195]) was used to detect the increase of the resorufin-linked fluorescence signal, which is the reaction product of H_2O_2 formed with AmR in the presence of horse radish peroxidase (HRP). At the beginning of each experiment, the O2k chambers were filled with 2 mL of reaction buffer (200 mM sucrose, 25 mM KCl, 5 mM $MgCl_2$, 4 mM KH_2PO_4, 5 mM MOPS, pH 7.4) and equilibrated with air at 37°C. Subsequently, 10 µM Amplex ®Red, 1 U/mL HRP, 5 U/mL SOD and 0.1 µM H_2O_2 were added in both chambers for initial calibrations. Upon calibration of the fluorescence signal with H_2O_2, 100-300 µg of freshly isolated RLM were injected into the 2-mL O2k chambers, followed by 1 µM rotenone and 12.5 mM succinate to support complex II-linked respiration. Subsequently, uncoupler 0.25 µM CCCP was added to obtain uncoupled respiration. Finally, a step-by-step titration with the drugs was performed to investigate changes in the endogenous ROS levels. The measured fluorescence values are expressed as a percentage of fluorescence with respect to the control group (baseline).

2.6. Cell Viability Assays (MTT)

The viability of HepG2 cells in the presence of several pharmaceutical drugs was tested using the 3-(4,5-dimethyl-2-thiazolyl)-2-diphenyl-2H-tetrazolium bromide (MTT) assay. Cells were seeded onto 96 well, clear bottom tissue culture plates at a density of 10,000 cells/well and left overnight to attach. Incubation media contained 1 mM sodium pyruvate, 25 mM glucose, 10% FCS (v/v) and 2 mM glutamine. Compounds were first prepared in DMSO and were serially diluted to give between a 5-11-point concentration curve. Dosing solutions were prepared by diluting each compound stock 1:10 in assay media (10% DMSO v/v final concentration) and the cells were dosed in triplicate by adding 5 µL of the dosing solution to the appropriate wells containing 95 µL assay media (0.5% DMSO (v/v)). Compound incubation was performed for 24 or 48 h in a humidified atmosphere with 5% CO_2 at 37ºC. After compound treatment, cells were loaded with the final MTT dye concentration of 0.5 mg/mL and incubated for 4 h in a humidified atmosphere with 5% CO_2 at 37ºC. After this incubation period, purple formazan salt crystals were solubilised by adding 100 µL solubilisation solution (10% SDS in 0.01 M HCl) and incubating overnight in a humidified atmosphere with 5% CO_2 at 37ºC. The solubilised formazan product was

spectrophotometrically quantified by measuring the absorbance at 570 nm (Thermo Scientific™ Multiskan™ GO microplate spectrophotometer).

2.7. The Glu/Gal Assay

In the first version of this assay, HepG2 cells were collected by trypsinisation and 10,000 cells/95 µL were plated per well in a 96 well clear bottom tissue culture plate and incubated overnight at 37°C and 5% CO_2 in DMEM containing 25 mM glucose, 1 mM sodium pyruvate, 10% FCS (v/v) and 2 mM glutamine. Six hours prior to the compound treatment, cells were washed twice with 95 µL DMEM containing either 10 mM glucose or 10 mM galactose (plus 1 mM sodium pyruvate, 10% FCS (v/v) and 2 mM glutamine). Dosing solutions were prepared by diluting the compound stocks in the appropriate assay media. After 24 h compound treatment, 0.5 mg/mL MTT dye was added to the wells and incubated for 4 h in a humidified atmosphere with 5% CO_2 at 37 ºC. Formazan salts were then solubilised as described before and the formazan product was spectrophotometrically quantified by measuring the absorbance at 570 nm.

In the second version of this assay, 6,000 HepG2 cells/well were plated in a 384-well black microplate and incubated overnight at 37°C and 5% CO_2 in DMEM containing 25 mM glucose, 1 mM sodium pyruvate, 10% FCS (v/v) and 2 mM glutamine. Six hours prior to the compound treatment, cells were washed twice with DMEM media containing either 10 mM glucose or 10 mM galactose (plus 1 mM pyruvate, 6 mM glutamine, 10% FBS and 1% NEAA). Compounds were prepared at a 200-fold final concentration in DMSO (0.5% v/v final concentration), except for metformin, valproic acid and vigabatrin, which were prepared at a 5-fold change final concentration in the appropriate assay media. Compounds were serially diluted in appropriate vehicle to give an eight-point concentration curve using a half-log dilution series. Dosing solutions were prepared by diluting the compound stocks 1:40 in the appropriate assay media (glucose or galactose). Cells were dosed with 12.5 µL of the dosing solution using the Bravo automated liquid handling platform (Agilent Technologies, Santa Clara, CA) and compound incubation was performed for 24 h in a humidified atmosphere with 5% CO_2 at 37ºC. After this incubation period, cellular ATP concentrations were assessed by using the CellTiter-Glo Cell Viability Assay as per manufacturer's instructions (Figure 2.1). A fold shift of the AC_{50} values obtained

through the dose-response curves in glucose media and galactose media was measured for identifying mitochondrial toxicants.

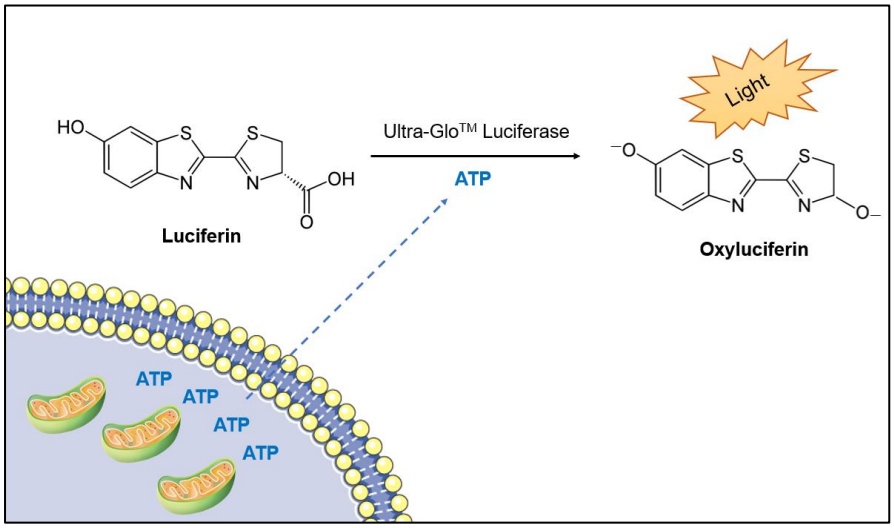

Figure 2.1. The CellTiter-Glo® Luminescent Cell Viability Assay. The assay allows quantification of the number of viable cells based on the ATP present, indicator of metabolically active cells. Cells are the source of ATP, required for the luciferase reaction. The luminescence produced is proportional to the number of viable cells.

2.8. Measurement of Cell Bioenergetics using an Extracellular Flux Analyser

2.8.1. Incubated Drug Effect

The Extracellular Flux Analyzer 8-well format (XFp, Seahorse Bioscience) was used to simultaneously measure in real-time the oxygen consumption rate (OCR) and the extracellular acidification rate (ECAR) in HepG2 cells. The analyser contains two fluorescent sensors per well which detect changes of oxygen and proton levels in the media. From the OCR profile, the effects of the drugs on several respiration parameters were evaluated, including basal respiration, ATP production, maximal respiratory capacity, proton leak and the spare respiratory capacity (Cell Mito Stress Test)[197], as illustrated in Figure 2.2. From the ECAR profile, changes in glycolysis were evaluated.

The day prior the assay, HepG2 cells were seeded on the Seahorse Bioscience XFp cell culture plates at a cell density of 2.0 x 10^5 cells/mL in 80 µL culture medium and incubated overnight at 37°C, 5% CO_2, 85% relative humidity. Respective XFp Flux Assay cartridge plates were hydrated with 200 µL/well of sterile water and were placed

in a non-CO_2 37°C incubator overnight. These disposable sensor cartridges contain fluorescent biosensors that detect changes in oxygen and pH, and they are also equipped with four delivery chambers per well for injecting test agents during the assay (Figure 2.3).

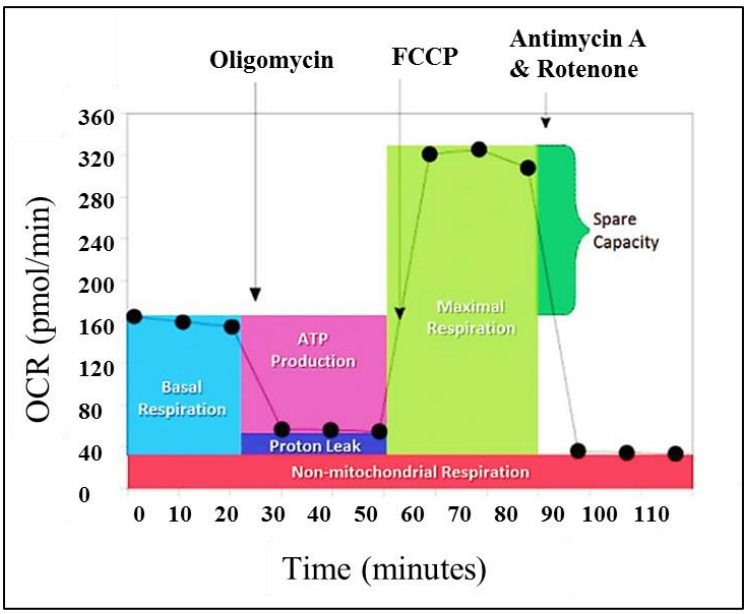

Figure 2.2. The fundamental parameters of mitochondrial function obtained using the Cell Mito Stress Test.

On the day of the assay, water from the utility plate of cartridges was discarded and replaced with 200 µL pre-warmed Seahorse XF calibrant medium. Moats around the outside of the wells were also filled with 400 µL. Cartridges were then incubated in a non-CO_2 37°C incubator for 60 min prior to loading drug ports. Cells in the culture plates were washed twice with non-buffered pre-warmed freshly prepared XF Base DMEM medium pre-warmed to 37°C, supplemented with 2 mM glutamine and adjusted to pH 7.4. Other supplements, such as 10 mM glucose, 10 mM galactose or 1 mM sodium pyruvate depended on the choice of experimental conditions. On each plate, 2 wells were used as background control (cell free), whereas the 6 remaining wells (containing cells) were divided into 3 controls wells (0.5% DMSO (v/v)) and 3 experimental wells (drug treatment).

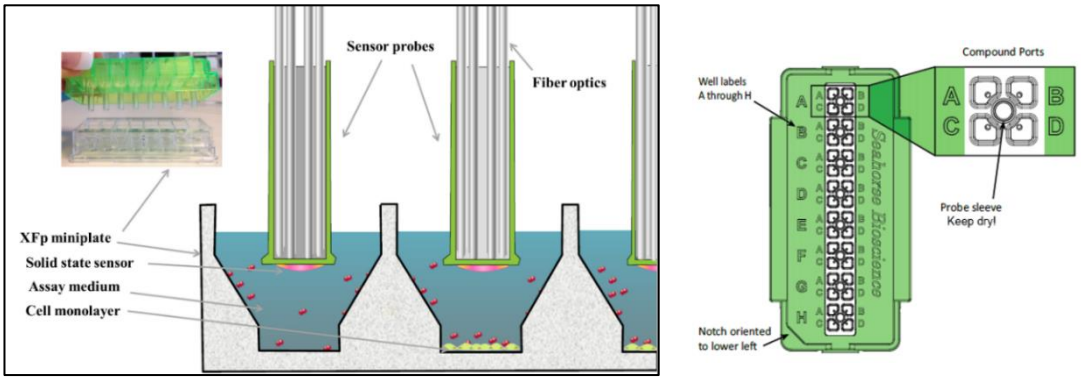

Figure 2.3. The XFp Extracellular Flux Analyzer. Each assay kit contains a sensor cartridge with 8 pairs of fluorescent biosensors (oxygen and pH) and four delivery chambers per well for injecting testing agents into the wells during the assay.

Cell plates were incubated with 50 µM of the drug in the experimental wells in a CO_2 free incubator for 1 h prior to the experiment. During this incubation period, the mitochondrial stressors oligomycin A, FCCP and the mixture of rotenone/antimycin A were loaded in ports A, B and C of the cartridge plates, respectively.

Figure 2.2 shows the typical bioenergetic profile that is generated during the Cell Mito Stress Test. Four initial baseline OCR and ECAR measurements were obtained followed by the injection of the first mitochondrial stressor, oligomycin A (1 µM), where further three measurement of OCR and ECAR were taken. Another three measurements were taken upon addition of the other mitochondrial stressors (0.5 µM FCCP and 1 µM rotenone/antimycin A). Each measurement consisted of a three-minute mix and three minute read cycle. As illustrated in Table 2.1 and Figure 2.4, each reagent targets a specific component of the ETC.

Table 2.1. Modulators of respiration used in the Cell Mito Stress Test (in order of injection).

Compound(s)	ETC target	Effect on OCR
Oligomycin	ATP synthase (complex V)	Decrease
FCCP	Inner mitochondrial membrane	Increase
Rotenone / Antimycin A	Complex I and III (respectively)	Decrease

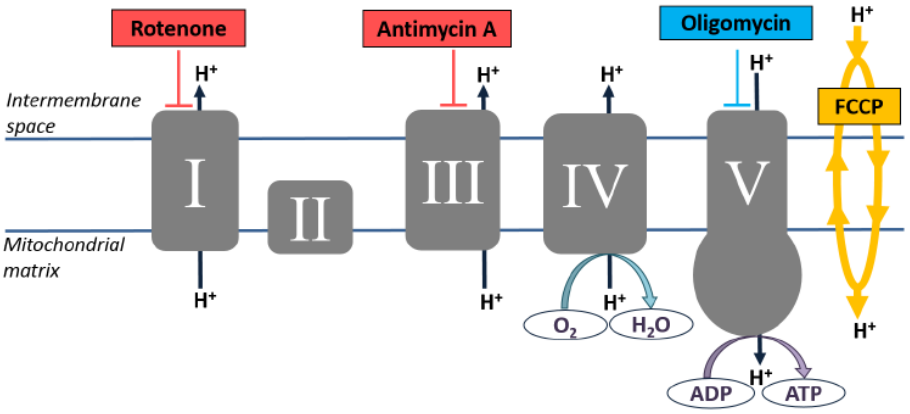

Figure 2.4. Cell Mito Stress Test Modulators of the ETC and their target of action. Adapted from the Agilent XFp Cell Mito Stress Test guide. See Figure 1.2 for a complete depiction of the ETC.

The OCR and ECAR parameters obtained in the presence of the drugs were compared to the values obtained with the controls. OCR is reported as pmol/min/µg and ECAR as mpH/min/µg. Parameters were calculated as follows:

- **Non-mitochondrial O_2 consumption:** oxygen consumption that persists due to a subset of cellular enzymes that continue to consume oxygen after rotenone and antimycin A addition. This is important for getting an accurate measure of basal mitochondrial respiration.
- **Basal respiration:** oxygen consumption used to meet cellular ATP demand. Shows energetic demand of the cell under baseline conditions. It is calculated as the average of the first measurements before the first injection minus the non-mitochondrial respiration rate.
- **Maximal respiratory capacity:** the maximal oxygen consumption rate attained by adding the uncoupler FCCP, which dissipates the mitochondrial membrane potential and therefore allows maximal uncoupled O_2 consumption. FCCP mimics a physiological "energy demand" by stimulating the respiratory chain to operate at maximum capacity, which causes rapid oxidation of substrates (sugars, fats, and amino acids) to meet this metabolic challenge. It shows the maximum rate of respiration that the cell can achieve.
- **Spare respiratory capacity or reserve capacity:** calculated from the difference between the basal and the maximal rate of respiration, this measurement indicates

the capability of the cell to respond to an increased energy demand as well as how closely the cell is to respire to its theoretical maximum. The cell's ability to respond to demand can be an indicator of cell fitness or flexibility.

- **H^+ (Proton) leak:** shows the remaining basal respiration not coupled to ATP production. High levels of proton leak can be a sign of mitochondrial damage. Proton leak can be used as a mechanism to regulate the mitochondrial ATP production. It is calculated from the difference between the respiration rate upon addition of oligomycin and the non-mitochondrial respiration (upon addition of rotenone/antimycin A).
- **ATP production:** the decrease in oxygen consumption rate upon injection of the ATP synthase inhibitor oligomycin represents the portion of basal respiration that was being used to drive ATP production. Shows ATP produced by the mitochondria that contributes to meeting the energetic needs of the cell.

Likewise, the XFp Analyzer registers variations in the extracellular pH. A major component of extracellular acidification is the glycolytic production of lactate, therefore ECAR is commonly used as an indirect measure of the rate of anaerobic glycolysis. However, it should be taken into account that HCO_3^- formation from CO_2 also causes acidification of the medium. When oxidative phosphorylation is disrupted by the addition of oligomycin, cells increase the rate of glycolysis to maintain ATP production, and thereby energy homeostasis. This elevated rate of glycolysis is referred to as the glycolytic capacity of the cell.

After each experiment on the Seahorse XFp, media was removed from the wells, cells were freeze-thawed twice, and protein content was quantified by Bradford method in order to normalise measurements with the protein content[194]. Absorbance was measured at 595 nm on a Thermo Scientific™ Multiskan™ GO microplate spectrophotometer. BSA was used as standard.

2.8.2. Acute Drug Effect

The Extracellular Flux Analyzer 96-well format (XFe96, Seahorse Bioscience) was used to simultaneously measure real-time OCR and ECAR changes upon acute injection of test compounds onto HepG2 cells. The day prior the assay, HepG2 cells were seeded on the Seahorse Bioscience XFe96 cell culture plates at a cell density of

20,000 cells/well in culture medium and incubated overnight at 37°C, 5% CO_2. Respective XFe96 Flux Assay cartridge plates were hydrated with 200 µL/well of calibrant and were placed in a 37°C, 85% relative humidity, non-CO_2 incubator overnight.

On the day of the assay, cells in the culture plates were washed with non-buffered, pre-warmed freshly prepared XF Base DMEM medium, supplemented with 10 mM glucose, 1 mM pyruvate and 2 mM glutaMAX, adjusted to pH 7.4. Cells were incubated in 180 µL assay media in a non-CO_2 incubator at 37°C for 60 min prior to the experiment. During this incubation period, the mitochondrial stressors oligomycin A, FCCP and the mixture of rotenone/antimycin A were loaded in ports B, C and D of the cartridge plates, respectively. Test compounds were prepared at 200-fold final concentration in appropriate vehicle (DMSO or water). Then, compounds were serially diluted to form a seven-point half-log dilution series and were further diluted 1:10 in assay media. Test compounds were injected in port A and the final DMSO concentration was 0.5% (v/v final volume) in all wells. On each plate, ten wells were cell free and used as controls. Six were used as compound controls, where the top concentrations of each compound were injected to identify interference with the measurements due to pH changes or colour. The remaining four wells were used as temperature controls.

At the start of each experiment, four initial baseline OCR and ECAR measurements were taken, prior to the addition of the test compounds. Subsequently, test compounds were injected from port A and a further six measurements of OCR and ECAR were taken. This was followed by the injection oligomycin A (1 µM), where further two measurements of OCR and ECAR were taken. Another two measurements were taken upon addition of 0.5 µM FCCP and rotenone (1 µM) plus antimycin A (1 µM). Each measurement consisted of a three-minute mix and four-minute read cycle.

The sixth OCR measurement following compound or vehicle addition, was normalised to baseline OCR measurements. Reserve capacity was calculated from the difference between the basal and the maximal rate of respiration. ATP production was measured upon injection of the ATP synthase inhibitor oligomycin. Proton leak was calculated from the difference between the respiration rate upon addition of oligomycin and the non-mitochondrial respiration rate. All measurements were determined as change

from baseline OCR and corrected for the non-mitochondrial OCR (the final OCR measurement following the addition of rotenone/antimycin A). ECAR measurements were also taken concurrently after the addition of test compounds/vehicle and normalised to the baseline ECAR.

2.8.3. Cell Permeabilised Assay

As previously explained in section 2.8.2, the Extracellular Flux Analyzer 96-well format (XFe96, Seahorse Bioscience) was used to track in real-time OCR changes in HepG2 cells. Since many oxidizable substrates are unable to cross the plasma membrane freely and, additionally, many cell types can store and oxidize endogenous substrates, it is difficult to control and determine which metabolic routes are fuelling respiration. Selective cell permeabilisation using recombinant perfringolysin O ($rPFO^{C459A}$) offers a solution to this without having to isolate mitochondria. In this protocol, 4 nM of rPFO was used to selectively permeabilise the plasma membrane of the HepG2 cells just before running the assay, and a combination of different metabolic substrates and inhibitors were used as an approach to study mitochondrial function *in situ* by exploiting the fact that oxidizable substrates feed differentially into mitochondrial pathways:

- **Complex I-mediated respiratory activity:** oxidation of the NADH-linked substrates pyruvate and malate is determined. Combination of both substrates is necessary for several reasons. On the one hand, addition of malate is required as accumulation of acetyl-CoA could inhibit pyruvate dehydrogenase (PDH) via feedback inhibition. Presence of malate allows for oxaloacetate production and condensation with acetyl-CoA and normal functioning of PDH. On the other hand, addition of just pyruvate may result in the loss of some TCA cycle intermediates through the dicarboxylate carrier. Also, in the presence of malate alone, TCA cycle intermediates are depleted: mitochondrial citrate and oxoglutarate can be depleted by antiport with malate through tricarboxylate and oxoglutarate carrier exchanges, respectively[198].
- **Complex II-mediated respiratory activity:** oxidation of succinate in the presence of complex I-inhibitor rotenone is determined. Transport of succinate into the mitochondria through the dicarboxylate carrier allows its oxidation to

fumarate, with concomitant reduction of FAD into $FADH_2$. Rotenone is present to prevent reverse electron transfer to complex I.

- **Complex IV-mediated respiratory activity:** by the addition of the non-physiological electron-donating compound tetramethyl-p-phenylene diamine (TMPD) and the reducing agent ascorbate (to regenerate the TMPD from its oxidised form) in the presence of complex III-inhibitor antimycin A. TMPD donates electrons to cytochrome *c*, which then reduces complex IV, which catalyses the transfer of four electrons to O_2, forming water.

The day prior the assay, HepG2 cells were seeded on the Seahorse Bioscience XFe96 cell culture plates and respective the cartridge plates were hydrated as previously explained in section 2.8.2. On the day of the assay, the test compounds and specific substrates/inhibitors were loaded into the different injection ports of the cartridges. Test compounds were prepared at 200-fold final concentration in appropriate vehicle, serially diluted to form a seven-point half-log dilution series and were further diluted 1:10 in MAS buffer (Table 2.2). Test compounds were injected from port A with a total of three technical repeats per assay per concentration. Port B was used for the injection of 10 mM succinate + 2 µM rotenone in MAS buffer. Port C was used for the injection of 10 mM ascorbate + 100 µM TMPD + 2 µM antimycin A in MAS buffer. Upon calibration of the cartridge, the cell plate was removed from the incubator and was washed once quickly with 0.15 mL MAS buffer + 0.2% BSA (w/v). Then, media was replaced with warm MAS buffer + 0.2% BSA (w/v) supplemented with 1 mM malate, 10 mM pyruvate, 4 mM ADP and 4 nM rPFO, adjusted to pH 7.4 to a final volume of 0.18 mL per well. Immediately after media replacement, the cell plate was inserted into the XF instrument to start the assay.

Since cell permeabilisation may result in the loss of ADP, the addition of high concentrations of ADP (4 mM) is required alongside the respiratory substrates for the formation of ATP. Additionally, it has been demonstrated that RCR values are much higher in the presence of bovine serum albumin (BSA), indicating that the presence of fatty-acid free BSA in the buffer may preserve mitochondrial coupling by buffering free fatty acids that can be released during the assay[198]. Therefore, BSA was added to the media in the cell plates. However, it was omitted in the injection ports to avoid compounds binding to albumin and to minimise the generation of oxygen bubbles.

Table 2.2. Mannitol and Sucrose (MAS) buffer recipe.

Reagent	Final concentration (mM)
Mannitol	220
Sucrose	70
KH_2PO_4	10
$MgCl_2$	5
HEPES	3
EGTA	1

2.9. Microscopic Observations of HepG2 Cells

2.9.1. Optical Microscopy

HepG2 cells were seeded onto 96 well, clear bottom tissue culture plates at a density of 1.0 x 10^4 cells/well and left overnight to attach. The next day, each concentration of the respective drug was added to one of the wells in triplicate and incubated for 24 h. After the incubation period, pictures were taken using Zeiss AxioVert with 10x/0.3 objective. The camera used was iXon DV885 from Andor Technology.

2.9.2. Confocal Microscopy

HepG2 cells were seeded onto sterile cover slips placed in 6-well plates at an initial cell density of 3.0 x 10^5 cells/mL/well. On the next day, cells were washed with pre-warmed Fluorobrite DMEM lacking FBS (ThermoFisher A1896701) and incubated with 500 nM MitoTracker™ Red CMXROS staining solution for 30 min at 37°C. Cells were washed again with Fluorobrite DMEM and fixated with 4% formaldehyde (Image-iT™ Fixative Solution, ThermoFisher FB002) for 10 min. Subsequently, cells were rinsed with 50 mM glycine/PBS and permeabilised with 0.2% Triton X-100 in PBS for 10 min. Finally, cells were covered with 1 mL 5µg/mL wheat germ agglutinin (WGA) conjugates solution to stain the plasma membrane for 10 min. After that incubation time, cells were washed twice with 1 mL PBS and incubated with 1µg/mL Hoescht for 10 min. After a final wash with 1 mL PBS, cover slips were mounted onto a microscope slide with 10 µL mounting media (ProLong Gold Antifade, ThermoFisher P36930). Samples were stored in dark at -20°C until visualized. Images were obtained using the Zeiss LSM880 confocal microscope with 63X objective using the “smartest” scanning method in the ZEN black software. Hoescht and WGA were

excited with the laser lines 405 and 633 nm, respectively. MitoTracker™ Red CMXROS was excited with laser line 561 nm. Emission was detected in the range 410-497 nm for Hoescht, 580-633 nm for MitoTracker and 653-755 nm for WGA. ImageJ was used to assemble and label the final figures.

2.10. Statistical Analysis

For establishment of significance, one-way ANOVA was performed followed by the Dunnet test to compare every mean to a control mean or the unpaired t-test student to compare one mean to the control mean. The following statistical significance values were reported: * for $p<0.05$, ** for $p<0.01$, *** for $p<0.001$ and **** for $p<0.0001$.

2.11. Molecular Docking

2.11.1. Structure Preparation

2.11.1.1. Protein Structures

All crystal structures were obtained from RCSB Protein Data Bank[199] and were of a reasonable resolution:

- Alternative oxidase of *Trypanosoma brucei* (TAO). PDB entry: 3W54, resolution of 2.3 Å[51].
- Complex I. PDB entry: 5XTD, resolution of 3.7 Å[27].
- Complex II. PDB entry: 3SFD, resolution of 2.6 Å[200].
- Complex III or the cytochrome bc_1 complex. PDB entry: 1PPJ, resolution of 2.1 Å[201].
- Complex IV. PDB entry: 5ZCP, resolution of 1.65 Å[202].
- Complex V. PDB entry: 2JIZ, resolution of 2.3 Å[203].

All protein structures were loaded into MOE software (Molecular Operating Environment, version 2019.01, Chemical Computing Group Inc., Montreal, Canada)[204] to carry out some preparatory steps. The hydrogen bond network was optimised, and protonation of amino acid residues was corrected using the Protonate 3D algorithm. AMBER99 forcefield was used to assign correct atomic charges. All crystallized water molecules and other coordinated molecules were preserved.

2.11.1.2. Compounds

3D structures of the compounds were built from their SMILES codes using the MOE-Builder tool. The molecules were washed, and partial atomic charges were assigned. Then, molecules were subjected to an initial energy minimisation using the AMBER10:EHT forcefield and to a second minimisation using the MOPAC semi-empirical energy function (PM3 Hamiltonian).

2.11.2. Docking of the Compounds

Molecular docking studies were performed using MOE software package (Molecular Operating Environment, version 2019.01, Chemical Computing Group Inc., Montreal, Canada)[204]. The binding pockets were defined as follows:

- Alternative oxidase of *Trypanosoma brucei* (TAO): the binding site of TAO was defined using colletochlorin B, the co-crystallised ligand in the structure.
- Complex I: the binding site of complex I was defined using the proposed ubiquinone-binding channel by Fedor *et al.*, 2017[205], formed by the residues E143, E192, D199, E202 and E227 on the ND1 chain (chain S) and H92, Y141 and D193 on the NDUFS2 chain (chain Q) in the mammalian structure.
- Complex III: inhibitors of Q_o site were docked into the quinol oxidation site, which was defined using the co-crystallised ligand stigmatellin. Likewise, Q_i inhibitors were docked into the quinone reduction site, which was defined using the co-crystallised ligand antimycin A.
- Complex II, IV and V: The binding sites were defined using the co-crystallised ligands pentachlorophenol, azide and resveratrol, respectively.

In the MOE dock panel, the placement method used was Triangle Matcher and the poses generated by this methodology were re-scored using London dG scoring (Equation 2.1). Subsequently, poses resulting from the placement stage were further refined using the Induced Fit method, which allows protein flexibility upon ligand binding, improving the prediction accuracy for the interaction. Poses were then rescored using the GBVI/WSA dG scoring function (Equation 2.2), and the top five best scoring poses were retained. The final output was analysed and docked poses that were not correctly orientated (for catalytic site) within the binding site were discarded and not included in the analysis.

Equation 2.1. London dG scoring. The London dG score estimates binding free energy using:

$$\Delta G = c + E_{flex} + \sum_{h-bonds} C_{HB} f_{HB} + \sum_{m-lig} C_M f_M + \sum_{atoms\ i} \Delta D_i$$

Where c is the average gain/loss of rotational and translational entropy, E_{flex} is the energy loss due to ligand flexibility, f_{HB} measures H-bond geometric imperfections and takes a value [0,1], C_{HB} is the ideal H-bond energy, f_M measures metal ligations geometric imperfections [0,1], C_M is the energy of an ideal metal ligation and D_i is the desolvation energy of atom i.

Equation 2.2. GBVI/WSA dG scoring. The GBVI/WSA dG score estimates binding free energy by:

$$\Delta G \approx c + \alpha \left[\frac{2}{3}(\Delta E_{Coul} + \Delta E_{sol}) + \Delta E_{vdW} + \beta \Delta SA_{weighted}\right]$$

Where c is the average gain/loss of rotational and translational entropy, α and β are equation constants determined during training, E_{Coul} is the coulombic electrostatic energy, E_{sol} is the solvation electrostatic term, E_{vdW} is the Van der Waals energy and $SA_{weighted}$ is the weighted surface area.

2.12. Quantitative-Structure Activity Relationship (QSAR) Models

2.12.1. QSAR for the Search of AOX Inhibitors

2.12.1.1. Data Sets

A series of 34 ascofuranone (AF) derivatives synthesized by Saimoto *et al.*[52] with inhibitory activities against the alternative oxidase of *Trypanosoma brucei* (TAO) were taken to perform the QSAR study. The molecular structures of these compounds, along with their respective 50% inhibitory concentrations (IC_{50}) against TAO are shown in Appendix I, Table 1.2. For the development of QSAR models, IC_{50} values

were converted to the logarithmic scale (-log IC_{50} or pIC_{50}) to ensure normal distribution in statistical analyses, and these were used as the dependent variable in the QSAR analyses. In addition to the 34 AF derivatives, IC_{50} values of a collection of 8 AOX inhibitors were calculated as outlined in section 2.5.1 and were used as the external test compounds.

The chemical structures of all compounds used in this research were drawn with ACD/ChemSketch 2016.2 software and their SMILES (Simplified Molecular Input Line Entry Specification) notations were generated for future uses in molecular modelling and QSAR studies.

2.12.1.2. Calculation of Molecular Descriptors

Molecular descriptors for the 34 AF derivatives and for the external test compounds were calculated using Advanced Chemistry Development (ACD/Labs) Percepta version 2016.1[206] and MOE software (QuaSAR descriptor panel)[204]. Initially, in order to reduce the number of non-significant variables, descriptors with missing values (>10%) or those with >97% of constant values were eliminated from the data set. Additionally, the best docking scores and the average docking scores of the retained top three and top five poses for each compound were used as additional molecular descriptors for the analysis. Furthermore, an indicator variable was devised which indicated the presence (value 1) or absence (value 0) of a hydrogen bond donor group in the meta position of the aromatic ring with respect to the longest hydrocarbon chain on the ring. This indicator variable was used as an additional molecular descriptor in QSAR analysis. As a result, a total of 331 predictors were used as independent variables in all statistical analyses.

2.12.1.3. Model Development and Validation

For the development of QSAR models and the internal validation, only the 34 AF derivatives were used as the training set (Appendix I, Table 1.2).

Stepwise Regression Analysis

To prune the number of initial molecular descriptors and select the predominant ones affecting the inhibitory activity of the AF derivatives against the trypanosomal alternative oxidase, stepwise regression analysis was performed using IBM SPSS Statistics software, version 24. Stepwise regression analysis is a linear feature

selection method in which a model is built by successively adding or removing predictor variables (molecular descriptors), generating a multiple linear regression equation that includes the variables that best explain the distribution of the dependent variable. The stepping criteria was set to default ('alpha to enter'= 0.05 and 'alpha to remove'= 0.10).

In order to perform this feature selection and identify the most important descriptors correlating with log IC_{50}, random allocation of compounds into various training sets was carried out, where each training set comprised of ~80% total number of compounds. To this end, MatLab® was used to carry out a random permutation to obtain 85 sets of different combinations of compounds (85 training sets). In these permutations, 7 compounds of the total set (~20%) were eliminated randomly each time in order to be used as the "internal validation set", whereas the remaining 27 compounds (~80%) were kept to be used as the "training set". Stepwise regression analysis was carried out for each training set (85 times) and the three most important molecular descriptors were selected in each analysis. A collection of these selected descriptors (48 descriptors in total) were used to perform the final stepwise regression analysis, from which top four best molecular descriptors were identified. The optimal QSAR model was then obtained by multiple regression analysis in IBM SPSS Statistics software using the top four best descriptors of the final stepwise regression analysis. For a statistically reliable model, we maintained a ratio of at least 5:1 between the number of compounds and number of descriptors used.

Model Validation

The final QSAR model was validated internally and externally. The internal validation procedure used was leave-one-out (LOO) cross validation, as well as leave-some-out (LSO) cross validation. For LSO method, compounds were divided into 5 groups (containing 7, 7, 7, 7 and 6 compounds), each group was removed once, and then multiple regression was performed using the remaining compounds. The predicted values for the internal validation set were collected and the Mean Absolute Error (MAE), as well as cross-validated R^2 (Q^2) were used to assess the accuracy of prediction of pIC_{50} (Equation 2.3 and Equation 2.4).

Equation 2.3. Cross-validated R^2 (Q^2).

$$Q^2 = 1 - \frac{\sum(Y_{obs} - Y_{pred})^2}{\sum(Y_{obs} - \bar{Y}_{pred})^2}$$

Where Y_{obs} and Y_{pred} correspond to the observed and LOO predicted pIC_{50} value, respectively. $\bar{Y}_{pred}$ refers to the average of the predicted pIC_{50} values based on the LOO technique.

The external validation was done by using the external test compounds, which are represented by the 8 specific AOX inhibitors that were not used to develop the model (Figure 3.1). pIC_{50} values for each compound were predicted using the QSAR model to examine its consistency and capability of predicting. Then the mean absolute error (MAE) (Equation 2.4) was calculated for the external test set. Furthermore, the square correlation coefficient (R^2) between the observed and the predicted activity values, another parameter proposed by Golbraikh and Tropsha for determining the external predictability of a QSAR model, was calculated. According to them, a QSAR model is considered predictive if $R^2 > 0.6$[167].

Equation 2.4. Mean absolute error (MAE)

$$MAE = \frac{\sum|(observed - predicted)|}{N}$$

Where "observed" refers to the experimentally obtained log IC_{50} value, "predicted" is the predicted log IC_{50} value for the internal validation set by the QSAR model, and N is the number of compounds.

2.12.2. QSAR to Identify Key Physicochemical Properties Required for SCR Inhibition

2.12.2.1. Data Sets

A total of 34 compounds which included 19 fungicides and 15 medical drugs were tested to study their inhibitory activity against succinate-cytochrome *c* reductase (SCR, a mixture of respiratory complex II and III). Cytochrome bc_1 inhibitors can be classified into three groups according to what catalytic site they bind to: the quinol oxidation site (Q_o site), the quinone reduction site (Q_i site) or both (Q_o/Q_i). In order to make the QSAR model consistent and robust, only Q_o inhibitors were included in this

study. Q_i inhibitors such as the classic natural inhibitor antimycin A and the synthetic compounds amisulbrom[207], cyazofamid[208] and diuron[209] were excluded from the model. Ascochlorin, a specific inhibitor that acts at both the Q_i and Q_o sites, was also excluded[34]. Q_o inhibitors used in the model included azoxystrobin, dimoxystrobin, fenamidone, fluoxastrobin, kresoxim-methyl, myxothiazol, picoxystrobin, pyraclostrobin and trifloxystrobin[210]. Because of the similarity in structure with some of the cytochrome bc_1 inhibitors, ascofuranone, a specific AOX inhibitor and ascofuranone–derivatives colletochlorin B, colletochlorin D, compound ISSF31 and compound ISSF33, were also tested and included in the analysis. The medical drugs tested included a wide variety of compounds such as antipsychotics (chlorpromazine), blood glucose lowering agents (ciglitazone and troglitazone), anti-inflammatory agents (salicylic acid, sulfasalazine), anticholesteremic agents (simvastatin, lovastatin, bezafibrate), anticoagulants (warfarin) and anti-infectives (atovaquone).

Additionally, some IC_{50} values obtained under the same experimental conditions were taken from the literature in order to achieve a good number of observations based on which a model could be developed and thereby build a robust QSAR model. Consequently, IC_{50} values for amectotradin, a Q_o inhibitor, and 12 derivatives of the parent drug reported by Zhu X. *et al*.[211], as well as IC_{50} values for famoxadone, a Q_o inhibitor, and 11 derivatives reported by Wang F. *et al*.[212] were taken to be included in the analysis. An IC_{50} value for pyribencarb, a Q_o inhibitor reported by Kataoka S. *et al*., was also considered in the analysis[213].

In total, 50 compounds were taken to perform this study. For the development of the QSAR model, the complete set of molecules (50 compounds) was divided into a training set (32 compounds) to generate the model and a test set (18 compounds) to examine its consistency and capability of predicting. Because splitting of the data set into training and test set is one of the most crucial steps for QSAR, and determines the quality of the generated model, compounds were divided into training and test set manually, by considering the structural diversity and a wide range of activity in the data set. This was achieved through Principal Component Analysis (PCA), a powerful tool in exploratory data analysis that transforms the data into lower dimensions called principal components (PCs), which can simplify the complexity in high-dimensional data[214]. For the development of the QSAR model, IC_{50}s were converted to the

logarithmic scale (-log IC_{50} or pIC_{50}) to ensure normal distribution of data in statistical analyses, and these were used as the dependent variable in the QSAR analyses.

2.12.2.2. Calculation of Molecular Descriptors

The chemical structures of all compounds used in this study were drawn with ACD/ChemSketch 2016.2 software. Subsequently, SMILES (Simplified Molecular Input Line Entry Specification) notations were generated to build the geometry of the compounds using MOE software (Molecular Operating Environment, version 2016.08, Chemical Computing Group Inc., Montreal, Canada)[204]. The data set molecules were washed, partial charges were assigned, and the molecules were then subjected to an initial energy minimisation using the AMBER10:EHT forcefield. A second minimisation was applied by the PM3 semi-empirical method in MOPAC. A total of 291 2D and internal 3D molecular descriptors were calculated using the QuaSAR descriptor panel within MOE software[204]. In addition, 38 physicochemical descriptors were calculated using Advanced Chemistry Development (ACD/Labs) Percepta version 2016.1[206]. Docking scores and fingerprints were also included as additional descriptors. With the aim of reducing the number of non-significant variables, descriptors with empty values or >97% of constant values were eliminated from the data set. As a result, a total of 325 predictors were used as independent variables in all statistical analyses.

2.12.2.3. Model Development and Validation

Stepwise Regression Analysis

In order to perform a pre-selection of the most important descriptors correlating with pIC_{50}, MatLab® was used to carry out a random permutation *(p = randperm(n))* to obtain 200 different samples containing 25 compounds as the "training set" from the total set of 32 compounds. The remaining 7 compounds of the total set (~20%) were used as the "internal validation set". A stepwise regression analysis using the stepwise regression algorithm in MatLab® *(b=stepwisefit(X,y))* was carried out for every combination of training set compounds (200 times) beginning with no terms in the model and using entrance/exit tolerances of 0.05/0.10 on the *p*-values. Finally, a histogram plot was generated to report the frequencies of each molecular descriptor in all 200 stepwise regression analyses. Descriptors with frequencies greater than 10 were selected and used to perform a final stepwise regression analysis (49 descriptors

in total). For a statistically reliable model, we maintained a ratio of at least 10:1 between the number of compounds and number of descriptors used, therefore the final QSAR models were obtained by multiple regression analysis using a maximum of 3 or 4 descriptors.

Model Validation

The QSAR models were validated internally and externally. The internal validation procedure used was Leave-One-Out (LOO) cross validation. The predicted values for the internal validation set was collected and cross-validated R^2 (Q^2) was used to assess the accuracy of prediction of pIC_{50}.

The external validation was performed by using an external test set of compounds, which were not used to develop the model. pIC_{50} values for each compound were predicted using the QSAR models to examine their consistency and capability of predicting. Then, MAE was calculated for the external test set.

Furthermore, several parameters proposed by Golbraikh and Tropsha for determining the external predictability of a QSAR model were calculated[167]. According to them, a QSAR model is considered predictive if the following conditions are satisfied:

i. $Q^2 > 0.5$
ii. $R^2 > 0.6$
iii. $R^2 – R_0^2 / R^2 < 0.1$ and $0.85 \leq k \leq 1.15$ or $R^2 – R'_0{}^2 / R^2 < 0.1$ and $0.85 \leq k' \leq 1.15$
iv. $| R_0^2 - R'_0{}^2 | < 0.3$
v. R^2 or $R'_0{}^2$ close to R^2

Mathematical definition of Q^2 (cross-validated R^2) is explained in Equation 2.3. R^2 and R_0^2 are the square correlation coefficients between the observed and the predicted activity values with and without intercept, respectively, while $R'_0{}^2$ represents the same information as R_0^2 does but with inverted axis (linear regression between the predicted against the observed values). These parameters can be calculated as follows:

Equation 2.5

$$R_0^2 = 1 - \frac{\sum(Y_{pred-} Y_{obs}^{r0})^2}{\sum(Y_{pred-} \bar{Y}_{pred})^2}$$

Equation 2.6

$$R'^2_0 = 1 - \frac{\sum(Y_{obs-} Y^{r0}_{pred})^2}{\sum(Y_{obs-} \bar{Y}_{obs})^2}$$

Where $\bar{Y}_{pred}$ and $\bar{Y}_{obs}$ refer to the mean values of the predicted and observed activity data, respectively. The regression lines through the origin are defined by $Y^{r0}_{obs} = k\, Y_{pred}$ and $Y^{r0}_{pred} = k' Y_{obs}$, while the slopes *k* and *k'* are calculated as follows:

Equation 2.7

$$k = \frac{\sum Y_{obs}\, Y_{pred}}{\sum {Y_{pred}}^2}$$

Equation 2.8

$$k' = \frac{\sum Y_{obs}\, Y_{pred}}{\sum {Y_{obs}}^2}$$

Likewise, R^2_m metrics proposed by Roy *et al* [215] for external validation were calculated to further evaluate the correlation between the observed and predicted activity:

Equation 2.9

$$\overline{R^2_m} = \frac{(R^2_m + R'^2_m)}{2}$$

Equation 2.10

$$\Delta R^2_m = |R^2_m - R'^2_m|$$

Where $R^2_m = R^2 \times \left(1 - \sqrt{(R^2 - R^2_0)}\right)$ and $R'^2_m = R^2 \times \left(1 - \sqrt{(R^2 - R'^2_0}\right)$

3. QSAR and Molecular Docking Studies for the Search of AOX Inhibitors: a Rational Drug Discovery Approach

3.1. Introduction

The alternative oxidase (AOX) represents an attractive target in the attempt to treat some important pathogenic parasites. For instance, the AOX of *T. brucei brucei* (TAO) has been considered a valid target in the treatment of trypanosomiasis for decades, which has led to the identification of a number of specific inhibitors, the structures of which are summarised in Figure 3.1. Among these, SHAM and propyl gallate represent the most studied compounds, having been known as inhibitors of TAO since 1971 and 1980, respectively[216, 217]. Ascofuranone (AF), an antibiotic isolated from the pathogenic fungus *Ascochytia visiae*, is the most potent inhibitor of the AOX family enzymes identified to date since it specifically inhibits TAO at subnanomolar concentrations ($IC_{50} = 0.13 \pm 0.04$ nM)[52]. In contrast, SHAM ($IC_{50} = 4$ μM) and propyl gallate ($IC_{50} = 200$ nM) require higher concentrations for inhibition[52]. Animal studies have shown how treatments with SHAM and derivatives are complicated and require coadministration of glycerol, due to the lack of specific TGK inhibitors. However, therapeutic dosage of glycerol is dangerously high, since it requires non-physiological amounts that would equally inhibit the mammalian glycerol kinase[218]. AF, on the other hand, has been known for over 20 years to have trypanocidal activity both *in vitro* and *in vivo*, with successful treatment of the *T. vivax*-infected mouse without coadministration of glycerol, as a single intramuscular dose of 50 mg/kg, or 6 mg/kg on 4 consecutive days[219, 220]. However, AF is still far from being the perfect candidate for treating HAT due to some unwanted features (e.g. electron rich aromatic ring, aldehyde group and lipophilic chain), which account for its rapid blood clearance, low oral bioavailability and potential toxicity[46]. However, even though AF undoubtedly constitutes a promising lead compound, the reality is that we still lack a TAO inhibitor at an advanced stage of clinical development despite TAO's unique and critical role.

Firstly, this can be explained by the fact that the complex chemical structure of AF, which requires long multistep synthetic strategies, results in high synthesis cost and limited access to synthetic analogues[46]. But secondly, and most importantly, the 3D structure of AOX was unknown until recently[221], therefore not much was known about the protein-ligand interactions, which hindered a rational strategy towards the design

of potent inhibitors. Upon elucidation of TAO's crystal structure, structure-aided design of TAO inhibitors became possible, and since then, several structure-activity relationship (SAR) analyses have been performed[52, 222].

Therefore, in this study, the trypanosomal alternative oxidase of *Trypanosoma brucei*, the only AOX crystal structure available to date[221], was used to identify the binding interactions occurring between the inhibitors and TAO, and to further understand their inhibitory mechanism. Molecular docking studies, combined with QSAR analysis, were used to offer insight into understanding the details of protein-inhibitor interactions and the factors affecting bioactivity, providing information for the design of new drug candidates and to predict the inhibitory activity of unknown compounds. To achieve these goals, a reliable set of inhibitors with consistently measured activity was obtained from a study published by Saimoto *et al.*, who recently synthesized several AF derivatives, for which they experimentally obtained the 50% inhibitory concentration (IC_{50})[52]. This data set provided an excellent resource for the development of models and docking studies and was used as the training set. Moreover, the IC_{50} values of a different set of compounds (Figure 3.1) were measured in our laboratory and used as the test set to assess the validity of the developed models.

3.2. Chapter Aims

The aim of this investigation was twofold: to elucidate the detailed mode of interaction of TAO protein and its inhibitors, in order to identify key interactions required for high potency of inhibitors, and to identify molecular characteristics in compounds that could contribute to the inhibitory activity towards TAO. These aspects are important for the discovery and design of novel, potent TAO inhibitors. Furthermore, because of the relative simplicity of the AOX structure, the present study was included in this research project to develop a QSAR methodology that could be applied for future studies on more complex ETC proteins, such as the cytochrome bc_1 complex. Specific objectives within this work included:

1. To predict the most favourable binding mode and interaction mechanism between experimentally identified TAO inhibitors and TAO using molecular docking.
2. To perform a QSAR analysis to correlate the experimentally obtained IC_{50} values with computed properties, such as molecular descriptors and

fingerprints, in order to investigate and highlight the structural features responsible for the AF derivatives inhibitory activity.

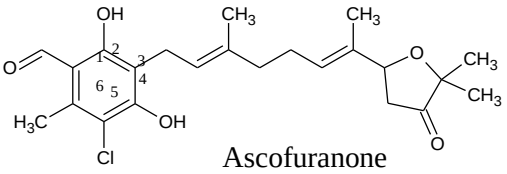

Ascofuranone

IC_{50} = 7.4 ± 5 nM

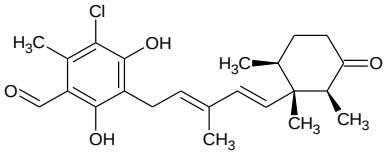

Ascochlorin

IC_{50} = 7.4 ± 3 nM

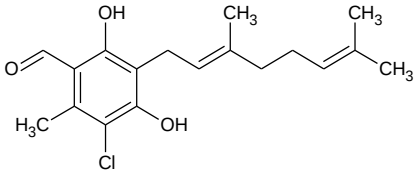

Colletochlorin B

IC_{50} = 7.5 ± 1 nM

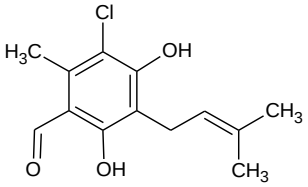

Colletochlorin D

IC_{50} = 33 ± 5 nM

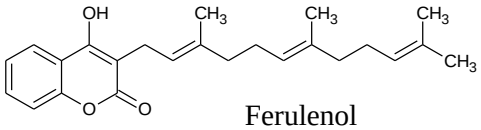

Ferulenol

IC_{50} = 53 ± 6 nM

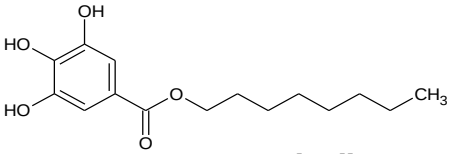

Octyl gallate

IC_{50} = 230 ± 6 nM

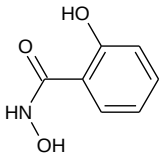

SHAM

IC_{50} = 6 µM

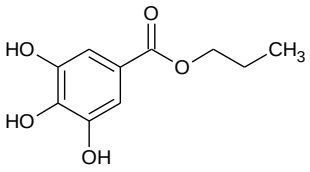

Propyl gallate

IC_{50} = 1.4 ± 0.1 µM

Figure 3.1. Chemical structure of AOX inhibitors and IC_{50} values obtained for recombinant AOX expressed in *E. coli* membranes. Data are mean ± SD of n = 3 isolations.

3.3. Results

3.3.1. Molecular Docking Analysis

3.3.1.1. Validation of Docking

To assess the reliability of the docking procedure used, the co-crystallized colletochlorin B (CB) was re-docked into the binding site of TAO. As a result, the root mean square deviation (RMSD) between the crystallographic conformation and the re-docked conformation of CB was 0.68 Å (Figure 3.2), suggesting an acceptable accuracy for the docking procedure to predict the binding mode of the TAO inhibitors. This is a satisfactory value that suggests that the docking method could be valid for the studied inhibitors.

	ΔG_{bind} (kcal/mol)	RMSD (Å)
Re-docked colletochlorin B	-9.28	0.68

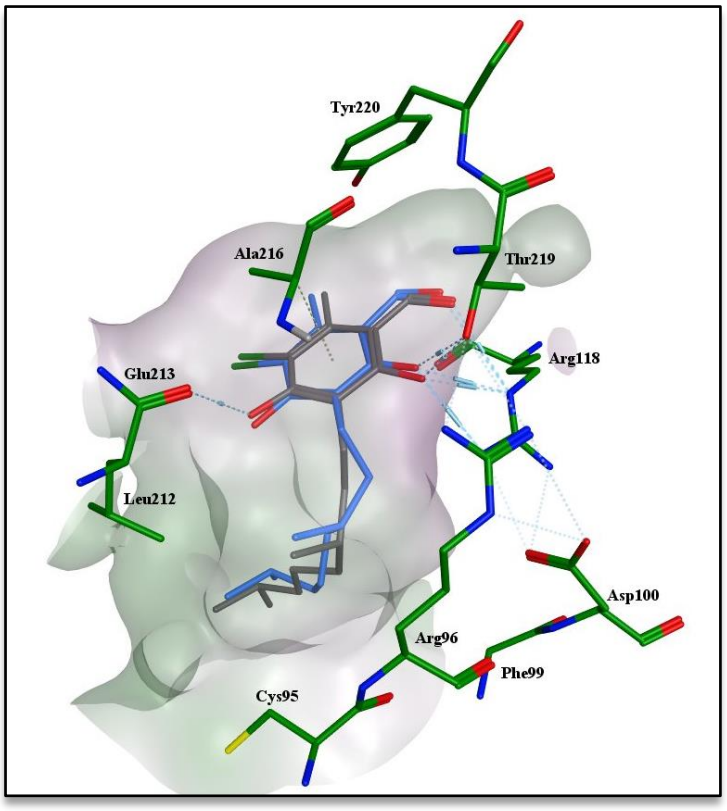

Figure 3.2. Superimposition of the crystallographic colletochlorin B (carbon atoms in grey) and the best ranked pose of the re-docked colletochlorin B (carbon atoms in blue). Hydrogen bonds are represented by light blue dashed lines. Oxygen, nitrogen and sulfur atoms are depicted in red, dark blue and yellow, respectively.

3.3.1.2. Interaction Fingerprint Analysis by PLIF

In this study, the 34 AF derivatives reported by Saimoto *et al*.[52] (Appendix I, Table 1.2), along with 8 specific AOX inhibitors with IC_{50} values measured here, as explained in Methods section 2.5.1 (Figure 3.1), were docked into the binding site of TAO. Based on the docking results, a protein–ligand interaction fingerprinting (PLIF) analysis was performed to provide detailed information on protein–ligand interactions. The PLIF tool within MOE summarised the interactions of the compounds and AOX residues using a fingerprint scheme, in which interactions were classified according to the residue of origin (Figure 3.3).

There are several types of interactions in which a residue may participate: sidechain hydrogen bonds (donor or acceptor), backbone hydrogen bonds (donor or acceptor), solvent hydrogen bonds (donor or acceptor), ionic interactions, surface interactions, metal binding interactions and arene interactions. The fingerprints present within the inhibitor-AOX complexes included surface contact interactions (C), backbone hydrogen bond donors (d), sidechain hydrogen bond acceptors (A) and donors (D) and arene interactions (R) (Figure 3.3). The bit selector tool within MOE provided detailed information about the nature and statistics of each fingerprint. The percentage abundance of each fingerprint (Table 3.1) is calculated in a way that if the fingerprint bit occurs in every entry, the percentage abundance will be 100. Among the residues that interact most often with the ligands are leucine 122 (C) (80.95%), arginine 118 (A) (46.66% and 40%), threonine 219 (A) (34.76% and 15.71%) and cysteine 95 (C, D) (26.19% and 14.76%) (Table 3.1).

Table 3.1. Percentage abundance of the fingerprint bit throughout the database.

Residue	Type of interaction	% Abundance	Strength of Interaction
Leu 122	Surface contact	80.95	
Arg 118	Sidechain hydrogen bond acceptor	46.66	Strong (1.5 kcal/mol)
Arg 118	Sidechain hydrogen bond acceptor	40.00	Weak (0.5 kcal/mol)
Thr 219	Sidechain hydrogen bond acceptor	34.76	Weak (0.5 kcal/mol)
Cys 95	Surface contact	26.19	
Thr 219	Sidechain hydrogen bond acceptor	15.71	Strong (1.5 kcal/mol)
Cys 95	Sidechain hydrogen bond donor	14.76	Weak (0.5 kcal/mol)
Cys 119	Sidechain hydrogen bond donor	11.90	Weak (0.5 kcal/mol)
Tyr 220	Arene interaction	9.04	

To better understand the interaction mechanisms, the significance of the fingerprints for a compound to be an active inhibitor was investigated. For this purpose, all compounds were classified as active or inactive based on their IC_{50} values. Because 76% of the IC_{50}s of the AF derivatives reported by Saimoto *et al*. ranged between 0.06 to 6 nM[52], the threshold was arbitrarily set up at 10 nM (compounds with an $IC_{50} \geq 10$ nM were considered inactive). As a consequence of this classification, the frequency bars in Figure 3.3B were annotated with a qualitative indication of the overabundance of active compounds with that particular residue interaction vs. overall number of active compounds. The extent to which the fraction of actives containing the bit was higher than the fraction of actives overall was indicated as a black line above the bar. If, on the contrary, the fraction of actives containing the bit was lower than the fraction of actives overall, it was indicated as an inverse (white) line below the top of the bar. Generally, the combination of height and overabundance is often an indication that the corresponding interaction is important for activity.

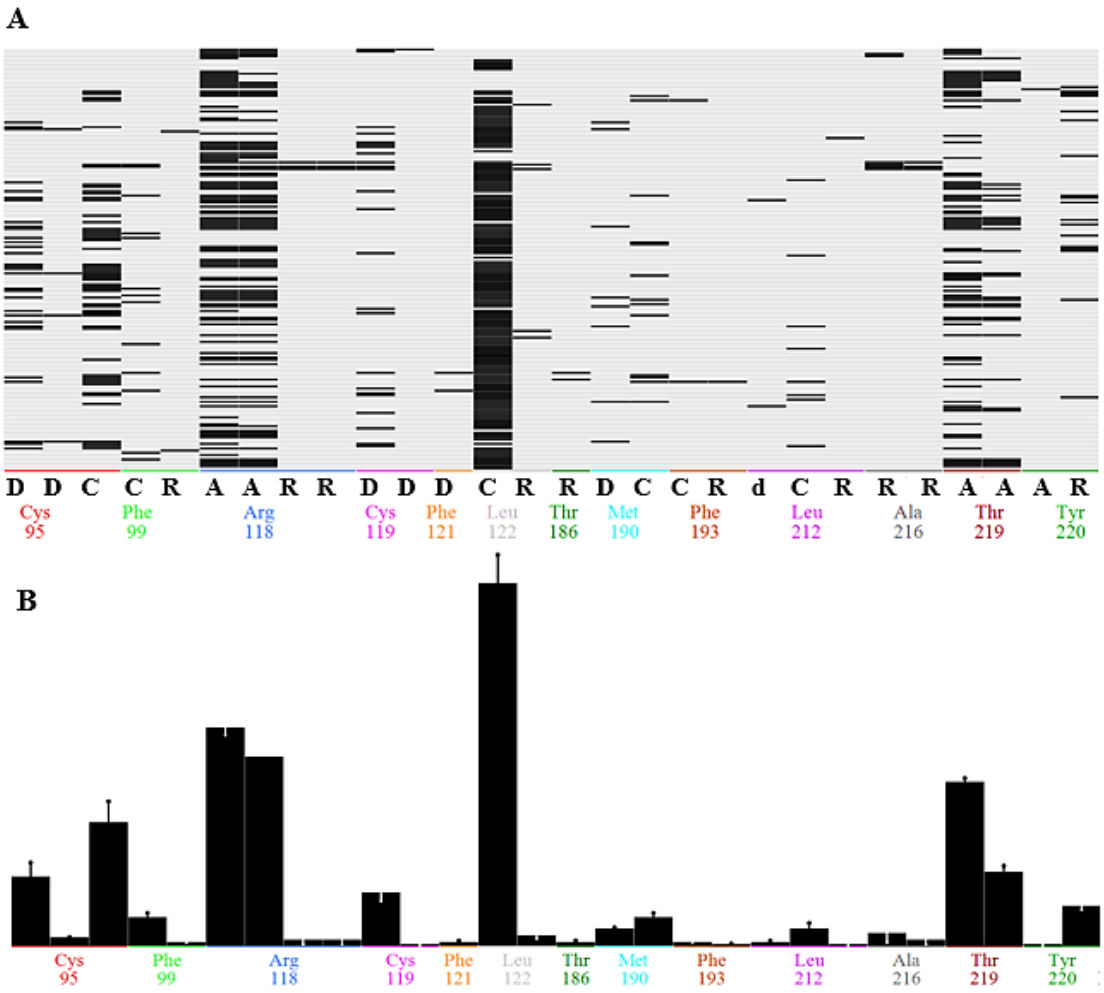

Figure 3.3. Interaction fingerprint analysis by PLIF. A) Interaction fingerprint matrix. The columns represent interactions, which are labelled with the residues (coded with an arbitrary colour) and corresponding type of interaction: sidechain hydrogen bond acceptors (A) and donors (D), surface contact interactions (C), backbone hydrogen bond donors (d) and arene interactions (R). Encoded fingerprints are present as black rectangles. The rows represent the top five ranked poses for each inhibitor. B) The population histogram shows the frequency of occurrence amongst the inhibitors for each of the selected fingerprint bits. The X-axis is constructed in the same way as for the interaction fingerprint matrix, while the Y-axis shows the relative counts for the bits. The bars contain a qualitative indication (black line above bar) that represent the fraction of actives containing the bit over all the active compounds, which indicates that the corresponding interaction is important for activity.

3.3.1.3. Binding Mode of the Inhibitors

Docking poses of the inhibitors within TAO were compared with those with point mutated TAO, where Arg 118 was replaced with an alanine. Figure 3.4 shows the top poses of ascofuranone and CB docked into the binding sites of the wild type and mutated TAO.

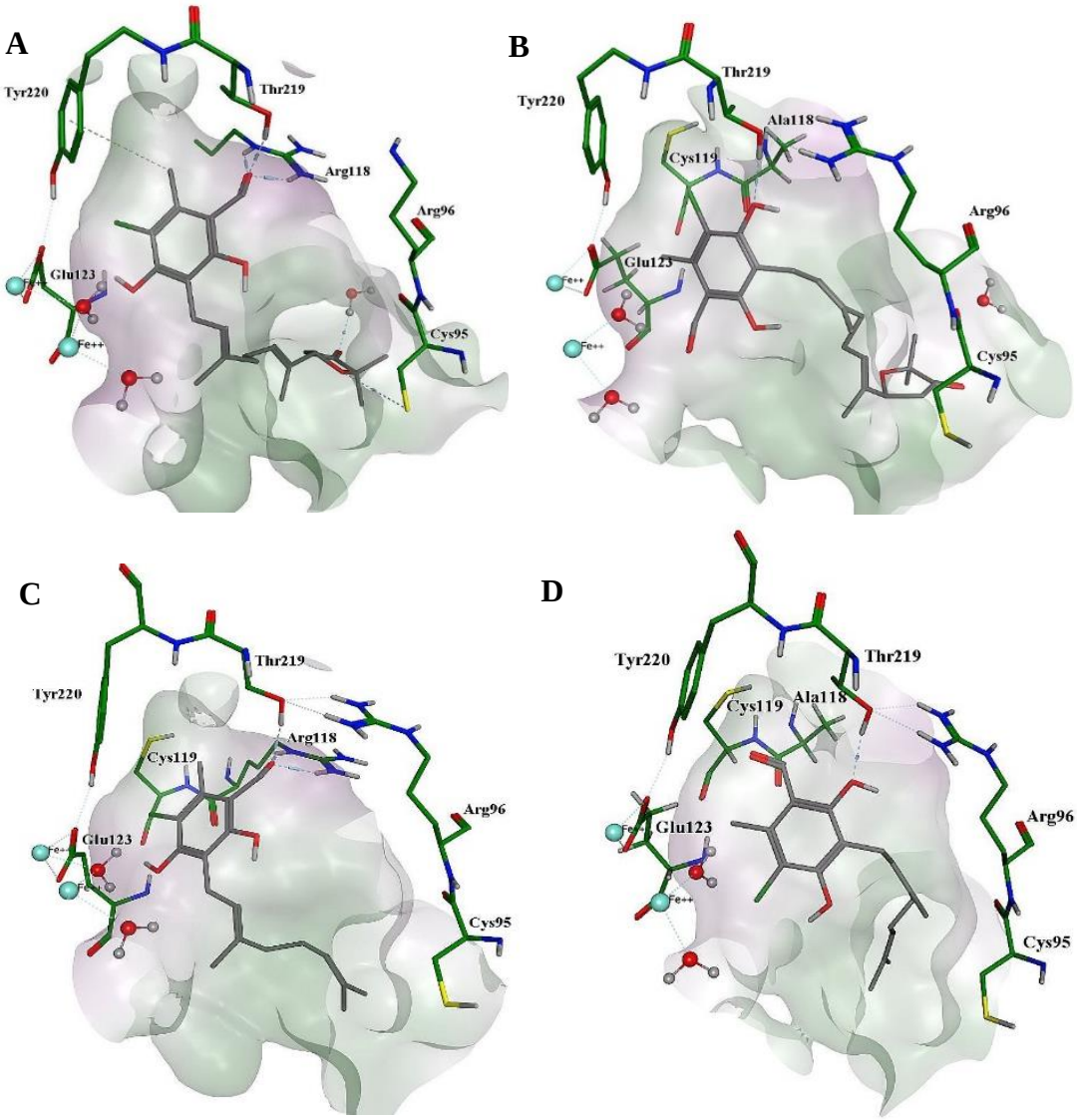

Figure 3.4. Predicted docked poses for inhibitors within the binding site of TAO (PDB: 3W54). A) Ascofuranone and wild type TAO. B) Ascofuranone and R118A mutated TAO. C) Colletochlorin B and wild type TAO. D) Colletochlorin B and R118A mutated TAO. The molecular surface is indicated in green for hydrophobic regions and in pink for hydrophilic regions. Hydrogen bonds are represented by blue dashed lines. Arene-H interaction is represented by a green dotted line. Diiron centre is represented by turquoise spheres. Oxygen, nitrogen and sulfur atoms are depicted in red, blue and yellow, respectively.

The active site of AOX is composed of a diiron centre, four glutamates (Glu 123, Glu 162, Glu 213 and Glu 266) and two histidine residues (His 165 and His 269), all being fully conserved[2]. Tyrosine residues also have a key role in the catalytic activity of AOX. For instance, Tyr 220, which is also identified in our PLIF analysis to interact with several inhibitors, is fully conserved across all AOXs, and is buried within 4 Å of the diiron centre (Figure 3.4)[1,2,51]. In addition to the catalytic site, AOX contains a binding site for its natural substrate ubiquinol. For docking analysis, this site was defined using the co-crystallised CB depicted in the crystal structure (see Methods section 2.11.2). From the results obtained, it is apparent that the inhibitors bind to the enzyme in a manner that the aromatic head remains close to the diiron center, as well as to the residues Arg 118, Thr 219 and Arg 96. This seems to be in agreement with the binding mode of CB to TAO previously reported by Shiba *et al.*[51]. Residues Arg 118 and Thr 219 are of particular importance, as they form hydrogen bonds with the functional groups on the aromatic ring of the inhibitors, establishing a strong interaction between the compounds and the protein. These hydrogen bonds are key for the potent inhibitory activities of the inhibitors[52], which is also shown by the PLIF analysis (Figure 3.3).

Figure 3.4 depicts AF and CB within the hydrophobic pocket of TAO. These two are phenolic acids, with 5-chloro orsellinaldehyde structures (see Figure 3.1). In the wild type TAO, the key interactions of these ligands with the protein occur through hydrogen bonding between the formyl group of the orsellinaldehyde (formyl group on the benzene ring) and Thr 219 and Arg 118 residues. The 4-OH of the orsellinaldehyde group, on the other hand, is seen to be interacting with the diiron centre. However, when the Arg 118 is mutated to alanine, the hydrogen bond formations are lost for both inhibitors, displacing the compounds away from the diiron centre[223] (Figure 3.4).

Similar docking experiments were performed with two other TAO mutants, L122A and T219A. As it can be seen from the docking scores obtained (Table 3.2), the importance of these residues was confirmed by comparison of the docking scores with the wild type TAO. As could be expected, mutations on these particular residues caused the docking scores to increase, indicating lower affinity and less favourable interactions. Furthermore, results showed that L122A and R118A mutations have a more profound effect on binding affinity than T219A mutations[224].

The extra hydrogen bond acceptors on the tail end of ascofuranone side chain did not appear to interact with any side chains in the majority of the determined poses, the most likely H-bond formation being with the Cys 95 backbone as shown in Figure 3.4A. Given the lack of improvement of inhibition by AF over CB, it is unlikely that this extra hydrogen bond plays a significant role in the efficacy of inhibition under the experimental conditions defined in this study.

Table 3.2. Docking scores of ubiquinol, some of the most potent and novel TAO specific inhibitors including those reported by Saimoto *et al.* (AF, CB, compound 16 and compound 24) and the classic inhibitors SHAM and propyl gallate and specific point mutants. Binding free energy is depicted in kcal/mol and IC_{50} is depicted in nM. IC_{50} values of wt were obtained by Saimoto *et al* [52].

	Calculated ΔG_{bind} (kcal/mol)				
Compound	**Wild type**	**L122A**	**R118A**	**T219A**	**IC_{50} (nM)**
Ubiquinol	-9.77	-8.36	-8.87	-9.18	-
Ascofuranone	-9.65	-8.92	-8.89	-9.50	0.13
Colletochlorin B	-8.76	-8.06	-7.94	-8.70	0.20
Compound 16	-9.21	-8.47	-8.58	-8.78	0.15
Compound 24	-8.52	-7.92	-7.72	-8.42	0.06
SHAM	-5.26	-5.48	-5.15	-5.35	4000
Propyl gallate	-6.67	-6.43	-6.43	-6.46	200

As can be seen in Table 3.2, docking scores (kcal/mol) rank correlate well with the potency of the inhibitors, which shows the docking procedure provides realistic results. For instance, ubiquinol, the natural substrate of TAO, gives the lowest docking score in the wild type (-9.77 kcal/mol), followed closely by ascofuranone, the most potent inhibitor of TAO (-9.65 kcal/mol). SHAM and propyl gallate, on the other hand, are the least potent inhibitors, which is reflected in their high docking scores (-5.26 and -6.67 kcal/mol, respectively).

The two mutations that affected the final docking scores the most were L122A and R118A, which is in agreement with the PLIF analysis shown in Table 3.1, which indicated that these were the residues that compounds interacted the most with. Interestingly, mutations of these key residues seemed to have a greater impact on the interactions of potent inhibitors (such as AF, CB, compound 16 and compound 24 (see Appendix I, Table 1.2) than on the classic inhibitors such as SHAM or propyl gallate. In summary, all the mutations that were performed (L122A, R118A, T219A) caused all scores to increase (except for L122A and T219A in the case of the weakest

inhibitor, SHAM), which proves their key role in the interactions between inhibitors and the enzyme[224].

3.3.2. QSAR Model

For the 34 AF derivatives, a QSAR model was developed using the molecular descriptors selected by stepwise regression analysis as explained in Materials and Methods section 2.12.1.3. The obtained linear model is shown below:

$$\mathbf{pIC_{50}} = - 0.124 + 2.252\ \textit{metaH-acceptor} - 2.527\ \textit{Neutral form}\ (\text{pH } 7.4) - 18.014\ \textit{PEOE\_VSA\_FPPOS} + 17.527\ \textit{petitjean}$$

$$N = 34,\ R = 0.85,\ R^2 = 0.72,\ SE = 0.63,\ F = 18.6,\ p = 0.000$$

Here, n is the number of compounds used in the development of the QSAR model; R and R^2 are the correlation coefficient and the squared correlation coefficient, respectively; SE is the standard error of the estimate, F is the Fischer ratio value and p is the statistical confidence level. All regression coefficients are significant at $p<0.05$.

The first molecular descriptor selected by the analysis is *metaH-acceptor*, which is an indicator variable showing the presence or absence of hydrogen bond donor group(s) in meta position with respect to the long alkyl side substituent of the benzene ring (corresponding to positions 1 or 5 of the orsellinaldehyde group as shown for ascofuranone in Figure 3.1). This descriptor takes binary values (0, 1) to indicate the absence or the presence of the hydrogen bond donor property, respectively. The positive coefficient of this parameter in the equation indicates that the presence of such groups in meta position provides greater ability for the compounds to interact more effectively with the protein. This is consistent with the fact that hydrogen bonds are key for strong interactions in the protein-ligand complexes. Accordingly, compounds that lack hydrogen bond donor groups in meta positions (compounds 19 and 23) show the lowest pIC_{50} values (Appendix I, Table 1.2). This agrees well with the docking results discussed earlier regarding the role of hydrogen bonding groups in this position for interaction of inhibitors with Arg 218 and Thr 219.

The second most important descriptor in the equation is *Neutral form*. This is the fraction of molecules that is unionised in acid/base protonations at pH 7.4, calculated by the classic ACD Percepta method[206]. Given that the compounds in the training set do not possess any basic groups, and only acid dissociation is possible for some of them, the negative coefficient of *Neutral form* indicates that the more acidic compounds (with lower unionized fractions) are better TAO inhibitors with higher pIC_{50} values. However, given that the presence of carboxylic acid groups at the end of the linker group (as described in the next paragraph) has a negative impact on pIC_{50}, it is only the acidity of the meta-phenolic groups that leads to increased potency. The negative impact of such carboxylic acid groups has been accounted for by *PEOE_VSA_FPPOS* parameter.

The third most important molecular descriptor in the equation is *PEOE_VSA_FPPOS*. It is a charge-dependent molecular descriptor where atomic charge is calculated through the Partial Equalization of Orbital Electronegativities (PEOE) method[225]. This molecular descriptor represents the fractional positive polar Van der Waals surface area. Based on the negative coefficient of this parameter in the equation, compounds with lower fraction of positively charged atoms, *i.e.* larger molecules with fewer (electronegative) heteroatoms, will present higher pIC_{50} values and a greater efficacy in inhibiting TAO. Within the data set, all compounds contain an aromatic group with phenolic hydroxyl(s) and a linker (alkyl side chain) group, with some compounds containing a carboxylic acid group attached to the other end of this linker. Presence of such carboxylic acid group reduces the inhibition potency (e.g. compounds 12 and 13, see Appendix I, Table 1.2).

Finally, the last descriptor selected in the model is *petitjean*, which is a "shape coefficient". This molecular descriptor is defined as the ratio (D-R)/R, where R is the generalised radius and D is the generalised diameter calculated using graph theoretical methods in MOE software [226]. Larger *petitjean* values in the AF derivatives correspond to more linear (longer linker chain) molecules, which according to the positive sign of this descriptor in the equation, will result in higher pIC_{50} values. In contrast, compounds with shorter linker chains, e.g. compounds 7a, 7b and 7c, have the lowest *petitjean* values.

The linear plot of the predicted pIC_{50} values based on the QSAR model developed in this study versus the experimental values is shown in Figure 3.5.

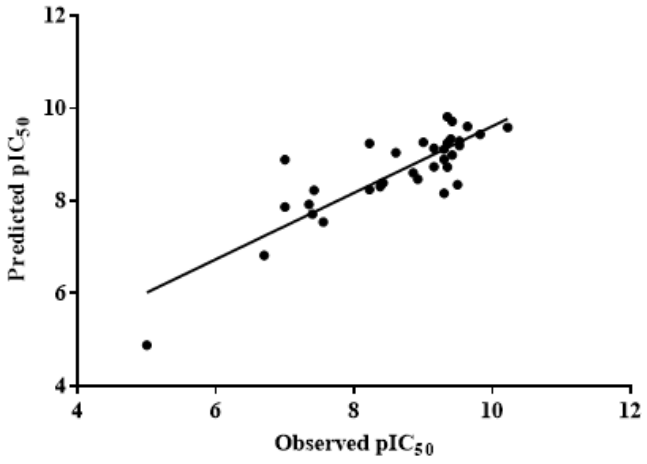

Figure 3.5. Predicted pIC_{50} values with QSAR model vs. experimentally obtained values (training set). Pearson correlation (R): 0.72; $p<0.0001$ (95% confidence interval). MAE of 100% data was 0.42.

3.3.2.1. Validation of the QSAR Model

The QSAR model was first internally validated to evaluate its accuracy. As described in Materials and Methods section 2.12.1.3, the internal validation procedure used was leave-one-out (LOO) cross validation, as well as leave-some-out (LSO) cross validation. For LSO method, four sets of 7 compounds and 1 set of 6 compounds were removed from the data set; QSAR model was then rebuilt based on the remaining compounds and the activity of the deleted compounds was predicted based on the resulting QSAR equation. In this exercise, every compound was left out once. Mean absolute error (MAE) of predicted pIC_{50} values for the validation set was 0.485 and Q^2 value was 0.637. The LOO method was also performed, where all the compounds were removed once, one at a time, and the QSAR model was rebuilt based on the remaining molecules. The activity of the deleted compounds was then calculated based on the resulting QSAR equation. The LOO Q^2 was 0.623, while MAE of predicted pIC_{50} values with the LOO cross-validation method was 0.487. According to Tropsha, a QSAR model is considered acceptable if the value of Q^2 exceeds the predetermined value of 0.5[227]. Appendix I, Table 1.1 shows individual absolute error values for each compound.

Based on the MAE obtained through internal validation, we can judge the goodness-of-fit of the model. However, this validation approach lacks predictability when the model is applied to an external data set. The external validation ensures predictability and applicability of the developed QSAR model for the prediction of untested molecules[228]. For that reason, the QSAR model was also externally validated by comparing the predicted and observed activities of the external test set of compounds with IC_{50} values measured in our laboratory (compounds in Figure 3.1), which were not used in the development of the model. The IC_{50} values for these compounds were experimentally determined as described in Materials and Methods section 2.5.1. It must be noted that it is expected to observe interlaboratory variations as the training set compounds and test set compounds have been measured in two different laboratories using different techniques and equipment. Table 3.3 shows the observed and predicted pIC_{50} values for the external compounds. On the one hand, despite the laboratory variations, the predicted pIC_{50} values correlate very well with the observed values, as seen in Figure 3.6 and Table 3.3. On the other hand, the predicted pIC_{50} values show large absolute error, which indicates that this QSAR model is valuable in predicting the rank order of compound's inhibitory potency, but not accurate in predicting the exact pIC_{50} values.

Table 3.3. Compounds used as external validation set, observed and predicted pIC_{50} values and absolute error.

Compounds	pIC_{50} Exp.	pIC_{50} Pred.	Abs. error
Ascofuranone	8.131	9.262	1.131
Ascochlorin	8.131	9.183	1.052
Colletochlorin B	8.125	9.637	1.512
Colletochlorin D	7.481	9.009	1.528
SHAM	5.222	4.884	2.591
Propyl gallate	5.853	4.296	1.558
Octyl gallate	6.638	6.340	0.298
Ferulenol	7.275	7.010	1.986

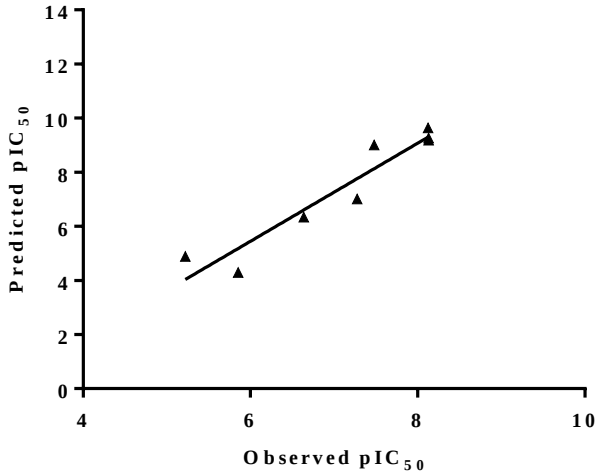

Figure 3.6. Predicted pIC_{50} values of external test compounds with the QSAR model vs. experimentally obtained ones. Pearson correlation (R): 0.90, p value = 0.0001 (95% confidence interval).

3.4. Discussion

Crystallisation of the trypanosomal alternative oxidase (TAO) has provided insights into its α-helical structure and its attachment to the membrane[51]. Additionally, co-crystallization of TAO with a number of ascofuranone (AF) derivatives has provided considerable structural details with respect to the active-site and nature of the substrate/inhibitor-binding site. Such insights can lead to the generation of new AOX specific inhibitors. AF, for instance, is a naturally occurring compound isolated from *Ascochyta viciae*, which has been demonstrated to be a highly potent AOX inhibitor and to have trypanocidal activity both *in vitro*[219] and *in vivo*[220]. Despite its high potency against TAO, survival of mice following AF treatment showed that AF is not an effective inhibitor of the mammalian cytochrome bc_1 complex, which makes it a promising clinical drug candidate. On the other hand, ascochlorin, which is a potent inhibitor of AOX activity in both *Trypanosoma brucei* [229] and *Trypanosoma vivax* [230], is also a potent inhibitor of cytochrome bc_1 complex [34], making this compound unsafe clinically. SHAM and the gallates have generally been considered, and indeed used as inhibitors to indicate the presence and potential contribution of AOX to the overall respiratory rate in isolated mitochondria, cells and tissues. However, outside of their use within isolated mitochondria, such inhibitors are not specific for AOX. For instance, it is well-documented that SHAM is able to inhibit other redox enzymes apart from AOX[231].

Knowledge on the nature of the substrate, inhibitor-binding site and catalytic mechanism of the enzyme is fundamental to a more rational design of highly targeted AOX inhibitors. The aim of this study was to explore molecular properties required for inhibition of AOX using computational modelling techniques, which can aid with the future design of further AOX specific inhibitors. To achieve this, inhibitory activities of a series of AF derivatives towards AOX reported by Saimoto *et al.*[52] were used for molecular docking purposes and QSAR, and a series of molecularly diverse compounds were used to assess the validity of these computational techniques in the prediction of AOX inhibition.

Docking results and PLIF analyses confirmed that the three residues mostly involved in binding to inhibitors (AF derivatives in the training set) are Leu 122, Arg 118 and Thr 219 (Figure 3.3). The significance of these residues was further validated by docking of the test set compounds to the wild and mutated receptors where mutations of L122A, R118A, T219A all caused a significant reduction in affinity, especially of the most potent inhibitors (Table 3.2). Two of these residues, Arg 118 and Thr 219, form hydrogen bonds with the functional groups on the aromatic ring of the inhibitors, establishing a strong interaction between the compounds and the enzyme. The importance of this interaction was further confirmed by QSAR, which showed that the most important factor to control pIC_{50} values of the inhibitors is the presence of a hydrogen bond donor group on the aromatic ring of the compounds.

The QSAR model produced here was successfully validated by internal validation and external set of compounds. The external set consisted of a series of classic and novel AOX inhibitors with the pIC_{50} values measured in our laboratory (pIC_{50} values of ascofuranone, ascochlorin, colletochlorin B, colletochlorin D, octyl gallate and SHAM were kindly obtained by Dr Luke Young). The QSAR model was able to predict the rank order of the pIC_{50} values of these diverse set of compounds, although the exact pIC_{50} values could not be predicted with a reasonable accuracy (Table 3.3, Figure 3.6). This was probably due to the differences of experimental procedures used in our laboratory and those used by Saimoto *et al.*[52] for the measurement of pIC_{50} values of the external compounds and the training set compounds, respectively.

In addition to the impact of hydrogen bond acceptor groups on the aromatic ring of compounds on the aromatic ring of ascofuranone derivatives, the QSAR model

highlighted the importance of acidity of the compounds, and a linear (non-spherical) shape of the compounds for higher inhibitory potency towards AOX. Overall, this analysis provides valuable information about the structural features that could be responsible for the interaction between the inhibitors and TAO and their mechanism of inhibition.

In summary, the AOX represents a promising target to address the threat posed by multiple human pathogenic organisms and numerous fungi of agronomic importance, particularly after the emergence of fungicide-resistant strains of phytopathogenic fungi[53, 232]. Hence, the data presented here may prove to be useful for future design and development of novel and specific AOX inhibitors. Furthermore, this investigation has offered an opportunity to develop a methodology with regards to QSAR model development that can be applied to other more complex protein targets (see chapter 7).

4. Characterisation of Isolated Rat Liver Mitochondria and Effects of Fungicides on Mitochondrial Function

4.1. Introduction

A wide variety of *in vitro* assay protocols and cell models have been used to study the effect of compounds on mitochondrial function. Measurements of different aspects of mitochondrial function post-compound-exposure can provide detailed understanding of the mechanisms and help to identify the suitable model systems that can effectively reflect clinical manifestations of mitochondrial impairment. Isolated mitochondria are a commonly used model system in the assessment of drug-induced mitochondrial dysfunction. One of the most informative ways of studying mitochondrial function is by measuring mitochondrial oxygen consumption through Clark-type oxygen electrodes, alongside measurements for reactive oxygen species (ROS) generation and changes in the mitochondrial membrane potential (MMP)[155]. The proton electrochemical gradient (ΔμH+) generated by the respiratory chain in the IMM is the energetic force which drives ATP production by the ATP synthase. Under physiological conditions, cells maintain stable levels of intracellular ATP and MMP, but prolonged perturbations of this fine balance compromise cell viability. MMP is not only essential for ATP production, but it is also a driving force for the transport of compounds into the mitochondrial matrix[233]. Due to its crucial role, MMP assessment is a commonly used technique to evaluate mitochondrial function, particularly in the studies of pathogenesis of cellular injury and cell fate determination. Reduction of MMP can be caused by compounds that inhibit the respiratory chain complexes or act as uncouplers.

Mitochondria are not only the primary source of aerobic ATP, but also the main producers of ROS within the cell[234]. ROS are a by-product of respiratory activity and serve multiple purposes, contributing to both physiological and pathological processes. Low levels of ROS may act as modulators of important cellular processes, including transcription factor activity, adaptation to stress conditions, kinase signalling and cellular differentiation[119]. Hence, in order to guarantee redox balance, ROS levels are tightly regulated by cellular antioxidant defence systems, such as the mitochondrial glutathione peroxidase, peroxiredoxin and thioredoxin, among others[18]. However, if ROS levels increase dramatically, to a point where the cellular antioxidant capacity is overwhelmed, the resulting oxidative stress can cause substantial damage

to lipids, proteins and DNA[129]. Hence, oxidative stress caused by mitochondrial dysfunction has been reported to play a major role in the pathogenesis of several diseases and in the ageing process[235].

In the first section of this chapter, freshly isolated rat liver mitochondria were employed as a model system to study the effects of different substrates, inhibitors and uncouplers using the Oroboros O2k-Fluorometer. This equipment allowed the simultaneous determination of mitochondrial respiration, MMP and ROS production. With regards to ROS measurement, superoxide anions (O_2^-) are the primary ROS produced by the ETC, which are rapidly converted to hydrogen peroxide (H_2O_2) in a reaction catalysed by the mitochondrial superoxide dismutase (SOD). H_2O_2 is a non-charged, relatively stable molecule capable of crossing the membranes and, for this reason, easily accessible to analytical probes. Therefore, the method of choice for estimation of mitochondrial ROS formation was the H_2O_2 sensitive probe Amplex Red (AmR). The AmR assay is based on the H_2O_2 dependent oxidation of AmR to the red fluorescent compound resorufin catalysed by the enzyme horseradish peroxidase (HRP) (Figure 4.1). Hence, an increase in the fluorescence signal is related to an increase in H_2O_2 production.

With regards to MMP measurement, due to the negative electrical potential difference across the membrane, MMP can be studied using fluorescent lipophilic cationic dyes such as rhodamine 123, safranin and tetramethylrhodamine methyl (TMRM) and ethyl (TMRE) esters[236]. As positively charged molecules, these dyes accumulate within the negative interior of mitochondria; more polarized mitochondria (i.e. hyperpolarized, where the interior is more negative) accumulate more cationic dye, whereas depolarized mitochondria (interior is less negative) accumulate less dye. Uptake of these compounds into the matrix space leads to self-quenching, decreasing the fluorescence signal. Here, mitochondria were assessed for their ability to generate a MMP using safranin as the fluorescent probe.

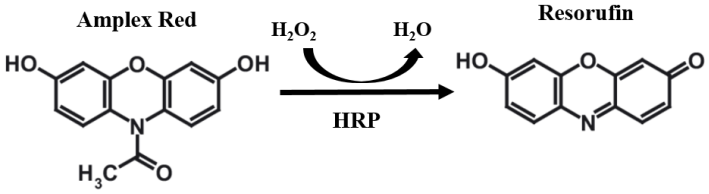

Figure 4.1. Conversion of Amplex® Red into Resorufin. Amplex Red acts as an electron donor in the reduction of hydrogen peroxide into water, a reaction catalysed by HRP. Final product is the fluorescent compound resorufin.

The second part of this chapter is dedicated to the study of the effects of a number of compounds, namely complex III and AOX inhibitors, on mitochondrial function. A total of 16 complex III inhibitors included ametoctradin, amisulbrom, antimycin A, ascochlorin, atovaquone, azoxystrobin, cyazofamid, dimoxystrobin, diuron, fenamidone, fluoxastrobin, kresoxim-methyl, myxothiazol, picoxystrobin, pyraclostrobin and trifloxystrobin. All of these inhibitors are fungicides, with the exception of diuron, a herbicide[209], and atovaquone, which is used as an anti-malarial agent[237]. AOX inhibitors included ascofuranone, colletochlorin B (CB), colletochlorin D (CD) and compounds ISSF31 and ISSF33, which were synthesised in-house and are derivatives of CB and CD, respectively.

First, the inhibitory effects of the compounds on the activity of succinate-cytochrome *c* reductase (SCR), which is a mixture of respiratory complex II and III, were investigated. The results obtained provide an excellent resource for the development of QSAR models for mechanistic understanding of effect of molecular structure on complex II+III inhibition. Following this, the inhibitory potency of the compounds was assessed using an Extracellular Flux Analyser and HepG2 cells.

4.2. Chapter Aims

The overall aims of this chapter were twofold: to examine the validity of the methodology for future studies using isolated mitochondria and to study the effects of some well-known complex III and AOX inhibitors on mitochondrial function. Specific objectives included:

1. To assess the quality of the mitochondrial preparations, which were evaluated by their ADP/O and RCR ratios.

2. To analyse the effects of different substrates, inhibitors and uncouplers on mitochondrial respiration, MMP and ROS production.
3. To measure the inhibitory potencies of several fungicides against complex II+III activities using isolated mitochondria for future QSAR studies.
4. To profile the acute effects of these fungicides on mitochondrial function using HepG2 cells and an Extracellular Flux Analyser.
5. To confirm the mechanism of action of the compounds by evaluating their activity on the mitochondrial ETC complexes using HepG2 cells permeabilised with rPFO.

4.3. Results

4.3.1. Characterisation of Isolated Rat Liver Mitochondria

4.3.1.1. Parameters of Energy Transduction: Respiratory Control Ratio and ADP/O Flux Ratio

A commonly used measure of the quality of the mitochondrial preparation is the respiratory control ratio (RCR)[24]. Therefore, mitochondrial bioenergetics was assessed in terms of RCR, an indicator of the coupling state of mitochondria, which is calculated as the ratio of state 3 vs. state 4 slopes. State 3 is attained during maximal ATP synthesis (i.e. in the presence of ADP), whereas state 4 is the rate of resting respiration in the absence of ATP synthesis (when all ADP has been consumed)[24]. State 4 is associated with proton leakage across the inner mitochondrial membrane, when mitochondria exhibit basal activity, i.e. they are respiring but not producing ATP.

RCR can evaluate the integrity of a mitochondrial preparation as damaged mitochondria tend to show an increased proton leak. A low ratio is indicative of "leaky" mitochondria that have difficulty in maintaining proton gradients in the resting state and, consequently, electron transport and oxygen consumption are increased. For isolated mitochondria, RCR values typically range from 3 to 15 in different preparations and a RCR greater than 6 is normally accepted as a highly intact and coupled preparation[24]. To determine RCR ratios, state 3 was achieved in two ways: in the presence of high ADP concentrations (state 3_{ADP}) and in the presence of increasing concentrations of ADP followed by the addition of an uncoupler, CCCP (state 3_U).

RCR calculated as state 3_{ADP}/state 4 was 2.72 ± 0.07, whereas RCR calculated as state 3_U/state 4 was 5.12 ± 0.68 (Figure 4.2).

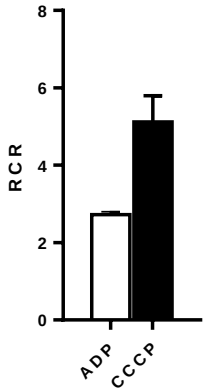

Figure 4.2. Respiratory control ratio (RCR) represents the mitochondrial coupling state. Results are mean ± SD (n = 3).

For the determination of ADP/O flux ratio, a limited amount of ADP (70 μM) was added to respiring mitochondria (Figure 4.3). This method can determine the extent of the burst of accelerated state 3 respiration; ADP added allowed the ATP synthase to synthesise ATP coupled to proton re-entry across the membrane. When all ADP is phosphorylated to ATP, mitochondria are in state 4 respiration and the oxygen uptake during the accelerated state 3 respiration can be quantified allowing an ADP/O ratio to be calculated as nmols of ADP added / nmols of O consumed[24]. It is generally assumed that during state 3 respiration proton leak ceases or is almost negligible, therefore the total oxygen consumed during state 3 is effectively used for ATP synthesis and hence used in the calculations. ADP/O ratios for succinate respiration can vary between 1.2 and 2.2[238]. Here, the mean ADP/O ratio with succinate as the substrate was found to be 1.54 ± 0.33 for n = 6 independent experiments.

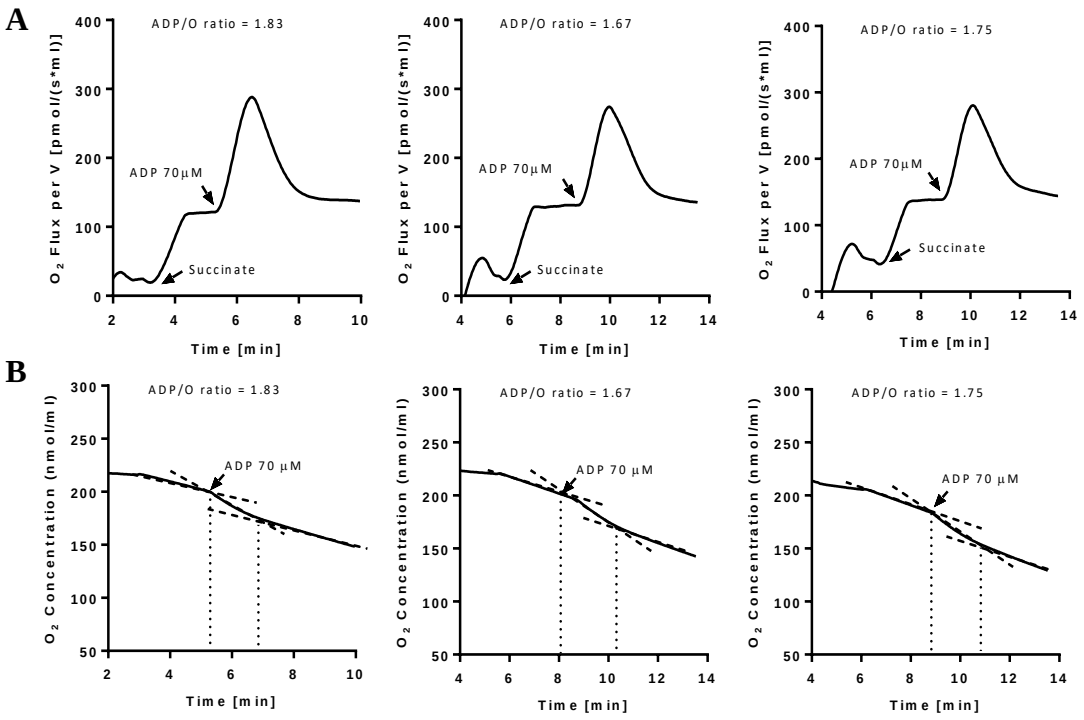

Figure 4.3. Representative experiments of high-resolution respirometry for the determination of ADP/O flux ratios at 70 µM ADP stimulation (rat liver mitochondria, 0.26-0.4 mg protein/mL). A) A sharp peak of oxygen flux is observed upon the addition of ADP, which is rapidly consumed and phosphorylated to ATP. B) Total oxygen uptake can be calculated by making linear extrapolations (dashed lines) during state 3 respiration (after ADP titration) and at state 4 (after ADP depletion). The difference of oxygen concentrations at the intercepts is the total oxygen uptake.

4.3.1.2. Determination of Membrane Potential and Reactive Oxygen Species Production

Changes in MMP and oxygen consumption were investigated simultaneously with an Oroboros® Oxygraph-2K.

Figure 4.4A shows an experiment in which safranin was titrated from 0.25 µM to a final concentration of 2 µM for initial calibration. Subsequently, 150 µg rat liver mitochondria (RLM) were added, followed by addition of 1 µM rotenone (complex I inhibitor) and 12.5 mM succinate as the substrate supporting complex II-linked respiration. This caused a sharp decrease in the fluorescence signal, reflecting an increase in the membrane potential and an increase in the oxygen consumption rate. Addition of the uncoupler CCCP (0.25 µM) maximized respiration and completely diminished membrane potential. Then, 2 mM malonate (complex II inhibitor) and 0.1 µM antimycin A (complex III inhibitor) were added to completely inhibit respiration,

but as expected, did not further increase fluorescence due to the complete dissipation of the membrane potential caused by CCCP.

An additional control experiment to simultaneously analyse mitochondrial respiration and ROS production was also performed. O_2 and H_2O_2 fluxes were determined in isolated mitochondria in a sequential addition of respiratory complex II substrate (12.5 mM succinate), a complex I inhibitor (1 μM rotenone), an uncoupler (0.25 μM CCCP) and a complex III inhibitor (2.5 nM antimycin A) (Figure 4.5). Addition of succinate induced an increase in oxygen consumption, as well as an increase in H_2O_2 flux. Addition of rotenone decreased H_2O_2 production possibly due to inhibition of reversed electron flow to complex I. CCCP titration further elevated respiration and reduced H_2O_2 flux to a baseline level. Uncouplers like CCCP decrease reactive oxygen species formation in the resting state by accelerating electron transport and thereby increasing the oxidised state of the respiratory complexes and carriers[239]. Finally, inhibition of complex III by antimycin A completely inhibited respiration and increased H_2O_2 flux, which is in accordance with previous literature[240].

A final control experiment to examine the reliability of the methodology was performed. Rat liver mitochondria in the presence of 12.5 mM succinate were exposed to increasing concentrations of antimycin A in the presence or absence of rotenone (1 μM). Figure 4.6 shows how the absence of rotenone allows reverse electron transport (RET), i.e. electrons from ubiquinol are transferred back to respiratory complex I, reducing NAD+ to NADH. This leads to complex I-linked ROS production which results in an increased H_2O_2 flux. On the contrary, RET is blocked when rotenone is present, keeping ROS levels low. The phenomenon of RET and its implications on ROS generation are discussed further in the Discussion.

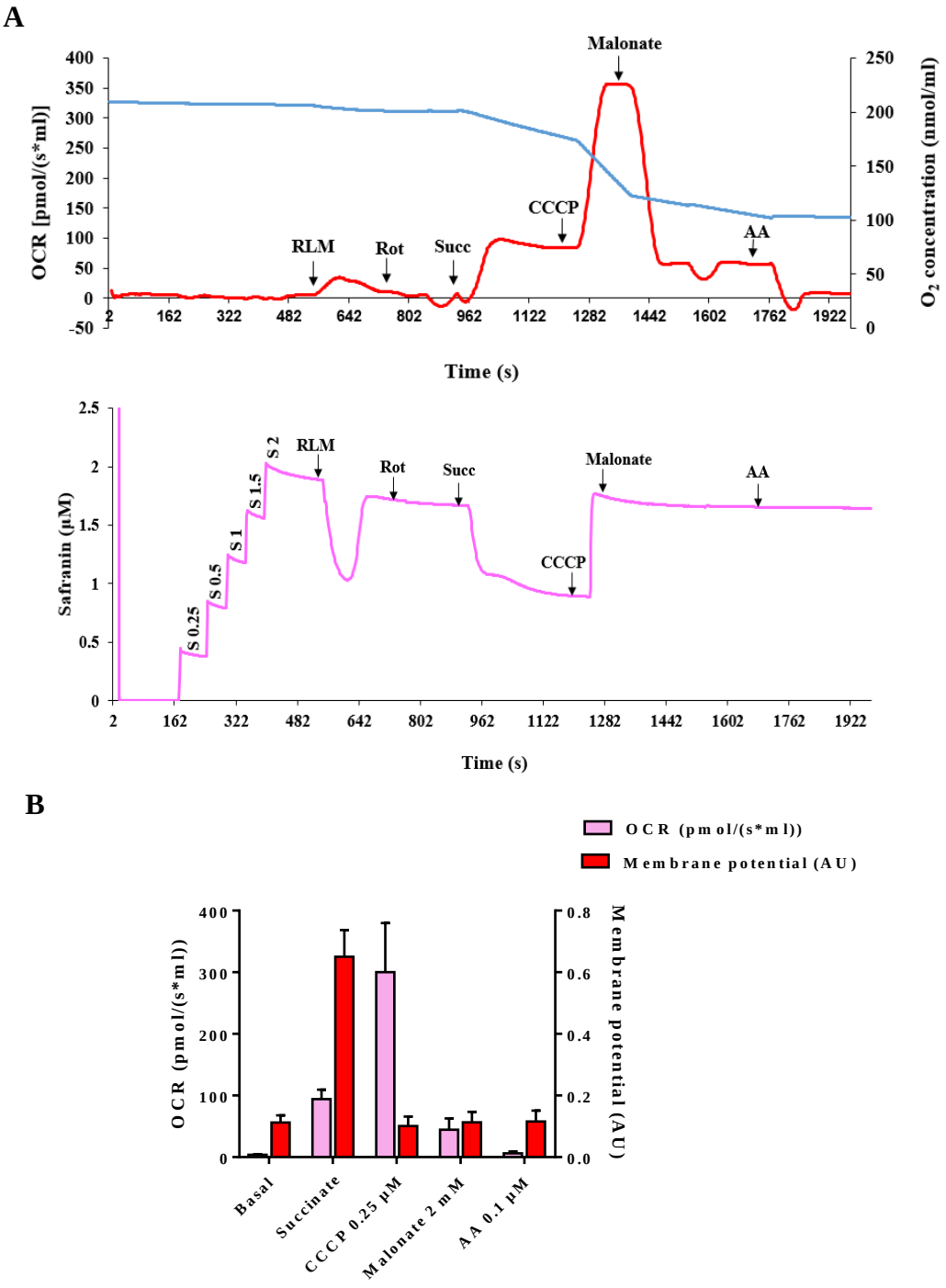

Figure 4.4. Simultaneous evaluation of oxygen consumption rate (OCR) and mitochondrial membrane potential (MMP) in isolated rat liver mitochondria. A) Representative experiment in the presence of 2 µM safranin (S) and 150 µg of rat liver mitochondria (RLM), following the sequential addition of 1 µM rotenone (Rot), 12.5 mM succinate (Succ), 0.25 µM CCCP, 2 mM malonate and 0.1 µM antimycin A (AA). OCR [pmol/(s*ml)] and oxygen concentration levels (nmol/ml) are illustrated in red and blue lines respectively, whereas MMP (in the form of a fluorescence signal) is depicted by a pink line. B) Mean ± SD of OCR and MMP (AU) in the presence of sequential additions of succinate, CCCP, malonate and antimycin A (n = 2). In this case, fluorescence signal for the membrane potential was normalised with 2 µM safranin concentration set as 0 (no membrane potential) and 0 µM safranin set as 1.

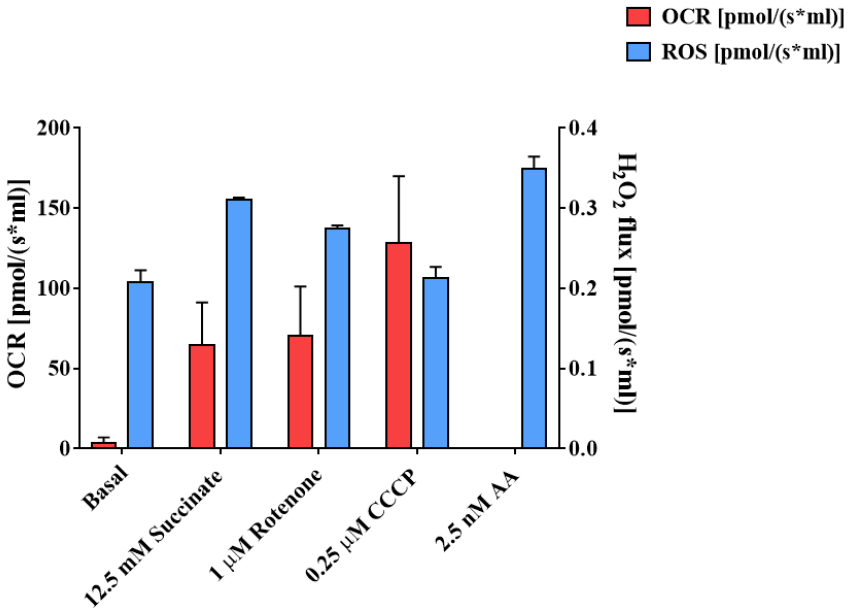

Figure 4.5. Simultaneous measurement of oxygen consumption and H_2O_2 flux by O2k – Fluorometry. Results show sequential additions of succinate, rotenone, CCCP and antimycin A to an initial basal state of isolated rat liver mitochondria (150 µg protein). Data are mean ± SD (n = 2).

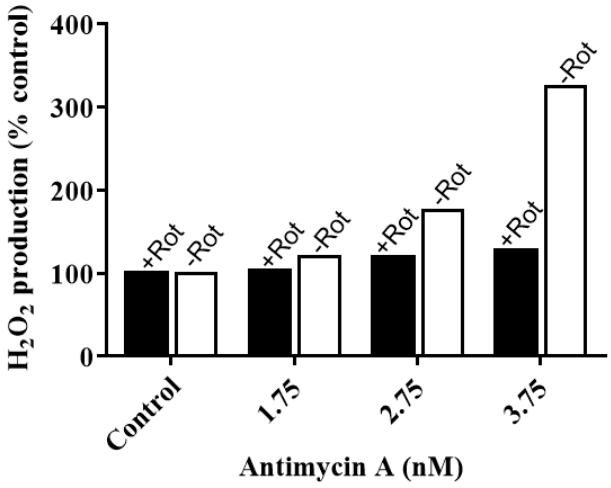

Figure 4.6. H_2O_2 flux in isolated rat liver mitochondria (150 µg protein) upon antimycin A titrations either in the presence (black bars) or absence (white bars) of rotenone (1 µM).

4.3.2. Effects of Fungicides on Mitochondrial Function

4.3.2.1. Succinate-Cytochrome *c* Reductase Inhibition

Isolated rat liver mitochondria were used to assess the inhibitory activities of several complex III and AOX inhibitors against succinate-cytochrome *c* reductase (SCR) activity, the mixture of respiratory complex II and III. Complex III inhibitors included both those that bind to the quinol oxidation site (Q_o site) and those that bind to the quinone reduction site (Q_i site). Due to their structural similarity with ascochlorin, a known inhibitor of the cytochrome bc_1 complex, ascofuranone, a specific AOX inhibitor, and ascofuranone–derivatives colletochlorin B, colletochlorin D, compound ISSF31 and compound ISSF33 were also included in the study, in order to investigate whether these compounds also inhibited the cytochrome bc_1 complex.

The SCR assay is a widely used method that measures electron flow through complex II to ubiquinone to form ubiquinol, which is then reoxidised by complex III with the transfer of electrons to cytochrome c[241]. Therefore, the overall activity of SCR in the presence of drugs was determined using succinate and cytochrome c as substrates. The half maximal inhibitory concentrations (IC_{50}s) were calculated from the dose-response curves of three independent experiments (biological repeats). Mode of action of compounds according to the literature and pIC_{50} values measured in this experiment can be found in Table 4.1.

Figure 4.7 shows a representative dose-response curve for each of the compounds tested. Results show that the most potent inhibitors were myxothiazol ($pIC_{50} = 9.15 \pm 0.11$) and antimycin A ($pIC_{50} = 8.55 \pm 0.14$). The rank order of potency of the complex III inhibitors regarding SCR inhibition was: myxothiazol > antimycin A > ascochlorin > pyraclostrobin> trifloxystrobin > picoxystrobin > fluoxastrobin > dimoxystrobin > atovaquone > azoxystrobin > kresoxim-methyl > fenamidone > amisulbrom > cyazofamid > diuron. The rank order of potency of the AOX inhibitors regarding the inhibition of SCR was: ISSF31 > colletochlorin B > ascofuranone > ISSF33 > colletochlorin D. An IC_{50} for ametoctradin could not be obtained due to solubility issues. In summary, compounds tested showed a wide range of potency in inhibiting SCR, constituting a valuable data set for future structure-activity and QSAR studies.

Table 4.1. Summary of compounds tested, pIC_{50} values against complex II+III activity and mode of action according to the literature. Data is shown as mean ± S.D. of n = 3 biological repeats. N/A = not available.

Compound	Complex II+III pIC_{50}	Mode of action	Reference
Ametoctradin	N/A	complex III Q_o inhibitor	Zhu X.L. *et al*., 2015
Amisulbrom	5.60 ± 0.05	complex III Q_i inhibitor	Fontaine S. *et al*., 2019
Antimycin A	8.55 ± 0.14	complex III Q_i inhibitor	Huang L. *et al*., 2005
Ascochlorin	8.29 ± 0.05	complex III Q_o/Q_i inhibitor	Berry E.A. *et al*., 2010
Ascofuranone	5.08 ± 0.09	AOX inhibitor	Shiba T. *et al*., 2013
Atovaquone	6.69 ± 0.05	complex III Q_o inhibitor	Kessl J.J. *et al*., 2003
Azoxystrobin	6.67 ± 0.09	complex III Q_o inhibitor	Gao A.H. *et al*., 2014
Colletochlorin B	5.98 ± 0.09	AOX inhibitor	Saimoto H. *et al*., 2012
Colletochlorin D	4.34 ± 0.04	AOX inhibitor	-
Cyazofamid	4.22 ± 0.16	complex III Q_i inhibitor	Mitani S. *et al*., 2001
Dimoxystrobin	6.90 ± 0.16	complex III Q_o inhibitor	FRAC[242]
Diuron	3.53 ± 0.01	complex III Q_i inhibitor	di Rago J.P. *et al*., 1988
Fenamidone	6.20 ± 0.05	complex III Q_o inhibitor	Mercer R.T. *et al*., 1998
Fluoxastrobin	6.98 ± 0.22	complex III Q_o inhibitor	FRAC[242]
ISSF31	6.04 ± 0.37	AOX inhibitor	-
ISSF33	4.39 ± 0.29	AOX inhibitor	-
Kresoxim-methyl	6.48 ± 0.15	complex III Q_o inhibitor	FRAC[242]
Myxothiazol	9.15 ± 0.11	complex III Q_o inhibitor	Lai B. *et al*., 2006
Pyraclostrobin	7.89 ± 0.14	complex III Q_o inhibitor	FRAC[242]
Picoxystrobin	7.25 ± 0.09	complex III Q_o inhibitor	FRAC[242]
Trifloxystrobin	7.58 ± 0.16	complex III Q_o inhibitor	Fisher N. *et al*., 2008

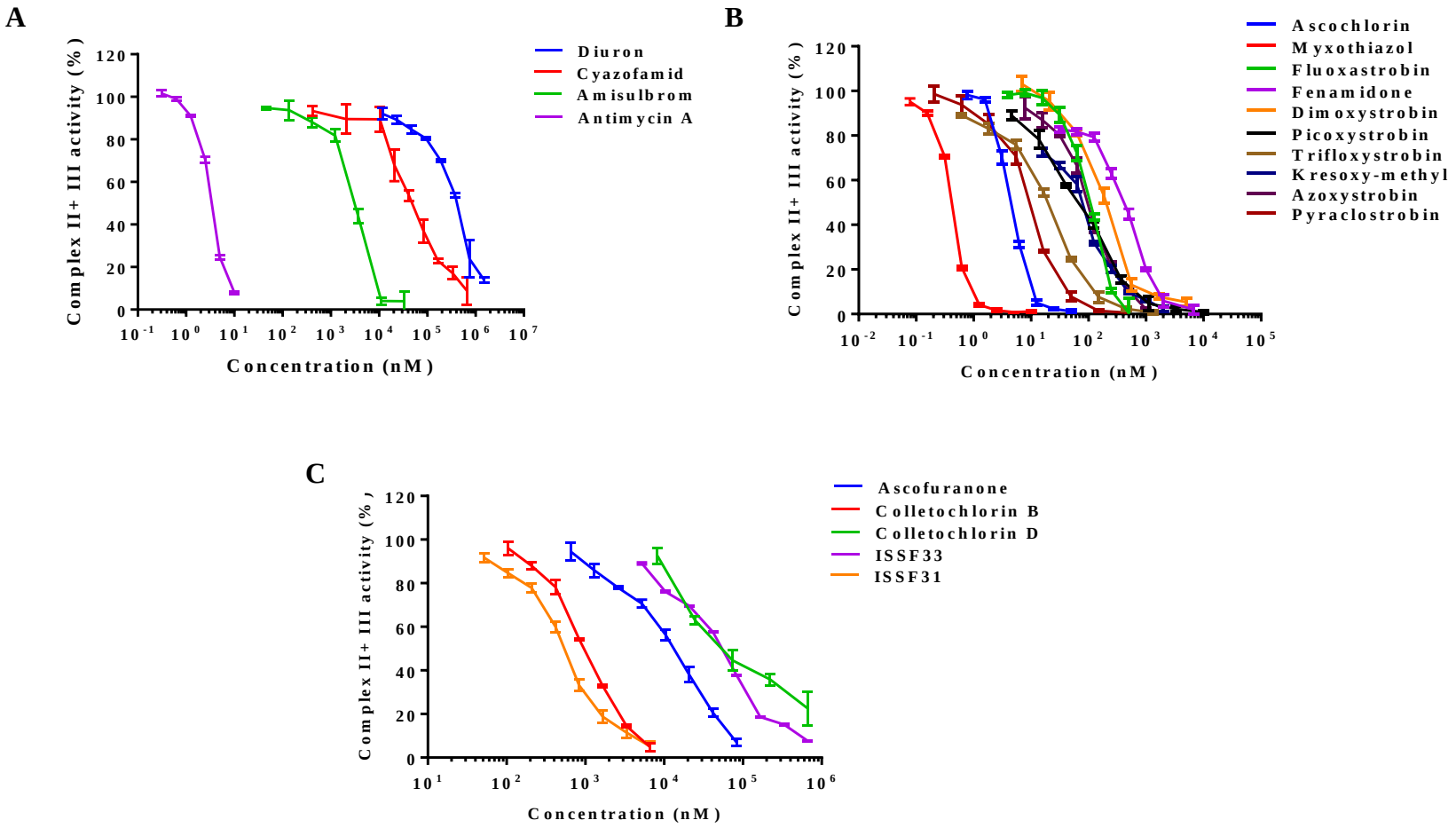

Figure 4.7. Representative dose-response curves for A) Q_i inhibitors B) Q_o inhibitors and C) AOX inhibitors. Data is expressed as percentage relative to vehicle control.

4.3.2.2. The Acute Extracellular Flux Assay to Investigate Real-Time Effects of Fungicides on Mitochondrial Function using HepG2 Cells

Following measurement of SCR inhibitory activities of fungicides, the effects of some of these complex III inhibitors were assessed in intact HepG2 cells for purposes of comparison. The real-time effects of such compounds on mitochondrial function were tested using the Seahorse Bioscience XF96 analyser, which, as described in the Materials and Methods section 2.8.2, can simultaneously measure changes in the oxygen consumption rate (OCR) and extracellular acidification rate (ECAR). In this assay, acute injection of compounds onto HepG2 cells was performed followed by a "Stress Test", which involved a sequential exposure to various mitochondrial stressors that allowed determination of various mitochondrial parameters, such as ATP turnover, reserve capacity or proton leak. Compounds were tested at 7 different concentrations by doing a half-log dilution, with 100 µM as the highest concentration tested, except for atovaquone, where the highest concentration was 50 µM.

Data obtained for all examined compounds and rotenone, a potent complex I inhibitor used as positive control, is summarised in Table 4.2 and Table 4.3. Figure 4.8 illustrates the dose-response curves of some of the mitochondrial parameters determined with this assay. Table 4.2 reports the direction of change of the mitochondrial parameters measured, whereas Table 4.3 reports the concentration which resulted in 50% maximum responses (AC_{50} values) and the minimum effective concentration (MEC), defined as the concentration that significantly changed the respiratory response with respect to the vehicle control.

Based on the OCR AC_{50} values listed in Table 4.3, rank order of potency of these compounds was: pyraclostrobin > dimoxystrobin > picoxystrobin > kresoxim-methyl > atovaquone > trifloxystrobin > fenamidone > fluoxastrobin > ametoctradin > diuron. Interestingly, cyazofamid was the only compound that showed an uncoupling activity instead of an ETC inhibitory activity, as can be seen in Figure 4.8. Acute injection of up to 30 µM cyazofamid caused a sharp increase in OCR and proton permeability, as shown in the increase in proton leak rate (Table 4.2 and Figure 4.8). Results suggest that at 100 µM cyazofamid becomes acutely toxic to the cells, resulting in decreased OCR and reserve capacity. Ametoctradin and diuron showed very low potency in OCR inhibition and ametoctradin showed a dose-dependent effect on reserve capacity, where it seemed to increase at concentrations lower than 1 µM. The rest of the compounds decreased OCR

and reserve capacity and increased ECAR in a dose-dependent manner, indicating inhibition of the ETC and upregulation of glycolysis (Table 4.2). IC_{50} values obtained from isolated mitochondria (SCR assay) and those from HepG2 cells (acute extracellular flux assay) are shown in Table 4.5 for comparative purposes.

Table 4.2. Acute extracellular flux assay (AEFA) for the detection of mitochondrial toxicity. List of compounds, ranges of concentrations tested and direction of change of mitochondrial parameters. Direction of change: ↑ = increase compared to vehicle control, ↓ = decrease compared to vehicle control, NR = no response compared to vehicle control.

Compounds	Concentration range (µM)	Direction of change					Summary mechanism
		OCR	Reserve capacity	ECAR	ATP	Proton leak	
Ametoctradin	0.1 – 100	↓	↓	↑	↓	NR	ETC inhibitor
Atovaquone	0.05 – 50	↓	↓	↑	↓	↓	ETC inhibitor
Cyazofamid	0.1 – 100	↑	↓	↑	↓	↑	Uncoupler
Dimoxystrobin	0.1 – 100	↓	↓	↑	↓	↓	ETC inhibitor
Diuron	0.1 – 100	↓	↓	↑	↓	↓	ETC inhibitor
Fenamidone	0.1 – 100	↓	↓	↑	↓	↓	ETC inhibitor
Fluoxastrobin	0.1 – 100	↓	↓	↑	↓	↓	ETC inhibitor
Kresoxim-methyl	0.1 – 100	↓	↓	↑	↓	↓	ETC inhibitor
Picoxystrobin	0.1 – 100	↓	↓	↑	↓	↓	ETC inhibitor
Pyraclostrobin	0.1 – 100	↓	↓	↑	↓	↓	ETC inhibitor
Trifloxystrobin	0.1 – 100	↓	↓	↑	↓	↓	ETC inhibitor
Rotenone	0.003 – 1	↓	↓	↑	↓	↓	ETC inhibitor

Table 4.3. Data summary of acute extracellular flux assay. MEC = minimum effective concentration that significantly crosses vehicle control threshold. AC_{50} = the concentration at which 50% maximum effect is observed. NR = no response observed.

Compounds	MEC (µM)					AC_{50} (µM)				
	OCR	Reserve capacity	ECAR	ATP production	Proton leak	OCR	Reserve capacity	ECAR	ATP production	Proton leak
Ametoctradin	1.8	3.96	7.04	32	NR	>31.6	80.6	>31.6	>31.6	NR
Atovaquone	1.52	1.52	3.14	2.30	5.10	8.08	3.15	29.9	6.54	29.1
Cyazofamid	0.999	35.7	8.97	0.374	0.544	3.54	86.4	>31.6	6.56	1.12
Dimoxystrobin	0.319	<0.1	1.59	1.02	0.654	2.27	0.387	>100	1.74	3.69
Diuron	10.9	1.17	69.8	0.615	84.8	>100	>100	>100	11.7	>100
Fenamidone	1.89	0.318	5.6	5.92	5.91	9.50	3.37	>100	9.62	48.1
Fluoxastrobin	1.32	2.27	4.53	3.34	1.76	10.1	4.93	>100	10.8	>100
Kresoxim-methyl	1.07	1.23	2.5	4.57	2.16	7.02	4.25	>100	7.88	29.8
Picoxystrobin	0.682	0.662	1.16	1.52	0.507	3.50	2.25	70.7	3.74	7.40
Pyraclostrobin	0.19	0.220	0.461	0.38	0.162	0.895	0.629	70.4	0.909	2.41
Trifloxystrobin	2.18	2.67	3.54	4.6	3.42	8.56	5.48	81.2	8.58	28.4
Rotenone	0.0053	<0.003	0.0274	0.0159	0.0120	0.0433	0.0106	>1	0.0459	0.213

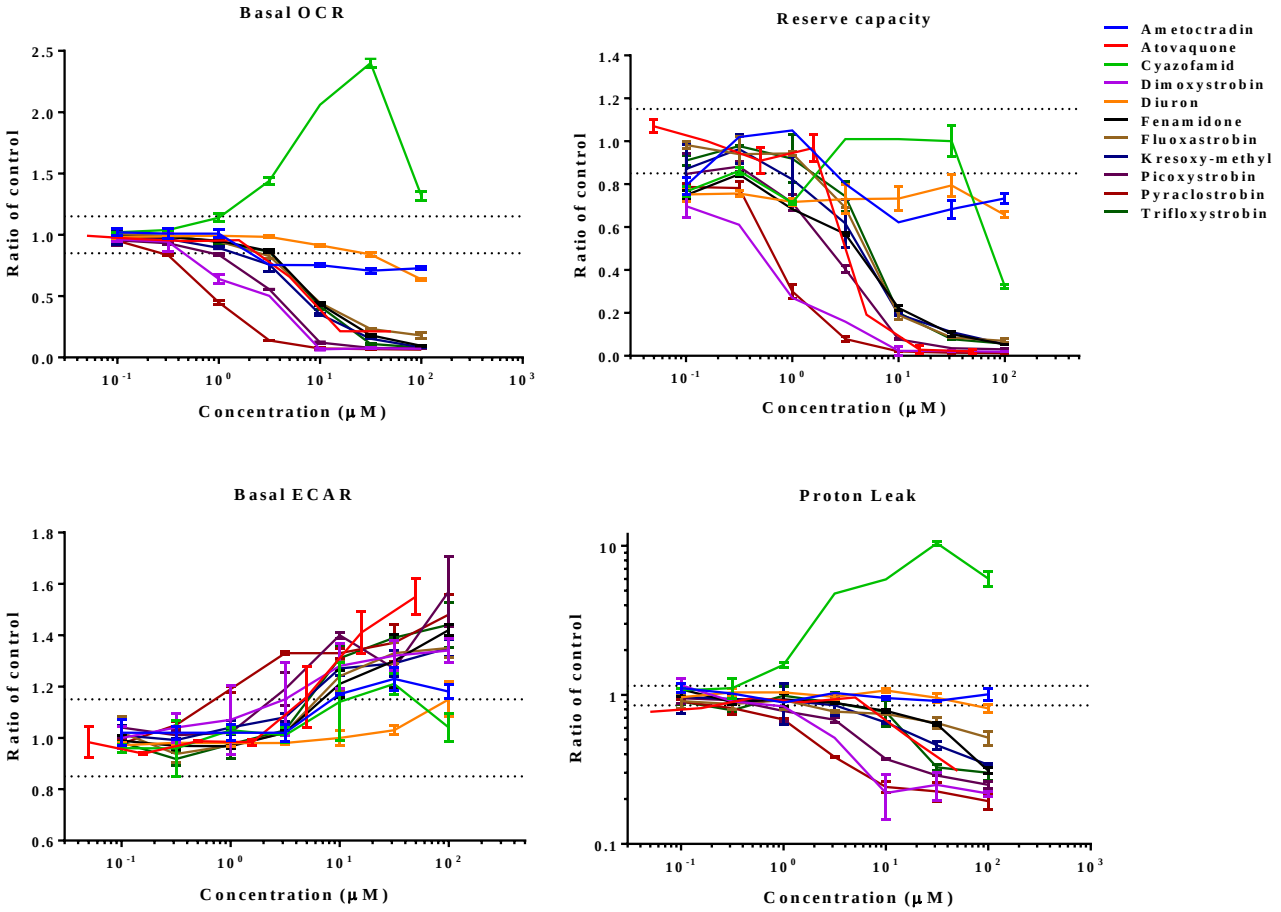

Figure 4.8. Bioenergetic profile of compounds tested using the Extracellular Flux Analyser. Dose-response curves show the acute effects of compounds in basal OCR, reserve capacity, proton leak and basal ECAR in 10 mM glucose, 1 mM pyruvate and 2 mM glutamine. Data is expressed as mean ratio to vehicle control ± SD of n = 3. Black dashed lines represent significant cut-off from vehicle control.

4.3.2.3. Measurement of Respiratory Activity using Permeabilised Cells with rPFO

The effects on mitochondrial function of the same set of compounds were investigated using a different assay protocol that employs permeabilised cells and a set of specific substrates of either complex I, complex II or complex IV. rPFO, the selective permeabiliser of the cytoplasmic membrane (see Materials and Methods section 2.8.3), allows permeation of these mitochondrial substrates to the mitochondria, thereby mitochondrial isolation is not required. The way the permeabilised assay identifies mitochondrial toxicants is on the basis of the recovery of mitochondrial function following the addition of the specific substrates and inhibitors. When pyruvate and malate are added at the beginning of the assay, theoretically there is a fully functioning ETC, and all complexes are involved in the reaction. When succinate and rotenone are added to the media, complex II-linked respiration is induced and RET is blocked. Finally, ascorbate + TMPD and antimycin A are injected to induce complex IV-linked respiration.

Figure 4.9 shows the responses of the different fungicides as well as the response of the complex I inhibitor rotenone (used as control) on complex I, complex II and complex IV-linked respiration. The response for rotenone-treated cells in the presence of pyruvate, succinate or ascorbate + TMPD substrates clearly indicates that the mechanism of action of rotenone is the inhibition of complex I, as a recovery in respiration is observed upon addition of succinate. All compounds included in this study, except for ametoctradin, diuron and cyazofamid, caused a strong inhibition of respiration that was only restored after addition of ascorbate + TMPD as the oxidizable substrates, which indicates that the mechanism of action of these mitochondrial toxicants is the inhibition of complex III. If a recovery had been seen with addition of succinate, this would have implied complex I inhibition as the mechanism of action. Table 4.4 provides a summary of the deduced inhibition mechanisms based on the results presented in Figure 4.9. The results presented in this section were kindly obtained by the toxicology team in Cyprotex Ltd (Alderley Park, UK).

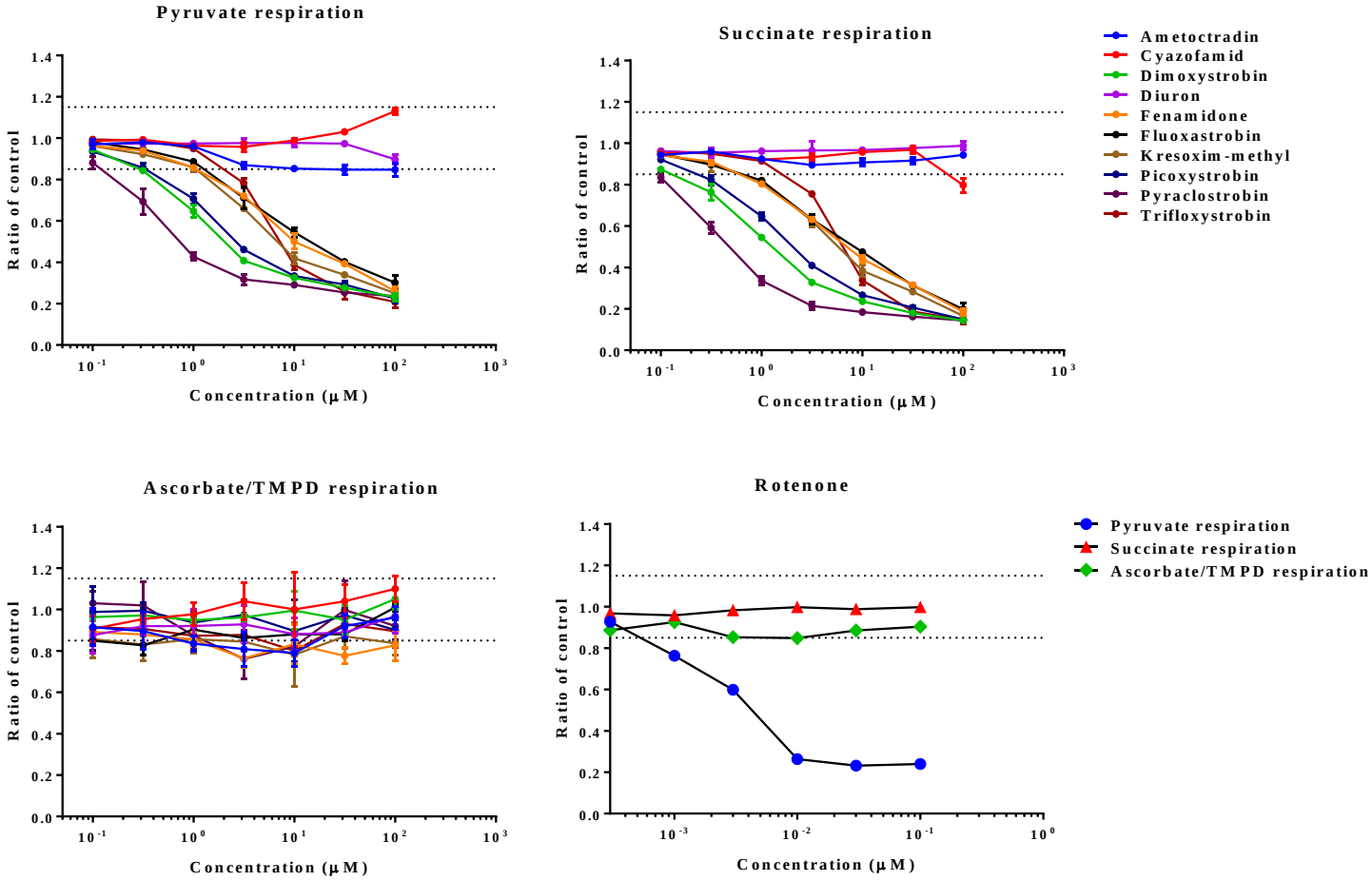

Figure 4.9. Dose-response curves of compounds in complex I-linked respiration (pyruvate respiration), complex II-linked respiration (succinate respiration) and complex IV respiration (ascorbate + TMPD) in HepG2 cells permeabilised with rPFO. Ratio of control refers to the ratio of the basal respiration in the presence and the absence of a test drug with respect to the control. Black dashed lines represent significant cut-off from vehicle control.

Table 4.4. Most sensitive mechanism of fungicides and rotenone using HepG2 cells permeabilised with rPFO. ↑↓= direction of change of mitochondrial respiration. MEC = minimum effective concentration that significantly crosses vehicle control threshold. AC_{50} = the concentration at which 50% maximum effect is observed. NR = no response observed.

Compounds	Most sensitive mechanism	↑↓	MEC (µM)	AC_{50} (µM)
Ametoctradin	NR	NR	NR	NR
Cyazofamid	succinate respiration	↓	79.9	>100
Dimoxystrobin	succinate respiration	↓	<0.1	1.44
Diuron	NR	NR	NR	NR
Fenamidone	succinate respiration	↓	0.531	7.84
Fluoxastrobin	succinate respiration	↓	0.571	8.69
Kresoxim-methyl	succinate respiration	↓	0.548	6.60
Picoxystrobin	succinate respiration	↓	0.177	2.32
Pyraclostrobin	succinate respiration	↓	<0.1	0.515
Trifloxystrobin	succinate respiration	↓	1.17	8.17
Rotenone	pyruvate respiration	↓	0.00054	0.00423

Table 4.5. IC_{50} values (µM) obtained in the SCR assay vs. OCR IC_{50} values obtained with the Extracellular Flux Analyser in whole and permeabilised cells.

Compound	SCR IC_{50} (µM)	OCR_{whole} IC_{50} (µM)	OCR_{perm} IC_{50} (µM)	OCR_{whole} / SCR IC_{50}	OCR_{perm} / SCR IC_{50}
Ametoctradin	N/A	>31.6	NR	-	-
Atovaquone	0.2	8.08	N/A	40.4	-
Cyazofamid	60.26	*	>100	-	-
Dimoxystrobin	0.12	2.27	1.44	18.91	12
Diuron	295	>100	NR	-	-
Fenamidone	0.63	9.50	7.84	15.07	12.44
Fluoxastrobin	0.10	10.1	8.69	101	86.9
Kresoxim-methyl	0.33	7.02	6.6	21.27	20
Picoxystrobin	0.05	3.50	2.32	70	46.4
Pyraclostrobin	0.01	0.895	0.515	89.5	51.5
Trifloxystrobin	0.02	8.56	8.17	428	408.5

*showed increase in respiration, not inhibition. N/A = not available

4.4. Discussion

In the first section of this present chapter the use of isolated mitochondria and high-resolution respirometry in simultaneous evaluation of MMP and ROS for the assessment of drug-induced mitochondrial dysfunction was explored. The goal was to study the effects of classic inhibitors and uncouplers to validate the methodology for future studies that employ isolated mitochondria (SCR assay in this chapter and experiments performed in chapter 5).

Firstly, the RCR and ADP/O ratios demonstrated good quality of the mitochondrial preparations and a functional respiratory chain. Secondly, the AmR assay showed congruous fluctuations in the ROS measurements according to the mitochondrial stressors that were added to the media. In this assay, superoxide is converted into H_2O_2 by the action of superoxide dismutases (SOD), which is then used by horseradish peroxidase (HRP) to oxidise the colorless substance Amplex red into resorufin, which can be detected by fluorescence measurements. It should not be overlooked that, during the course of the experiment, the concentration of AmR diminishes, whereas the concentration of resorufin increases, which could lead to allosteric inhibition of HRP. Therefore, experiments using this technique should be performed in a short timeframe[243]. It should also be noted that ROS generation was determined in the presence of 1 μM rotenone and 12.5 mM sodium succinate using freshly isolated mitochondria (instead of frozen mitochondria), which, in theory, allows preservation of the phosphorylation state and therefore maintenance of more physiological conditions[244].

As shown in Figure 4.6, increasing concentrations of antimycin A led to an increase in ROS production in complex II-linked respiration. However, such increase was suppressed in the presence of rotenone, which confirmed the existence of the phenomenon of reverse electron transfer (RET). During RET, electrons leak at either I_F or I_Q sites of complex I, leading to a considerable increase in ROS production. Addition of rotenone blocks the I_Q site during RET, preventing coenzyme Q from transferring electrons back to complex I and consequently reducing ROS generation[245].

Next, changes in MMP were measured using safranin as the fluorescent probe. As shown in Figure 4.4, complex II-linked respiration led to the generation of a MMP (shown by a decrease in the fluorescent signal) consistent with a more negatively charged mitochondrial interior and consequent accumulation of safranin in the mitochondria.

Upon addition of the uncoupler CCCP, the membrane potential was completely dissipated, (shown by the increase in the fluorescent signal) consistent with a reduced negative charge in the mitochondrial matrix. When taken together, these results demonstrate first the integrity of the isolated mitochondria, which have been used in several assays throughout the thesis, and second the validity of this methodology in detecting simultaneous changes in oxygen consumption and either MMP or ROS production.

Confirmation of the quality of the mitochondrial preparations allowed their use in SCR inhibition studies, where reduction of cytochrome *c* was monitored spectrophotometrically. In this assay, IC_{50} values of several complex III and AOX inhibitors were consistently measured, constituting a promising data set for future structure-activity and QSAR studies. As for the compounds that were synthesised in-house (AOX inhibitors such as ISSF31, ISSF33, colletochlorin B and colletochlorin D), no previous data was available with regards to inhibition of mammalian complex III. However, this information is of great value given the potential those compounds may have in the treatment of relevant pathogenic organisms through AOX inhibition, as previously explained in chapter 3. Successful candidates in the treatment of fungal and parasitic infections acting as AOX inhibitors should show reduced inhibition of mammalian complex III to avoid mammalian toxicities. In this regard, colletochlorin D (IC_{50} = 45.7 µM) and ISSF33 (IC_{50} = 40.73 µM) seem the most promising candidates, whereas colletochlorin B (IC_{50} = 1.04 µM) and ISSF31 (IC_{50} = 0.91 µM) showed relatively high potency against complex II+III in isolated mitochondria.

While isolated mitochondria allow the determination of direct mitochondrial interactions, they suffer from low-throughput and possible damage and alterations in mitochondrial morphology during the isolation process. They also lack cellular context, meaning that such interactions might not be as relevant to clinical situations as experiments that use whole cells, due to the unrestricted access of the drug to the ETC in isolated mitochondria and lack of protective mechanisms, such as the cell membrane and transporter proteins. Conversely, it can also lead to certain toxicities going unnoticed in situations where multiple mechanisms of toxicity or xenobiotic activation of drugs are involved. Here, the acute effects of some of the same compounds were investigated in intact and permeabilised HepG2 cells using the Extracellular Flux Analyser. The results from intact HepG2 cells rank the compounds IC_{50} values for the basal OCR reduction in the same

order as permeabilised HepG2 cells. However, the rank order of potency differs between SCR test and OCR effects (Table 4.5). Despite this, compounds showing minimum inhibition of OCR, such as cyazofamid and diuron, also showed the lowest pIC_{50} values in the SCR assay.

Cyazofamid, which has classically been considered a complex III-Qi inhibitor (Table 4.1)[246], here it exerted an uncoupling effect on intact mammalian cells at ≤30 μM (Figure 4.8). This could be due to the interspecies differences in inhibition specificity towards fungal complex III, where the original complex III inhibition had been reported[246] vs. mammalian (HepG2) results obtained here. Additionally, studies on cyazofamid's inhibitory activity using isolated mitochondria without a fully functioning ETC[246] may not reflect the reality of what actually happens in the cellular environment of a mammalian cell in the presence of cyazofamid. In fact, cyazofamid fully exerted its uncoupling effects in intact cells, and only slightly in permeabilised cells where there was a fully functioning ETC supported by pyruvate respiration (AC_{50} > 100 μM, see Figure 4.9). In permeabilised cells supported by complex II-linked respiration, cyazofamid inhibited respiration moderately (AC_{50} > 100 μM, see Figure 4.9), and a recovery was seen upon addition of complex IV substrates, which may indicate inhibition of complex III.

OCR IC_{50} values obtained in HepG2 cells, both permeabilised and intact cells, were significantly higher than those obtained in isolated mitochondria. For instance, OCR IC_{50} values obtained in intact cells for fenamidone, dimoxystrobin and kresoxim-methyl were around 15, 19 and 21 times higher respectively, while values for atovaquone, picoxystrobin, pyraclostrobin, fluoxastrobin, and trifloxystrobin were around 40, 70, 90, 101 and 428 times higher than those obtained in isolated mitochondria, respectively (Table 4.5). This is probably due to the nature of the endpoint being measured in each of the experiments, i.e. enzyme inhibition in SCR vs. the oxygen consumption rate in the Extracellular Flux Analyser. It is evident that the variability of OCR data shows a much narrower data distribution than SCR test results, making OCR inconvenient for decisions on quantitative measures of toxicity, although much more suitable to qualitatively identify the toxicants and their mechanisms of action. OCR IC_{50} values obtained from permeabilised cells and those from intact cells were comparable, with intact cells showing slightly higher values that could be attributed to the media and cell condition used in each experiment.

Finally, the permeabilised cell assay confirmed that, for all the compounds tested, except for ametoctradin and diuron, complex III is the mechanism of action by which the compounds tested inhibit the mitochondrial ETC (Table 4.4).

In summary, this data show that discrepancies can exist among results obtained using various assay protocols and cell or isolated mitochondria systems. These results are often complementary, which highlights the importance of combining different tests results for a better assessment of drug's activities.

5. The Effect of Antidiabetic Drugs, Lipid-Lowering Agents, Anti-Inflammatory Drugs and other widely Prescribed Drugs on Mitochondrial Function

5.1. Introduction

Drug-induced mitochondrial toxicity has been described for a wide range of different drug classes, which could be associated with side effects, limiting their success in the clinic. More specifically, there is increasing evidence that mitochondrial dysfunction is implicated in the aetiology of drug toxicity caused by some antidiabetic, antihyperlipidemic and anti-inflammatory medications[85, 103]. In this chapter, the effects on mitochondrial function of some members of these drug classes were assessed using a combination of different *in vitro* approaches. In addition to these compounds, a selection of some widely prescribed members of other drug classes (ranked in some cases as "essential medicines" by the World Health Organisation[247]) were also included in the study.

Cardiovascular diseases are the leading cause of death globally, accounting for >17 million deaths every year, causing lipid-lowering agents such as statins to be the most commonly prescribed drug class in the world[248]. Statin-induced myotoxicity varies between 5% and 30% of patients and it is the most common reason for discontinuation of therapy. Rhabdomyolysis, the most serious form of myotoxicity, has an incidence of approximately 1 in 10,000[249]. The mechanisms leading to such toxicities are yet to be fully elucidated, although there is growing evidence that indicates mitochondrial dysfunction may be the primary cause[249, 250].

Similarly, there are over 451 million adults with type 2 diabetes mellitus, and it has been predicted that this figure will rise to 693 million by 2045 if trends continue[251]. However, current treatments are not exempt from serious side effects and, in fact, they have been strongly associated with mitochondrial toxicity. Two important biguanides, phenformin and buformin, were withdrawn from the market due to fatal lactic acidosis, while metformin remains on the market although it is also associated with lactic acidosis as a persistent adverse effect[252]. Other antidiabetic treatments, such as the thiazolidinediones have also been strongly associated with mitochondrial toxicities[85, 145, 253].

Likewise, analgesic/anti-inflammatory drugs are widely prescribed therapeutic agents often used long-term in the treatment of chronic diseases. They have been associated with

gastrointestinal injury and, in some cases, with idiosyncratic hepatotoxicity with severe cases resulting in fatal fulminant hepatitis[254]. The mechanisms contributing to such injuries are not completely understood and, again, mitochondrial dysfunction has been proposed as one of the contributing factors[255].

The first section of this chapter reports the effects of the drugs from these therapeutic classes on mitochondrial function using different cell-based *in vitro* assays. Subsequently, drugs that presented some degree of toxicity in the cell assays were shortlisted for further studies using mitochondria isolated from rat liver to gain more insight into mechanisms of toxicity. Additionally, binding affinity of compounds into the mitochondrial ETC complexes was investigated through docking studies.

All cell assays were performed using the HepG2 cell line due to several reasons. First, drug-induced liver injury (DILI) is the most common cause for withdrawal of an approved drug and is a major issue for public health and pharmaceutical companies[57, 73, 256]. Although the exact mechanisms of DILI are not fully understood, mitochondrial liability is often present when drug-induced impairment of mitochondrial function is investigated[257, 258]. Moreover, unlike primary hepatocytes, HepG2 cells have the ability to utilise glycolysis as an additional mechanism to produce ATP in order to meet the energy demands implicated in high rates of cell proliferation, a phenomenon known as the Warburg effect[259]. Hence, due to their altered bioenergetic profile, HepG2 cells allow the detection of mitochondrial toxicity when forced to rely on OXPHOS by substituting glucose for galactose in the growth media[58]. Finally, HepG2 cells are the most widely used preclinical model for toxicity predictions in the pharmaceutical industry, due to availability, reproducibility and display of many genotypic and phenotypic features of normal liver cells[140, 260]. Whilst the use of primary human hepatocytes has some important advantages, such as retention of xenobiotic metabolism, current protocols do not allow the maintenance of this function for more than a few hours, which means that the option to use these cells to test chronic toxicity remains limited[261]. Also, complicated isolation procedures, limited availability and inter-individual variability reduce their utility[140].

5.2. Chapter Aims

The overall aim of this chapter was to investigate the effects of some antidiabetic, antihyperlipidemic and anti-inflammatory drugs, as well as other widely prescribed drugs, on mitochondrial bioenergetics using molecular docking and different *in vitro* methods

performed on two model systems: isolated rat liver mitochondria and the human hepatoblastoma cell line HepG2. This will help identify in detail the mechanisms of any drug effects on mitochondria by comparing the results obtained from the different *in vitro* assays and model systems. A total of 16 pharmaceutical drugs were investigated in detail. The objectives of this study were:

1. To investigate in detail the mechanisms of any drug effects on mitochondria by comparing the results obtained from the different *in vitro* assays and model systems.
2. To evaluate the results obtained here in light of literature data, including those from *in vitro, in vivo* or clinical studies.
3. To obtain further mechanistic evidence by determining the binding affinities of drugs in the ligand-binding pocket of the different ETC complexes through protein-ligand docking studies.
4. To obtain consistent experimental data for QSAR investigations for the establishment of relationships between inhibitory activity and chemical characteristics of compounds.

In order to achieve these objectives, the metabolic flexibility of HepG2 cells was first characterised using the Extracellular Flux Analyser.

5.3. Results

5.3.1. Bioenergetic Profile of HepG2 Cells in the presence of Glucose or Galactose

To investigate the metabolic flexibility of the HepG2 cell line as a model system to test drug-induced mitochondrial dysfunction, the effect of glucose replacement with galactose was examined. The rationale for this assay is that cells grown in galactose as the only source of sugar are forced to rely on mitochondrial oxidative phosphorylation (OXPHOS), while cells grown in glucose media can rely on glycolysis for ATP generation, and are therefore less susceptible to mitochondrial toxicities[262].

Cells were grown under standard conditions and transferred to unbuffered DMEM (containing 2 mM glutamine), either in the presence or absence of 10 mM glucose or 10 mM galactose and either in the presence or absence of 1 mM sodium pyruvate. Real-time changes in oxygen consumption rate (OCR) and extracellular acidification rate (ECAR) were determined after 1 h and 2 h glucose starvation.

Figure 5.1 illustrates that glycolytic capacity is not reduced after 1 or 2 hours of glucose starvation, and that noticeable reduction is observed only after overnight starvation (24 hours), with or without 1 mM pyruvate. This clearly indicates the presence of enough endogenous glucose for efficient glycolysis, pyruvate metabolism and TCA, even after it is removed from the medium for 1 or 2 hours.

With regards to basal ECAR, Figure 5.1 illustrates that after 1 h glucose starvation (and in the presence of 10 mM galactose), ECAR remains the same as in 10 mM glucose media. On the contrary, OCR decreases (although not significant at $p<0.05$), therefore the lack of ECAR signal reduction in the absence of exogenous glucose cannot be justified by an increase in CO_2 from respiration. To determine whether this response was justified by increased lactic fermentation, pyruvate was removed from the media. Pyruvate is a metabolic intermediate with several potential fates. On the one hand, pyruvate can get converted into lactate in the cytosol by lactate dehydrogenase. On the other hand, pyruvate can be converted into acetyl-coA, entering the TCA cycle within mitochondria, producing CO_2 along the way. Removal of pyruvate from the media led to an increased ECAR response, which could be interpreted as a higher demand for glycolytic ATP in the absence of pyruvate. This explanation correlates with the reduced OCR in the absence of pyruvate, due to less TCA-cycle generated substrates. It also suggests cells were not relying on lactic fermentation, since a reduction in the ECAR signal was not observed in the absence of pyruvate.

Since the glycolytic capacity and basal ECAR were maintained up to 2 hours of glucose starvation, it is likely that there is enough endogenous glucose within the cells allowing for continued glycolysis. However, the absence of both pyruvate and exogenous glucose probably caused a reduction in the TCA cycle activity, and consequently a lower production of mitochondrial substrates, which resulted in a decreased maximal respiration.

Results in Figure 5.1 (where o/n stands for overnight, i.e. 24 h glucose starvation) show that, after 24 h, the basal rate of respiration increases as it would be expected if the cells were Crabtree-positive, whereas the glycolytic capacity is reduced. This suggests that after 24 h cells have consumed all the endogenous glucose and have activated the “metabolic switch” from aerobic glycolysis to OXPHOS. A metabolic switch to OXPHOS was confirmed by a higher respiratory capacity, which suggests a potentiation

in the mitochondrial OXPHOS system that could be due to an increased mitochondrial mass or even changes in mitochondrial dynamics that could cause, for example, an increase in fusion and generation of an extended mitochondrial network. Preservation of a similar ECAR response is not striking, as it could be explained by at least two reasons: increased CO_2 production by respiration and presence of galactose, which can still be converted into glucose by the Leloir pathway, allowing glycolysis to take place. However, the Leloir pathway reduces net glycolysis ATP yield. Because the conversion of galactose to glucose consumes an amount of ATP equivalent to that which is directly generated by glycolysis, galactose can support a full glycolysis flux but does not permit net glycolysis ATP production[263]. Consequently, after 24 h glucose starvation, cells rely more on OXPHOS than glycolysis, which is reflected in a higher OCR/ECAR ratio (Figure 5.1).

Finally, the effects of 24 h glucose starvation in the absence of 10 mM galactose were investigated (Figure 5.1, orange bar). This time, deprival of both galactose and glucose led to an important decrease in both basal ECAR and glycolytic capacity. Under these conditions, as previously discussed, cells not only lack endogenous glucose, but in the absence of galactose, the Leloir pathway cannot take place. Consequently, as shown in the OCR/ECAR ratio, cells are completely reliant on OXPHOS for energy production. Since OXPHOS is the only energy-yielding pathway, cells must increase their mitochondrial coupling efficiency, which may be supported by changes in the mitochondrial fusion. This agrees with a higher spare respiratory capacity (Figure 5.1).

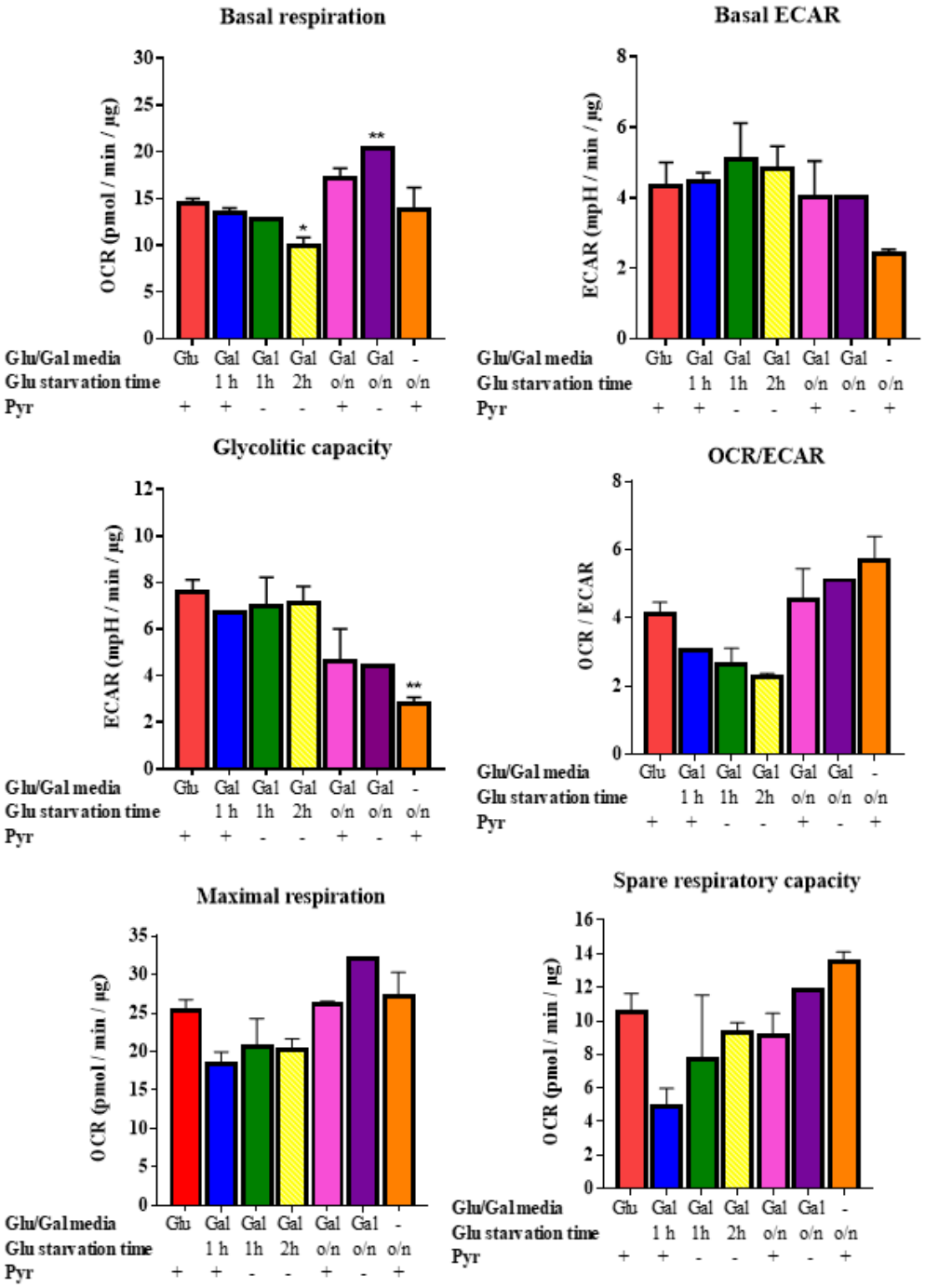

Figure 5.1. Bioenergetic profile of HepG2 cells after 1 h, 2 h and 24 h (o/n) of glucose starvation in the presence or absence of 1 mM pyruvate and 10 mM galactose. Values are expressed as mean ± SEM (n = 2-10 independent experiments) *p<0.05, **p<0.01, Dunnett's test one-way ANOVA, glucose media (red bar) as control.

5.3.2. Data set of compounds

A total of 16 pharmaceutical drugs were included in this study. A summary of drug names, drug class and literature mechanisms of mitochondrial toxicity is given in Table 5.1. A majority of the compounds had known mitochondrial liabilities, except for baclofen and warfarin, which, to the best of my knowledge, had no reported effects on mitochondria to this date. For the cell assays, the maximum concentrations of tested compounds were set at least at 100-fold C_{max} (maximum plasma concentration) (Table 5.2), unless not possible due to solubility limitations. C_{max} values are influenced by several different factors, such as species, gender, age and co-medications, therefore, when possible, values were obtained from the literature for plasma or serum of adult humans for consistency.

Table 5.1. Summary table of compounds tested, drug class and literature mechanism.

Compounds	Drug class	Literature mechanism	Reference
Acetaminophen	Analgesic, antipyretic	MPTP opening (oxidative stress)	Masubuchi Y. *et al.*, 2005
		complex I inhibitor	Chrøis K.M. *et al.*, 2019
Baclofen	Skeletal muscle relaxant	no reported effects	N/A
Bezafibrate	Lipid-lowering agent (fibrate)	increased mitochondrial mass and mitochondrial protein synthesis	Noe N. *et al.*, 2013
		complex I inhibitor	Nadanaciva S. *et al.*, 2007
Ciglitazone	Antidiabetic (thiazolidinedione)	complex II+III, IV and V inhibitor	Nadanaciva S. *et al.*, 2007
Clonidine	Antihypertensive agent	loss of MMP, activation of caspases 2, 3, 8 and 9 (apoptosis)	Fan D. *et al.*, 2017
Colchicine	Antimitotic agent	loss of MMP, activation of caspases 3 and 9 (apoptosis)	Chen X.M. *et al.*, 2012
Lovastatin	Lipid-lowering agent (statin)	complex II+III, IV and V inhibitor	Nadanaciva S. *et al.*, 2007
Memantine	Alzheimer's disease	increased complex I activity	McAllister J. *et al.*, 2008
		decreased complex IV activity	
		complex I inhibition/activation	Reus G.Z. *et al.*, 2012
Metformin	Antidiabetic (biguanide)	complex I inhibitor	Fontaine E., 2018
Pioglitazone	Antidiabetic (thiazolidinedione)	complex I and III inhibitor	Garcia-Ruiz I. *et al.*, 2013
Rosiglitazone	Antidiabetic (thiazolidinedione)	complex I inhibitor	Nadanaciva S. *et al.*, 2007
Salicylic acid	Nonsteroidal anti-inflammatory agent (NSAID)	mitochondrial FAO inhibition	Deschamps D. *et al.*,1991
		oxidative stress	Doi H. *et al.*, 2010
		MPTP opening	Battaglia V. *et al.*, 2005
		OXPHOS uncoupling	Norman C. *et al.*, 2004
		complex III inhibitor	Liu R. *et al.*, 2018
Simvastatin	Lipid-lowering agent (statin)	complex I, II+III, IV and V inhibitor	Nadanaciva S. *et al.*, 2007
Sulfasalazine	Anti-inflammatory	oxidative stress and mitochondrial injury	Niknahad H. *et al.*, 2017
Troglitazone	Antidiabetic (thiazolidinedione)	complexes II+III, IV and V inhibitor	Nadanaciva S. *et al.*, 2007
		mtDNA damage	Lyudmila I. *et al.*, 2009
		MPTP induction	Okuda T. *et al.*, 2010
Warfarin	Anticoagulant	no reported effects	N/A

5.3.3. The Acute Extracellular Flux Assay (AEFA) to Assess Real-Time Effects of Compounds on Mitochondrial Function

Mitochondrial toxicity was assessed by measuring real-time changes in OCR and ECAR upon injection of compounds using the Seahorse Bioscience XF96 analyser. Cells were then subjected to a "Stress Test", whereby sequential exposure to various mitochondrial stressors allowed the determination of five mitochondrial bioenergetic parameters, namely basal OCR, reserve capacity, basal ECAR, ATP production and proton leak. Essentially, based on the effects of the compounds on these mitochondrial parameters, this test allows the generation of a bioenergetic profile that allows identification of possible mechanisms of mitochondrial effects.

Data obtained for all examined compounds and rotenone, a potent complex I inhibitor used as the positive control, is summarised in Table 5.2 and Table 5.3. Table 5.2 summarises the effects of the 16 drugs tested on the five mitochondrial bioenergetic parameters qualitatively, while Table 5.3 reports the minimum effective concentration that significantly crosses vehicle control threshold (MEC) and the concentration at which 50% maximum effect is observed (AC_{50}). Additionally, a dose-response curve of the drugs tested for basal OCR, basal ECAR, reserve capacity and ATP production can be found in Figure 5.2 and Figure 5.3.

Table 5.2 shows that, of the 16 drugs tested, 9 may be identified as potential mitochondrial toxicants, while baclofen, clonidine, colchicine, memantine, metformin, simvastatin and sulfasalazine demonstrated no acute effects on the respiratory parameters at the concentrations tested.

It has been suggested that ETC inhibitors may be defined as those that decrease mitochondrial respiration, resulting in an increase in glycolysis as an adaptive response, which is reflected by a decreased basal OCR, reserve capacity and ATP production, alongside a simultaneous increase in basal ECAR[136]. Compounds classified as ETC inhibitors based on these criteria included ciglitazone, lovastatin, rosiglitazone and troglitazone. None of the compounds tested here showed an uncoupling activity, which represents another important mechanism of mitochondrial toxicity where compounds increase basal OCR while decreasing ATP production[136]. Similarly, none of the compounds showed a cytotoxic response, where both basal OCR and basal ECAR are simultaneously decreased[136].

Acetaminophen was the only compound classified as “substrate inhibitor”, where mitochondrial respiration is decreased due to a reduced substrate availability (via transporter inhibition, for example), but glycolysis is often not increased to compensate[136]. A few other compounds were labelled as “other” within the table due to their mode of action being poorly defined using this system (not consistent with any of the groups mentioned, i.e. ETC inhibitors/uncouplers/substrate inhibitors). These included the compounds bezafibrate, pioglitazone, salicylic acid and warfarin.

The lowest MEC and AC_{50} values have been highlighted in bold in Table 5.3 to indicate the most potent compounds affecting each aspect of mitochondrial respiration. The table shows that, based on the AC_{50} values, ciglitazone is the most potent in terms of reducing ATP production and increasing proton leak, and troglitazone is the most potent in terms of reducing respiration and increasing ECAR. It can also be observed that all four thiazolidinediones tested here (ciglitazone, pioglitazone, rosiglitazone and troglitazone) have the lowest MEC values (<1 μM) and AC_{50} values (<50 μM) for OCR reduction. These compounds, with the exception of pioglitazone, also have the lowest MEC values (<3 μM) and AC_{50} values (<10 μM) for the reduction of reserve capacity.

It must be noted that the potency of OCR inhibition of rotenone, used as positive control, is much higher than the pharmaceutical drugs tested.

Table 5.2. Acute extracellular flux assay for the detection of mitochondrial toxicity. List of compounds, clinical C_{max} values from references and ranges of concentrations tested. Direction of change in basal OCR, reserve capacity, basal ECAR, ATP production and proton leak, where: ↑ = increase compared to vehicle control, ↓ = decrease compared to vehicle control, NR = no response compared to vehicle control. N/A = not available. Summary mechanism is the conclusion made based on the direction of change in the bioenergetic parameters.

Compounds	C_{max} (µM)	C_{max} reference	Concentration range (µM)	Direction of change					Summary mechanism
				OCR	Reserve capacity	ECAR	ATP	Proton leak	
Acetaminophen	120	Choi, L. *et al*., 2012	10 - 10000	↓	↓	NR	NR	↓	Substrate inhibitor
Baclofen	0.5	Vlavonou, R. *et al*., 2014	0.05 - 50	NR	NR	NR	NR	NR	-
Bezafibrate	13.5	Kajosaari, L. *et al*., 2004	0.75 - 750	↓	↓	↓	↓	NR	Other
Ciglitazone	N/A	N/A	0.1 - 100	↓	↓	↑	↓	↑	ETC inhibitor
Clonidine	0.004	Ehrlich, J. *et al*., 2016	0.0005 - 0.5	NR	NR	NR	NR	NR	-
Colchicine	0.01	Davis, M.W. *et al*., 2014	0.02 - 20	NR	NR	NR	NR	NR	-
Lovastatin	0.01	Kyrklund, C. *et al*., 2001	0.05 - 50	↓	↓	↑	↓	↑	ETC inhibitor
Memantine	0.03	Lenuzza, N. *et al*., 2016	0.1 - 100	NR	NR	NR	NR	↑	-
Metformin	11.7	Chappell, J. *et al*., 2018	6 - 6000	NR	NR	NR	NR	↓	-
Pioglitazone	1.5	Jaakkola, T. *et al*., 2006	0.1 - 100	↓	NR	NR	↓	NR	Other
Rosiglitazone	0.2	Joy, M.S. *et al*., 2007	0.1 - 100	↓	↓	↑	↓	↑	ETC inhibitor
Salicylic acid	115	Weiser, T. *et al*., 2019	10 - 10000	↓	↓	↓	↓	↑	Other
Simvastatin	0.01	Nishimura, Y. *et al*., 2008	0.1 - 100	NR	NR	NR	↑	NR	-
Sulfasalazine	0.03	Kashihara, Y. *et al*., 2017	1.5 - 1500	NR	NR	↓	NR	↓	-
Troglitazone	2.8	Young, M.A. *et al*., 1998	0.225 - 225	↓	↓	↑	↓	↑	ETC inhibitor
Warfarin	5.7	Jiang, X. *et al*., 2004	0.5 - 500	↑	NR	↓	NR	↑	Other
Rotenone	N/A	N/A	0.003 - 1	↓	↓	↑	↓	↓	ETC inhibitor

Table 5.3. Data summary of the acute extracellular flux assay. MEC = minimum effective concentration that significantly crosses vehicle control threshold. AC_{50} = the concentration at which 50% maximum effect is observed. NR = no response observed.

Compounds	MEC (µM)					AC_{50} (µM)				
	OCR	**Reserve capacity**	**ECAR**	**ATP production**	**Proton leak**	**OCR**	**Reserve capacity**	**ECAR**	**ATP production**	**Proton leak**
Acetaminophen	604	2440	NR	NR	25.9	7440	>10000	NR	NR	46.0
Baclofen	NR	NR	NR	NR	NR	NR	NR	NR	NR	NR
Bezafibrate	21.1	561	310	335	NR	>750	>750	>750	>750	NR
Ciglitazone	0.979	2.61	6.28	2.44	**1.35**	18.7	5.52	>100	**4.87**	**4.01**
Clonidine	NR	NR	NR	NR	NR	NR	NR	NR	NR	NR
Colchicine	NR	NR	NR	NR	NR	NR	NR	NR	NR	NR
Lovastatin	22.1	12.6	24.2	12.1	15.4	>50	>50	>50	>50	34.1
Memantine	NR	NR	NR	NR	32.0	NR	NR	NR	NR	>100
Metformin	NR	NR	NR	NR	3620	NR	NR	NR	NR	>6000
Pioglitazone	0.486	NR	NR	2.62	NR	41.6	NR	NR	5.13	NR
Rosiglitazone	**0.368**	1.88	3.05	2.28	14.2	15.9	7.59	>31.6	9.70	86.7
Salicylic acid	772	459	125	<10	126	1820	1510	555	1300	284
Simvastatin	NR	NR	NR	**1.09**	NR	NR	NR	NR	>100	NR
Sulfasalazine	NR	NR	11.5	NR	181	NR	NR	68.4	NR	>1500
Troglitazone	0.473	**0.321**	**1.66**	2.40	6.46	**11.8**	**3.94**	**49.4**	5.37	17.5
Warfarin	164	<0.5	8.94	NR	57.3	>500	NR	>158	NR	93.5
Rotenone	0.00456	<0.003	0.0292	0.0277	0.0326	0.0416	0.0107	0.229	0.0626	0.323

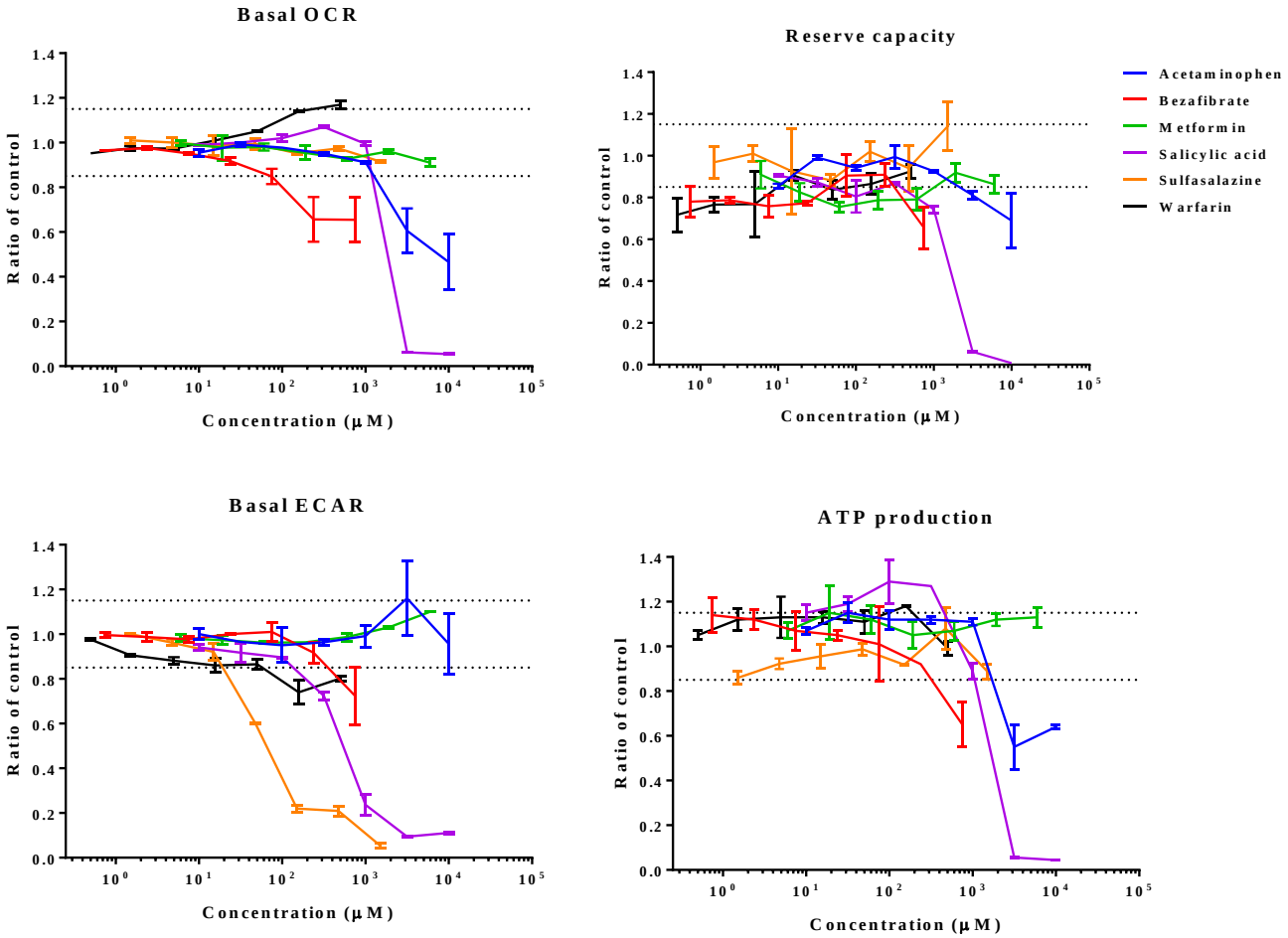

Figure 5.2. Bioenergetic profile of acetaminophen, bezafibrate, metformin, salicylic acid, sulfasalazine and warfarin using the Extracellular Flux Analyser. Dose-response curves show the acute effects of compounds in basal OCR, reserve capacity, basal ECAR and ATP production in 10 mM glucose, 1 mM pyruvate and 2 mM glutamine. Data is expressed as mean ratio to vehicle control ± SD of n = 3. Dashed lines represent significant cut-off from vehicle control.

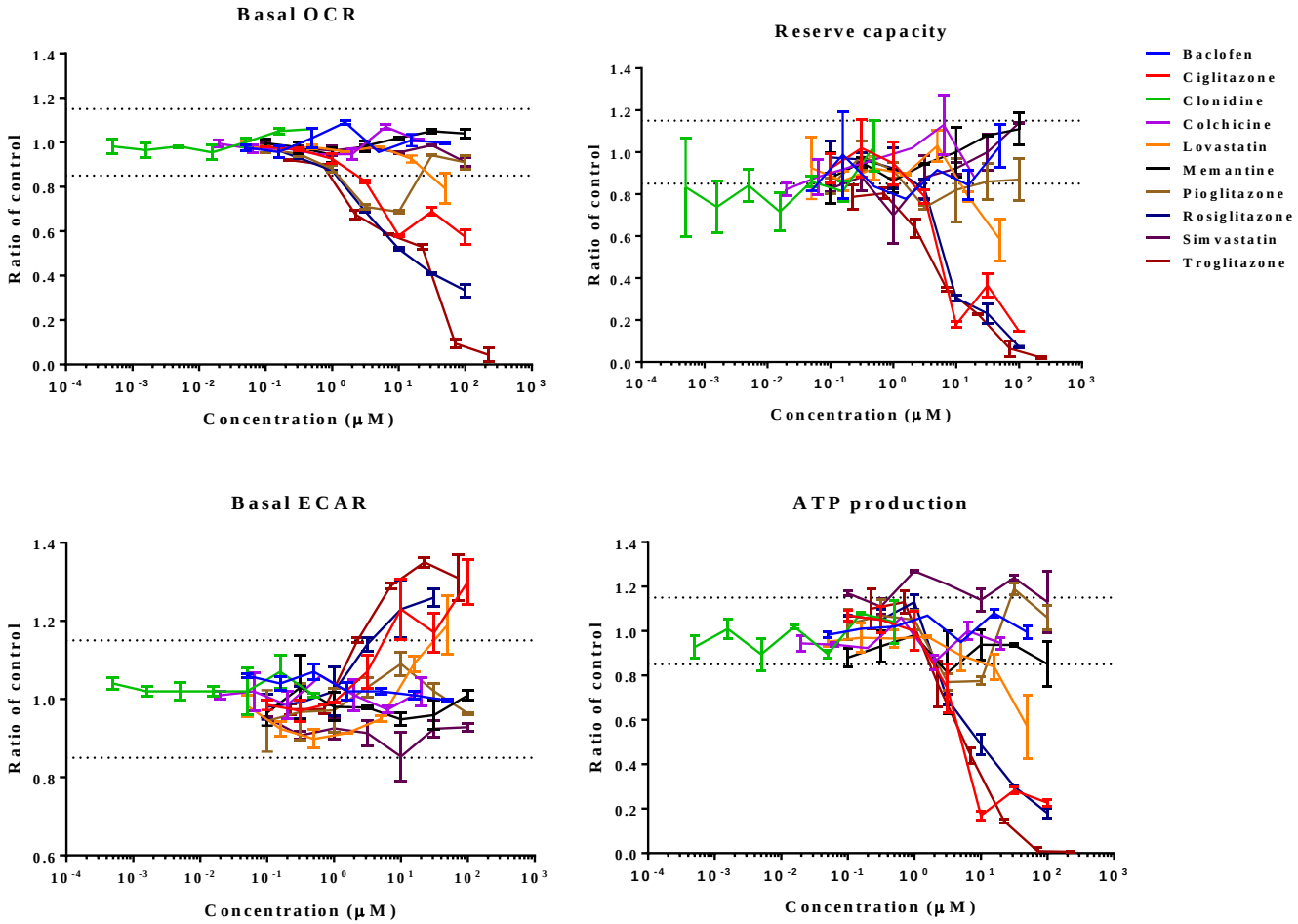

Figure 5.3. Bioenergetic profile of baclofen, ciglitazone, clonidine, colchicine, lovastatin, memantine, pioglitazone, rosiglitazone, simvastatin and troglitazone using the Extracellular Flux Analyser. Dose-response curves show the effects of compounds in basal OCR, reserve capacity, basal ECAR and ATP production in 10 mM glucose, 1 mM pyruvate and 2 mM glutamine. Data is expressed as mean ratio to vehicle control ± SD of n = 3. Dashed lines represent significant cut-off from vehicle control.

5.3.4. Measurement of Respiratory Activity using Permeabilised Cells with rPFO

The use of permeabilised HepG2 cells allowed further analysis of the mode of action of compounds that showed an effect on the acute extracellular flux assay (AEFA), particularly those classified as ETC inhibitors, since it can assess the effects of the compounds on the function of different ETC complexes, based on the recovery of mitochondrial function in the presence of a specific inhibitor. Nonetheless, one limitation of the assay is that it is not possible to discriminate between direct ETC complex inhibition and inhibition of substrate transport/metabolization mediated by other enzymes such as the pyruvate dehydrogenase, the mitochondrial pyruvate carrier or the mitochondrial dicarboxylate carrier due to the nature of the endpoint being measured (basal OCR).

Figure 5.4 shows that in HepG2-permeabilised cells, all drugs but ciglitazone, lovastatin, pioglitazone and warfarin, decreased complex I-linked respiration in a dose-dependent manner. Comparison of the MEC values with C_{max} values indicates that acetaminophen, bezafibrate and sulfasalazine reduce respiration at supra-therapeutic concentrations, whereas rosiglitazone and troglitazone may reduce respiration at therapeutic concentrations (Table 5.4). Except for salicylic acid, mitochondrial respiration was restored upon addition to the media of complex II substrate succinate, indicating that these compounds act either as complex I inhibitors or inhibitors of NADH-linked substrates. Salicylic acid decreased complex II-linked respiration, which was restored upon addition of complex IV electron donors ascorbate/TMPD, suggesting it may be a complex III inhibitor. Ciglitazone showed no decrease in respiration, instead a concentration-dependent increase in ascorbate/TMPD respiration was observed. Finally, even though lovastatin was classified as an ETC inhibitor in the acute extracellular flux assay (AEFA) (Table 5.2), here it did not show a significant response, making it impossible to pinpoint a precise site of action. Table 5.4 shows a summary of these results indicating the most prominent mode of mitochondrial action for each compound.

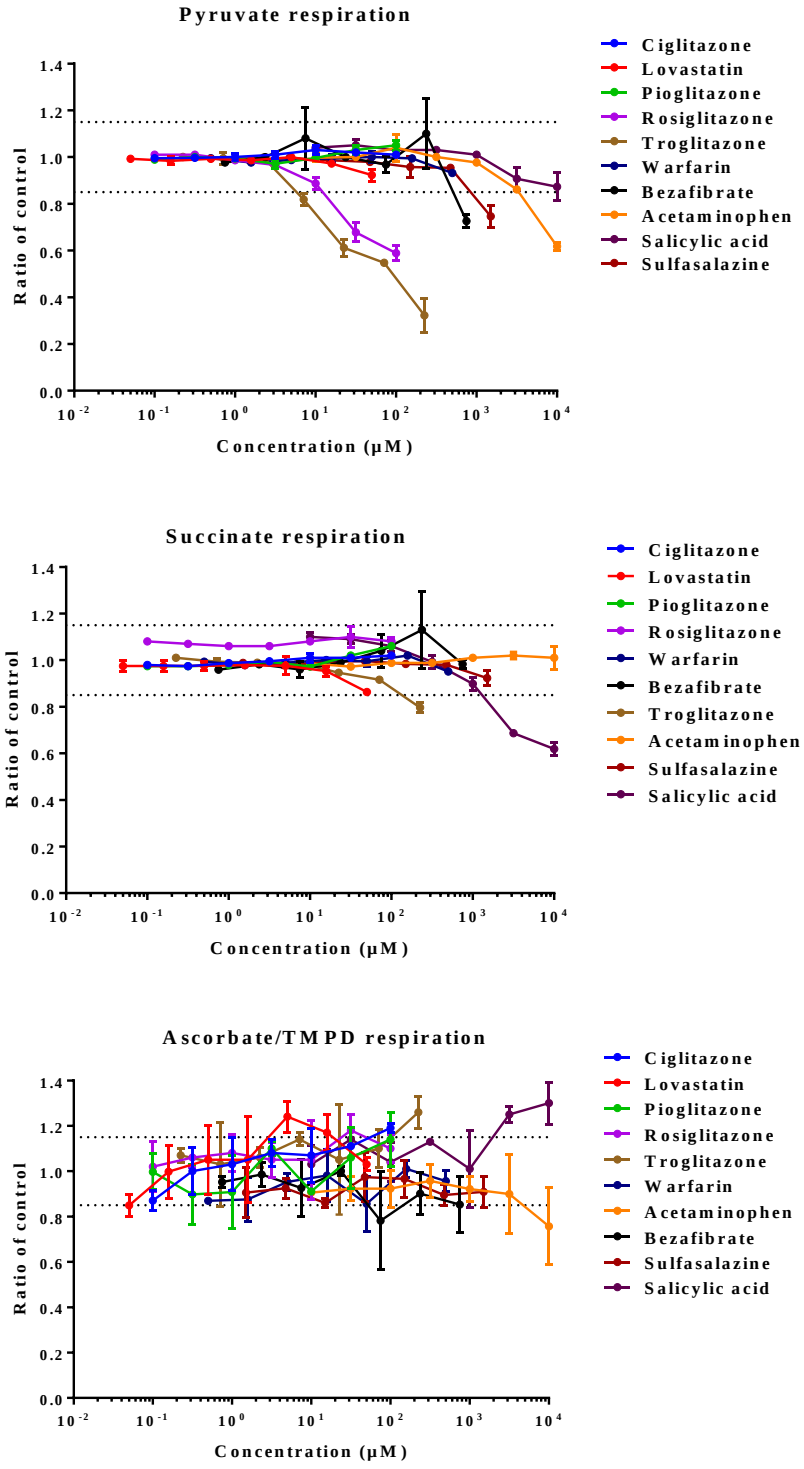

Figure 5.4. Dose-response curves of compounds tested in complex I-linked respiration (pyruvate respiration), complex II-linked respiration (succinate respiration) and complex IV respiration (ascorbate+TMPD) in HepG2 cells permeabilised with rPFO. Data is expressed as mean ratio to vehicle control ± SD of n = 3. Black dashed lines represent significant cut-off from vehicle control.

Table 5.4. Most sensitive mechanism of action of compounds on mitochondrial function using HepG2 cells permeabilised with rPFO. ↑↓ = Direction of change of mitochondrial respiration, where: ↑ = increase compared to vehicle control, ↓= decrease compared to vehicle control, NR = no response compared to vehicle control. MEC = minimum effective concentration that significantly crosses vehicle control threshold. AC_{50} = the concentration at which 50% maximum effect is observed.

Compounds	Most sensitive mechanism	↑↓	MEC (μM)	AC_{50} (μM)
Acetaminophen	pyruvate respiration	↓	3600	>10000
Bezafibrate	pyruvate respiration	↓	655	>750
Ciglitazone	ascorbate respiration	↑	53.8	>100
Lovastatin	NR	NR	NR	NR
Pioglitazone	NR	NR	NR	NR
Rosiglitazone	pyruvate respiration	↓	12	>100
Salicylic acid	succinate respiration	↓	1670	>10000
Sulfasalazine	pyruvate respiration	↓	1020	>1500
Troglitazone	pyruvate respiration	↓	6.1	66
Warfarin	NR	NR	NR	NR

5.3.5. Measurement of Cytotoxicity in HepG2 Cells grown in either Glucose or Galactose to Identify Mitochondrial Toxicants (Glu/Gal assay)

Drug-induced mitochondrial toxicity was assessed in HepG2 cells cultured in galactose or glucose containing media (Glu/Gal assay). The Glu/Gal assay is a commonly used *in vitro* assay that was developed to increase the detection of deleterious mitochondrial effects of xenobiotics and drugs that are often missed using glycolytic cells. In this assay, HepG2 cells in galactose media are forced to rely mainly on OXPHOS rather than glycolysis for energy production by substituting galactose (Gal) for glucose (Glu) in the growth media. The main route of galactose metabolism – the Leloir pathway – results in the conversion of galactose into glucose-1-phosphate, which can enter the glycolytic pathway[264]. However, the cost of an additional ATP consumption in this pathway renders glycolysis less efficient, demanding a higher mitochondrial activity, which increases the susceptibility of the cells to mitochondrial toxicants.

To this end, cellular ATP levels were measured after 24 h compound treatment to determine cell viability in either media conditions. Antimycin A and rotenone, classic mitochondrial toxicants with well-defined mitochondrial targets, were used as positive controls, whereas digitonin, a non-mitochondrial targeted cytotoxic detergent, was used as a negative control (Figure 5.5 and Table 5.5).

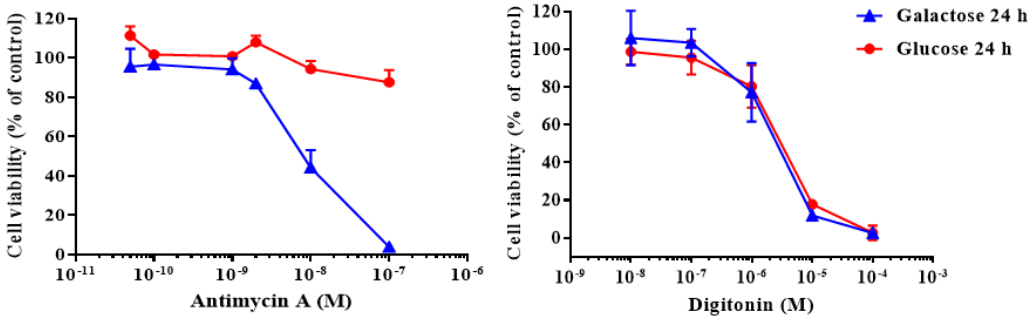

Figure 5.5. The effect of antimycin A and digitonin on HepG2 cells cytotoxicity compared to the vehicle control after 24 h incubation either in 10 mM glucose or 10 mM galactose media. Values are expressed as percentage of those of the vehicle control ± S.D. (n = 2). Dashed lines represent significant cut-off from vehicle control.

The Crabtree effect is an adaptation of highly proliferative cells grown in high glucose media that allows them to generate almost all ATP via glycolysis despite abundant O_2 and functional mitochondria[58]. Figure 5.5 clearly shows this phenomenon, where HepG2 cells grown in the presence of glucose become resistant to antimycin A. By replacing glucose in the growth media with galactose, HepG2 cells are forced to rely on mitochondrial OXPHOS rather than glycolysis. Under these conditions, antimycin A leads to a dramatic reduction in cell viability due to inhibition of mitochondrial respiration. On the contrary, HepG2 cells treated with digitonin were equally susceptible in both glucose and galactose-conditioned media, which indicates that toxicity is due to other mechanisms rather than mitochondrial impairment.

The fact that HepG2 cells derive most of their energy from glycolysis rather than mitochondrial OXPHOS despite having functionally competent mitochondria was further investigated using confocal microscopy. According to Marroquin *et al.*, HepG2 cells grown in galactose media increase mitochondrial respiration rates to generate sufficient ATP for survival[58]. This was confirmed with the images obtained, where 24 h glucose deprivation resulted in an increased mitochondrial activity as assessed by an increased fluorescence signal using MitoTracker™ Red CMXROS (Figure 5.6).

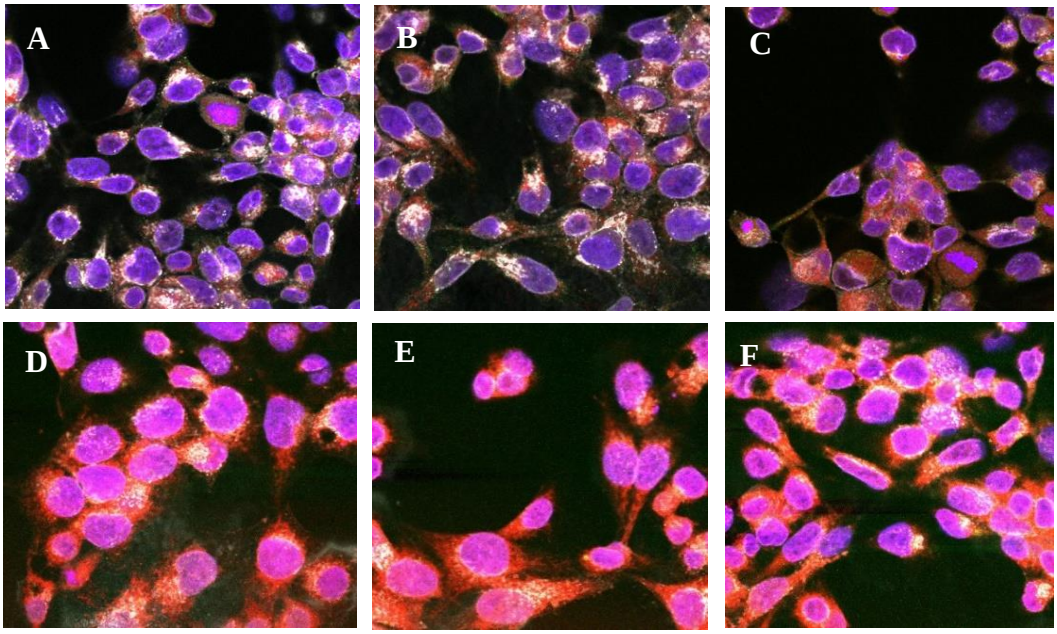

Figure 5.6. Confocal microscopy of HepG2 cells grown in 25 mM glucose media (A, B, C) vs. HepG2 cells grown in 10 mM galactose media after 24 h glucose withdrawal (D, E, F). Mitochondria stained with MitoTracker™ Red CMXROS (red), nuclei stained with Hoescht (blue) and plasma membrane stained with WGA (white).

The total of 16 compounds included in this study (Table 5.1) were evaluated with this assay, despite the absence of effects in the acute extracellular flux assay (AEFA) (Table 5.2). Within this assay, compounds are incubated for 24 hours, which may increase the susceptibility of the cells, and in some cases, reveal unobserved effects in acute treatments. This was the case for metformin, which showed no real-time changes in basal OCR or ECAR under acute treatment, however, in this assay metformin caused a >2.4-fold shift of the dose-response curves (Figure 5.7). According to Eakins *et al*., a ≥3-fold shift in AC_{50} values provides the most predictive cut-off for identifying the mitochondrial toxicants, with a sensitivity of 51%, specificity of 97% and an overall accuracy of 72%[136].

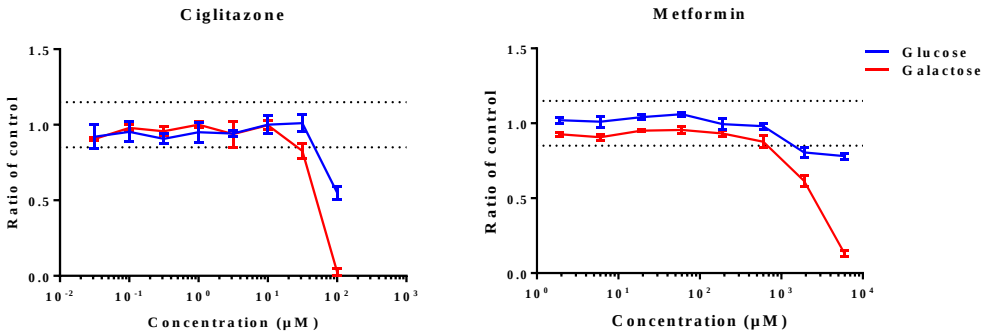

Figure 5.7. The effect of ciglitazone and metformin on HepG2 cells cytotoxicity after 24h incubation either in 10 mM glucose or 10 mM galactose media. Data is expressed as mean ratio to vehicle control ± S.D. (n = 3). Dashed lines represent significant cut-off from vehicle control.

A summary of the AC_{50} values and fold shifts is shown in Table 5.5. In some cases, fold change could not be determined due to insufficient response to calculate AC_{50} values. As in the AEFA (section 5.3.3), compounds baclofen, clonidine, colchicine and memantine showed no response. The only two compounds of the data set that showed a marked difference in cell viability between the two conditioned-media were ciglitazone (Gal MEC = 32 µM; Glu MEC = 70 µM) and metformin (Gal MEC = 852 µM; Glu MEC = 2450 µM) as shown in Figure 5.7. However, it should be noted that although this assay has a specificity of almost 100% (according to Eakins *et al.*[136]), its sensitivity is very low, meaning that it will often fail to detect true mitochondrial toxicants (high rates of false negatives). Out of 9 compounds with potential mitochondrial toxicity identified by the AEFA, three of the thiazolidinediones (pioglitazone, rosiglitazone and troglitazone), acetaminophen, bezafibrate, lovastatin, salicylic acid and warfarin have not been picked in this assay. However, it must be noted that among these compounds, only some had detectable AC_{50} values for OCR reduction: thiazolidinediones with an AC_{50}<50 µM and acetaminophen and salicylic acid with AC_{50} values in the mM range.

A possible explanation for the low sensitivity of this assay could be down to cytotoxicity. Swiss *et al.*[265] and Eakins *et al.*[136], both identified troglitazone as a cytotoxic compound rather than a mitochondrial toxicant, despite its known effects on mitochondria *in vivo*[136]. Another explanation could be low availability of the free

form of highly protein-bound compounds. This may be the case for the thiazolidinediones due to their high plasma protein bindings (Table 5.5).

Table 5.5. Summary table of the Glu/Gal assay including compounds tested and positive control rotenone. ↑↓ = Direction of change of cell viability, where: ↓ = decrease compared to vehicle control, NR = no response compared to vehicle control. AC_{50} = the concentration at which 50% maximum effect is observed. UD = undetermined mitochondrial toxicity. N/A = not available. Fold change = Glu AC_{50}/Gal AC_{50}. Protein binding values were retrieved from DrugBank[266].

Compounds	↑↓	Glucose AC_{50} (μM)	↑↓	Galactose AC_{50} (μM)	Fold Change	Protein binding (%)
Acetaminophen	NR	NR	↓	>10000	UD	10-25
Baclofen	NR	NR	NR	NR	NR	30
Bezafibrate	NR	NR	NR	NR	NR	94-96
Ciglitazone	↓	>100	↓	46.3	>2.16	N/A
Clonidine	NR	NR	NR	NR	NR	20-40
Colchicine	NR	NR	NR	NR	NR	40
Lovastatin	↓	43.2	↓	>50	UD	>95
Memantine	NR	NR	NR	NR	NR	45
Metformin	↓	>6000	↓	2510	>2.39	Negligible
Pioglitazone	NR	NR	NR	NR	NR	>99
Rosiglitazone	NR	NR	NR	NR	NR	99.8
Salicylic acid	↓	4630	↓	5830	0.794	N/A
Simvastatin	↓	>100	NR	NR	UD	95
Sulfasalazine	↓	1230	↓	1240	0.992	N/A
Troglitazone	↓	115	↓	103	1.12	>99
Warfarin	NR	NR	NR	NR	NR	99
Rotenone	↓	27.8	↓	0.00605	4600	N/A

5.3.6. Measurement of Activities of Individual Respiratory Complexes using Isolated Mitochondria

A total of 12 medical drugs were selected for the measurement of inhibitory potency against the succinate-cytochrome *c* reductase (SCR). The aims of this assay were to compare the results with those obtained using whole cells, to gain insight into the mechanisms of action, assess accuracy of various *in vitro* methods in identifying mitochondrial toxicants and, finally, to obtain valuable data for QSAR studies. To this end, a minimum of three biological samples of rat liver mitochondria were used for the calculation of IC_{50} values, as outlined in Materials and Methods 2.4.4. The generation of consistently measured IC_{50} values using this assay provided valuable data for QSAR studies performed in chapter 7. Although CNS drugs, chlorpromazine, haloperidol and valproic acid are not part of the data set contemplated in this chapter, the results obtained for these compounds were included here for convenience and will be further discussed in chapter 6.

The low throughput of this assay only allowed the study of a few compounds out of the total data set. These are either amongst the top most prescribed drugs in the world[267] (acetaminophen, warfarin, sulfasalazine), have been withdrawn from the market due to unacceptable risk of toxicities[268] (ciglitazone, troglitazone) or have been reported to have a mitochondrial effect before (simvastatin, lovastatin, salicylic acid, bezafibrate). In addition, compounds were selected considering a wide structural diversity for QSAR purposes.

IC_{50} values for SCR activity were determined for all compounds as shown in Figure 5.8, except for acetaminophen (IC_{50} > 5000 µM), haloperidol (IC_{50} > 600 µM) and valproic acid (IC_{50} > 6600 µM) due to solubility limitations not allowing higher concentrations to be tested. The two statins studied here, simvastatin and lovastatin, showed inhibitory activity in the micromolar range. Simvastatin showed a greater inhibitory activity (IC_{50} = 11 ± 1 µM) than lovastatin (IC_{50} = 35 ± 3 µM), which is in agreement with the rank order of potency reported by Nadanaciva *et al.*[85], where complex II+III IC_{50} values were 28 ± 1 µM for simvastatin and 57.2 ± 3 µM for lovastatin in a similar assay using bovine heart mitochondria. The two thiazolidinediones tested, ciglitazone and troglitazone, caused 50% inhibition of complex II+III at 3.4 ± 1 µM and 19 ± 5 µM, respectively. In this case, the order of potency does not correlate with studies done by Nadanaciva *et al.*[85], where IC_{50}

values were 60 ± 1 µM for ciglitazone and 30 ± 1 µM for troglitazone. Bezafibrate was the only fibrate tested here. IC_{50} value for bezafibrate was 920 ± 304 µM. The top concentration tested by Nadanaciva *et al.*[85] for bezafibrate was 500 µM and no inhibition of complex II+III was reported at such concentration. IC_{50} values obtained here for chlorpromazine, salicylic acid, sulfasalazine and warfarin were 194 ± 67 µM, 2476 ± 475 µM, 709 ± 130 µM and 1359 ± 358 µM, respectively.

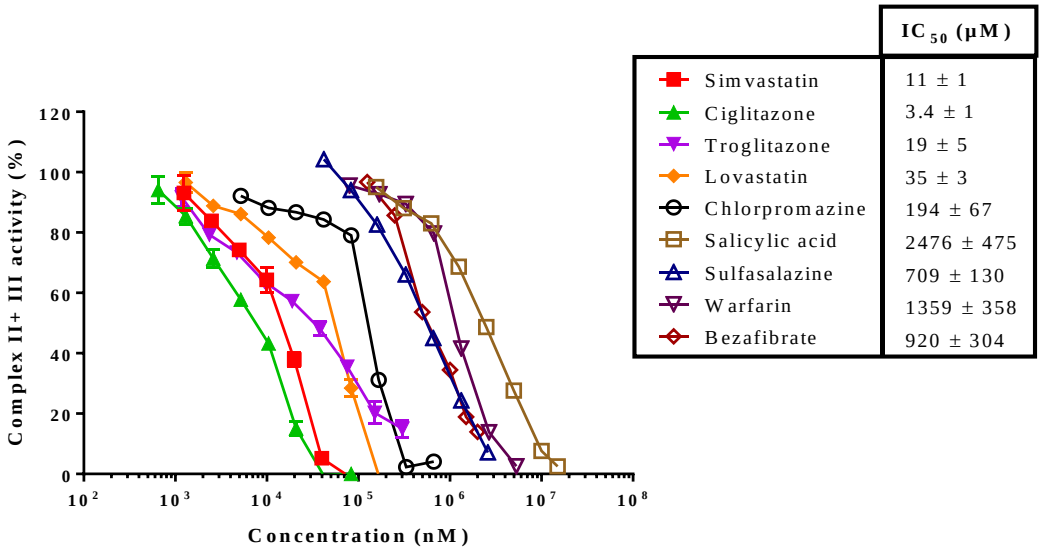

Figure 5.8. Representative dose-response curves for the pharmaceutical drugs tested and SCR IC_{50} values of compounds. Table: IC_{50} values are a mean average of 3 replicates ± SEM. Graph: Complex II+III activity is the percentage activity normalised to controls as outlined in Materials and Methods section 2.4.1.

In order to ascertain whether the test compounds were selectively inhibiting complex II or complex III, the activity towards each complex was assayed separately as outlined in Materials and Methods sections 2.4.2 and 2.4.3. Figure 5.9 shows the enzyme activities of both mitochondrial complexes compared to the vehicle control (0.6% DMSO) in response to drug exposure at the IC_{50} concentrations determined by the SCR assay. Atovaquone, an analogue of ubiquinone, was used as a positive control, as it selectively inhibits the cytochrome bc_1 complex[269]. At its IC_{50} value (200 nM, determined in chapter 4), atovaquone caused little inhibition of complex II activity, however it caused a significant inhibition of complex III (Figure 5.9). Lovastatin, chlorpromazine, bezafibrate and ciglitazone also showed greater inhibition against complex III. Warfarin and salicylic acid showed similar inhibition against both complex II and complex III, suggesting low specificity for either

complex. Nevertheless, direct inhibition of complex III by salicylic acid has been previously reported[270]. Inhibition of complex II but not complex III by sulfasalazine was observed. Simvastatin and troglitazone showed no inhibition against either complex II or complex III, which suggests that they may be acting as quinol competitive antagonists, i.e. they compete with endogenous ligand ubiquinol at the binding site. Consequently, high concentrations of quinol in the assays lead to no inhibition by such compounds.

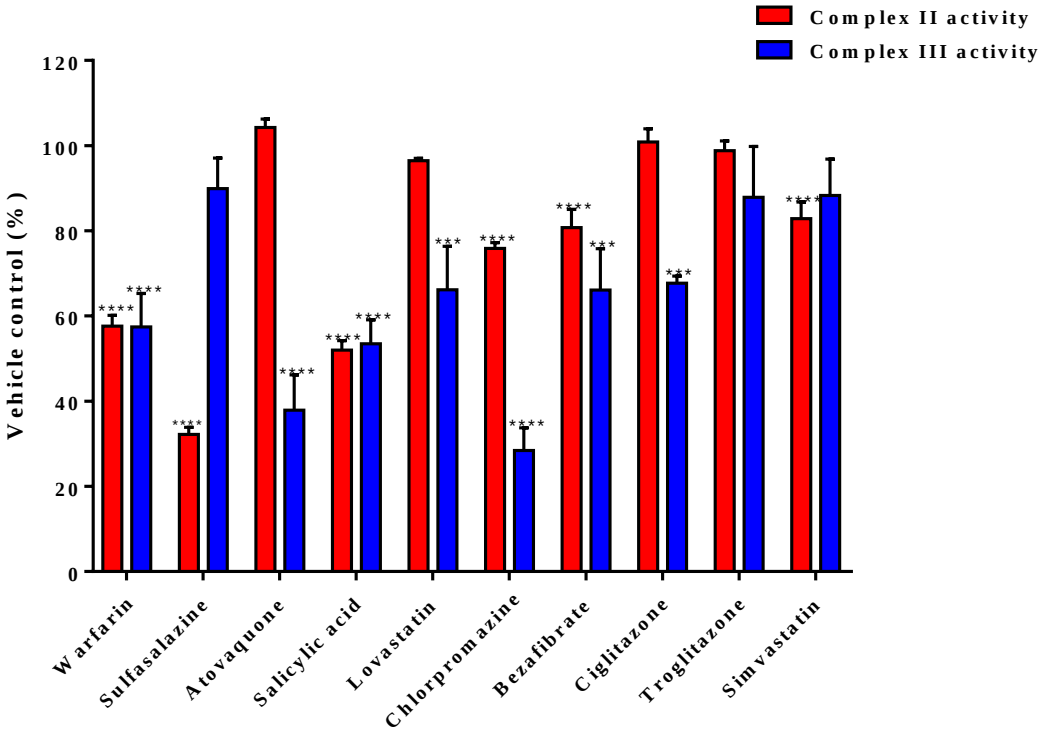

Figure 5.9. Effect of the IC_{50} concentrations obtained in the SCR activity assay of 10 pharmaceutical drugs on either complex II or complex III activity. Data are expressed as mean ± SD (n = 3) of the normalised values with the 100% activity (the activity of the uninhibited enzyme) and 0% activity (obtained with 5 mM malonate for complex II activity and 0.6 µM antimycin A for complex III activity). Statistically significant values compared with the control are reported as follows: ***: for $p \leq 0.001$ and ****: for $p \leq 0.0001$.

Given the increasing number of medical drugs that have been reported to target complex I, different protocols were set up to spectrophotometrically measure enzymatic activity of complex I. The assay was performed by monitoring NADH oxidation (600 µM) through the decrease in absorbance at 340 nm using isolated rat liver mitochondria (10 to 20 µg/ml) that had been sonicated according to Long *et al.*[271] and subjected to at least three freezing-thawing cycles to achieve

permeabilization to NADH[272]. Different electron acceptors were used in the enzymatic reaction, such as DCPIP (450 µM)[271], UQ_2 (50 µM) or UQ_1 (50 µM)[272] and the reaction was always performed in the presence of 2 µM antimycin A and 1 mM KCN to avoid electron flow through complex III and IV. The assay medium was the same used for the SCR assay. Investigation of complex I activity was difficult to perform and was considerably hampered by the lack of inhibition by 2 µM rotenone (likely due to the high rotenone-insensitive activity of the NADH-dehydrogenase present in the outer mitochondrial membrane of the rat liver)[272]. Numerous attempts were performed to try and overcome this issue, such as inhibition of the NADH-dehydrogenase on the outer membrane with 500 µM dicoumarol[273] or the use of hypotonic buffers (assay buffer diluted 10 times in water) followed by high-speed centrifugation of mitochondrial fractions to achieve disruption of the outer membrane, all without success, as rotenone insensitive respiration was still observed.

5.3.7. Combined Determination of Oxygen Consumption and Mitochondrial Membrane Potential in Rat Liver Mitochondria

Upon initial calibration with 2 µM safranin, rat liver mitochondria, 1 µM rotenone and 12.5 mM succinate were added to the Oroboros® Oxygraph-2K chambers to induce complex II-linked OXPHOS. Then, pharmaceutical drugs were subsequently added to the chambers to investigate their effects on oxygen consumption (OCR) and mitochondrial membrane potential (MMP) simultaneously. Changes in OCR were normalised to the baseline and were displayed as a percentage, with the control (no drug) having a 100% OCR. Changes in fluorescence signal, corresponding to MMP, were normalised within a maximum fluorescence (which corresponds to the basal signal elicited upon addition of rat liver mitochondria) and a minimum (which corresponds to the fluorescence signal upon addition of succinate). A 100% MMP generation was therefore established for the distance between basal signal and succinate signal, and the proportional dissipation of that percentage by the addition of drugs is shown in Table 5.6.

A total of 7 drugs were selected to be investigated with this assay. This assay has very low through-put because: 1) it uses freshly isolated mitochondrial preparations, 2) the Oroboros® Oxygraph-2K has only two chambers per instrument, 3) for statistical analyses purposes, experiments had to be repeated using different mitochondrial preparations, 4) each independent experiment had to be performed

quickly to avoid running out of oxygen once the chambers were closed and mitochondria started respiring, and 5) freshly isolated mitochondria could only be used for a few hours in order to keep their physiological properties. Therefore, a selection of compounds with questionable modes of action from the previous sets of assays were selected to be studied here.

All drugs tested caused a significant dissipation of the MMP to different extents, except for bezafibrate (at 450 and 750 μM) and simvastatin (at 12 μM). However, not all showed the same effects on respiration. In fact, most of the drugs increased basal respiration, showing an OXPHOS uncoupling activity, except for bezafibrate, which inhibited respiration, and simvastatin, which caused no changes in respiration rate at the concentration tested. Troglitazone dissipated the membrane potential to 36% and increased respiration to around 200% at a concentration around four times its C_{max} (C_{max} = 6.4 μM)[274]. In the case of ciglitazone, an OXPHOS uncoupling activity was observed with subsequent inhibition of respiration as concentrations increased further from 11 to 16 μM (Table 5.6). Hence, these results suggest that once the maximal response is reached, higher concentrations become acutely toxic to cells, resulting in decreased OCR. This dual effect of ciglitazone drugs on OXPHOS (i.e. uncoupling followed by inhibition) seems to be concentration-dependent and uncoupling is only observed at low concentrations. This behaviour has been described before with other pharmaceutical drugs, such as amiodarone, perhexiline, alpidem, tamoxifen and buprenorphine[275-278].

Table 5.6. Concentration of compounds tested and effect on the MMP and OCR in isolated rat liver mitochondria (basal respiration). Data are mean ± SD of n = 2-10 (biological repeats). *p<0.05, **p<0.01, ***p<0.001, ****p<0.0001 vs. control (baseline).

Drug	Concentration (µM)	% MMP	% OCR
Bezafibrate	450	100 ± 0.9	****87 ± 2.7
	750	99.5 ± 2.9	****76 ± 7.8
Ciglitazone	3	****61 ± 3.4	***170 ± 10.6
	6	****37 ± 2.7	****200 ± 13.7
	11	****14 ± 0.01	****248 ± 3
	16	****-1.82 ± 3.4	****224 ± 15.2
Lovastatin	45	*61 ± 23.5	110 ± 7
Salicylic acid	2500	*37 ± 10.4	*144 ± 16.7
Simvastatin	12	95 ± 2.3	97 ± 6.4
Troglitazone	22.5	***36 ± 1.8	*204 ± 30
Warfarin	1100	***34 ± 2.1	**168 ± 11.9

5.3.8. Combined Determination of Oxygen Consumption and Reactive Oxygen Species Production in Rat Liver Mitochondria

The simultaneous effects of the pharmaceutical drugs on uncoupled respiration and ROS production were studied using the Oroboros® Oxygraph-2K. Mitochondrial respiration was initiated by addition of 12.5 mM succinate (in the presence of 1 µM rotenone) and stimulated with the classic uncoupler CCCP (0.25 µM). Therefore, mitochondrial oxygen consumption measurements were performed in uncoupled complex II-linked respiration.

Here, the effects on respiration by some of the drugs differed with results previously obtained in basal respiration (section 5.3.7). For instance, in basal respiration, 11 µM ciglitazone increased respiration to around 250% (Table 5.6), whereas in uncoupled respiration ciglitazone decreased respiration to 43% (Table 5.7). This leads to the conclusion that the dual activity of drugs can be attributed not only to the concentration, but also to the mitochondrial state. A similar behaviour was observed with salicylic acid (SA), whose dual activity on the ETC has been reported before[279, 280]. In basal respiration, 2.5 mM SA markedly increased OCR to 144% (Table 5.6), while in uncoupled respiration it significantly decreased OCR to 38% (Table 5.7).

The effects of higher concentrations than 2.5 mM of SA were not tested for basal respiration, therefore a concentration-dependent activity cannot be ruled out. In fact, it has been reported in the literature that at high concentrations (5 mM) SA can inhibit respiration by preventing electron flow from the substrate dehydrogenases to the UQ pool[280]. This hypothesis has been proposed due to the phenolic nature of SA, which could act as a quinone analogue at millimolar concentrations, preventing the interaction between the dehydrogenases and the UQ pool[280]. Nevertheless, results suggest that in isolated mitochondria, SA can act as both an uncoupler and an inhibitor depending on the respiration state. Other compounds that showed dual effects included lovastatin, troglitazone and warfarin. Due to technical issues, a direct comparison of the effect of troglitazone and simvastation between the two mitochondrial states could not be made, as concentrations tested in uncoupled respiration were much higher than those in basal respiration experiments. Therefore, conclusions cannot be made as to whether the uncoupling effect is attributable to the higher concentrations or to the mitochondrial state. On the other hand, the opposite effects of warfarin on respiration were clearly determined by the mitochondrial state. Similar to ciglitazone and SA, in basal respiration warfarin (1.1 mM) increased respiration to 168% (Table 5.6), whereas, in uncoupled respiration, 1.1 mM warfarin inhibited respiration to 58% (Table 5.7). Finally, bezafibrate was the only compound that showed an inhibitory effect in both coupled and uncoupled mitochondria. Simultaneous evaluation of the effects of sulfasalazine on MMP and basal respiration was not possible due to interactions of this drug with the fluorescent sensors. However, sulfasalazine effects were assessed here, and results indicate that, in uncoupled respiration, sulfasalazine decreases OCR and ROS production at concentrations ranging from 200-1700 µM (Table 5.7).

With regards to ROS production, drugs could be divided into two groups: those that increased ROS production along with a simultaneous decrease in OCR in a concentration-dependent manner (ciglitazone, lovastatin, simvastatin, troglitazone), and those that simultaneously decreased ROS production and OCR (bezafibrate, sulfasalazine and warfarin) (Table 5.7). Since complex II-linked respiration was measured in the presence of rotenone, the phenomenon of RET could not take place, as established during control experiments in chapter 4 (see section 4.3.1.2). Hence, in the forward direction of electron transfer, CoQ is reduced by complex II and,

during this process, the flavin site in complex II (II_F) and the ubiquinol-oxidising site in complex III (III_{Qo}) probably account for most of the mitochondrial ROS production[116]. It has been observed that if compounds act downstream of a given electron leak site, they lead to reduction of the site and increased electron leak, whereas if they act upstream, due to the absence of reduced electron donors, they lead to oxidation of the site and less electron leak[116]. Hence, based on the results obtained, lovastatin, simvastatin and troglitazone may inhibit complex III, causing the observed increase in ROS production. On the other hand, bezafibrate, sulfasalazine and warfarin may either inhibit complex II or act as ROS scavengers, since they cause a decrease in ROS production in a dose-dependent manner (Table 5.7). Ciglitazone showed a variable behaviour in terms of the effect on ROS production. At 3 and 7 μM, it reduced ROS, while at 11 μM, ROS production increased slightly.

Table 5.7. Concentrations of compounds tested and the effect on ROS production and OCR in isolated rat liver mitochondria (uncoupled succinate-respiration). Data are mean ± SD of n = 2-10. *p<0.05, **p<0.01, ***p<0.001, ****p<0.0001 vs. control (baseline).

Drug	Concentration (µM)	% ROS	% OCR
Bezafibrate	250	**72 ± 5	94 ± 0.3
	450	**66 ± 10	*87 ± 1.1
	750	**64 ± 9.6	**77 ± 5
Ciglitazone	3	****72 ± 2.8	90 ± 3.5
	7	****64 ± 2	**73 ± 2.6
	11	**89 ± 3	****43 ± 14
Lovastatin	25	90 ± 10	*82 ± 8.2
	45	*127 ± 22	***71 ± 6.1
Salicylic acid	2500	**56 ± 13.8	****38 ± 5
	5000	***33.7 ± 13.3	****22 ± 5.5
	7500	****23.8 ± 11.1	****14 ± 2.1
	10000	****17.2 ± 13	****6 ± 1.6
Simvastatin	36	**137 ± 6.7	*83 ± 6
	60	**146 ± 16.5	**74 ± 10.2
	132	****190 ± 8.6	***65 ± 11
	252	****235 ± 7.5	****52 ± 8
Sulfasalazine	200	****54 ± 4.6	*81 ± 5.2
	400	****40 ± 3	**65 ± 3.4
	700	****31 ± 4.5	***47 ± 4
	1100	****27 ± 7	****30 ± 8
	1700	****16 ±8	****12 ± 6
Troglitazone	90	**123 ± 3	****21 ± 0.4
	112	****262 ± 5.1	****3.8 ± 1.3
Warfarin	400		*84 ± 4.5
	1100	***58 ± 6.2	****57 ± 9.6
	2100	****54 ± 7.6	****30 ± 11
	3100	****53 ± 10	****16 ± 3.6
	4600	****49 ± 5.4	****10 ± 1.8

5.3.9. Molecular Docking

Molecular docking was performed to computationally evaluate the binding affinities of the 16 pharmaceutical drugs to the different ETC complexes (complex I-IV) and the ATP synthase (complex V). All 3D structures of compounds were built from their SMILES codes using the MOE-Builder tool[204], then all molecules were subjected to energy minimisation as explained in Materials and Methods 2.11.1.2. Binding pockets were defined as outlined in Materials and Methods 2.11.2. In the case of complex III, the Q_o site was the chosen binding pocket. All crystal structures used were from a mammalian source and were of a reasonable resolution (i.e. below 3 Å) (Table 5.8). Complex I presented the lowest resolution (3.7 Å), however it was the only human structure available on PDB at a resolution less than 4 Å at the time of writing.

The co-crystallized ligands of each complex (except for complex I, which lacked one) were redocked into their respective binding sites to analyse the root mean square deviation (RMSD) in order to validate the reliability of the docking calculations. RMSD values obtained were lower than 2 Å in all cases, indicating acceptable accuracy of the docking procedure (Table 5.8).

Table 5.8. PDB entries, resolution of ETC complexes and ATP synthase and RMSD values of co-crystallised ligands.

PDB entry	Complex	Resolution (Å)	Organism	Re-docked ligand	RMSD (Å) co-crystallised ligand
5XTD	I	3.7	*Homo sapiens*	-	-
3SFD	II	2.6	*Sus scrofa*	Pentachlorophenol	0.32
1PPJ	III	2.1	*Bos Taurus*	Stigmatellin	1.5
5ZCP	IV	1.65	*Bos Taurus*	Azide	0.75
2JIZ	V	2.3	*Bos Taurus*	Resveratrol	0.22

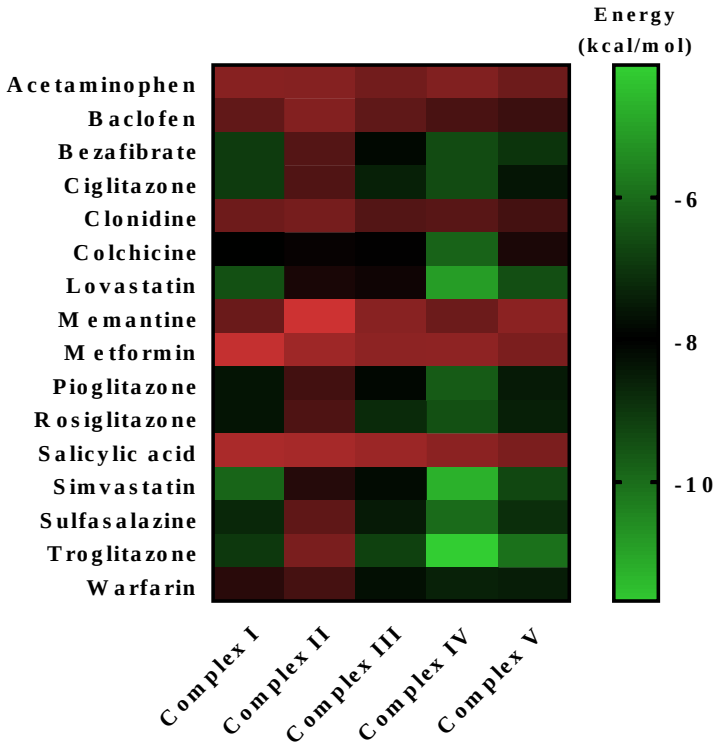

Figure 5.10. Top docking scores of the compounds against the ETC complexes (complex I-IV) and ATP synthase (complex V) presented on a heat map.

Upon confirmation of validity of the docking methodology, the 16 compounds were subsequently docked into the binding pockets of each ETC complex and ATP synthase (complex V) and the top scores were collected. Table 5.9 shows the highest and lowest docking score for each drug.

Figure 5.10 shows a heat map assembled from the top docking scores for each complex. Qualitatively speaking, there is an appreciable correlation between the docking results and the OCR results obtained through the acute extracellular flux assay (Table 5.3). A majority of compounds (8 out of 10 compounds) that showed no response or a mild response only at high concentrations (acetaminophen, baclofen, clonidine, colchicine, memantine, metformin, salicylic acid and warfarin) also had the least negative docking scores indicating low affinity (sulfasalazine and simvastatin were exceptions of this). On the other hand, compounds that reduced OCR in the micromolar range, such as bezafibrate (AC_{50} = 750 µM), ciglitazone,

(AC_{50} = 18.7 µM), lovastatin (AC_{50} = 50 µM), pioglitazone (AC_{50} = 41.6 µM), rosiglitazone (AC_{50} = 15.9 µM) and troglitazone (AC_{50} = 11.8 µM) (Table 5.3) generally showed the lowest docking scores that can be seen in the heatmap, indicating highly favourable binding. The best docking scores were observed for lovastatin (-10.79 kcal/mol for complex IV), simvastatin (-9.77 kcal/mol for complex I and -11.16 kcal/mol for complex IV), pioglitazone (-9.59 kcal/mol for complex IV), sulfasalazine (-9.87 kcal/mol for complex IV), troglitazone (-11.66 kcal/mol for complex IV and -9.98 kcal/mol for complex V) and colchicine (-9.72 kcal/mol for complex IV).

Based on the docking results, it is possible to classify compounds into OCR active and OCR inactive compounds. Weka was used to see if a decision tree could be developed to classify compounds based on the results from docking analysis. The decision tree method REPTree was used with minimum number of cases of 1. The model is shown in Figure 5.11. This decision tree correctly classified 13 out of 16 compounds (81.25%). In the model, 'scores' refers to docking top score against any of the ETC complexes, and 'Ratio of high/low score' is the top score (against any of the complexes) divided by the top score against the least favourable ETC complex (according to docking scores).

```
REPTree
============

scores < -9.73 : A (3/2) [1/0]
scores >= -9.73
|   scores < -7.67 : A (3/0) [3/1]
|   scores >= -7.67
|   |   scores < -6.37 : B (1/0) [1/0]
|   |   scores >= -6.37
|   |   |   Ratio of high/low score < 1.24 : A (2/0) [0/0]
|   |   |   Ratio of high/low score >= 1.24 : B (1/0) [1/0]
```

Figure 5.11. Decision tree based on REPTree to identify compounds that have been identified to reduce OCR in AEFA (class A) from those that showed no effect on OCR (class B).

Table 5.9. Highest and lowest docking scores for the compounds screened alongside OCR AC_{50} values from the AEFA.

Compound	Lowest/Highest scores (kcal/mol)	ETC complex	OCR AC_{50} values (μM) from the AEFA (Table 5.3)
Acetaminophen	-5.91	V	7440
	-5.43	I	
Baclofen	-6.83	V	NR
	-6.13	I	
Bezafibrate	-9.29	IV	>750
	-6.37	II	
Ciglitazone	-9.28	IV	18.7
	-6.45	II	
Clonidine	-6.67	V	NR
	-5.47	II	
Colchicine	-9.72	IV	NR
	-7.42	V	
Lovastatin	-10.79	IV	>50
	-7.46	II	
Memantine	-5.97	I	NR
	-4.14	II	
Metformin	-5.66	V	NR
	-4.32	I	
Pioglitazone	-9.59	IV	41.6
	-6.70	II	
Rosiglitazone	-9.37	IV	15.9
	-6.48	II	
Salicylic acid	-5.66	V	1820
	-4.80	I	
Simvastatin	-11.16	IV	NR
	-7.22	II	
Sulfasalazine	-9.87	IV	NR
	-6.17	II	
Troglitazone	-11.66	IV	11.8
	-5.67	II	
Warfarin	-8.51	IV	>500
	-6.64	II	

5.4. Discussion

In this study, the effects on mitochondrial bioenergetics of some antidiabetic, antihyperlipidemic and anti-inflammatory drugs, as well as other widely prescribed drugs, were investigated using rat liver isolated mitochondria and HepG2 cells. HepG2 cells are still the most widely used preclinical model for hepatotoxicity; their tumorigenic phenotype allows determining whether cytotoxicity is due to mitochondrial dysfunction using the technique of metabolic modification, an advantage that primary human hepatocytes lack[58, 140]. On the other hand, isolated mitochondria from hepatocytes have long been a model of choice for the study of drug-induced mitochondrial dysfunction due to the inability of many mitochondrial substrates to freely permeate the cell membrane[198]. The use of permeabilised cells overcomes the limitations associated with the use of isolated mitochondria and whole cell model systems, as this method allows the mitochondrial structure to remain intact and in its *in-situ* environment, thereby increasing physiological relevance while allowing mitochondrial access to a variety of substrates. Therefore, in order to correctly interpret the results obtained, chemical characteristics of compounds, as well as potential benefits and limitations of each model system, must be carefully considered.

The results obtained from the experimentations can help identify mechanism of mitochondrial effect of compounds at a molecular level. Hence, the next few paragraphs give an overview of the possible mechanisms of action, before discussing the results obtained for individual classes of drugs. Generally speaking, compounds that cause disruption of OXPHOS can be classified into two main categories: ETC inhibitors or uncouplers of the electrochemical potential gradient of protons across the IMM. In the cases where OXPHOS is uncoupled with no inhibition of the ETC proteins, ATP synthesis is hindered by the reduction of the electrochemical gradient. In the cases where the ETC proteins are inhibited but the mitochondria remain coupled, the electrochemical gradient is unable to form due to a reduction of protons pumping across the membrane. In addition to these two main mechanisms, compounds can also affect OXPHOS by acting as substrate inhibitors.

Uncouplers typically provoke a loss of mitochondrial $\Delta\Psi$, a reduction in mitochondrial ATP production and increased levels of substrate oxidation. Previous

research indicate that potent uncouplers show protonophoric activity and, generally speaking, are lipophilic weak acids (with a pKa in the range of 5-7) that possess an acid-dissociable group, such as phenolic –OH and anilino –NH groups[102, 281]. However, other chemical characteristics are commonly found in potent uncouplers, such as the presence of a bulky lipophilic group (-tert-butyl-, -Cl, -CF_3), which may help the molecule bind to the mitochondrial membrane and remain in the membrane, or the presence of a strong electron-withdrawing group (-CN, -NO_2, CF_3 or -$CH=C(CN)_2$), which could influence release or binding of H^+ to the acid-dissociable group[102]. The logarithm of the partition coefficient in the octanol-water system (log P) is used as an indicator of the lipophilic character of a molecule. QSAR studies have shown that compounds with low (-2 to 3.99) and very high (>6) log P values were less likely to have an effect on mitochondrial respiration, which could be partially attributed to low membrane permeability and accumulation in lipophilic membranes, in either case[282]. Compounds with a log P value ranging from 4 to 6, on the other hand, were more likely to alter mitochondrial respiration[282]. In the cytoplasm, these molecules may exist in their ionized anionic state, but become protonated upon reaching the IMS due to the high concentration of protons, losing their charge and becoming significantly more lipophilic. In this state, they can pass through the IMM via diffusion, and once in the matrix (where there is an increased alkaline environment), they deprotonate[70]. The proton re-entry mediated by these molecules effectively dissipates the mitochondrial $\Delta\Psi$, thereby inhibiting the ATP synthase through dissolution of its driving force.

ETC inhibitors interact with the respiratory chain complexes reducing the rate of proton pumping. Furthermore, ETC inhibition causes secondary impairment of mitochondrial β-oxidation and TCA cycle: inhibition of the oxidation of NADH and $FADH_2$ leads to their accumulation and impedes the activity of the different FAD-dependent and NAD^+-dependent dehydrogenases of the β-oxidation and TCA cycle pathways[283]. This impairment can lead to hyperlactatemia and lactic acidosis because the conversion of lactate from pyruvate by lactate dehydrogenase is favoured by NADH accumulation[284]. Another important consequence of ETC inhibition can be the enhanced production of ROS. ETC inhibitors can either rise or lower the rate of ROS production depending on whether they act predominantly upstream or downstream of an electron leak site, even though they lower protonmotive force in

either case[116]. If they act downstream, this leads to reduction of the site and increased electron leak. On the contrary, if they act upstream, this leads to oxidation of the site and decreased electron leak[116]. Eventually, drug-induced mitochondrial ROS overproduction can result in the damage of macromolecules such as proteins and mtDNA, and eventually lead to apoptosis[285].

5.4.1. Antidiabetic drugs

Metformin and thiazolidinediones (TZDs) are drugs used for the treatment of type 2 diabetes. TZDs are a class of peroxisome proliferator-activated receptors (PPAR-γ) agonists, which ameliorate hyperglycaemia by increasing insulin-stimulated glucose uptake by skeletal muscle. However, activation of PPAR may not be the only mechanism of action, since these drugs have also been reported to inhibit complex I[253]. By inhibiting complex I, TZDs may cause acceleration of glycolytic flux as an adaptive response to loss of aerobically generated ATP, lowering serum glucose[69]. Metformin is a biguanide agent used as the first-line medication for the treatment of type 2 diabetes[286]. Exact molecular mechanisms of metformin are not completely understood, however, its antidiabetic properties have also been attributed to inhibition of mitochondrial respiratory complex I[287, 288], which may explain the elevated plasma lactate concentrations observed in patients[289]. Nonetheless, these drugs have been associated with a variety of negative pharmacological profiles, especially hepatotoxicity cases[290]. The initial marketed drug in this class, troglitazone, was withdrawn from the market worldwide after three years of use due to rare but severe hepatotoxicity, which, in some occasions, resulted in liver failure and even death[291]. The exact toxicity mechanisms are still speculative, however it is likely that mitochondrial OXPHOS dysfunction might have played a role[291, 292]. Development of ciglitazone, a drug considered the prototypical compound for the thiazolidinedione class, was discontinued and was never used as medication because of its association with a dose-dependent increase in the incidence and severity of nuclear cataract formation in rats[293].

A study by Nadanaciva *et al.*[85] reported IC_{50} values during state 3 respiration (ADP-stimulated, in the presence of complex I substrates glutamate + malate) in rat liver mitochondria of 23 nmol/mg mitochondrial protein for ciglitazone and 6 nmol/mg for troglitazone; values that are much lower than the other TZDs that were later

developed and remain in the market, such as pioglitazone (IC_{50} > 100 nmol/mg) and rosiglitazone (IC_{50} > 100 nmol/mg). Additionally, another study showed that troglitazone and ciglitazone induced opening of the mitochondrial permeability transition pore (MPTP), whereas rosiglitazone and pioglitazone were much less effective[292].

In this investigation, various assay protocols were used to enable characterisation of the exact mechanisms involved in mitochondrial effect of these drugs. A summary of the results from these tests (Table 5.10), indicates multiple mechanisms may be involved in mitochondrial toxicity by TZDs. First, it can be seen from the inhibitory concentrations reported in this table that troglitazone and ciglitazone are indeed more potent inhibitors of various aspects of mitochondrial function than the marketed analogues pioglitazone and rosiglitazone. These two latter drugs were not identified as mitochondrial toxicants by the Glu/Gal assay, and furthermore, pioglitazone was also identified as safe with the permeabilised HepG2 extracellular flux assay. Despite this, the AEFA showed that both drugs reduced basal OCR and ATP production at relatively low concentrations (but at higher concentrations than their clinical plasma concentrations, see Table 5.2).

All TZDs reduced basal OCR and ATP production, and all but pioglitazone also reduced reserve capacity and increased ECAR and proton leak dose-dependently in the AEFA (Table 5.10). Therefore, this leads to the conclusion that these compounds may act as ETC inhibitors. On the other hand, the permeabilised HepG2 assay was not able to show any ETC effect in terms of pyruvate respiration for pioglitazone and ciglitazone (only a slight increase in respiration for ciglitazone under ascorbate/TMPD/Antimycin A-driven respiration). Furthermore, for rosiglitazone and troglitazone, the AC_{50} values for OCR inhibition were higher in this assay, than those observed in the AEFA. This contradictory result between the AEFA and the permeabilised flux assay may stem from the differences between the assay protocols, for example, the constituents of the nutrients in the buffer used during the assays. Similar conflicting results between intact vs. permeabilised cells were observed by Divakaruni *et al.* for pioglitazone, while for three other TZDs (troglitazone, rosiglitazone and MSDC-0160) they observed acute respiratory inhibition in both intact and permeabilised cells[145]. Divakaruni *et al*. showed TZDs to be specific inhibitors of the mitochondrial pyruvate carrier (MPC) in permeabilised C2C12

myoblasts and a number of permeabilised primary cells, and the inhibitory effect could be reversed by the specific MPC substrate, methyl pyruvate[145]. Similar to the extracellular flux results from permeabilised cells, they also observed no respiratory inhibition for succinate- or ascorbate/TMPD-driven respiration.

Despite this, two separate assay protocols have provided evidence that indicate additional mitochondrial targets for the TZDs that were investigated further. Both ciglitazone and troglitazone inhibited complex II+III when tested against the succinate-cytochrome c reductase (SCR) in isolated rat liver mitochondria. Similar results have been observed for these two drugs previously[76]. In addition, while both these drugs increased basal succinate-driven OCR (and reduced MMP), the uncoupled succinate-driven respiration was inhibited in a dose-dependent manner in isolated rat liver mitochondria. These observations collectively indicate that, in addition to MPC inhibition, there may be other multiple mechanisms involved in the mitochondrial toxicity caused by these drugs, i.e. ETC inhibition at complex II+III level and uncoupling effects.

In addition to these, there are literature reports suggesting complex I inhibitory effect of these compounds[251]. A study published by Brunmair *et al.* showed that TZDs and metformin cause a reduction of enzymatic activity of complex I in homogenates of rat gastrocnemius muscle and rat liver, which were sonicated to disrupt both cell and mitochondrial membranes. The effects of pioglitazone and troglitazone on complex I were observed only at the highest concentration used (100 µM), while rosiglitazone and metformin showed a dose-dependent behaviour[253].

Brunmair *et al.* also showed that metformin, rosiglitazone and pioglitazone failed to affect state 3 respiration in the presence of complex II substrate succinate + rotenone. However, a TZD-induced increase in state 4 was seen with succinate as substrate, but not with glutamate + malate[253]. Consequently, TZDs seem to also have uncoupling properties, which would be in agreement with what was observed in this study: in complex II-linked basal respiration, both ciglitazone and troglitazone significantly increased OCR and dissipated the MMP at low micromolar concentrations (Table 5.6). Furthermore, both ciglitazone and troglitazone meet the requirements proposed for a potent uncoupler: both have a pKa value of 6.61, have an acid-dissociable group,

strong electron-withdrawing groups and log P values are 4.28 and 5.5, respectively[266].

Finally, the fold change values obtained for metformin and ciglitazone in the Glu/Gal assay may suggest that they ought to be considered mitochondrial toxicants. Both rosiglitazone and pioglitazone are avidly protein-bound (99.8% and 97% bind to plasma proteins, respectively, see Table 5.5)[294], which may explain why they were not picked up as mitochondrial toxicants by the Glu/Gal assay, even at the highest concentration tested. Protein binding of troglitazone is also very high (>99%), however, troglitazone showed a similar cytotoxic response in both culture conditions, suggesting the possible existence of other toxicity mechanisms apart from mitochondrial toxicity.

Table 5.10. Summary of assays performed to investigate the mitochondrial effects of metformin and thiazolidinediones (TZDs). Direction of change in basal OCR, reserve capacity, basal ECAR, ATP production and proton leak, where: ↑ = increase compared to vehicle control, ↓ = decrease compared to vehicle control, NR = no response compared to vehicle control, N/A = not available. Values in brackets show the concentrations used in μM.

Assays		Ciglitazone	Pioglitazone	Rosiglitazone	Troglitazone	Metformin
Acute HepG2 Extracellular Flux Assay (AEFA)	OCR AC_{50} (μM)	18.7↓	41.6↓	15.9↓	11.8↓	NR
	Reserve capacity AC_{50} (μM)	5.52↓	NR	7.59↓	3.94↓	NR
	ECAR AC_{50} (μM)	>100↑	NR	>31.6↑	49.4↑	NR
	ATP production AC_{50} (μM)	4.87↓	5.13↓	9.7↓	5.37↓	NR
	Proton leak AC_{50} (μM)	4.01↑	NR	86.7↑	17.5↑	>6000↓
	Summary mechanism	ETC inhibitor	Other	ETC inhibitor	ETC inhibitor	N/A
Permeabilised HepG2 Extracellular Flux Assay (OCR)	Most sensitive mechanism (AC_{50} μM)	ascorbate respiration↑ >100	NR	pyruvate respiration↓ >100	pyruvate respiration↓ 66	N/A
Glu/Gal assay (cell viability reduction)	Glucose AC_{50} (μM)	>100↓	NR	NR	115↓	>6000↓
	Galactose AC_{50} (μM)	46.3↓	NR	NR	103↓	2510↓
	Fold Change	>2.16	NR	NR	1.12	>2.39
SCR inhibition	IC_{50} (μM)	3.4	N/A	N/A	19	N/A
Basal succinate-driven respiration	% MMP (Conc. μM)	61 (3), 37 (6), 14 (11), -1.8 (16)	N/A	N/A	36 (22.5)	N/A
	% O_2 consumption (Conc. μM)	170 (3), 200 (6), 248 (14), 224 (16)	N/A	N/A	204 (22.5)	N/A
Uncoupled succinate-driven respiration	% ROS (Conc. μM)	72 (3), 64 (7), 89 (11)	N/A	N/A	123 (90), 262 (112)	N/A
	% O_2 consumption (Conc. μM)	90 (3), 73 (7), 43 (11)	N/A	N/A	21 (90), 3.8 (112)	N/A
C_{max} (μM)		N/A	1.5	0.2	2.8	11.7

5.4.2. Lipid-lowering agents

Statins and fibrates are medical drugs used to lower elevated plasma lipid levels. Statins are inhibitors of 3-hydroxy-3-methyl-glutaryl coenzyme A reductase (HMG-CoA), the rate-controlling enzyme of the cholesterol biosynthetic pathway. This pathway generates a range of other products in addition to cholesterol, such as coenzyme Q10, heme A and isoprenylated proteins[295]. As a class, they are among the most frequently prescribed drugs worldwide and, generally speaking, they are considered safe medications[296]. However, myopathies are the most common adverse reactions observed with these medications, ranging from muscle pain to very rare cases of life-threatening rhabdomyolysis[297]. Lovastatin was the first drug introduced in the market in 1987 and, since then, other drugs have been used clinically, such as simvastatin, pravastatin, fluvastatin, atorvastatin or cerivastatin, among others. All marketed statins have a comparable incidence of producing myopathy, except cerivastatin, which was withdrawn from clinical use due to an unacceptable number of rhabdomyolysis cases[298]. Acute liver failure and death have been rarely reported, however, although rare, statin-induced liver injury can be severe, and as an increasing number of patients take statins, monitoring side effects and understanding mechanisms of toxicity is essential to identify susceptible patients and improve the safety of these drugs[274]. Mitochondrial dysfunction has been suggested as the main toxicity mechanism, but still very little is known[274, 299].

Here, two of the most widely commercialised statins, lovastatin and simvastatin, were investigated. A summary of the results obtained for these two drugs is shown in Table 5.11. A number of reports have described acute effects of these drugs on the ETC. For instance, acute doses of simvastatin (10, 30 and 100 μM) caused significant inhibition of complex I activity in human skeletal muscle fibers[300], while a subsequent study showed that *ex vivo* treatment with simvastatin caused mitochondrial membrane depolarisation (EC_{50} = 1.96 μM) and triggered release of cytoplasmic calcium (EC_{50} = 7.8 μM) in human skeletal muscle fibres[301]. In addition, a study employing an immunocapture technique indicated that statins at 150 μM were able to cause a direct inhibition of the ETC complexes I, II+III, IV and V, with simvastatin and lovastatin showing the most pronounced effects[85]. The same study found that in state 2 respiration (where substrates glutamate + malate were provided in the absence of exogenous ADP), both lovastatin and simvastatin showed

uncoupling activity; whereas in state 3 respiration (ADP-stimulated) they caused significant inhibition of respiration. Here, in isolated rat liver mitochondria with succinate as substrate in the absence of exogenous ADP, 45 µM lovastatin increased OCR consumption to 110% and dissipated MMP to 61%, whereas that same concentration in uncoupled respiration decreased OCR to 71% and increased ROS production to 127% (see summary in Table 5.11). Simvastatin inhibition in uncoupled respiration also caused an increase in ROS generation as seen in Table 5.11. Interestingly, lovastatin and simvastatin constitute lipophilic statins, and share some characteristics of those proposed for potent uncouplers, including the presence of an acid-dissociable group and log P values of 4.11 and 4.51, respectively[266]. However, they lack strong electron withdrawing groups and pKa values are high with the degradation products, hydroxy acid analogues, having a stronger acidic property (pKa of 14.91 for simvastatin compared with 4.21 for the hydroxy acid analogue according to ChemAxon calculations).

Enzymatic assays using isolated mitochondria showed that lovastatin and simvastatin inhibit 50% of complex II+III activity at 35 µM and 11 µM, respectively (Figure 5.8). In agreement with this, lovastatin was identified as an ETC inhibitor by the AEFA using intact HepG2 cells, whereas no effect on respiration was reported with up to 100 µM simvastatin (Figure 5.3 and Table 5.3). This could lead to the conclusion that IC_{50} values obtained in isolated mitochondria may not be physiologically relevant due to the unrestricted access of the drug to isolated mitochondria in the absence of cell membrane.

C_{max} values for lovastatin and simvastatin (0.02 µM)[274, 302] are much lower than the toxic concentrations determined in this study, which raises the question of to what extent the findings obtained *in vitro* are relevant in *in vivo* situations. It has been observed before that compounds may bioaccumulate in tissues and mitochondria, reaching higher concentrations and exerting a toxic effect through inhibition of the ETC (and build-up of free radicals within the organelle). In fact, a study published in 2015, showed how decreased complex III activity and ATP production was associated with statin accumulation in muscle biopsies of patients with statin-induced myopathies[303]. On the other hand, a more recent study published in 2017, showed how incubation of muscle biopsies of healthy individuals with simvastatin led to no effect on mitochondrial respiration using therapeutic concentrations, but

supratherapeutic concentrations yielded a dose-dependent inhibition of mitochondrial respiration[304]. It should also be noted that lovastatin is a substrate for MCT-4, a transporter of a wide array of substrates that is expressed in skeletal muscle. This would be in agreement with a bioaccumulation of lovastatin in the muscle via MCT-4, resulting in a greater susceptibility of the muscle to statin-induced rhabdomyolysis[305].

Table 5.11. Summary of assays performed to investigate the mitochondrial effects of simvastatin and lovastatin. Direction of change in basal OCR, reserve capacity, basal ECAR, ATP production and proton leak, where: ↑ = increase compared to vehicle control, ↓ = decrease compared to vehicle control, NR = no response compared to vehicle control, N/A = not available. Values in brackets show the concentrations used in μM.

Assays		**Simvastatin**	**Lovastatin**
Acute HepG2 Extracellular Flux Assay (AEFA)	OCR AC_{50} (μM)	NR	>50↓
	Reserve capacity AC_{50} (μM)	NR	>50↓
	ECAR AC_{50} (μM)	NR	>50↑
	ATP production AC_{50} (μM)	>100↑	>50↓
	Proton leak AC_{50} (μM)	NR	34.1↑
	Summary mechanism	NR	ETC inhibitor
Permeabilised HepG2 Extracellular Flux Assay (OCR)	Most sensitive mechanism	N/A	NR
Glu/Gal assay (cell viability reduction)	Glucose AC_{50} (μM)	>100↓	43.2↓
	Galactose AC_{50} (μM)	NR	>50↓
	Fold Change	UD	UD
SCR inhibition	IC_{50} (μM)	11 ± 1	35 ± 3
Basal succinate-driven respiration	% MMP (Conc. μM)	95 ± 2.3 (12)	61 ± 23.5 (45)
	% O_2 consumption (Conc. μM)	97 ± 6.4 (12)	110 ± 7 (45)
Uncoupled succinate-driven respiration	% ROS (Conc. μM)	137 (36), 146 (60), 190 (132), 235 (252)	90 (25), 127 (45)
	% O_2 consumption (Conc. μM)	83 (36), 74 (60), 65 (132), 52 (252)	82 (25), 71 (45)
C_{max} (μM)		0.01	0.01

Another issue that requires consideration is individual susceptibility due to underlying metabolic conditions or variations in mitochondrial DNA mutations (degree of heteroplasmy). In other words, some individuals may be more susceptible to the onset and severity of side effects due to severe heteroplasmic mitochondrial disorders (i.e. higher level of mutations in mitochondrial DNA)[306]. Individual differences in the capacity for absorption, transport and elimination of statins could also play an important role. For instance, deficiencies in cytochrome P450 3A4 (CYP3A4), which metabolises simvastatin, could potentially result in an increased bioavailability of simvastatin in some patients, and possibly, elevated intramuscular concentrations, which would increase the chances of developing myopathies[307]. Additionally, it has also been suggested that drug-drug interactions could magnify the toxicity of statins by impeding their metabolism and therefore increasing their plasma concentrations[308, 309]. Finally, it is important to bear in mind that the mevalonate pathway, which statins inhibit, also produces CoQ10 and heme A, which have their own central involvement in the ETC[310-314]. Consequently, depletion of either may be a contributing factor to the impairment of the mitochondrial respiratory chain. As a matter of fact, a number of studies have found evidence of a 27-50% decrease in CoQ10 levels in both serum and plasma of patients following statin treatment[315, 316].

Fibrates comprise another class of compounds that act as PPAR agonists, the PPAR-α isoform regarded as their major target[317]. They are used for the treatment of hypertriglyceridemia by inducing activity of peroxisomes containing high palmitoyl-CoA ligase, which metabolises fatty acids, lowering serum triglycerides and LDL cholesterol. They are often prescribed in combination with statins, and even though they have been used safely for decades, all fibrates including gemfibrozil, fenofibrate and bezafibrate, can cause skeletal muscle myopathy[318]. Several studies have also linked fibrate treatment to hepatotoxicity in rodent models[319]. The mechanisms of fibrate-induced adverse side effects are unknown, however, fibrates have been shown to impair mitochondrial function in several studies, usually by inhibiting respiration at high micromolar concentrations[69]. For instance, in a study using freshly isolated rat liver mitochondria energised with succinate, gemfibrozil induced the mitochondrial permeability transition pore, fenofibrate and clofibrate exerted a direct dose-dependent depolarisation of the MMP while bezafibrate showed no effects on

succinate-supported respiration[320]. Nadanaciva *et al*. showed that at 500 nmol/mg, fenofibrate, clofibrate and gemfibrozil significantly increased basal state 2 respiration in rat liver mitochondria, whilst bezafibrate caused no effects[85]. In state 3 respiration, bezafibrate showed slight inhibition. Further experiments revealed that 500 µM bezafibrate caused 18% inhibition of complex I activity, whilst it did not cause inhibition of any other ETC complex[85]. This is in agreement with other studies which have revealed inhibition of complex I activity by bezafibrate, such as a study by Yamada *et al.* where complex I-linked state 3 respiration was inhibited following exposure of rat liver mitochondria to 200 µM bezafibrate[321, 322].

Here, the permeabilised cell assay corroborated that complex I inhibition was the most sensitive mechanism of bezafibrate (MEC = 655 µM) (Table 5.4). Furthermore, data obtained using isolated mitochondria also confirmed that bezafibrate, in contrast with the TZDs and statins, did not show an uncoupling activity: 750 µM bezafibrate decreased OCR to 76 ± 7.8% in basal complex II-linked respiration and to 77 ± 5% in uncoupled respiration (Table 5.6 and Table 5.7). Finally, the AEFA confirmed that acute injection of bezafibrate not only reduced OCR but also ECAR (AC_{50}>750 µM), which suggests that it may exert cell toxicity through additional mechanisms. Nevertheless, no response was observed in the Glu/Gal assay, but this may be explained by the fact that bezafibrate is a highly protein-bound compound (94-96% bezafibrate is bound to protein in human serum)[323]. In summary, although bezafibrate has demonstrated to have effects on mitochondrial bioenergetics, previous studies have revealed that such effects are weaker than other fibrates, suggesting that bezafibrate might be the least toxic fibrate and hence more suitable for long-term *in vivo* use as an antihyperlipidemic drug[85, 322].

5.4.3. Anti-inflammatory and Analgesic drugs

5.4.3.1.1 Salicylic acid

Salicylic acid (SA) is a beta hydroxyl acid known for its anti-infective and exfoliating properties. Additionally, it is an important active metabolite of aspirin (acetylsalicylic acid), which is included in the list of essential medicines by the WHO[247]. Aspirin is one of the most widely consumed analgesic, antipyretic and anti-inflammatory agents, yet serious toxicities such as hepatotoxicity have been associated with its use[279, 324]. While most of aspirin dose is absorbed quickly, mostly

from the upper small intestine and distributed throughout body tissues as it is, some enters the systemic circulation as SA after hydrolysis by esterases in the liver and gastrointestinal tract[324, 325].

A large body of evidence has confirmed a dual activity of SA on the ETC, depending on the concentration, the mitochondria state and the substrates provided[279, 280]. For instance, a study using isolated rat liver mitochondria with succinate as the substrate, showed how increasing concentrations of SA decreased OCR in state 3 respiration, whereas, in state 4, respiration increased at up to 0.1 mM SA and then decreased at higher concentrations[279]. Another study done on mitochondria isolated from tobacco showed that at all concentrations tested (0.1-5 mM) SA inhibited state 3 respiration with succinate or malate + pyruvate as substrates. However, at concentrations lower than 1 mM, oxygen uptake was stimulated in state 4 respiration with malate + pyruvate as substrates[280]. Furthermore, reduction in the ubiquinone redox poise upon increasing concentrations of SA suggested block of electron flow from the substrate dehydrogenases to the ubiquinone pool[280]. It has been hypothesised that due to its phenolic nature, SA may act as quinone analogue at millimolar concentrations, preventing the interaction between the dehydrogenases and the UQ pool[280]. Other studies have pointed out the inhibition of complex III activity by SA. A recent study published by Liu *et al*. reported a decrease in complex III activity to 25% with respect to the control with 0.4 mM SA using isolated mitochondria from fungi[326]. Another study using isolated mitochondria from plant mitochondria reported inhibition of complex III activity to 25% with respect to the control with 0.5 mM SA[327].

Here, the AEFA confirmed that millimolar concentrations of SA inhibited OCR (AC_{50} = 1.8 mM), reserve capacity (AC_{50} = 1.5 mM) and ECAR (AC_{50} = 0.5 mM) in HepG2 cells (Table 5.2 and Figure 5.2). The permeabilised cell assay identified succinate respiration as the most sensitive mechanism (AC_{50} > 10 mM), which would suggest inhibition of complex III (Table 5.4 and Figure 5.4). The SCR assay performed using isolated mitochondria revealed an IC_{50} value of 2.5 mM (Figure 5.8). Further studies done on the individual complexes showed similar inhibition towards complex II and III by SA (Figure 5.9). Studies done using freshly isolated mitochondria showed the uncoupling activity of SA. In basal complex II-linked respiration, 2.5 mM SA increased OCR to 144% and dissipated the MMP to 37% with respect to the control (Table 5.6). In contrast, in CCCP-stimulated respiration

2.5 mM SA decreased OCR to 38% (Table 5.7). These results suggest that the dual activity of SA is dependent on the respiration state, however, a concentration-dependent activity cannot be ruled out as it was not investigated here. The fact that SA has an acidic group and a strong electron withdrawing group suggests that it could make a good uncoupler candidate like other NSAIDs[328, 329], however, it has a low log P value (1.98), which could explain why millimolar concentrations are required to observe an uncoupling effect.

5.4.3.1.2 Sulfasalazine

Sulfasalazine is a widely used sulphonamide drug for the treatment of rheumatoid arthritis and inflammatory bowel diseases such as ulcerative colitis and Crohn's disease[330]. Nearly all the prodrug taken orally reaches the colon intact, but only 10-30% is absorbed through the colon unchanged, the rest is converted into its two metabolites by bacterial azoreductases: 5-aminosalicylic acid (5-ASA) and sulfapyridine[330, 331]. The exact mechanism of action of sulfasalazine is still under investigation, although it appears to vary depending on the inflammatory disorder. For instance, in inflammatory bowel disease, 5-ASA seems to be primarily responsible for clinical efficacy due to its anti-inflammatory properties[332, 333]. A number of studies have shown that 5-ASA inhibits the prostaglandin E2 mediated inflammatory response[334], the synthesis of IL-1, IL-6 and the TNF-α [335] and the activation of NF-kβ[336]. Furthermore, only around 30% of 5-ASA is absorbed and transported to the liver, so most of it remains in the colon[337]. Sulfapyridine, on the other hand, is completely absorbed through the colon and has been proposed as the active moiety in rheumatoid arthritis, but its mechanism of action remains to be elucidated[338].

Long-term treatments with sulfasalazine have reported a wide range of side effects: from nausea, headache, vomiting and stomach pain to nephrotoxicity, hepatotoxicity, infertility, pancreatitis and skin disorders[337]. The possible relation between sulfasalazine-induced toxicities and mitochondrial injury has not been extensively investigated and consequently there is not much information about it in the literature. Only recently, a study published by Niknahad *et al.* defined oxidative stress and mitochondrial injury as the mechanism of sulfasalazine-induced renal injury[339]. In that study, kidney mitochondria obtained from sulfasalazine-treated rats revealed

mitochondrial swelling and depolarisation, increased ROS formation and decreased mitochondrial succinate dehydrogenase activity[339]. Results presented here have shown that acute dosing of up to 1.5 mM sulfasalazine to HepG2 cells had no effect on either OCR, reserve capacity or ATP production, although there was a significant reduction of ECAR at low micromolar concentrations (AC_{50} = 68.4 µM) (Table 5.2 and Figure 5.2). This is somehow different with observations in kidney cells described above[337] and cortical neurons from embryonic CD1 mice[340]. In the latter study, neuronal maximal respiration was diminished after 24 h treatment with 1 mM sulfasalazine. Moreover, both glycolysis and glycolytic capacity were reduced in neurons with sulfasalazine at 300 µM – 1 mM range[340].

The permeabilised cell assay indicated pyruvate respiration as the most sensitive mechanism, but only at high concentrations (AC_{50} > 1.5 mM) (Table 5.4 and Figure 5.4). Nonetheless, studies using isolated mitochondria showed that sulfasalazine inhibited 50% of SCR activity at 709 µM (Figure 5.8), and that at that concentration inhibition of succinate dehydrogenase (complex II) but not complex III, was displayed (Figure 5.9), which may be in agreement with the decreased activity of succinate dehydrogenase observed by Niknahad *et al.*[339]. The effects of sulfasalazine on MMP using the Oroboros® Oxygraph-2K could not be investigated due to interactions of the drug with the fluorescent sensors. In complex II-linked uncoupled respiration, sulfasalazine reduced respiration in a dose-dependent manner with a similar IC_{50} value as the SCR assay (700 µM decreased respiration to 47 ± 4%) (Table 5.7). Interestingly, in the same context, sulfasalazine also decreased ROS production in a dose-dependent manner (Table 5.7), which would be consistent with a sulfasalazine-induced complex II inhibition that would lead to a more oxidised ubiquinone-pool and reduced electron leak. However, another hypothesis has been proposed elsewhere that sulfasalazine may have ROS-scavenging effects that could account for its anti-inflammatory effects[341]. This may well be the case at lower (therapeutic) doses of this drug (C_{max} = 0.03 µM) not investigated here.

The Glu/Gal assay showed no significant difference between the two culture media conditions, with citotoxity observed at AC_{50} ~ 1.2 mM (Table 5.5). This may suggest that the observed cytotoxicity is not primarily related to mitochondrial function. In summary, further investigations on the effects of sulfasalazine and sulfasalazine's

metabolites need to be performed for a better insight into sulfasalazine-induced toxicities and mitochondrial function.

5.4.3.1.3 Acetaminophen

Acetaminophen (N-acetyl-*p*-aminophenol) also known as paracetamol, is the most commonly taken analgesic worldwide and is recommended as first-line therapy in pain conditions by the WHO[342]. It is also used for its antipyretic effect. Its exact mechanism of action has not been fully established, but it has been historically categorised along with nonsteroidal anti-inflammatory drugs (NSAIDs)[343, 344]. However, acetaminophen has proven to be ineffective as an anti-inflammatory drug, which suggests that its site of pharmacological action is within the central nervous system[344]. Although acetaminophen is generally safe at therapeutic doses, overdose is the most common cause of acute drug-induced liver failure in the United States and other countries in Europe[345].

Excessive acetaminophen dosing results in excessive formation of the reactive metabolite N-acetyl-*p*-benzoquinone imine (NAPQI) by CYP450 in the liver, which depletes the gluthathione stores (GSH, an antioxidant defense) in both the cytosol and mitochondria. Depletion of GSH stores allows NAPQI to freely react with mitochondrial proteins, which leads to mitochondrial oxidative stress[346], inhibition of mitochondrial respiration[90, 347] and ATP depletion[348]. Therefore, mitochondria are the primary target of NAPQI in acetaminophen-induced liver injury[348]. Furthermore, studies have shown that acetaminophen inhibits state 3 respiration (ADP-stimulated) in mouse liver mitochondria with an IC_{50} value of 1.8 mM for NADH-linked respiration (in the presence of complex I substrates glutamate + malate) and an IC_{50} of >10 mM for succinate-supported respiration[90]. On the other hand, NAPQI inhibited state 3 respiration with an IC_{50} value of 0.12 mM for NADH-linked respiration and an IC_{50} value of 0.39 mM for succinate-supported respiration[90]. Therefore, acetaminophen inhibition is most likely specific to complex I, whereas NAPQI is most likely inhibiting other ETC elements common to the oxidation of both NADH and succinate, like complex III[90].

In another work, mitochondrial respiratory capacity measured in primary human hepatic cells by high-resolution respirometry showed how therapeutic concentrations of acetaminophen (≤0.13 mM) did not inhibit state 3-complex I respiration, however,

concentrations of ≥2.0 mM significantly reduced mitochondrial respiration in a dose-dependent manner[349]. The same study showed that complex II-linked mitochondrial respiration was not inhibited, suggesting that the mechanism of action of acetaminophen is complex I inhibition[349].

Here, it was seen in the AEFA that acetaminophen reduces both OCR (AC_{50} = 7.4 mM) and reserve capacity in a dose-dependent manner (Figure 5.2). The use of permeabilised HepG2 cells confirmed that complex I inhibition was the most sensitive mechanism of action of acetaminophen (AC_{50} > 10 mM), as only pyruvate and not succinate respiration was inhibited (Table 5.4 and Figure 5.4). Nonetheless, even though acute injection of acetaminophen significantly reduced OCR and reserve capacity, it did not increase ECAR to compensate for reduced respiration (Table 5.2), hence according to this assay acetaminophen may be categorised as a "substrate inhibitor" instead of an ETC inhibitor, implying that mitochondrial respiration is decreased due to a reduced substrate availability. Accordingly, inhibition of NADH-linked substrates by acetaminophen (transport/metabolization mediated by other enzymes) cannot be ruled out.

Although acetaminophen can itself inhibit mitochondrial respiration, previous studies suggest that cytochrome P450-generated metabolite NAPQI is more likely to be responsible for the toxicities[90]. Consequently, identification of acetaminophen-induced toxicity may be hampered by the low CYP450 activity found in HepG2 cells, and could explain why no response was observed upon 24 incubation in the Glu/Gal assay[350, 351]. The lack of CYP450s in HepG2 cells may reduce the propensity for ROS production upon acetaminophen treatment, which may lead to an underestimation of toxicity when using HepG2 cells as model system[352].

5.4.4. Other drugs

5.4.4.1.1 Memantine

Memantine is an uncompetitive NMDA receptor antagonist that is used for the treatment of moderate to severe Alzheimer's disease[353]. It is believed that, in Alzheimer's disease, the loss of cholinergic neurons may occur partly due to excessive glutamate levels in the synaptic cleft and over-stimulation of NMDA receptors, which leads to excessive calcium influx and activation of enzymes that lead to neuronal death[353]. Memantine exerts its neuroprotective properties by

moderately inhibiting excitatory activity of glutaminergic neurons, however, other mechanisms that could potentially mediate its clinical effects have been proposed and require further investigation[354]. For instance, McAllister *et al.* found that memantine can influence mitochondrial function independently of NMDA channel antagonism[355]. In their study, isolated mitochondria from an embryonal carcinoma cell line (NT2 cells) were acutely exposed to 10 or 60 µM memantine. Both concentrations significantly reduced V_{max} of complex IV, while at 60 µM memantine increased V_{max} of complex I significantly. Furthermore, they showed that chronic treatment with both 10 and 60 µM memantine increased peroxide production, while acute treatment with the same concentrations of memantine reduced mitochondrial peroxide levels[355]. In another study, acute and chronic treatments with memantine altered the respiratory chain complexes in rat brain; depending on the treatment protocol (acute or chronic), ETC complex and the brain area[356]. For instance, acute treatment with 5 mg/kg memantine increased complex I activity in the hippocampus and striatum, but not in the prefrontal cortex. It also increased complex II activity only in the hippocampus, increased complex II+III activity only in the striatum and had no effect on complex IV activity in any of the brain areas. Then, upon chronic treatment with 20 mg/kg memantine, complex I activity was increased in the prefrontal cortex and hippocampus, but reduced in the striatum, complex II+III activity was highly increased in prefrontal cortex and to a lesser extent in the hippocampus, and complex IV activity was increased at the dose of 5 mg/kg in the hippocampus and striatum, at 10 mg/kg in prefrontal cortex and at 20 mg/kg in the striatum[356]. From these results, it can be concluded that screening the effects of drugs on mitochondria can be challenging, as results may vary depending on drug exposure time, dose and tissue.

In the present work, the AEFA showed no significant effect of acute injection of up to 100 µM memantine on mitochondrial respiration using HepG2 cells (Table 5.2). Chronic treatment of up to 100 µM memantine did not seem to affect HepG2 cell viability either, as assessed by the Glu/Gal assay, regardless of its low plasma protein binding (around 45%) (Table 5.5). There may be two possible explanations for this. Firstly, it may be the case that memantine has a stronger impact on brain bioenergetics than other tissues due to the existing link between NMDA receptors and mitochondria[355]. In their study, Reus *et al.* argued that the effects observed by

memantine on energy metabolism may be neuroprotective and related with oxidative stress[356]. Secondly, there is a possibility that assessing the activities of the ETC complexes individually, like in the study published by McAllister *et al.*[355], may be limited and do not necessarily reflect the mechanisms occurring in live intact cells.

5.4.4.1.2 Clonidine

The main therapeutic use of clonidine is in the treatment of hypertension, because of activation of presynaptic α2 receptors in central brainstem, although it also has apparent efficacy in the treatment of a range of other disorders such as attention deficit hyperactivity disorder, drug withdrawal, menopausal flushing, diarrhea and certain pain conditions[324]. Precise mechanisms of action of clonidine are not completely understood yet, and adverse effects associated with clonidine use include dry mouth, sedation, sexual dysfunction and contact dermatitis, among others[324].

A recent study using an *in vitro* model of human corneal epithelial cells (HCEP) showed that cells treated with various doses of clonidine for 1-28 h entered apoptosis via a mitochondrial-mediated pathway. As a result, they observed disruption of the MMP and release of cytochrome *c* to the cytosol[357]. Here, concentrations up to 0.5 µM clonidine (100 x C_{max}) showed no effects on HepG2 cell viability after 24 h incubation treatment in the Glu/Gal assay, even though plasma protein binding for clonidine is low (around 20%)[324] (Table 5.5). The AEFA also showed no effects on mitochondrial function (Figure 5.3 and Table 5.2).

5.4.4.1.3 Baclofen

Baclofen is considered the first-line treatment for muscle spasticity such as from a spinal cord injury or multiple sclerosis. It is an agonist of GABA-B receptors, leading to membrane hyperpolarisation, restriction of calcium influx and restriction of endogenous excitatory neurotransmitters from being released. Adverse effects include sedation, fatigue and hepatotoxicity[358]. To the best of my knowledge, no mitochondrial effects have been reported in the literature and, in this study, no effects were observed with up to 50 µM baclofen (100 x C_{max}) in any of the assays performed (Table 5.2, Table 5.3 and Table 5.5).

5.4.4.1.4 Colchicine

Colchicine is one of the oldest available drugs for the treatment of acute gout, as plant extracts containing colchicine were used for joint pain in the sixth century[324]. It is, however, a second-line therapy because of its narrow therapeutic window and high rate of side effects. Its exact mechanisms of action remain to be elucidated, but it is known to have antimitotic effects which may interfere with gout inflammation[324]. Colchicine also exhibits a variety of other pharmacological effects and adverse effects such as diarrhea, nausea, myelosuppression, leukopenia and rhabdomyolysis[324]. Like baclofen, colchicine has also been reported to induce apoptosis in cells through mitochondrial-mediated pathways[359], but no direct effects on mitochondrial function have been reported before. Here, concentration of up to 20 µM (2000 x C_{max}) colchicine did not affect mitochondrial function in any of the assays performed (Table 5.2, Table 5.3 and Table 5.5).

5.4.4.1.5 Warfarin

Warfarin (Coumadin) is a widely prescribed anticoagulant used to treat blood clots and to prevent stroke in patients with heart disorders. Warfarin inhibits vitamin K epoxide reductase (VKORC1), an enzyme essential for recycling vitamin K, which activates the clotting factors II, VII, IX and X[360]. It is on the WHO's list of essential medicines[247]. The bioavailability of warfarin is nearly complete when the drug is administered orally or intravenously[324] and it is almost completely bound to plasma proteins (99%), principally to albumin[361]. Bleeding is the major toxicity of warfarin, but other complications have been observed such as birth defects, skin necrosis or the purple toe syndrome[324]. Warfarin not only is of great importance for the health system, but from a mitochondrial point of view it is an interesting compound to test because of its chemical resemblance to its analogue ferulenol, as can be seen in Figure 5.12. Ferulenol is a natural product derived from *Ferula communis*[362], which has recently been found to be a novel potent inhibitor of the alternative oxidase (see Figure 3.1)[363], a potent inhibitor of the *Plasmodium falciparum* malate:quinone oxidoreductase (MQO)[364] and a weak inhibitor of the rat mitochondrial respiratory enzyme succinate ubiquinone reductase (SQR, IC_{50} = 17 µM)[365].

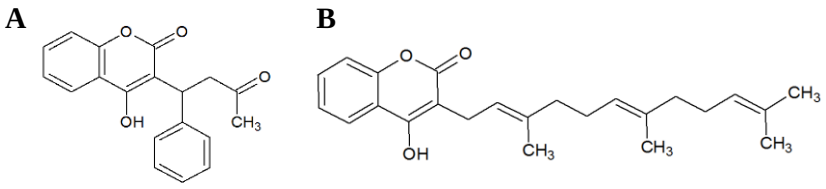

Figure 5.12. Chemical structures of warfarin (A) and ferulenol (B)

To the best of my knowledge, effects of warfarin on mitochondrial function have not been reported before, therefore it was considered valuable to gain further understanding of possible warfarin-induced mitochondrial toxicities. Studies done on isolated mitochondria showed that, in basal respiration using succinate as the substrate, 1.1 mM warfarin increased OCR to 168% and dissipated the MMP to 34% of the control (Table 5.6). However, in CCCP-stimulated (uncoupled) respiration using isolated mitochondria, warfarin provoked inhibition of respiration and ROS production in a dose-dependent manner (Table 5.7). This shows that the effect of warfarin on mitochondrial respiration is controlled by the mitochondrial state.

In the AEFA using intact HepG2 cells, 0.5 mM warfarin resulted in a mild increase in basal OCR (17%) and proton leak (47%) (Table 5.2), which could suggest an uncoupling activity, however a decrease of ATP production was not observed despite this. This indicates that warfarin might have some protonophoric effect, but this is insufficient to depolarise the mitochondrial membrane potential. Like with other drugs tested, this phenomenon suggests that once mitochondria have already reached the maximal uncoupled state, presence of other chemicals with certain degree of protonophoric activity leads to compromised mitochondrial membrane integrity, inevitably resulting in decreased OCR and ROS. In the SCR assay, which was performed on freeze-thawed mitochondria, warfarin showed inhibition of the ETC complexes with an IC_{50} of = 1.4 mM (Figure 5.8), and further studies on individual complex II and III activities revealed similar degree of inhibition towards both (Figure 5.9). As a general conclusion, it seems evident that warfarin probably contributes to the disruption of the electrochemical potential gradient due to its mild protonophoric activity at low milimolar concentrations. Finally, the fact that 99% of warfarin binds to plasma proteins might explain why no effects were observed in the Glu/Gal assay after 24 incubation treatment (Table 5.5)[361].

5.4.5. Docking of ETC complexes to identify OCR active compounds

All the drugs included in this chapter were docked against the five ETC complexes and the highest and lowest scores were used in the decision tree analysis (Figure 5.11). A decision tree (REPTree algorithm) using the docking scores was able to classify compounds into active and inactives groups, i.e. those that can significantly reduce basal OCR and those that cannot. This decision tree (Figure 5.11) is made up of 4 rules; compounds with docking scores lower than -7.67 are active against mitochondrial respiration, while those with docking scores ≥-7.67 are inactive, unless their scores is ≥-6.37 and the ratio of highest score against any ETC complex (least favourable) to the lowest score against any ETC complex is <1.24. This latter ratio can be regarded as an indication of specificity towards a particular target enzyme. Although this decision tree correctly classified 13 out of 16 compounds (81.25%), it is not possible to statistically validate this accuracy due to the small set of available data that does not allow the use of external test set. It is also noteworthy that all the 9 active compounds are predicted correctly as active, but out of 7 inactive compounds, this model predicts incorrectly 3 to be active.

With regards to OCR active compounds (9 compounds), the reported AC_{50} values show a correlation with the docking scores. Figure 5.13 is the scatter graph between the pIC_{50} values (calculated from OCR reduction, AC_{50}s are reported in Table 5.3 and the top docking scores (from Table 5.9). The fact that compounds with higher affinity to the ETC complexes have higher potency in reducing the OCR despite their differing mechanisms of action can be explained based on the relationship of docking scores with general chemical properties of the drugs such as their lipophilicity and molecular size. Hence the relationship does not necessarily indicate drugs binding to these specific ETC enzymes. It is obvious from the figure that the correlation is only a trend and docking score is not a perfect predictor of OCR pIC_{50}. This is only expected given the multiple mechanisms involved in the mitochondrial effect of compounds.

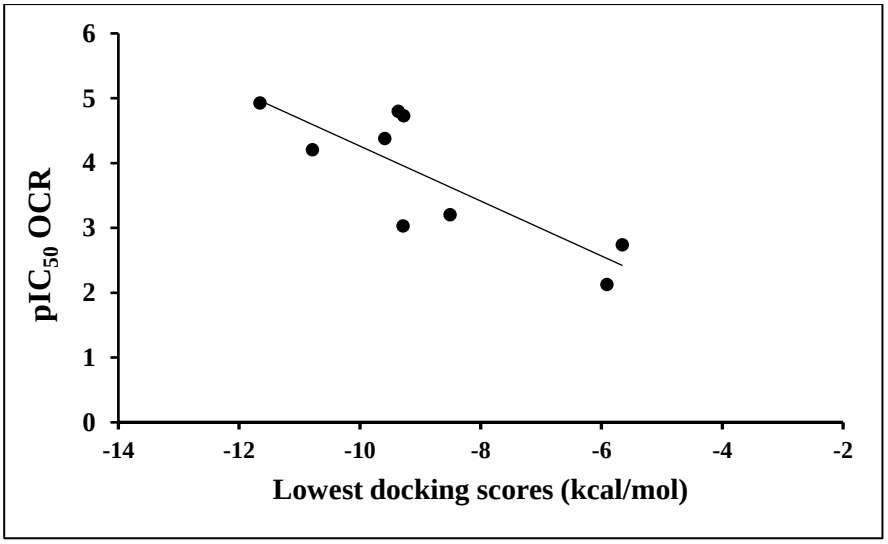

Figure 5.13. Scatter graph between OCR pIC_{50} values and the top docking scores.

6. The Effect of Antipsychotics, Anticonvulsants and other Psychotropic Drugs on Mitochondrial Function

6.1. Introduction

Antipsychotics (APs), also known as neuroleptics, are pharmacological drugs used for the treatment and management of several psychiatric conditions. They are classified as typical or "first-generation" antipsychotics and as atypical or "second-generation" antipsychotics. Acting mainly as dopamine type 2 (D2) receptor antagonists, typical APs were first introduced in the 1950s, and were commonly prescribed for schizophrenia[366]. However, owing to their high and non-specific occupation of D2 receptors in mesolimbic areas, they were soon associated with some serious side effects, among which extrapyramidal symptoms and hyperprolactinemia are the most prominent[367]. Examples of typical antipsychotics include chlorpromazine, levomepromazine, trifluoperazine and haloperidol, which are FDA-approved medications used for the treatment and management of multiple disorders, including schizophrenia, acute mania, agitation and bipolar disorder. The atypical APs were introduced later in the 1980s to treat a wide range of conditions, including depression, dementia/agitation, autism, obsessive–compulsive disorder or schizoaffective disorder. Examples include risperidone, quetiapine, clozapine, aripiprazole, ziprasidone, olanzapine, reserpine, zotepine, sertindole and amisulpride. With the use of second-generation APs, the risk of extrapyramidal symptoms decreased due to a lower affinity and occupancy for the D2 receptors and higher affinity for the serotoninergic receptors (such as 5-HT2A) and other receptors[368]. However, there is still an on-going debate as to whether second-generation APs are superior than first-generation APs in terms of efficacy[369]. In fact, two publicly funded effectiveness trials, the CUtLASS trial[370] and the CATIE trial[371] confirmed no clear difference in effectiveness between treatment with atypical and typical APs. The safety advantages of the atypical APs have also been questioned as they have been linked to a wide range of side effects, including reproductive dysfunction and metabolic effects, such as weight gain[372, 373], dyslipidaemia and diabetes mellitus [374-378]. Clozapine and olanzapine are associated with high risk of metabolic side effects[379], followed by the medium-risk drugs quetiapine and risperidone and the low-risk drugs ziprasidone and aripiprazole[380-382]. Furthermore, although less frequently, atypical APs can also induce extrapyramidal symptoms[383].

One of the most common extrapyramidal symptoms induced by neuroleptics is drug-induced Parkinsonism: patients on a long-term use of APs show a tardive dyskinesia prevalence of about 20% with atypical APs and 30% with typical APs[384]. Other common symptoms include dystonia, akathisia, rigidity and tardive dyskinesia[385]. The underlying mechanisms of these adverse effects are still not well understood, however, an increasing body of evidence has linked treatment with both typical and atypical APs to a disturbed mitochondrial function, however the exact mechanisms remain to be elucidated[386,387].

Anticonvulsants (ACs), also commonly known as antiepileptic or antiseizure drugs, are a diverse group of pharmacological agents that help prevent or treat seizures. Antiepileptic drugs are extensively used for the treatment of epilepsy, a chronic disease of the brain characterized by recurrent seizures that affects around 50 million people worldwide[388], but they are also increasingly being used in a broad spectrum of psychiatric and neurological disorders, such as bipolar disorder, neuropathic pain and trigeminal neuralgia[389-391]. ACs can be broken down into two categories: narrow-spectrum, which are designed for specific types of seizures (i.e. if the seizure occurs in a specific part of the brain on a regular basis), or broad-spectrum, which treat a wide variety of seizure types[392]. ACs are numerous and have a variety of mechanisms of action. For instance, some act on the sodium channels by blocking their repetitive activation (phenytoin, carbamazepine), while others block calcium channels (valproic acid) or bind to gamma-aminobutyric acid (GABA-A) receptors (phenobarbital)[392, 393]. Like other medical drugs, ACs have side effects depending on the dosage, toxicity and individual tolerability, and some have been attributable in the literature to mitochondrial toxicity [394]. In fact, ACs have been reported to interfere with various mitochondrial pathways, structure and functions, including the respiratory chain, OXPHOS, the TCA cycle and β-oxidation[395]. The most widely investigated AC in relation to mitochondrial toxicity has been valproic acid, probably due to its pronounced liver toxicity and because it causes the most severe side effects in patients with mitochondrial disorders[395, 396]. Nevertheless, other ACs have also been associated with hepatic mitochondrial function and elucidation of mechanisms of action will require further investigations[397, 398]. In this study, the effects on mitochondrial function of several narrow-spectrum ACs, including phenytoin,

phenobarbital, carbamazepine and vigabatrin, and some broad-spectrum ACs, including valproic acid, lamotrigine and primidone were investigated.

Finally, other psychotropic drugs including three antidepressants (citalopram, fluoxetine and tianeptine) and two anxiolytic drugs (buspirone and lorazepam) were investigated. Antidepressants (ADs) are widely used for the treatment of several conditions, such as bipolar disorder, obsessive-compulsive disorder, clinical depression and more. Their mechanism of action is very diverse, such as inhibition of monoamine or serotonin reuptake, but currently the selective serotonin reuptake inhibitors (SSRIs) are the first-choice drugs for depression therapy[399, 400]. Although SSRIs are generally well tolerated, cases of liver injury have been documented, as well as other side effects such as nausea, vomiting and sexual disorders[400, 401]. A number of SSRIs, like the widely prescribed ADs fluoxetine or sertraline, have been reported to have mitochondrial off-targets and impair mitochondrial function[402,401, 403].

In summary, although the mechanisms of action of most of the psychotropic drugs presented in this study are well known, their effects on mitochondria and cell energy metabolism remain to be fully elucidated. For that reason, different *in vitro* approaches were used to investigate the effects of a total of 22 psychotropic drugs, including a series of antipsychotics, anticonvulsants, antidepressants and anxiolytic drugs on rat liver mitochondria (RLM) and the human hepatoblastoma cell line HepG2. Subsequently, docking studies were performed to examine the binding affinities of the compounds to the different ETC complexes. The rationale behind using different *in vitro* assays lies in the fact that multiple assays may be required to fully understand the mechanisms of toxicity given that drugs may induce mitochondrial impairment through multiple mechanisms. Since conflicting and contradictory effects have been described in the literature, the main goal of this chapter was to compare multiple *in vitro* assays using different model systems and mitochondrial endpoints to shed light on the mitochondrial bioenergetics effects of the drugs.

6.2. Chapter Aims

The overall aim of this chapter was to investigate the effects of 22 psychotropic drugs belonging to different drug classes (antipsychotics, anticonvulsants, antidepressants and anxiolytic drugs) on mitochondrial function. Specific objectives for all 22 drugs contemplated in this chapter were:

1. To investigate the OCR and ECAR response of HepG2 cells upon acute injection of drugs at different concentrations, generally including clinical maximum plasma concentrations (C_{max}) and 100 x C_{max} concentrations when possible for clinical relevance.
2. To select those drugs that showed some effect in the AEFA for further investigations to determine inhibition of the different mitochondrial ETC complexes using HepG2 cells permeabilised with rPFO and incorporating various substrates/inhibitors.
3. To use the Glu/Gal assay for additional evidence in the determination of mitochondrial toxicants.
4. To determine the binding affinities of drugs in the ligand-binding pocket of the different ETC complexes through docking studies.
5. To compare results obtained with the literature mechanisms.

Additionally, chlorpromazine, haloperidol and olanzapine were subjected to further investigations. Experimental aims included:

1. To generate a bioenergetic profile of HepG2 cells grown in glucose media upon 1 h incubation with 50 µM of the drugs.
2. To generate a bioenergetic profile of HepG2 cells after 1 h and 24 h glucose deprivation upon 1 h incubation with 50 µM of the drugs.
3. To simultaneously investigate OCR and MMP in freshly isolated mitochondria using high-resolution respirometry.
4. To assess viability of HepG2 cells grown in high-glucose media (25 mM) after 24 h or 48 h treatment with the drugs through MTT assays.
5. To assess and compare viability of HepG2 cells grown in glucose media (25 mM) or galactose media (10 mM) after 24 h treatment with the drugs through MTT assays.

6.3. Results

6.3.1. Data set of compounds

A total of 22 psychotropic drugs were included in this study: 10 antipsychotics, 7 anticonvulsants, 3 antidepressants and 2 anxiolytic drugs. A summary of these drugs and literature mechanisms of mitochondrial toxicity is given in Table 6.1. All compounds had some reported mitochondrial liabilities, except for amisulpride, lorazepam and vigabatrin. For the cell assays, the top concentrations tested of each compound were at least 100 x C_{max} (Table 6.2), unless not possible due to solubility limitations. When possible, C_{max} values were obtained from the literature for plasma or serum of adult humans for consistency.

This section has been divided into three main groups: “Antipsychotics”, “Anticonvulsants” and “Antidepressants and Anxiolytic drugs” for ease of understanding and clarity of comparison between compounds of the same drug class.

Table 6.1. Summary table of compounds tested, drug class and literature mechanism of action on mitochondria.

Compounds	Drug class	Literature mechanism	Reference
Amisulpride	Antipsychotic	no reported effects	N/A
Aripiprazole	Antipsychotic	complex I inhibitor	Cikánkova T. *et al.*, 2019[404]
Buspirone	Anxiolytic	complex I inhibitor	Dykens JA. *et al.*, 2008[60]
Carbamazepine	Anticonvulsant	decreased ATP production	Berger I. *et al.*, 2010[405]
		complex I and IV inhibitor	Cikankova T. *et al.*, 2019[400]
Chlorpromazine	Antipsychotic	complex I and IV inhibitor	Elmorsy E. *et al.*, 2017[375] Cikankova T. *et al.*, 2019[404]
Citalopram	Antidepressant	complex I and II inhibitor	Hroudova J. *et al.*, 2010[406]
		increased ROS, loss of MMP	Xia Z. *et al.*, 1999[407]
Clozapine	Antipsychotic	complex I, II+III and IV inhibitor	Cikánková T. *et al.*, 2019[404] Elmorsy E. *et al.*, 2017[375] Modica-Napolitano J. *et al.*, [408]
Fluoxetine	Antidepressant	F_1F_0 ATPase inhibitor / decreased state 3 respiration and RCR	Curti C *et al.*, 1999[105] Souza M *et al.*, 1994[409]
		MPTP inhibition	Nahon E. *et al.*, 2005[410]
		decreased mitochondrial complex I and II-linked respiration	Hroudova J. *et al.*, 2012[411]
Haloperidol	Antipsychotic	complex I inhibitor	Cikánková T. *et al.*, 2019[404]
Lamotrigine	Anticonvulsant	increased ATP production	Berger I. *et al.*, 2010[405]
		neuroprotective effect against the toxicity of rotenone	Kim YJ. *et al.*, 2007[412]
Lorazepam	Anxiolytic	no reported effects	N/A
Olanzapine	Antipsychotic	complex I and IV inhibitor	Hroudova J. *et al.*, 2010[406]
		activation of citrate synthase activity	Hroudova J. *et al.*, 2010[406]
Phenobarbital	Anticonvulsant	complex I, II and IV inhibitors	Santos, NA. *et al.*, 2008[397]
Phenytoin	Anticonvulsant	decreased state-3 respiration and ATP synthesis	Santos, NA. *et al.*, 2008[397]
Primidone	Anticonvulsant	enhanced SOD activity and decrease of monoamine oxidases	Bodganov G. *et al.*, 2009[413]
Quetiapine	Antipsychotic	complex I inhibitor	Cikánková T. *et al.*, 2019[404]
Reserpine	Antipsychotic	uncoupler	Maina G., 1974[414]
Tianeptine	Antidepressant	mitochondrial FAO inhibitor	Fromenty B. *et al.*, 1989[415]
		complex I and IV inhibitor	Abdel-Razaq W. *et al.*, 2011[402], Hroudova J. *et al.*, 2010[406]
Trifluoperazine	Antipsychotic	ETC inhibitor	Cheah, KS. *et al.*, 1983[416]
		ATPase inhibitor	Ruben L *et al.*, 1981[417]
Valproic acid	Anticonvulsant	complex I and IV inhibitor	Hroudova J. *et al.*, 2010[406]
		mitochondrial FAO inhibitor	Silva MF. *et al.*, 2001[418]
		MPTP opening	Begriche K. *et al.*, 2011[68]
		decreased OCR, MMP, ATP and increased ROS	Komulainen T. *et al.*, 2015[419]
Vigabatrin	Anticonvulsant	no reported effects	N/A
Ziprasidone	Antipsychotic	complex II, III and IV inhibitors	Scaini G. *et al.*, 2018[374]
			Cikánková T. *et al.*, 2019[404]

N/A = not available

6.3.2. Antipsychotics

In this section, the effects of three typical antipsychotics (APs) (chlorpromazine, haloperidol and trifluoperazine) and seven atypical antipsychotics (amisulpride, aripiprazole, clozapine, olanzapine, quetiapine, reserpine and ziprasidone) were investigated. Chemical structures of compounds are depicted in Figure 6.1.

6.3.2.1. The Acute Extracellular Flux Assay (AEFA) to Assess Real-Time Effects of Antipsychotics on Mitochondrial Function

The Seahorse Bioscience XF96 analyser was used to assess real-time changes in oxygen consumption rate (OCR) and extracellular acidification rate (ECAR) upon injection of 10 different APs onto HepG2 cells. Top concentrations tested were at least 100 x C_{max} (Table 6.2), unless not possible due to solubility limitations. Cells were then subjected to sequential exposure to various mitochondrial stressors that allowed determination of several mitochondrial parameters, such as ATP turnover, reserve capacity or proton leak. Figure 6.2 and Figure 6.3 show the effect of various drug concentrations on basal OCR, basal ECAR, reserve capacity, and ATP production. Data obtained for all examined APs and rotenone, a potent complex I inhibitor used as positive control, are summarised in Table 6.2 and Table 6.3.

This assay identified one ETC inhibitor, one uncoupler and one substrate inhibitor out of the 10 APs tested (Table 6.2). Aripiprazole showed a dose-dependent drop in basal OCR alongside an increase in ECAR (indirect indicative of glycolysis), suggesting inhibition of the ETC. Chlorpromazine caused a drop in both OCR and ECAR, hence it was classified as a cytotoxic compound. Quetiapine reduced OCR but had no effect on ECAR, therefore it was classified as a substrate inhibitor. This means that reduction of oxygen consumption may be due to reduced substrate availability, explained by decreased substrate transport/metabolization mediated by other enzymes, such as the pyruvate dehydrogenase (PDH), the mitochondrial pyruvate carrier (MPC) or the mitochondrial dicarboxylate carrier (DIC). Trifluoperazine only caused a small decrease in reserve capacity, while OCR and ECAR responses remained unaffected. Hence it was categorised as “other”. Finally, 100 µM reserpine showed a strong uncoupling activity, increasing OCR and proton leak while causing a decrease in mitochondrial ATP production. The rest of the APs

tested showed no significant real-time effects on mitochondrial function upon acute injection.

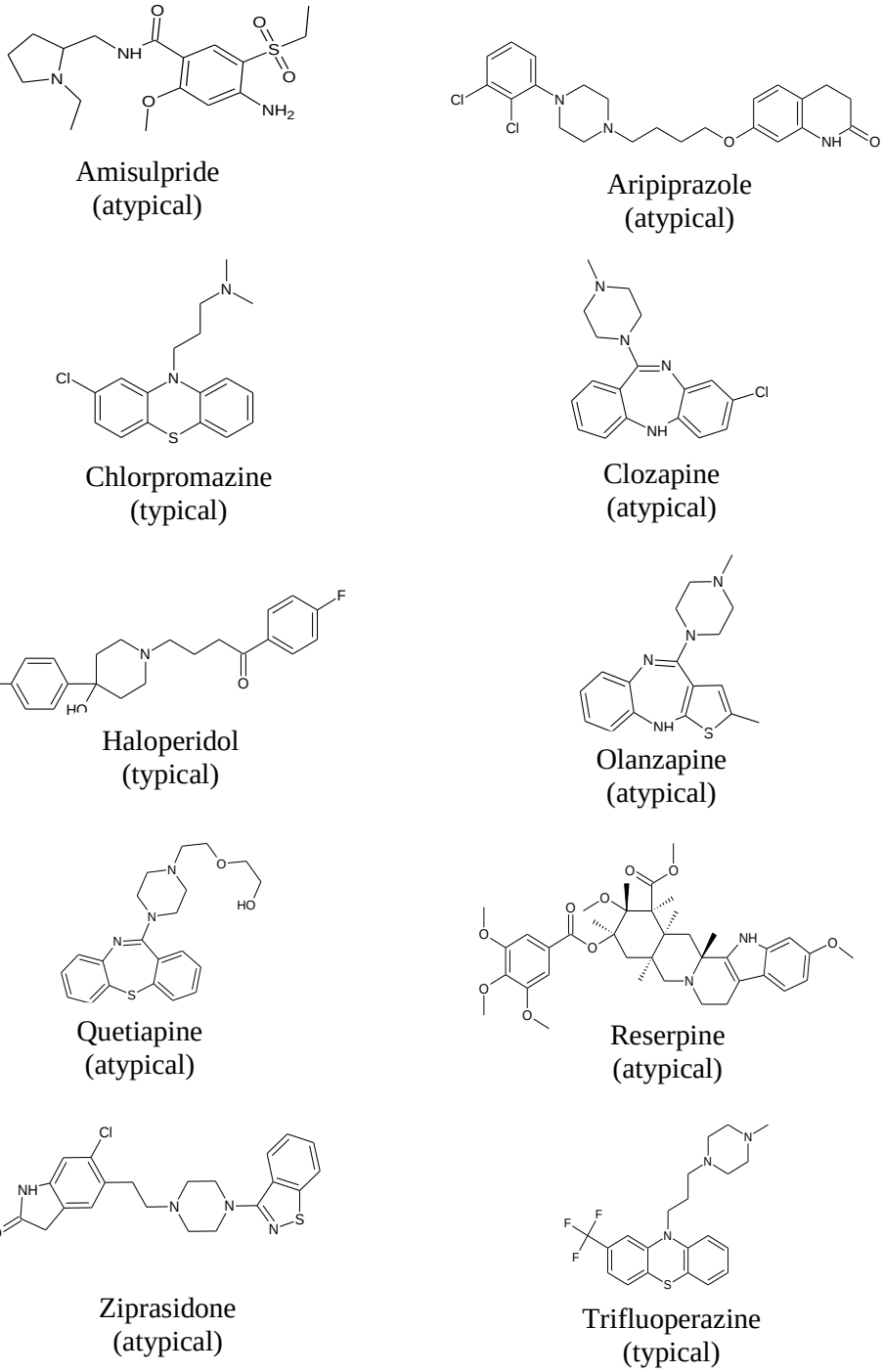

Figure 6.1. Chemical structures of the typical and atypical antipsychotics tested.

Table 6.2. Acute extracellular flux assay for the detection of mitochondrial toxicity. List of antipsychotics, clinical C_{max} values from references and ranges of concentrations tested. Direction of change in basal OCR, reserve capacity, basal ECAR, ATP production and proton leak, where: ↑ = increase compared to vehicle control, ↓ = decrease compared to vehicle control, NR = no response compared to vehicle control. N/A = not available. Summary mechanism is the conclusion made based on the direction of change in the bioenergetic parameters.

Compounds	C_{max} (µM)	C_{max} reference	Concentration range (µM)	Direction of change					Summary mechanism
				OCR	Reserve capacity	ECAR	ATP	Proton leak	
Amisulpride	2.56	Mogili, R. *et al*., 2011	0.1 - 100	NR	NR	NR	NR	NR	-
Aripiprazole	0.17	Mallikaarjun, S. *et al*., 2000	0.01 - 10	↓	↓	↑	↓	NR	ETC inhibitor
Chlorpromazine	0.9	Nadanaciva, S. *et al*., 2007	0.1 - 100	↓	↓	↓	NR	↑	Cytotoxicity
Clozapine	0.22	Chang, W. *et al*., 1999	0.1 - 100	NR	NR	↓	↓	NR	-
Haloperidol	0.02	Gupta, S.K. *et al*., 1995	0.1 - 100	NR	NR	NR	NR	NR	-
Olanzapine	0.02	Gossen, D., *et al*., 2002	0.05 - 50	NR	NR	NR	NR	NR	-
Quetiapine	1.42	Darwish, M. *et al*., 2012	0.15 - 150	↓	↓	NR	↓	NR	Substrate inhibitor
Reserpine	0.0004	El-Din, M.M. *et al*., 2016	0.1 - 100	↑	NR	NR	↓	↑	Uncoupler
Trifluoperazine	0.0009	Iyama, Y. *et al*., 2019	0.002 - 2	NR	↓	NR	NR	NR	Other
Ziprasidone	0.11	Darwish, M. *et al*., 2014	0.04 - 40	NR	NR	NR	NR	NR	-
Rotenone	N/A	N/A	0.003 - 1	↓	↓	↑	↓	↓	ETC inhibitor

Table 6.3. Data summary of acute extracellular flux assay. MEC = minimum effective concentration that significantly crosses vehicle control threshold. AC_{50} = the concentration at which 50% maximum effect is observed. NR = no response observed.

Compounds	MEC (µM)					AC_{50} (µM)				
	OCR	**Reserve capacity**	**ECAR**	**ATP production**	**Proton leak**	**OCR**	**Reserve capacity**	**ECAR**	**ATP production**	**Proton leak**
Amisulpride	NR	NR	NR	NR	NR	NR	NR	NR	NR	NR
Aripiprazole	2.06	0.344	9.20	3.49	NR	>10	>10	>10	>10	NR
Chlorpromazine	73.4	78.4	15.6	NR	29.8	>100	>100	>100	NR	84.4
Clozapine	NR	NR	20.2	37.3	NR	NR	NR	>100	>100	NR
Haloperidol	NR	NR	NR	NR	NR	NR	NR	NR	NR	NR
Olanzapine	NR	NR	NR	NR	NR	NR	NR	NR	NR	NR
Quetiapine	19	26.1	NR	92.3	NR	>150	124	NR	>150	NR
Reserpine	60.3	NR	NR	59.4	30	>100	NR	NR	77.3	36.8
Trifluoperazine	NR	<0.002	NR	NR	NR	NR	0.157	NR	NR	NR
Ziprasidone	NR	NR	NR	0.949	0.12	NR	NR	NR	NR	NR
Rotenone	0.0053	<0.003	0.0274	0.0159	0.0120	0.0433	0.0106	>1	0.0459	0.213

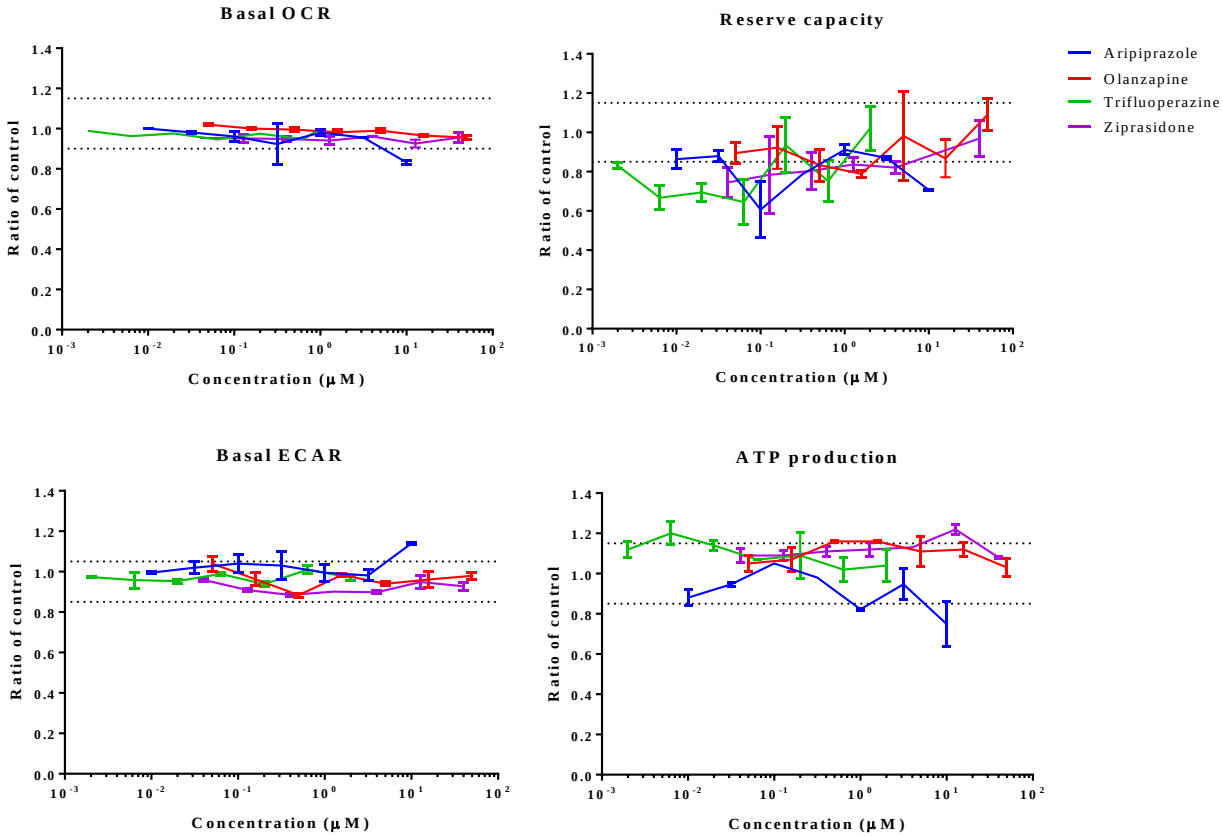

Figure 6.2. Bioenergetic profile of aripiprazole, olanzapine, trifluoperazine and ziprasidone using the Extracellular Flux Analyser. Dose-response curves show the effects of compounds in basal OCR, reserve capacity, basal ECAR and ATP production in 10 mM glucose, 1 mM pyruvate and 2 mM glutamine. Data is expressed as mean ratio to vehicle control ± SD of n = 3. Dashed lines represent significant cut-off from vehicle control.

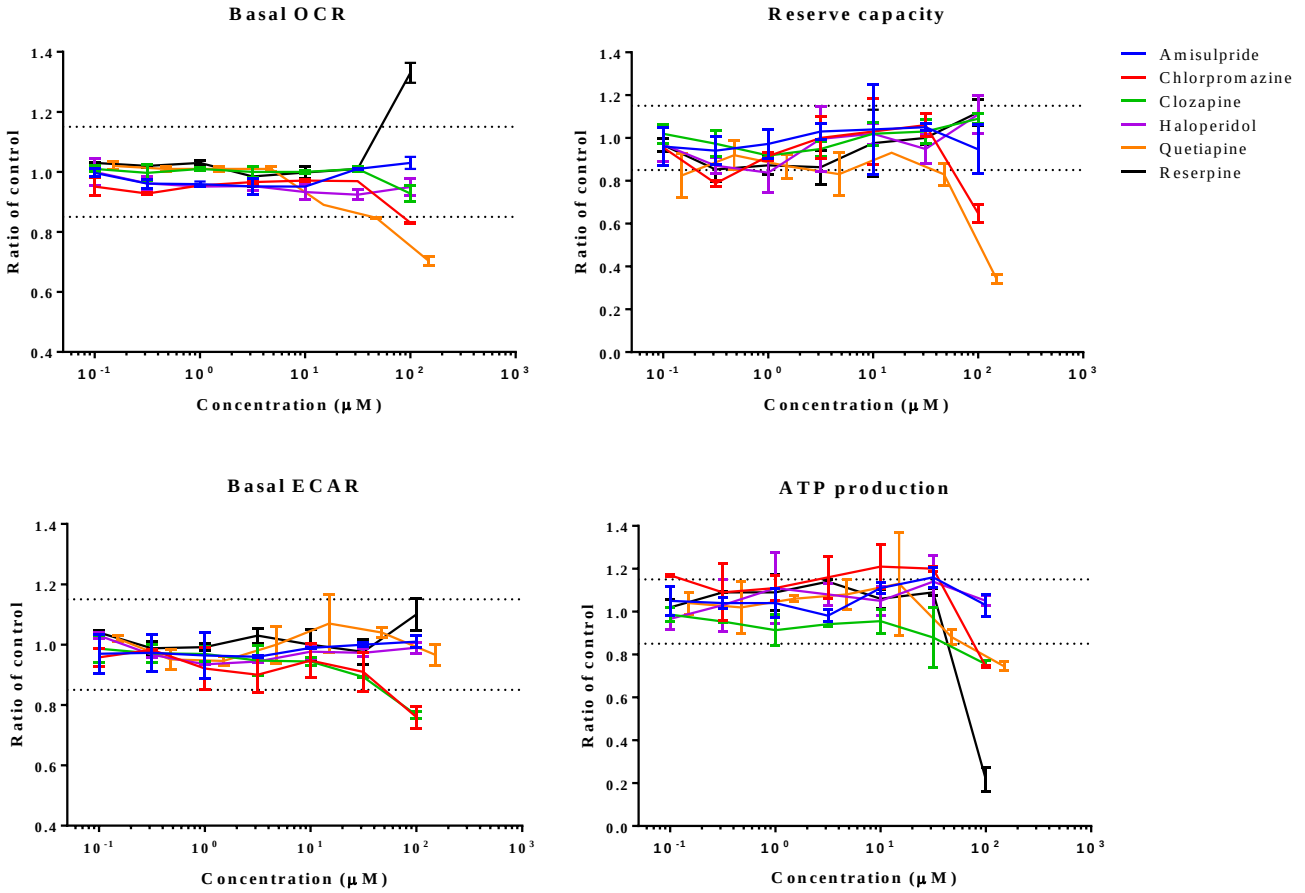

Figure 6.3. Bioenergetic profile of amisulpride, chlorpromazine, clozapine, haloperidol, quetiapine and reserpine using the Extracellular Flux Analyser. Dose-response curves show the effects of compounds in basal OCR, reserve capacity, basal ECAR and ATP production in 10 mM glucose, 1 mM pyruvate and 2 mM glutamine. Data is expressed as mean ratio to vehicle control ± SD of n = 3. Dashed lines represent significant cut-off from vehicle control.

6.3.2.2. Measurement of Respiratory Activity using Permeabilised Cells with rPFO

Those compounds that showed a response in the AEFA (chlorpromazine, aripiprazole, reserpine, trifluoperazine and quetiapine) and haloperidol (due to the extensive literature data regarding inhibition of complex I by this compound) were included here for further investigations. At the beginning of the assay, the compounds were injected onto permeabilised HepG2 cells in media containing complex I-linked substrates and ADP. Then, changes in OCR with respect to basal respiration prior to the injection of compounds were recorded. The rest of the assay involved the injection of other substrates/inhibitors for the determination of the effects of the compounds on other ETC complexes.

Among all the compounds tested, a response would be expected from all the compounds that were previously categorised as ETC inhibitors or substrate inhibitors: aripiprazole and quetiapine, respectively. However, only quetiapine showed a response inhibiting complex I-linked respiration at supra-therapeutic concentrations (Figure 6.4). Mitochondrial respiration was restored upon addition of complex II substrate succinate to the media, indicating that quetiapine may act as a complex I inhibitor or an inhibitor of substrates linked to complex I respiration.

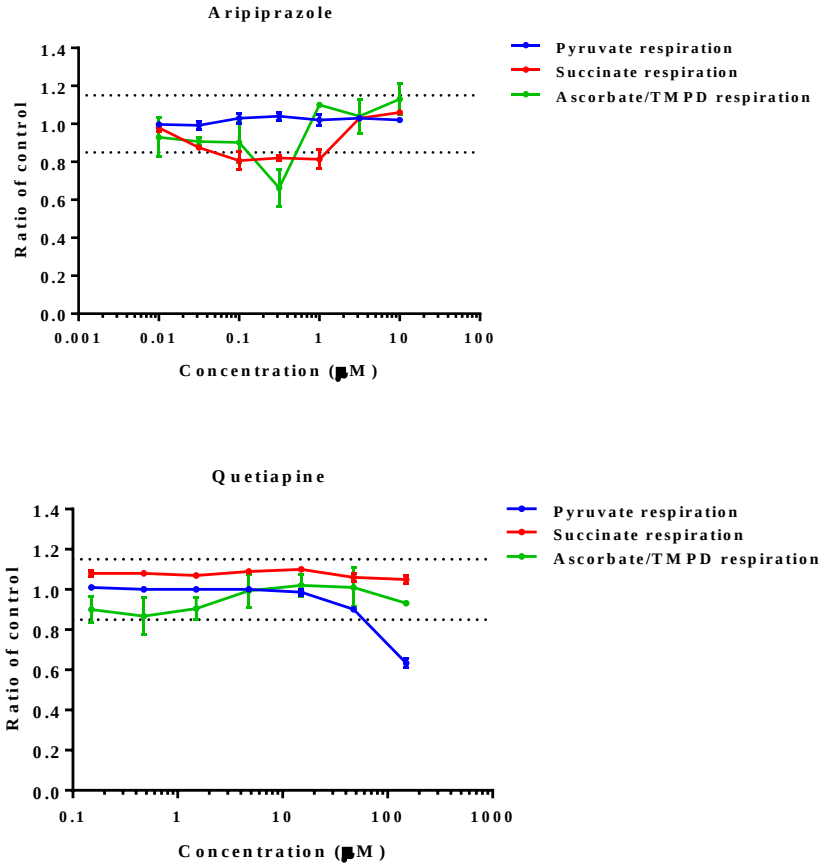

Compound	Most sensitive mechanism	⇅	MEC (μM)	AC_{50} (μM)
Aripiprazole	NR		NR	NR
Quetiapine	pyruvate respiration	↓	66.3	>150

Figure 6.4. Dose-response curve of quetiapine in the permeabilised cell assay. Black dashed lines represent significant cut-off from vehicle control. MEC = minimum effective concentration that significantly crosses vehicle control threshold. AC_{50} = the concentration at which 50% maximum effect is observed. Data is expressed as mean ratio to vehicle control ± SD of n = 3.

6.3.2.3. Assessment of Mitochondrial Toxicity of Antipsychotics using Selective Media Conditions (Glu/Gal assay)

APs-induced mitochondrial toxicity was assessed in HepG2 cells cultured in galactose (Gal) or glucose (Glu) containing media. To this end, cellular ATP levels were measured after 24 h compound treatment to determine cell viability in either media conditions. As explained in chapter 5, this assay was developed to increase the susceptibility of glycolytic cells to mitochondrial toxicants by forcing them to rely solely mainly on mitochondrial OXPHOS for energy production. AC_{50} values obtained in either media conditions, as well as fold-change values are shown in Table 6.4. Rotenone was used as positive control, causing a 4600-fold change in the AC_{50} values (Table 6.4). With the exception of ziprasidone, none of the antipsychotics had increased toxicity in galactose media, indicating the assay did not identify any mitochondrial toxicity at the concentrations used. Amisulpride and aripiprazole didn't show any response in any of the media conditions (top concentrations were 100 μM and 10 μM, respectively). Compounds that showed similar toxicity in both media conditions included chlorpromazine (100 μM top concentration), clozapine (100 μM top concentration), quetiapine (150 μM top concentration) and trifluoperazine (2 μM top concentration). Compounds that showed slightly higher toxicity in Glu media included haloperidol (100 μM top concentration), olanzapine (50 μM top concentration) and reserpine (100 μM top concentration). Ziprasidone was the only compound that showed a higher toxicity in Gal media (40 μM top concentration), despite not being toxic in AEFA. The toxicity in this current assay could be due to metabolism/degradation of this compounds during incubation period. Ziprasidone is known to be extensively metabolized *in vivo* with only a small amount excreted as unchanged drug. In clinical settings, oxidation by cytochrome P450 and, more importantly, reduction by aldehyde oxidase are the main routes of metabolism[420].

Table 6.4. Summary table of the Glu/Gal assay performed on antipsychotics. AC_{50} = the concentration at which 50% maximum effect is observed. ↑↓ = Direction of response. NR = no response observed. UD = undetermined toxicity.

Compounds	↑↓	Glucose AC_{50} (μM)	↑↓	Galactose AC_{50} (μM)	Fold Change
Amisulpride		NR		NR	NR
Aripiprazole		NR		NR	NR
Chlorpromazine	↓	15.9	↓	16.9	0.941
Clozapine	↓	56.7	↓	60.8	0.933
Haloperidol	↓	57.5	↓	78.6	0.732
Olanzapine	↓	>50		NR	UD
Quetiapine	↓	76.7	↓	79	0.971
Reserpine	↓	48.9	↓	79	0.619
Trifluoperazine	↓	1	↓	1.13	0.885
Ziprasidone		NR	↓	>40	UD
Rotenone	↓	27.8	↓	0.00605	4600

6.3.2.4. Further Investigations on the Typical Antipsychotics Chlorpromazine and Haloperidol and the Atypical Antipsychotic Olanzapine

6.3.2.4.1 Measurement of Cell Bioenergetics: Incubated Drug Effect using the Extracellular Flux Analyzer 8-well format

The effects of incubation for 1 h of the typical APs chlorpromazine (Chl) and haloperidol (Hlp) and the atypical AP olanzapine (Olz) on mitochondrial function were further investigated using the Extracellular Flux Analyzer 8-well format (XFp, Seahorse Bioscience). In this assay, HepG2 cells were incubated with 50 μM of the drugs for 1 h prior the commencement of "stress test"[421]. The Seahorse XFp Analyser is an 8-well format: it allowed 2 background wells, 3 vehicle control wells and 3 experimental wells per assay. Each assay was repeated at least three times using different biological samples and all measurements were normalised to protein content.

The effects of the compounds on mitochondrial bioenergetics were initially studied in glucose containing media (10 mM) supplemented with 1 mM sodium pyruvate and 2 mM glutamine. Figure 6.6 shows the bioenergetic profile of the HepG2 cells after 1 h incubation with 50 μM Chl, 50 μM Hlp or 50 μM Olz vs. vehicle control (0.5% DMSO). Results in Figure 6.6 show that, in growing cells, where mitochondria are actively synthesising ATP (state 3), Hlp caused a slight significant decrease in basal respiration (*$p<0.05$). This decrease in the rate of respiration was compensated by an increase in glycolysis (*$p<0.05$) to maintain the energy status. The maximal respiratory capacity was also highly reduced, reaching practically the same levels of

oxygen consumption as in basal respiration, indicating the total absence of spare respiratory capacity. For 50 μM Chl, although a decrease in OCR is visible in Figure 6.5, data normalised to protein content showed no significant changes neither in basal OCR nor in basal ECAR (Figure 6.6). However, 50 μM Chl caused a decrease in maximal respiration and spare respiratory capacity (Figure 6.6). In addition, a significant reduction in cell viability was observed under the microscope, which could explain the decrease in raw OCR data (Figure 6.5). Hence, a loss of mitochondrial mass due to cytotoxicity caused by Chl could account for the significant decrease in the spare respiratory capacity observed in Figure 6.6. Such reduction in cell viability was not observed in the case 50 μM Hlp 1 h incubation. Finally, 1 h incubation with 50 μM Olz led to a small non-significant (at *p<0.05) decrease in basal OCR and a small significant decrease in basal ECAR (*p<0.05). In contrast with the typical APs, maximal respiratory capacity and spare respiratory capacity were less affected by 50 μM Olz (Figure 6.6).

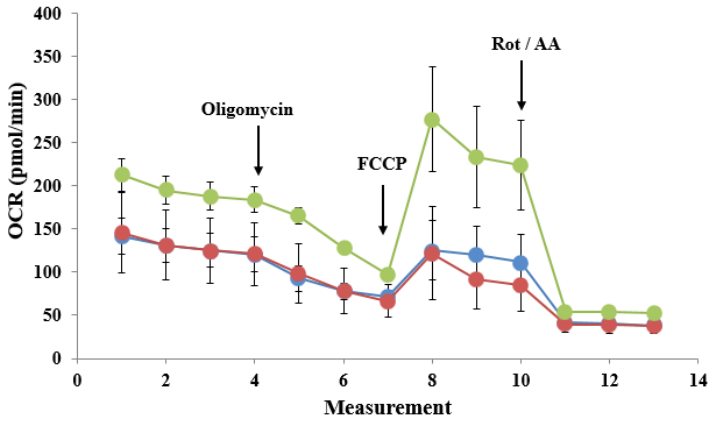

Figure 6.5. Effect of the typical antipsychotics Hlp and Chl on the energy metabolism of HepG2 cells. The figure represents the raw data of two representative experiments (n = 2) in which HepG2 cells were previously incubated in 10 mM glucose, 1 mM sodium pyruvate and 2 mM glutamine (pH = 7.4) with either 0.5% DMSO (control in green), 50 μM Chl (blue) or 50 μM Hlp (red).

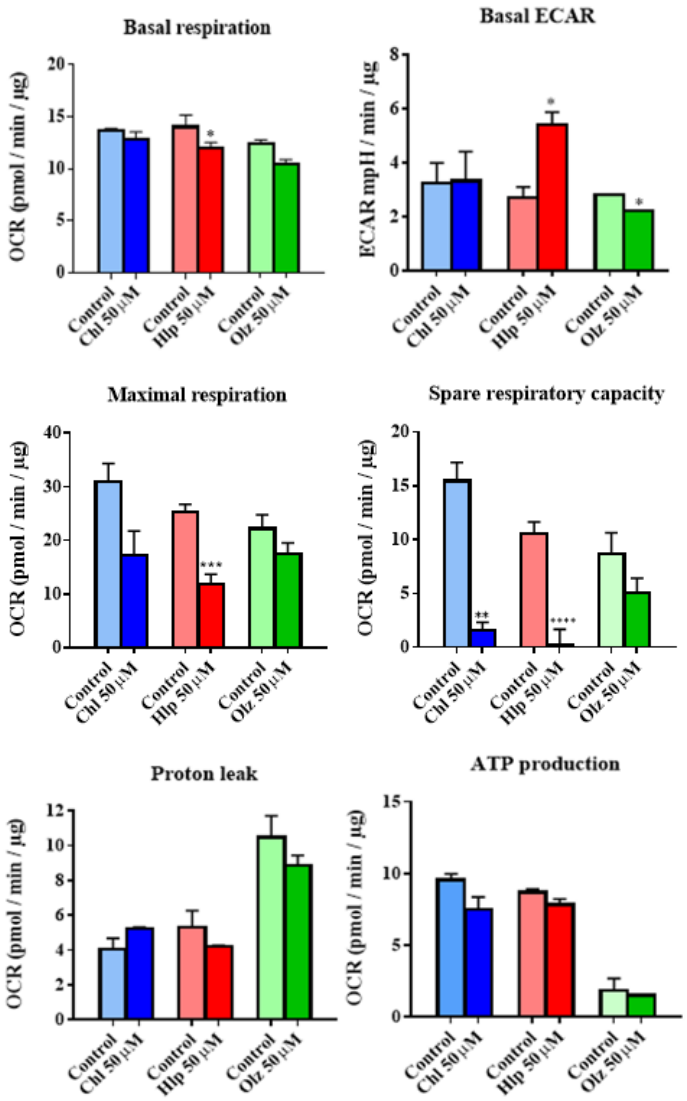

Figure 6.6. Bioenergetic profile of HepG2 cells after 1 h incubation with 50 µM chlorpromazine (Chl), 50 µM haloperidol (Hlp) or 50 µM olanzapine (Olz) vs. vehicle control. Assay media contained 10 mM glucose, 2 mM glutamine and 1 mM sodium pyruvate. Results are mean ± S.D. of n = 3 independent experiments, *p<0.05, **p<0.01, ***p<0.001.

Subsequently, the metabolic flexibility of HepG2 cells in the presence of either 50 µM Hlp or 50 µM Olz, was further investigated by depriving the cells of glucose (Glu) for 1 h or 24 h. Instead, media contained 10 mM galactose and was supplemented with 1 mM sodium pyruvate and 2 mM glutamine.

Figure 6.7 depicts the effects of 1 h incubation with 50 µM Hlp vs. vehicle control (0.5% DMSO) in Glu media, compared with 1 h and 24 h glucose deprivation (Gal media instead). Results show that Hlp decreased basal OCR with respect to the vehicle control in all media conditions. However, only in Glu media cells could increase

glycolysis to maintain the energy status. No change in basal ECAR and glycolytic capacity was observed after 1 h Glu starvation, and a decrease in these was observed after 24 h Glu starvation (although non-significant at *$p<0.05$). It was also striking to find that only in Glu media Hlp led to a strong diminishment in the maximal respiration and complete abolishment of the spare respiratory capacity. A possible explanation for this phenomenon could be that, as demonstrated in chapter 5, only after 24 h glucose deprivation cells become completely dependent on OXPHOS for energy production, which could trigger changes in the mitochondrial dynamics, such as an increase in mitochondrial fusion to improve mitochondrial efficiency (as shown in chapter 5, Figure 5.6). This could possibly explain why respiratory capacity is preserved in non-Glu containing media in the presence of Hlp, however confirmation of this hypothesis will require further investigations.

50 μM Olz did not cause a significant decrease in basal OCR, however, it reduced basal ECAR and the glycolytic capacity with respect to the vehicle control, which may be explained by a decrease in glycolysis (i.e. lactate production), given that the OCR response remained unaffected (therefore reduction in ECAR signal cannot be explained by a reduction in CO_2 formation from respiration). Confirmation of inhibition of glycolytic activity by olanzapine and resulting decrease in lactate production will require further testing and specific measurements of cellular lactate concentration. Interestingly, reduction in glycolysis would be in agreement with some of the side effects caused by olanzapine, which include hyperglycaemia and weight gain[422].

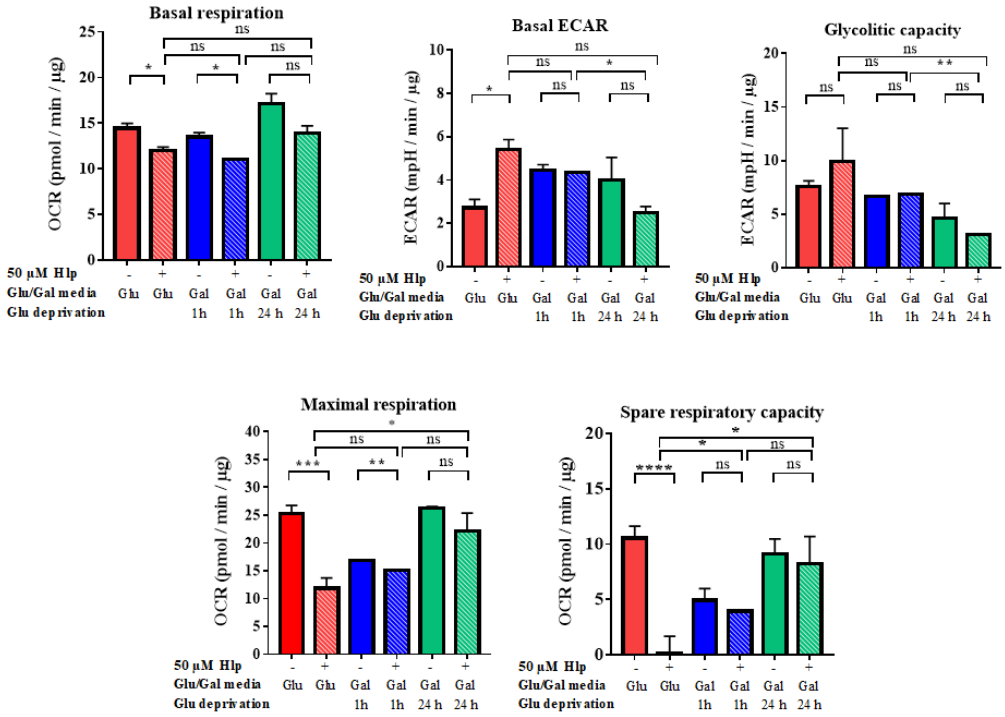

Figure 6.7. Bioenergetic profile of HepG2 cells after 1 h treatment with 50 µM haloperidol (Hlp) (+) or vehicle control (-). Cells were grown either in the presence of 10 mM glucose or 10 mM galactose (glucose-deprived for 1 h or 24 h). Results are mean ± S.D. of n = 3 independent experiments, ns = non-significant, *p<0.05, **p<0.01, ***p<0.001 and ****p<0.0001.

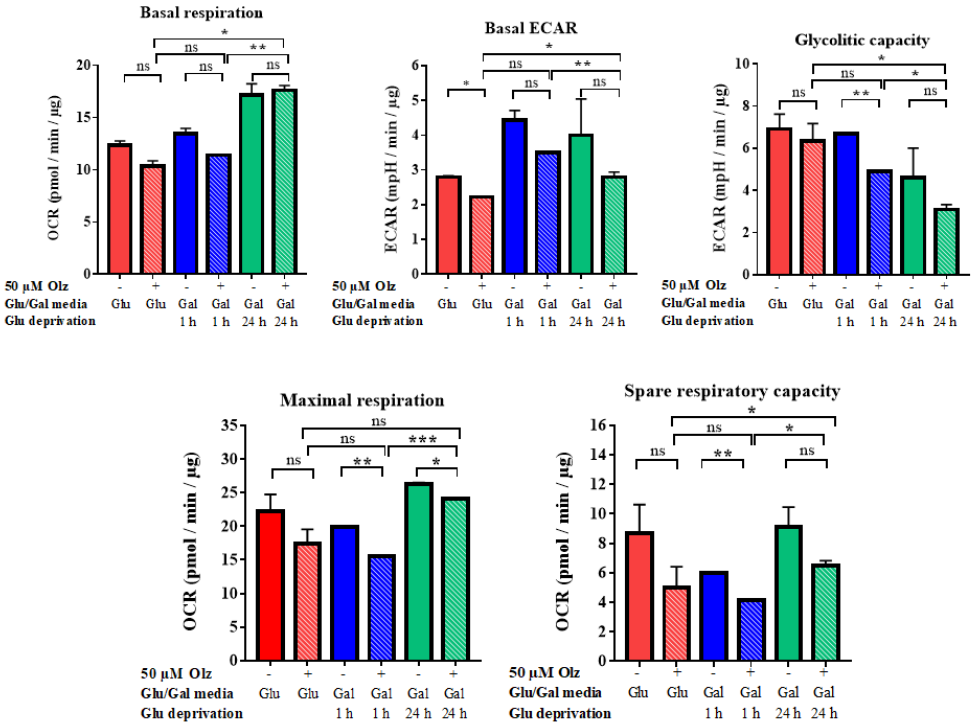

Figure 6.8. Bioenergetic profile of HepG2 cells after 1 h treatment with 50 µM olanzapine (Olz) (+) vs. vehicle control (-). Cells were grown either in the presence of 10 mM glucose or 10 mM galactose (glucose-deprived for 1 h or 24 h). Results are mean ± S.D. of n = 3 independent experiments, ns = non-significant, *p<0.05, **p<0.01, ***p<0.001.

6.3.2.4.2 High-Resolution Respirometry Readings

Subsequently, the effects of Chl, Hlp and Olz on OCR and mitochondrial membrane potential (MMP) were simultaneously investigated using freshly isolated rat liver mitochondria and high-resolution respirometry (Oroboros® Oxygraph-2K). Upon initial calibration with 2 µM safranin, rat liver mitochondria (RLM), 1 µM rotenone and 12.5 mM succinate were added to the Oroboros® chambers to induce complex II-linked respiration. Then, increasing concentrations of the pharmaceutical drugs were titrated into the chambers. Results show that the three drugs displayed very different effects on the ETC. On the one hand, Chl behaved as an uncoupler of OXPHOS, as it increased the respiratory rate to 111% at 20 µM, to 125% at 50 µM and to 131% at 100 µM, while it significantly dissipated the MMP to 88% at 20 µM, to 79% at 50 µM and to 72% at 100 µM (normalised to control, i.e. succinate respiration) (Figure 6.9). Hlp, on the other hand, decreased respiration to 85% at 20 µM and 77% at 50 µM. It also dissipated the MMP to 88% at 20 µM and to 69% at 50 µM. Finally, Olz didn´t affect respiration, but caused a mild dissipation of the MMP at 50 µM (Figure 6.9).

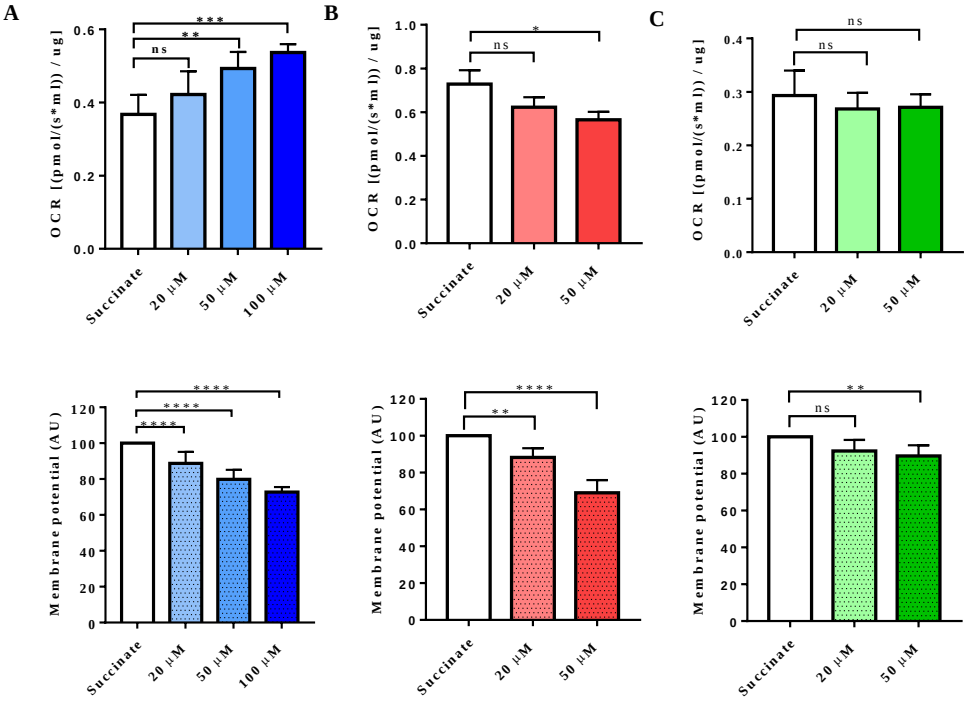

Figure 6.9. Simultaneous evaluation of OCR normalised to protein content and MMP in freshly isolated RLM in the presence of A) chlorpromazine (blue) B) haloperidol (red) and C) olanzapine (green). Data are mean ± SD of n = 3-6 independent experiments. For establishment of significance, one-way ANOVA was performed followed by the Dunnet test. Statistically significant values compared with the control are reported as follows: *p<0.05, **p<0.01, ***p<0.001 and ****p<0.0001.

The uncoupling effect of Chl was investigated further by the simultaneous measurement of uncoupled respiration and ROS production using the Oroboros® Oxygraph-2K. Here, 100-300 µg of freshly isolated RLM was added to each chamber and then respiration was initiated with 12.5 mM succinate + 1 µM rotenone and stimulated with 0.25 µM CCCP. Here, in contrast to what was observed in basal respiration (not stimulated by CCCP), Chl reduced respiration in a dose-dependent manner (50–400 µM) with an IC_{50} of 135 ± 5 µM. Likewise, increasing concentrations of Chl led to a reduction in the production of ROS (Figure 6.10). Both O_2 consumption and ROS production values are expressed as a percentage with respect to the baseline (succinate respiration).

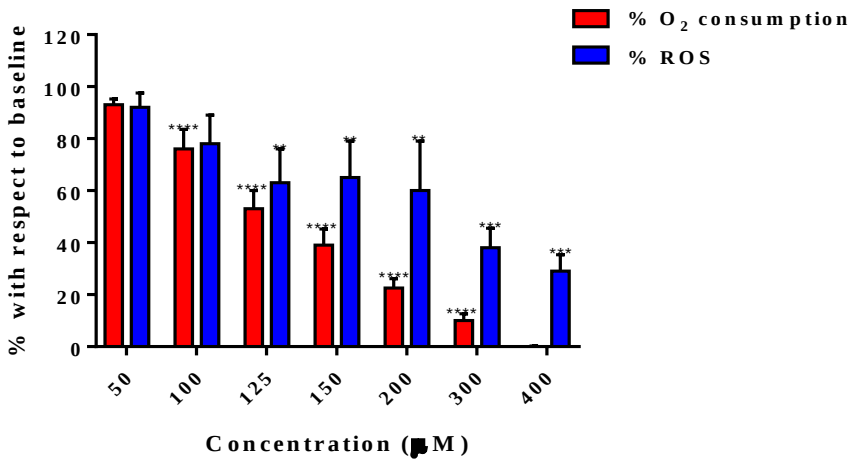

Figure 6.10. Chlorpromazine effects on ROS production and O_2 consumption in isolated RLM (uncoupled respiration). Data are mean ± SD of at least 3 independent experiments. **p<0.01, ***p<0.001, ****p<0.0001 vs. control (succinate respiration).

6.3.2.4.3 Cell Viability Measurements (MTT assay)

Finally, the effect of the drugs on cell viability was examined through MTT assays. In these assays, HepG2 cells were first grown in high glucose (Glu) media (25 mM) and were treated with different concentrations of the drugs for 24 h and 48 h (Figure 6.11). Then, the same was assessed on cells cultured in galactose (Gal) media (Figure 6.12). Available literature C_{max} values of drugs (Table 6.2) were considered and tested.

The results obtained in Glu containing media (Figure 6.11), suggest that all literature C_{max} values for the drugs were safe, as these concentrations showed no cytotoxic effect after 24 h or 48 h incubation treatment. C_{max} values were 1 µM for Chl[423] (103 ± 0.9% cell viability after 24 h), 0.02 µM for Hlp[424] (96 ± 4.2% cell viability after 24 h) and

0.02 μM for Olz[425] (101 ± 0.15% cell viability after 24 h) (Figure 6.11). From the dose-response curves of the relative cell viability with respect to the vehicle-treated controls, it can be concluded that Chl was the most toxic drug among the three antipsychotics. Chl reduced cell viability to 83 ± 0.6% at 15 μM and to 13 ± 5.3% at 75 μM. Same effects were observed after 48 h incubation (Figure 6.11). The fact that Chl reduced cell viability by 17% at a concentration just about 15 times its C_{max} value (0.9 μM)[423] indicates that bioaccumulation or poor metabolism of this drug can potentially lead to serious toxic events. Hlp showed a milder toxicity in Glu media than Chl, as cell viability was reduced to 88 ± 7.8% at 20 μM and to 42 ± 1.2% at 50 μM after 24 h incubation, whereas 48 h incubation reduced cell viability to 87 ± 18.3% at 20 μM and to 9 ± 6.9% at 50 μM. Olz did not show cytotoxicity in any of the concentrations tested (Figure 6.11). Testing higher concentrations than 50 μM Olz was not possible due to poor water solubility.

MTT toxicity of the drugs in Gal media was comparable to cytotoxicity measured using cellular ATP levels reported earlier in Table 6.4. Here, in MTT assay, Chl also equally induced cell death in both Glu (IC_{50} = 24.3 μM) and Gal media (IC_{50} = 28.2 μM) (Figure 6.12). Interestingly, treatment with 50 μM Hlp led to a bigger reduction in cell viability in cells grown in high Glu containing media (42 ± 1.2%) than in cells grown in Gal media (95 ± 9%) (Figure 6.12). Similarly, in assays where cellular ATP was the endpoint, toxicity caused by Hlp was found to be higher in Glu media (AC_{50} = 57.5 μM) than in Gal media (AC_{50} = 78.6 μM) (Table 6.4). A better understanding of this phenomenon will require further investigations. Finally, MTT assays revealed that Olz at concentrations up to 50 μM did not reduce cell viability neither in Glu nor in Gal media (Figure 6.12), which agrees with previous cytotoxicity assays that used cellular ATP as endpoint (Table 6.4).

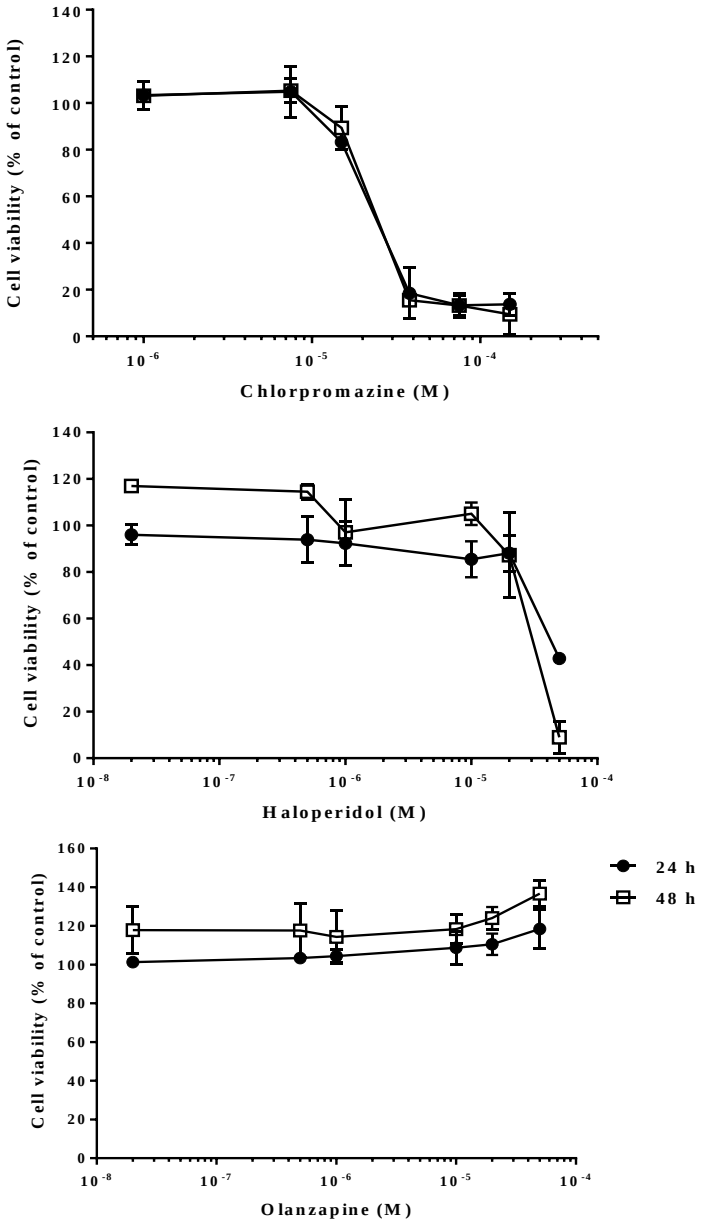

Figure 6.11. Viability percentage change of HepG2 cells grown in 25 mM glucose after 24 h (black circles) and 48 h (white squares) treatment with chlorpromazine (1-150 µM), haloperidol (0.02-50 µM) and olanzapine (0.02-50 µM). Data points represent mean ± S.D. (n=3 independent experiments).

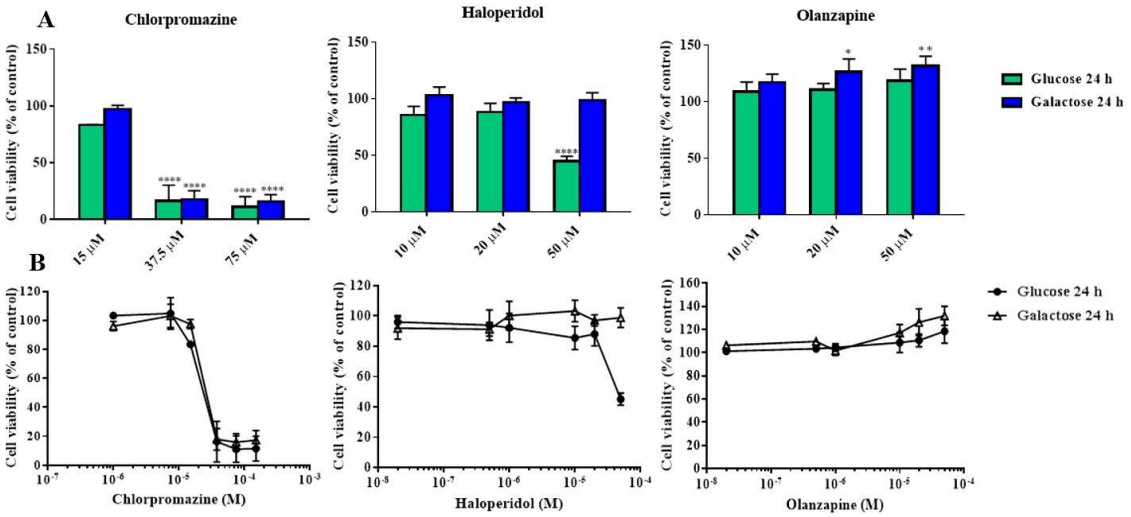

Figure 6.12. The effects of chlorpromazine, haloperidol and olanzapine on HepG2 cells viability after 24 h incubation in glucose or galactose media. A) Cell viability values expressed as percentage with respect to the vehicle control (100%). Statistically significant values compared with the control are reported as follows: *p<0.05, **p<0.01 and ****p< 0.0001 (one-way ANOVA followed by the Dunnet test). B) Dose-response curves of cell viability with chlorpromazine (1-150 µM), haloperidol (0.02-50 µM) or olanzapine (0.02-50 µM). Data points represent mean ± S.D. (n = 3 independent experiments).

6.3.2.4.4 Microscopic observations

Significant changes in the appearance and morphology of HepG2 cells were observed when incubated for 24 h with Chl and Hlp. While cells incubated in vehicle control (0.5% DMSO (v/v)) appeared healthy and confluent, 15 µM Chl visibly reduced cell viability and altered cell morphology, a concentration that is only 15-fold greater than its C_{max}[302]. At 37.5 µM, practically all cells were dead, which was clearly appreciated by the rounded shape that indicated cells were completely detached from the wells. Exposure to 50 µM Hlp for 24 h, significantly decreased cell number and led to rounding and detachment of the cells, which is a classic hallmark of the induction of cellular apoptosis[426] (Figure 6.13).

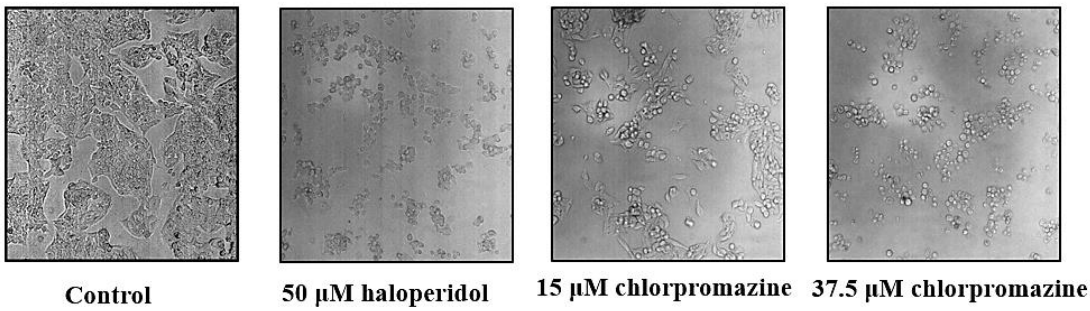

Figure 6.13. Microscopic observation of HepG2 cells cultured in glucose-containing media treated with 0.5% DMSO (v/v) (control), chlorpromazine or haloperidol for 24 h. Pictures were taken using Zeiss AxioVert with 10x/0.3 objective.

6.3.2.5. Molecular Docking of Antipsychotics

The 10 antipsychotics included in this research were virtually screened against the ETC complexes and ATP synthase by molecular docking. 3D structures of compounds were built from their SMILES codes using the MOE-Builder tool[204] and then all molecules were subjected to energy minimisation as outlined in Materials and Methods 2.11.1.2. Binding pockets were defined as outlined in Materials and Methods 2.11.2. The level of accuracy of the docking procedure was reported previously (Table 5.8). In general, all compounds showed high binding affinities for the protein targets, but the least favourable scores were observed for complex II. Drugs that displayed good docking scores included amisulpride (-9.94 kcal/mol for complex I and -10.22 kcal/mol for complex IV), aripiprazole (-9.96 kcal/mol for complex I, -11.55 kcal/mol for complex IV and -10.68 kcal/mol for complex V), haloperidol (-9.88 kcal/mol for complex IV), quetiapine (-9.37 kcal/mol for complex I, -9.53 kcal/mol for complex III and -10.15 kcal/mol for complex IV), reserpine (-11.59 kcal/mol for complex I, -14.59 kcal/mol for complex IV and -11.26 kcal/mol for complex V), trifluoperazine (-10.20 kcal/mol for complex IV and -9.47 kcal/mol for complex V) and ziprasidone (-10.27 kcal/mol for complex IV and -9.44 kcal/mol for complex V) (Figure 6.14 and Table 6.5). Table 6.5 shows that, out of 4 compounds that tested positive for mitochondrial OCR effect in the AEFA, 3 have a docking score below -10. However, 3 out of 6 non-inhibitor compounds also show ≤10 docking scores (amisulpride, trifluoperazine and ziprasidone).

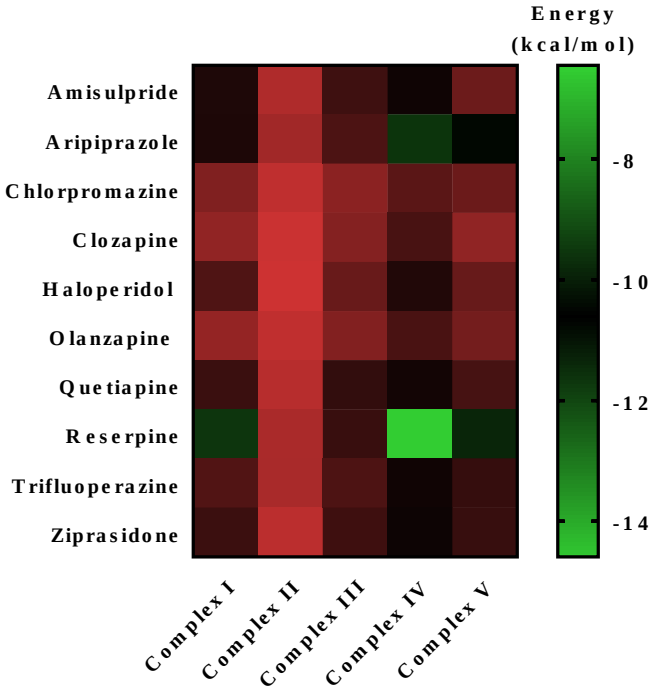

Figure 6.14. Top docking scores of the antipsychotics against the ETC complexes (complex I-IV) and ATP synthase (complex V) presented on a heat map.

Table 6.5. The lowest and highest docking scores for each of the APs screened alongside OCR AC_{50} values from the AEFA.

Compound	Lowest/Highest scores (kcal/mol)	ETC complex	OCR AC50 values (μM) from the AEFA (Table 6.3)
Amisulpride	-10.22	IV	NR
	-7.06	II	
Aripiprazole	-11.55	IV	>10
	-7.34	II	
Chlorpromazine	-8.74	IV	>100
	-6.74	II	
Clozapine	-9.10	IV	NR
	-6.52	II	
Haloperidol	-9.88	IV	NR
	-6.45	II	
Olanzapine	-9.08	IV	NR
	-6.72	II	
Quetiapine	-10.15	IV	>150
	-6.90	II	
Reserpine	-14.59	IV	>100
	-7.16	II	
Trifluoperazine	-10.20	IV	NR
	-7.17	II	
Ziprasidone	-10.27	IV	NR
	-6.82	II	

6.3.3. Anticonvulsants

In this section, the effects of seven anticonvulsants (ACs) were investigated: carbamazepine, lamotrigine, phenobarbital, phenytoin, primidone, valproic acid and vigabatrin. Chemical structures of compounds are depicted in Figure 6.15.

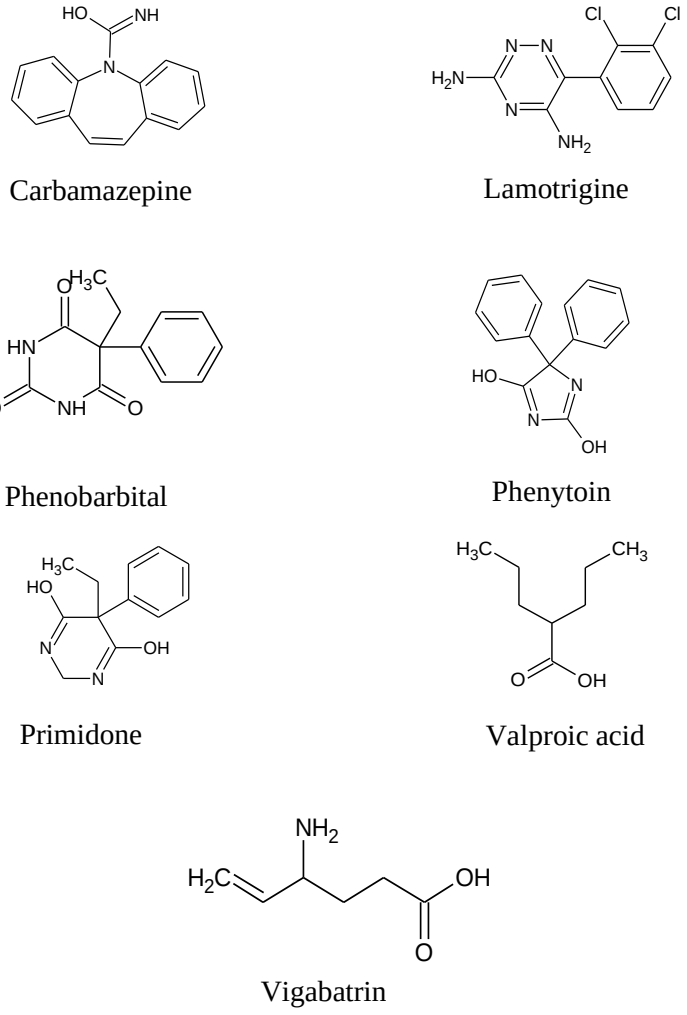

Figure 6.15. Chemical structures of anticonvulsants tested.

6.3.3.1. The Acute Extracellular Flux Assay (AEFA) to Assess Real-Time Effects of Anticonvulsants on Mitochondrial Function

The Seahorse Bioscience XF96 analyser was used to assess real-time changes in oxygen consumption rate (OCR) and extracellular acidification rate (ECAR) upon injection of seven different anticonvulsants onto HepG2 cells. Compounds were serially diluted in appropriate vehicle to give a seven-point concentration curve using a half-log dilution series. Top concentrations tested of each compound were at least 100 x C_{max} (Table 6.6) unless not possible due to solubility limitations. Figure 6.16 shows the bioenergetic profile of these drugs. Data obtained for all examined anticonvulsants and rotenone were analysed and summarised in Table 6.6 and Table 6.7.

This assay identified one ETC inhibitor, one substrate inhibitor and one cytotoxic compound out of the seven ACs tested (Table 6.6). Phenytoin caused a mild dose-dependent decrease in OCR (AC_{50} > 200 µM), reserve capacity and ATP production, which was accompanied by a dose-dependent increase in ECAR (AC_{50} > 200 µM), hence it was categorised as an ETC inhibitor. The effects observed in this assay occurred at concentrations that were close to its C_{max} value (180 µM) (Table 6.6)[427]. Carbamazepine was categorised as a possible substrate inhibitor, as it caused a dose-dependent decrease in OCR (AC_{50} > 600 µM), reserve capacity and ATP production but had no effect on ECAR. In the case of carbamazepine, top concentration tested was 100 x C_{max} (Table 6.6). At C_{max} (6 µM), carbamazepine had no effect on any of the bioenergetic parameters measured. The effects of 100 x valproic acid's C_{max} concentration could not be investigated here due to solubility limitations. Instead, the highest concentration tested was 10000 µM, which is around 28 x the C_{max} value. Results showed that valproic acid induced a dose-dependent decrease in all bioenergetic parameters, except for proton leak, which increased, and for this reason, it was categorised as a cytotoxic compound (Table 6.6). Compounds that showed no response in practically any of the mitochondrial parameters measured included lamotrigine (100 µM top concentration), phenobarbital (100 µM top concentration), primidone (100 µM top concentration) and vigabatrin (1000 µM top concentration).

Table 6.6. Acute extracellular flux assay for the detection of mitochondrial toxicity. List of anticonvulsants, clinical C_{max} values from references and ranges of concentrations tested. Direction of change in basal OCR, reserve capacity, basal ECAR, ATP production and proton leak, where: ↑ = increase compared to vehicle control, ↓ = decrease compared to vehicle control, NR = no response compared to vehicle control, N/A = not available. Summary mechanism is the conclusion made based on the direction of change in the bioenergetic parameters.

Compounds	**C_{max} (µM)**	**C_{max} reference**	**Concentration range (µM)**	**Direction of change**					**Summary mechanism**
				OCR	**Reserve capacity**	**ECAR**	**ATP**	**Proton leak**	
Carbamazepine	6	Darwish, M. *et al.*, 2015[428]	0.6 - 600	↓	↓	NR	↓	↓	Substrate inhibitor
Lamotrigine	4	Burger, D.M. *et al.*, 2008[429]	0.1 - 100	NR	NR	NR	↓	NR	-
Phenobarbital	89	Vernillet, L. *et al.*, 2018	0.1 - 100	NR	NR	NR	NR	NR	-
Phenytoin	180	Inoue, Y. *et al.*, 2013[427]	0.2 - 200	↓	↓	↑	↓	NR	ETC inhibitor
Primidone	N/A	N/A	0.1 - 100	NR	NR	NR	NR	NR	-
Valproic acid	364	Lee, S.Y. *et al.*, 2015[430]	10 -10000	↓	↓	↓	↓	↑	Cytotoxicity
Vigabatrin	4	He, Y.L. *et al.*, 2005[431]	1 - 1000	NR	NR	NR	NR	NR	-
Rotenone	N/A	N/A	0.003 - 1	↓	↓	↑	↓	↓	ETC inhibitor

Table 6.7. Data summary of acute extracellular flux assay. MEC = minimum effective concentration that significantly crosses vehicle control threshold. AC_{50} = the concentration at which 50% maximum effect is observed. NR = no response observed.

Compounds	MEC (µM)					AC_{50} (µM)				
	OCR	Reserve capacity	ECAR	ATP production	Proton leak	OCR	Reserve capacity	ECAR	ATP production	Proton leak
Carbamazepine	13.1	137	NR	165	97	>600	>190	NR	363	>600
Lamotrigine	NR	NR	NR	14	NR	NR	NR	NR	75.7	NR
Phenobarbital	NR	NR	NR	NR	NR	NR	NR	NR	NR	NR
Phenytoin	90.9	1.45	138	197	NR	>200	26.6	>200	>200	NR
Primidone	NR	NR	NR	NR	NR	NR	NR	NR	NR	NR
Valproic acid	520	3090	2600	5200	1140	>10000	>10000	>10000	>10000	9180
Vigabatrin	NR	NR	NR	NR	NR	NR	NR	NR	NR	NR
Rotenone	0.0053	<0.003	0.0274	0.0159	0.0120	0.0433	0.0106	>1	0.0459	0.213

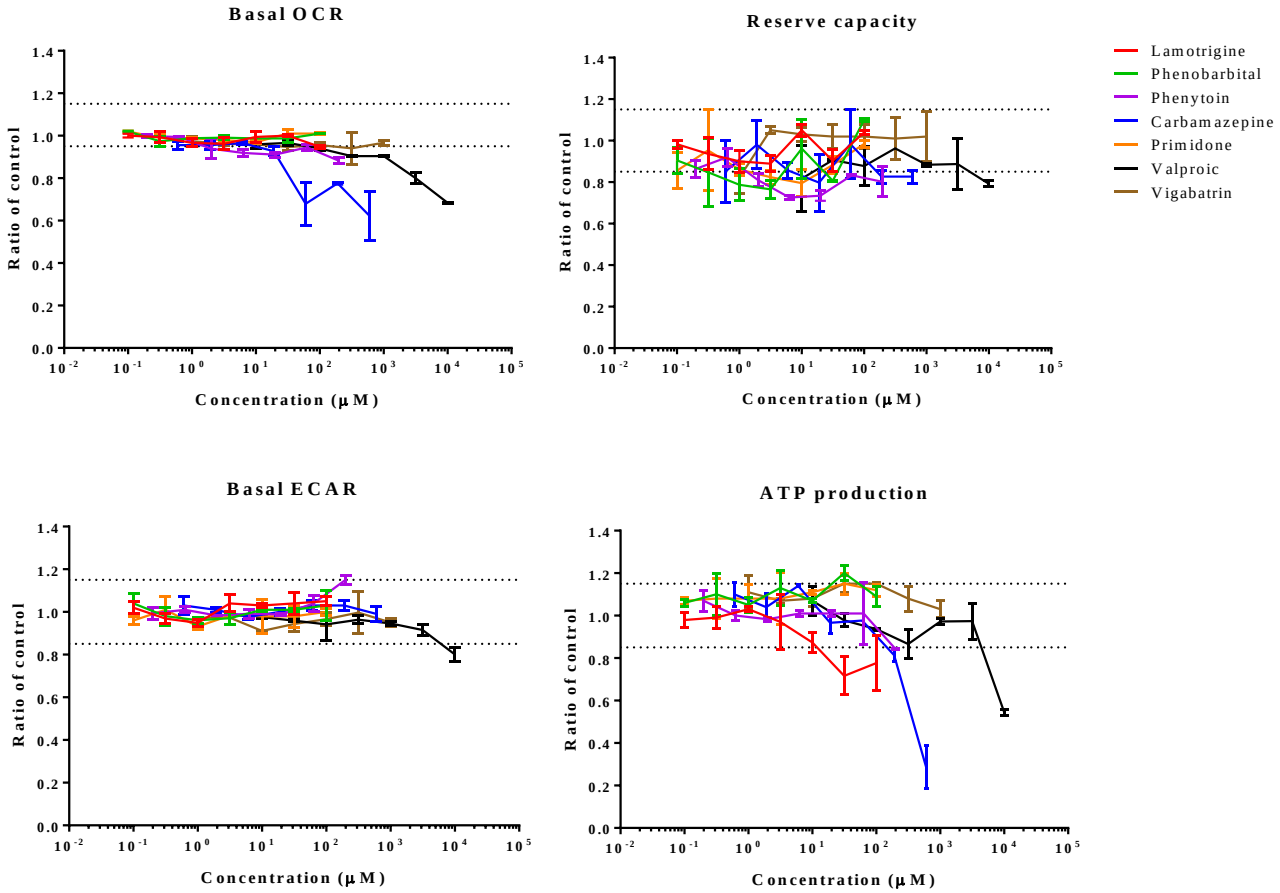

Figure 6.16. Bioenergetic profile of anticonvulsants tested using the Extracellular Flux Analyser. Dose-response curves show the effects of compounds in basal OCR, reserve capacity, basal ECAR and ATP production in 10 mM glucose, 1 mM pyruvate and 2 mM glutamine. Data is expressed as mean ratio to vehicle control ± SD of n = 3. Black dashed lines represent significant cut-off from vehicle control.

6.3.3.2. Measurement of Respiratory Activity using Permeabilised Cells with rPFO

Compounds that showed a response in the AEFA (carbamazepine, phenytoin, valproic acid) were selected for further investigations using permeabilised HepG2 cells with rPFO to further assess the effects on the ETC complexes. The only compound categorised as an ETC inhibitor in the AEFA using intact HepG2 cells was phenytoin, whereas carbamazepine was categorised as a substrate inhibitor and valproic acid as a cytotoxic compound. Here, only valproic acid showed a significant OCR response with respect to the vehicle control. The most sensitive mechanism of action was inhibition of complex I-linked respiration (MEC = 6370 µM, AC_{50} = 10000 µM) (Figure 6.17).

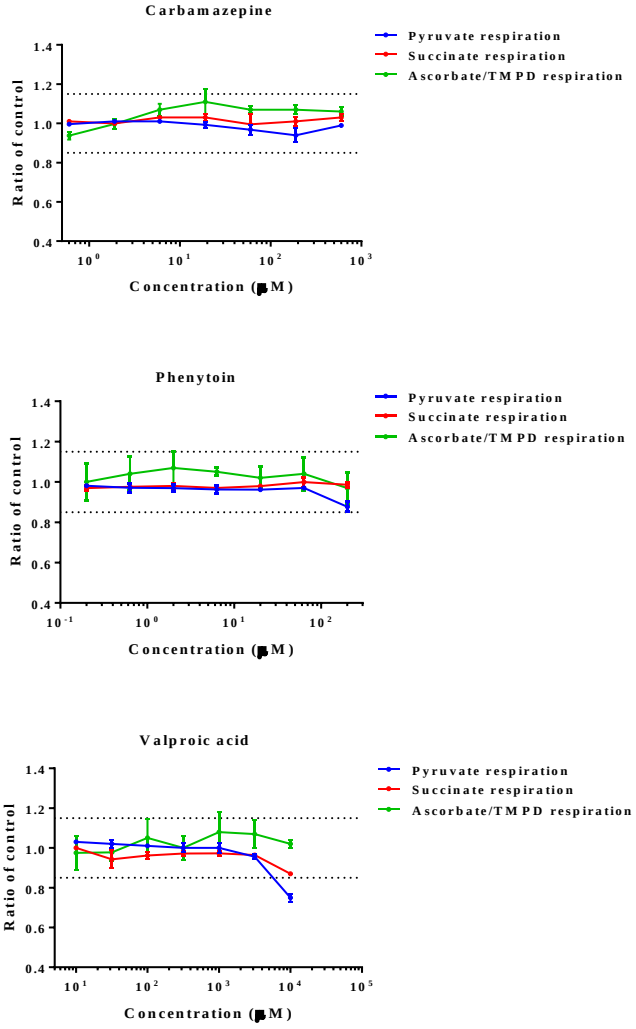

Figure 6.17. Dose-response curves of carbamazepine, phenytoin and valproic acid obtained in the cell permeabilised assay. Black dashed lines represent significant cut-off from vehicle control. Data is expressed as mean ratio to vehicle control ± SD of n = 3.

6.3.3.3. Assessment of Mitochondrial Toxicity by Anticonvulsants using Selective Media Conditions (Glu/Gal assay)

A Glu/Gal assay was performed where HepG2 cell viability was assessed after incubation with the 7 ACs in either Glu or Gal media for 24 h. A significant response (outside the cut-off from the vehicle control) was observed when cells where incubated with carbamazepine in both Glu and Gal media (Figure 6.18). However, an AC_{50} value could not be calculated due to not testing high enough concentrations (AC_{50} > 600 µM). Therefore, a fold-change between the two media conditions could not be established (Table 6.8). Incubation with all the other anticonvulsants for 24 h led to no significant effects on cell viability at the concentrations tested (stated in Table 6.8) in any of the media conditions. This included both valproic acid (at 3-10000 µM) and phenytoin (at 0.03-100 µM) (Figure 6.18).

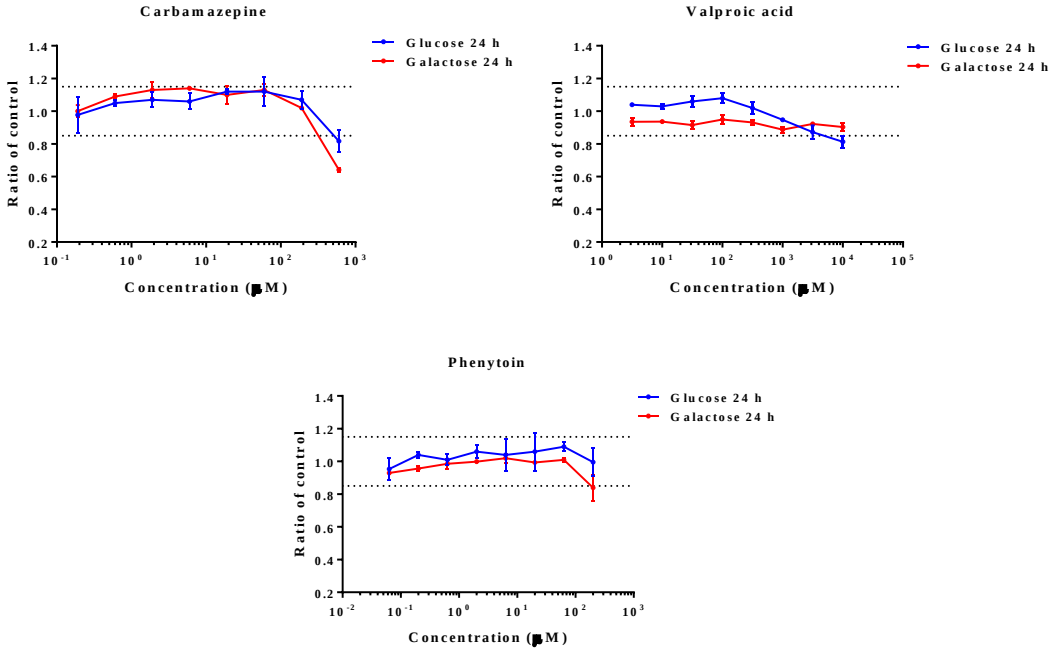

Figure 6.18. Dose-response curves of HepG2 cell viability upon 24 h incubation with carbamazepine, valproic acid and phenytoin either in 10 mM glucose or 10 mM galactose media. Black dashed lines represent significant cut-off from vehicle control. Data is expressed as mean ratio to vehicle control ± SD of n = 3.

Table 6.8. Summary table of the anticonvulsants Glu/Gal assay. AC_{50} = the concentration at which 50% maximum effect is observed. ↑↓ = Direction of response. NR = no response observed. UD = undetermined mitochondrial toxicity. Rotenone was used as positive control.

Compounds	↑↓	Glucose AC_{50} (μM)	↑↓	Galactose AC_{50} (μM)	Fold Change
Carbamazepine	↓	>600	↓	>600	UD
Lamotrigine		NR		NR	NR
Phenobarbital		NR		NR	NR
Phenytoin		NR		NR	NR
Primidone		NR		NR	NR
Valproic acid		NR		NR	NR
Vigabatrin		NR		NR	NR
Rotenone	↓	27.8	↓	0.00605	4600

6.3.3.4. Molecular Docking of Anticonvulsants

Binding affinities of the 7 ACs included in this research towards the ETC complexes (complex I-IV) and ATP synthase (complex V) were investigated as in previous sections (5.3.9 and 6.3.2.5). Docking scores displayed by the ACs were higher (hence less favourable) than previous antipsychotics investigated in this chapter, which could be due to their lower molecular weight (Figure 6.15). Here, the best docking scores ranged between -5 and -7.65 kcal/mol (Figure 6.19 and Table 6.9), whereas the antipsychotics scores ranged between -7 and -14 kcal/mol. Interestingly, the two compounds that showed mitochondrial toxicity in the AEFA, carbamazepine and phenytoin, also showed the best docking scores (Table 6.6 and Table 6.9). Phenytoin was the only compound categorised as an ETC inhibitor and it displayed a binding affinity of -6.83 kcal/mol for complex I, -7.28 kcal/mol for complex III, -7.65 kcal/mol for complex IV and -7.13 kcal/mol for complex V. Carbamazepine displayed a binding affinity of -6.59 kcal/mol for complex I, -6.42 kcal/mol for complex III, -7.09 kcal/mol for complex IV and -7.03 kcal/mol for complex V (Figure 6.19 and Table 6.9).

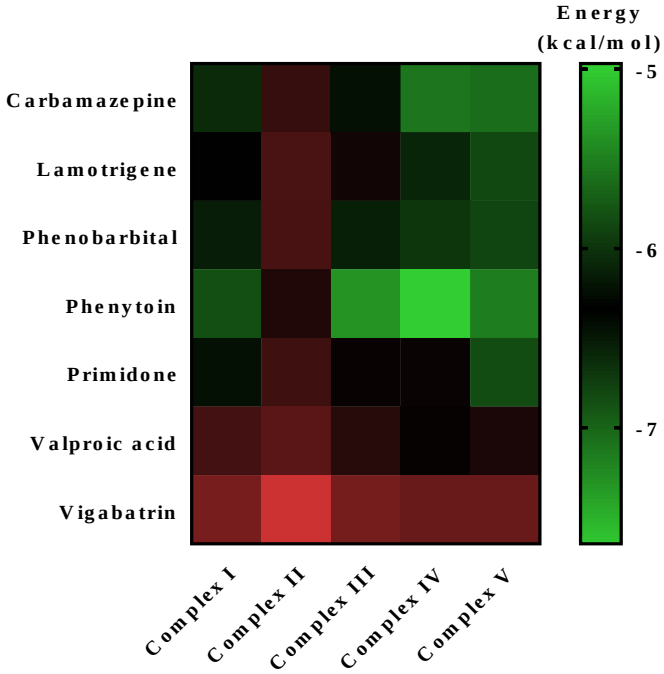

Figure 6.19. Top docking scores of the anticonvulsants against the ETC complexes (complex I-IV) and ATP synthase (complex V) presented on a heat map.

Table 6.9. The lowest and highest docking scores for each of the ACs screened alongside OCR AC_{50} values from the AEFA

Compound	Lowest/Highest scores (kcal/mol)	ETC complex	OCR AC_{50} values (μM) from the AEFA (Table 5.3)
Carbamazepine	-7.086	IV	>600
	-5.95	II	
Lamotrigine	-6.78	V	NR
	-5.82	II	
Phenobarbital	-6.75	V	NR
	-5.83	II	
Phenytoin	-7.64	IV	>200
	-6.09	II	
Primidone	-6.81	V	NR
	-5.90	II	
Valproic acid	-6.27	IV	>10000
	-5.72	II	
Vigabatrin	-5.63	IV	NR
	-4.96	II	

6.3.4. Antidepressants and Anxiolytic Drugs

In this section, the effects of three antidepressants (citalopram, fluoxetine and tianeptine) and two anxiolytic drugs (buspirone and lorazepam) on mitochondrial function were investigated. Chemical structures of these compounds are depicted in Figure 6.20.

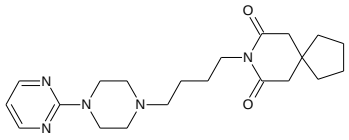

Buspirone
(anxiolytic)

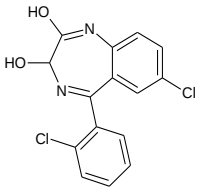

Lorazepam
(anxiolytic)

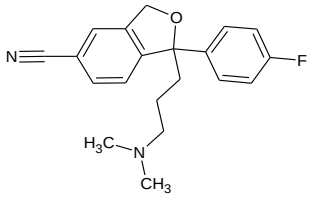

Citalopram
(antidepressant)

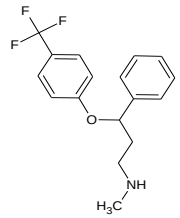

Fluoxetine
(antidepressant)

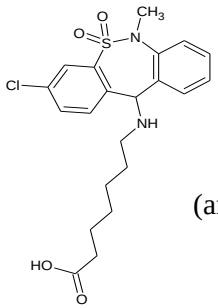

Tianeptine
(antidepressant)

Figure 6.20. Chemical structures of the antidepressants and anxiolytic drugs tested.

6.3.4.1. The Acute Extracellular Flux Assay (AEFA) to Assess Real-Time Effects of Antidepressants and Anxiolytic Drugs on Mitochondrial Function

The results of acute real-time bioenergetics assay using the Seahorse Bioscience XF96 analyser and HepG2 cells have been reported in Figure 6.21 and summarised in Table 6.10 and Table 6.11 along with the range of concentrations tested. All drugs were tested at concentrations that ranged from 0.1 – 100 µM, except for citalopram, which was tested at concentrations ranging from 0.01 – 10 µM.

According to this assay results, buspirone and tianeptine may be considered as substrate inhibitors and fluoxetine as an ETC inhibitor. The reason for this classification is that both buspirone and tianeptine reduced OCR (AC_{50}s > 100 µM), reserve capacity (AC_{50} = 43.7 and > 21.6 µM, respectively) and ATP production (AC_{50}s > 100 µM), but they did not increase ECAR, which suggests that the reduced OCR could be due to reduced substrate availability. Fluoxetine, in contrast, caused a dose-dependent reduction in OCR (AC_{50} > 100 µM), reserve capacity (AC_{50} = 70.4 µM) and ATP production (AC_{50} > 100 µM), and an increase in ECAR (AC_{50} > 100 µM), hence it was categorised as an ETC inhibitor.

Lorazepam decreased OCR (AC_{50} > 100 µM) and ATP production (AC_{50} > 100 µM) and increased proton leak (AC_{50} > 15 µM), with no significant effect on ECAR or reserve capacity. Hence it could not be classified as an ETC inhibitor, as an uncoupler or as a substrate inhibitor and, hence it was categorised as “other” due to its mode of action being poorly defined using this system. Citalopram was negative for mitochondrial toxicity using this assay (Table 6.10).

Table 6.10. Acute extracellular flux assay for the detection of mitochondrial toxicity. List of anxiolytic and antidepressant drugs, clinical C_{max} values from references and ranges of concentrations tested. Direction of change in basal OCR, reserve capacity, basal ECAR, ATP production and proton leak, where: ↑ = increase compared to vehicle control, ↓ = decrease compared to vehicle control, NR = no response compared to vehicle control. N/A = not available. Summary mechanism is the conclusion made based on the direction of change in the bioenergetic parameters.

Compounds	C_{max} (µM)	C_{max} reference	Concentration range (µM)	Direction of change					Summary mechanism
				OCR	Reserve capacity	ECAR	ATP	Proton leak	
Buspirone	0.003	Gammans, R.E. *et al*., 1986	0.1 – 100	↓	↓	NR	↓	NR	Substrate inhibitor
Lorazepam	0.1	Blin, O. *et al*., 1999	0.1 – 100	↓	NR	NR	↓	↑	Other
Citalopram	0.0003	Baumann, P. *et al*., 1995	0.01 – 10	NR	NR	NR	NR	↓	-
Fluoxetine	0.0004	Nelson, J.C. *et al*., 1991	0.1 – 100	↓	↓	↑	↓	NR	ETC inhibitor
Tianeptine	0.62	Zheng, R. *et al*., 2014	0.1 – 100	↓	↓	NR	↓	NR	Substrate inhibitor
Rotenone	N/A	N/A	0.003 – 1	↓	↓	↑	↓	↓	ETC inhibitor

Table 6.11. Data summary of acute extracellular flux assay. MEC = minimum effective concentration that significantly crosses vehicle control threshold. AC_{50} = the concentration at which 50% maximum effect is observed. NR = no response observed.

Compounds	MEC (μM)					AC_{50} (μM)				
	OCR	**Reserve capacity**	**ECAR**	**ATP production**	**Proton leak**	**OCR**	**Reserve capacity**	**ECAR**	**ATP production**	**Proton leak**
Buspirone	4.83	8.57	NR	80.9	NR	>100	43.7	NR	>100	NR
Lorazepam	63.7	NR	NR	3.2	3.14	>100	NR	NR	>100	15
Citalopram	NR	NR	NR	NR	7.17	NR	NR	NR	NR	>10
Fluoxetine	8.12	25.2	62.9	63.5	NR	>100	70.4	>100	>100	NR
Tianeptine	5.5	0.182	NR	40.3	NR	>100	21.6	NR	>100	NR
Rotenone	0.0053	<0.003	0.0274	0.0159	0.0120	0.0433	0.0106	>1	0.0459	0.213

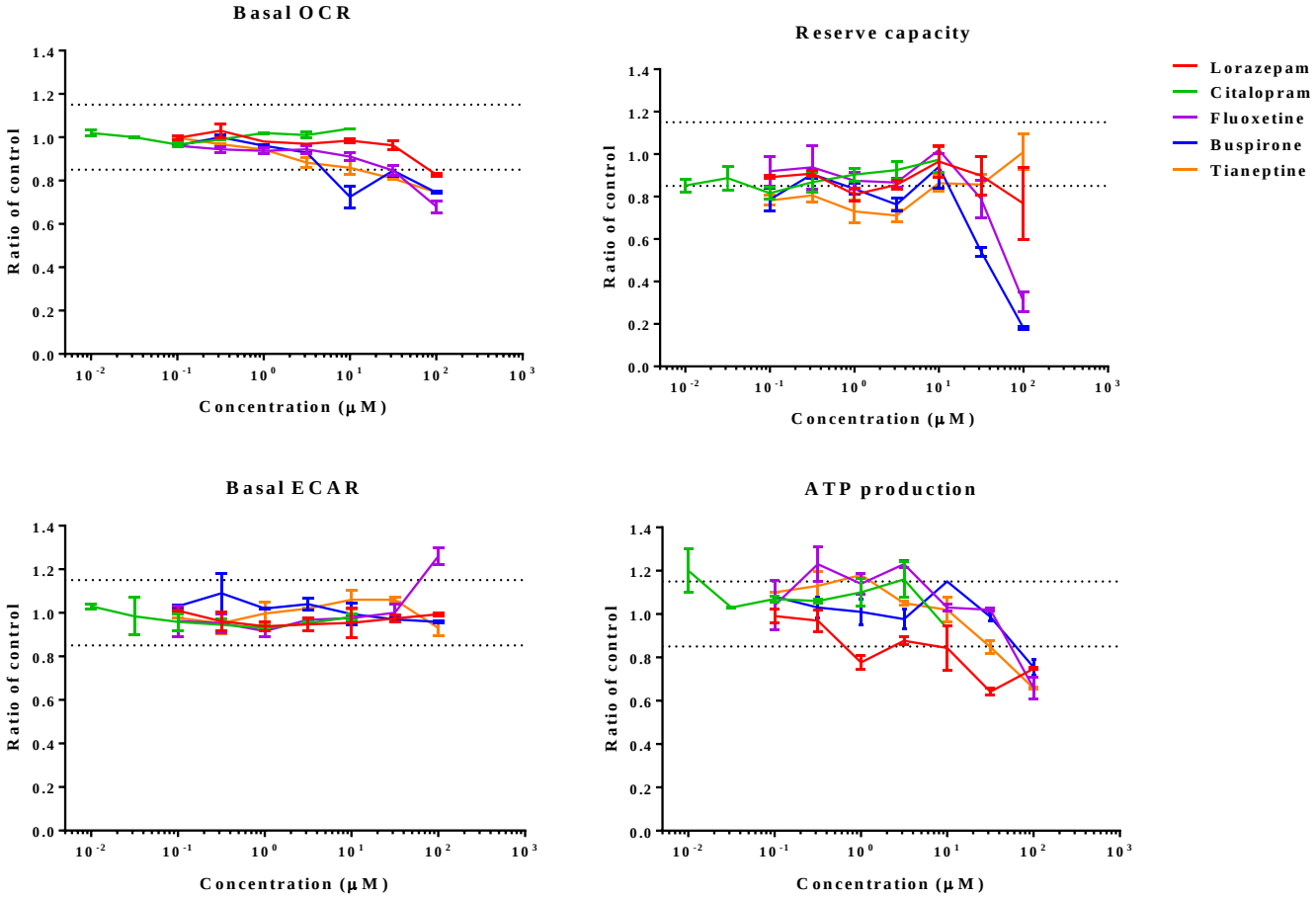

Figure 6.21. Bioenergetic profile of antidepressants and anxiolytic drugs tested using the Extracellular Flux Analyser. Dose-response curves show the effects of compounds in basal OCR, reserve capacity, basal ECAR and ATP production in 10 mM glucose, 1 mM pyruvate and 2 mM glutamine. Data is expressed as mean ratio to vehicle control ± SD of n = 3. Black dashed lines represent significant cut-off from vehicle control.

6.3.4.2. Measurement of Respiratory Activity using Permeabilised Cells with rPFO

Given the results obtained in the acute assay, buspirone, lorazepam, fluoxetine and tianeptine were selected for further investigations using HepG2 cells permeabilised with rPFO to identify any mechanisms of ETC inhibition. Figure 6.22 shows that the two compounds that showed a significant dose-dependent inhibitory activity against OCR were buspirone and fluoxetine. For both drugs, the most sensitive mechanism was pyruvate respiration, while succinate respiration was not affected. Injection of buspirone resulted in a decrease in pyruvate respiration with a MEC value of 44.5 µM. Fluoxetine also decreased pyruvate respiration with a MEC value of 72.1 µM. Given that buspirone was identified as a substrate inhibitor and fluoxetine as an ETC inhibitor in the AEFA, and given the results obtained here, it is likely that buspirone acts as an inhibitor of NADH-linked substrates, while fluoxetine probably inhibits complex I directly. Lorazepam and tianeptine both showed a small drop in pyruvate respiration at 100 µM, but this response was not significantly different from the vehicle response (Figure 6.22).

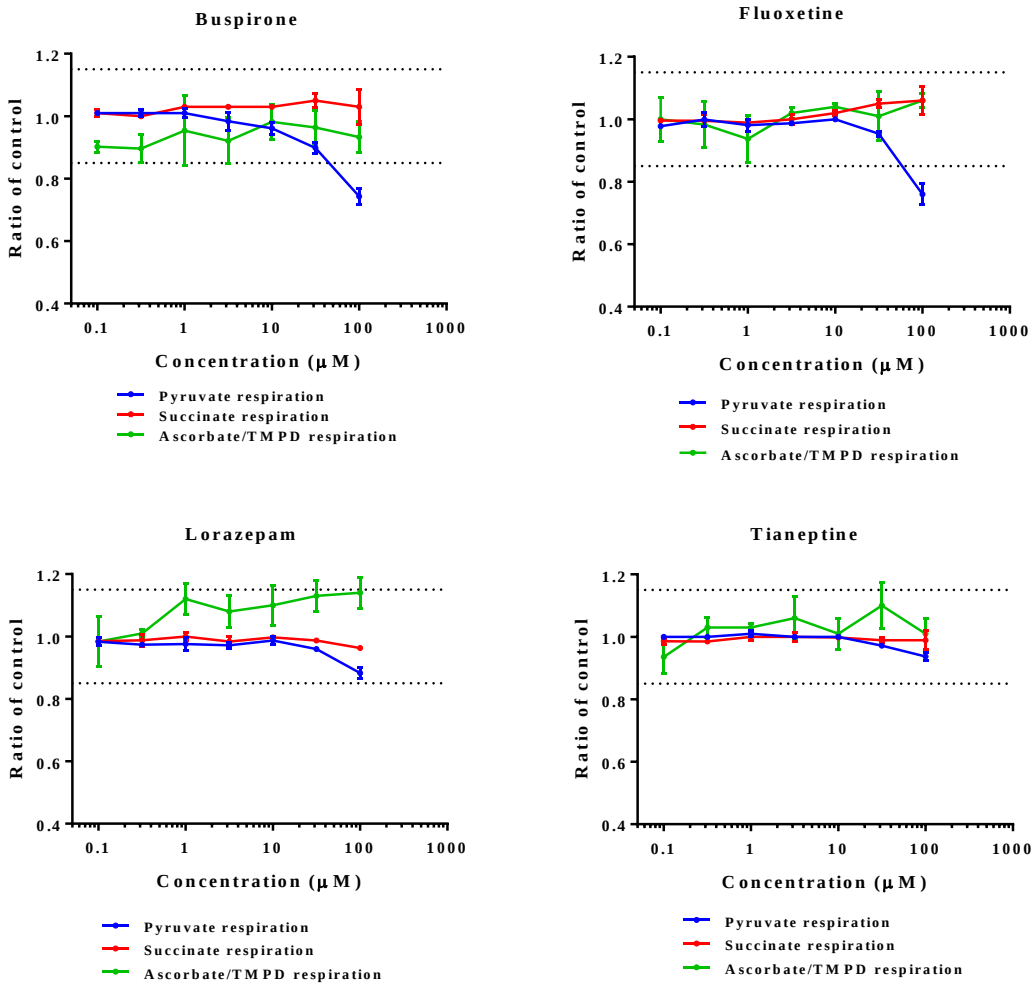

Compound	Most sensitive mechanism	⇅	MEC (µM)	AC_{50} (µM)
Buspirone	pyruvate respiration	↓	44.5	>100
Lorazepam	NR	NR	NR	NR
Fluoxetine	pyruvate respiration	↓	72.1	>100
Tianeptine	NR	NR	NR	NR

Figure 6.22. Dose-response curves of buspirone, lorazepam, fluoxetine and tianeptine in the cell permeabilised assay. Graphs: Black dashed lines represent significant cut-off from vehicle control. Data is expressed as mean ratio to vehicle control ± SD of n = 3. Table: a summary of the most sensitive mechanism, MEC and AC_{50} values.

6.3.4.3. Assessment of Mitochondrial Toxicity by Antidepressants and Anxiolytic Drugs using Selective Media Conditions (Glu/Gal assay)

The Glu/Gal assay was performed to find the potential mitochondrial impairment caused by the drugs and to help identify whether it is a primary effect or secondary to other cytotoxic mechanisms. Table 6.12 gives a summary of the results obtained from this assay and Figure 6.23 shows the dose-response curves for some of the test compounds. Figure 6.23 shows that buspirone treatment in Glu media (24 h) led to a dose-dependent reduction in cell viability that did not significantly cross the vehicle control threshold at the concentrations tested. However, in Gal media, buspirone significantly reduced cell viability with an AC_{50} = 99 µM. Fold change could not be determined due to a lack of AC_{50} in Glu media, so it was categorised as "undetermined" in terms of mitochondrial toxicity. Lorazepam did not show any response at any of the concentrations tested (0.03 – 100 µM) in either media conditions. Fluoxetine and citalopram showed similar toxicity in both media, which may suggest the existence of mechanisms of toxicity other than mitochondrial toxicity. In previous assays, fluoxetine was found to be an ETC inhibitor, however fold change between AC_{50} values was 0.76, which indicates that mitochondrial toxicity is probably not the primary mechanism of toxicity of this drug and suggests the existence of other cytotoxic mechanisms. Tianeptine at 100 µM was found to cause a dramatic reduction in cell viability in Gal media (AC_{50} = 57.6 µM), while ATP levels remained high in Glu media. This result indicates greater susceptibility of HepG2 cells to tianeptine when they rely heavily on OXPHOS for energy production (Gal media) which would indicate that fluoxetine's primary cytotoxic mechanism is mitochondria related. Citalopram was not found to have an effect in respiration in previous assays, and again these results prove that citalopram's primary mechanism of cytotoxicity is probably not related to mitochondrial toxicity.

Table 6.12. Summary table of the Glu/Gal assay done on antidepressants and anxiolytic drugs. AC_{50} = the concentration at which 50% maximum effect is observed. ↑↓= Direction of response. NR = no response observed. UD = undetermined mitochondrial toxicity. Rotenone was used as positive control.

Compounds	↑↓	Glucose AC_{50} (µM)	↑↓	Galactose AC_{50} (µM)	Fold Change
Buspirone		NR	↓	99	UD
Lorazepam		NR		NR	NR
Citalopram	↓	>10		NR	UD
Fluoxetine	↓	13.3	↓	17.5	0.76
Tianeptine		NR	↓	57.6	UD
Rotenone	↓	27.8	↓	0.00605	4600

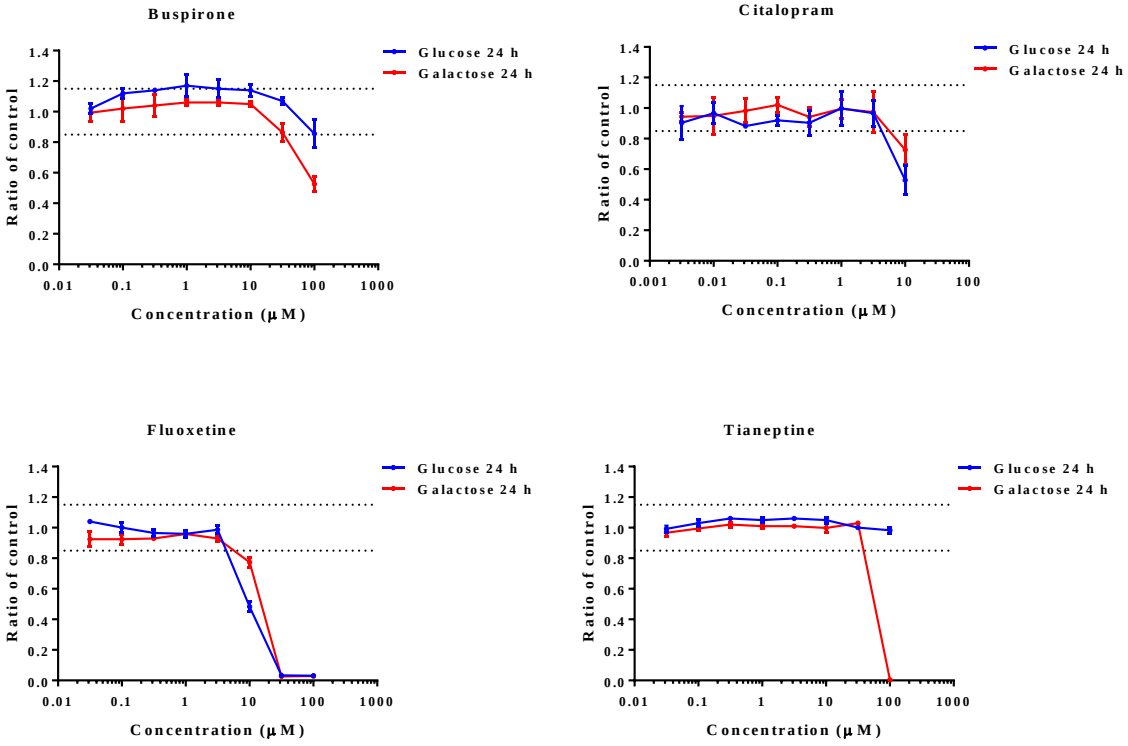

Figure 6.23. Dose-response curves of HepG2 cell viability upon 24 h incubation with tianeptine (0.1 – 100 µM), buspirone (0.1 – 100 µM), fluoxetine (0.1 – 100 µM) and citalopram (0.01 – 10 µM) either in 10 mM glucose or 10 mM galactose media. Black dashed lines represent significant cut-off from vehicle control. Data is expressed as mean ratio to vehicle control ± SD of n = 3.

6.3.4.4. Molecular Docking of Antidepressants and Anxiolytic Drugs

Finally, binding affinities of all six antidepressants and anxiolytic drugs towards the ETC complexes (complex I-IV) and ATP synthase (complex V) were investigated by molecular docking like in previous sections (5.3.9, 6.3.2.5). The top docking scores for these drugs ranged between -6 and -10.7 kcal/mol (Figure 6.24). Compounds with the best docking scores were buspirone (-9.29 kcal/mol for complex I, -9.58 kcal/mol for complex III, -11 kcal/mol for complex IV and -9.56 kcal/mol for complex V), citalopram (-8.34 kcal/mol for complex I, -8.73 kcal/mol for complex IV and -8.54 kcal/mol for complex V), fluoxetine (-8.5 kcal/mol for complex IV) and tianeptine (-9.34 kcal/mol for complex I, -10.7 kcal/mol for complex IV and -9.53 kcal/mol for complex V) (Table 6.13 and Figure 6.24).

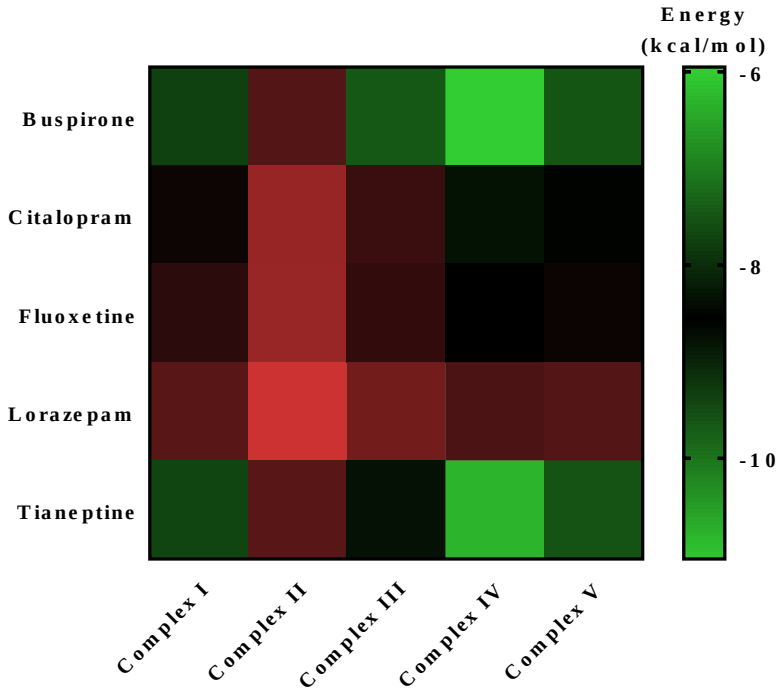

Figure 6.24. Top docking scores of the antidepressants and anxiolytic drugs against the ETC complexes (complex I-IV) and ATP synthase (complex V) presented on a heat map.

Table 6.13. The lowest and highest docking scores for each of the antidepressants and anxiolytic drugs screened alongside OCR AC_{50} values from the AEFA.

Compound	Lowest/Highest scores (kcal/mol)	ETC complex	OCR AC_{50} values (μM) from the AEFA (Table 6.11)
Buspirone	-11.04	IV	>100
	-7.46	II	
Lorazepam	-7.57	IV	>100
	-5.95	II	
Citalopram	-8.73	IV	NR
	-6.63	II	
Fluoxetine	-8.50	IV	>100
	-6.61	II	
Tianeptine	-10.74	IV	>100
	-7.39	II	

Table 6.13 shows the lowest docking scores for each of the antidepressants/anxyolytics alongside OCR AC_{50} values from the AEFA. According to the table, two of the strongest mitochondrial toxicants, at least according to Glu/Gal cell viability assay, i.e. buspirone and tianeptine, also have the lowest docking scores. On the other hand, docking score for lorazepam is high, despite the effect seen in AEFA, and the score for citalopram is low despite no effect in any of the *in vitro* tests.

6.4. Discussion

6.4.1. Antipsychotics

In this study, the effects of several typical and atypical antipsychotics (APs) on mitochondrial bioenergetics were investigated using different *in vitro* assays performed using both rat liver mitochondria and HepG2 cells.

6.4.1.1. Typical antipsychotics

Three typical APs were studied: chlorpromazine, haloperidol and trifluoperazine. To aid with the discussion of the effects of these drugs on mitochondria, a summary of all the results from various assays is presented in Table 6.14.

Chlorpromazine (Chl) is a tricyclic aliphatic phenothiazine which is indicated for the treatment of acute and chronic psychosis, as well as nausea and intractable hiccups[432]. Chlorpromazine use is strongly associated with high drug-induced liver injury (DILI) risk, as liver test abnormalities, such as increase of serum aminotransferases, have been reported to occur in up to 40% of patients on long term therapy. It is also a well-known cause of acute cholestatic liver injury[433,432, 434]. Haloperidol (Hlp), also known as Haldol, is a high potency typical AP and one of the most frequently used worldwide for the treatment of severe manifestations of several psychotic disorders, including schizophrenia, acute psychosis and Tourette syndrome[435]. Trifluoperazine is another typical AP agent primarily used to treat schizophrenia, but it has been replaced in the recent years in large part by the atypical APs[432].

Typical APs such as Chl and Hlp have long been reported as inhibitors of mitochondrial complex I[81, 436, 437], which has been suggested to be correlated with extrapyramidal side effects. This hypothesis has been supported by studies performed on both rat brain cortex[438] and normal human brain cortex[439], which showed that haloperidol was the most potent complex I inhibitor (IC_{50} = 100 μM), followed by chlorpromazine (IC_{50} = 400 μM), risperidone (IC_{50} = 500 μM) and clozapine (IC_{50} > 500 μM)[439]. In pig brain mitochondria, both chlorpromazine and haloperidol strongly inhibited complex I-linked respiration (Chl IC_{50} = 116 μM, Hlp IC_{50} = 64.9 μM), while they were partial inhibitors of complex II-linked respiration (Chl IC_{50} = 262 μM, Hlp IC_{50} = 467 μM)[440]. Furthermore, haloperidol and trifluoperazine have been observed to cause depolarization of mitochondrial membranes with disruption of mitochondrial membrane potential[441, 442]. Reduced

mitochondrial bioenergetics has also been associated with APs-induced reproductive toxicity, where chlorpromazine and haloperidol, decreased ATP levels, oxygen consumption rates and mitochondrial membrane potential in rat ovarian theca cells in a concentration-dependent manner[375].

Table 6.14. Summary of *in vitro* assays performed to investigate the mitochondrial effects of the APs. Direction of change in basal OCR, reserve capacity, basal ECAR, ATP production, proton leak and cell viability, where: ↑ = increase compared to vehicle control, ↓ = decrease compared to vehicle control, NR = no response compared to vehicle control. N/A = not available.

Assays		Amisulpride	Aripiprazole	Chlorpromazine	Clozapine	Haloperidol	Olanzapine	Quetiapine	Reserpine	Trifluoperazine	Ziprasidone
Acute HepG2 Extracellular Flux Assay (AEFA)	OCR (AC_{50} μM)	NR	>10↓	>100↓	NR	NR	NR	>150↓	>100↑	NR	NR
	Reserve capacity (AC_{50} μM)	NR	>10↓	>100↓	NR	NR	NR	124↓	NR	0.157↓	NR
	ECAR (AC_{50} μM)	NR	>10↑	>100↓	>100↓	NR	NR	NR	NR	NR	NR
	ATP production (AC_{50} μM)	NR	>10↓	NR	>100↓	NR	NR	>150↓	77.3↓	NR	NR
	Proton leak (AC_{50} μM)	NR	NR	84.4↑	NR	NR	NR	NR	36.8↑	NR	NR
	Summary mechanism	NR	ETC inhibitor	Cytotoxicity	NR	NR	NR	Substrate inhibitor	Uncoupler	Other	NR
Permeabilised HepG2 Extracellular Flux Assay (OCR)	Most sensitive mechanism (AC_{50} μM)	N/A	NR	N/A	N/A	N/A	N/A	Pyruvate respiration↓ >150	N/A	N/A	N/A
Glu/Gal assay (cell viability reduction)	Glucose (AC_{50} μM)	NR	NR	15.9↓	56.7↓	57.5↓	>50↓	76.7↓	48.9↓	1	NR↓
	Galactose (AC_{50} μM)	NR	NR	16.9↓	60.8↓	78.6↓	NR	79↓	79↓	1.13	>40↓
	Fold Change	NR	NR	0.941	0.933	0.732	UD	0.971	0.619	0.885	UD
SCR inhibition	IC_{50} μM	N/A	N/A	194 ± 67	N/A	N/A	N/A	N/A	N/A	N/A	N/A
Basal succinate-driven respiration	% MMP (Conc. μM)	N/A	N/A	88 (20), 79 (50), 72 (100)	N/A	88 (20), 69 (50)	92 (20), 90 (50)	N/A	N/A	N/A	N/A
	% O_2 consumption (Conc. μM)	N/A	N/A	111 (20), 125 (50), 131 (100)	N/A	85 (20), 77 (50)	90 (20), 92 (50)	N/A	N/A	N/A	N/A

Assays		Amisulpride	Aripiprazole	Chlorpromazine	Clozapine	Haloperidol	Olanzapine	Quetiapine	Reserpine	Trifluoperazine	Ziprasidone
Uncoupled succinate-driven respiration	% ROS (Conc. μM)	N/A	N/A	92 (50), 78 (100), 62 (125), 65 (150), 60 (200), 38 (300), 28 (400)	N/A	N/A	N/A	N/A	N/A	N/A	N/A
	% O_2 consumption (Conc. μM)	N/A	N/A	97 (50), 76 (100), 53 (125), 39 (150), 22 (200), 10 (300), 0.05 (400)	N/A	N/A	N/A	N/A	N/A	N/A	N/A
MTT assay (Glu media, 24 h incubation treatment)	% Cell viability (Conc. μM)	N/A	N/A	103 ± 0.9 (1), 104 ± 10 (7.5), 83 ± 0.6 (15), 18 ± 10 (37.5), 13 ± 5.3 (75), 13 ± 4.8 (150)	N/A	96 ± 4.2 (0.02), 93 ± 10 (0.5), 88 ± 7.8 (20), 42 ± 1.2 (50)	101 ± 0.15 (0.02), 103 ± 3 (0.5), 110 ± 5.5 (20), 118 ± 10 (50)	N/A	N/A	N/A	N/A
MTT assay (Gal media, 24 h incubation treatment)	% Cell viability (Conc. μM)	N/A	N/A	103 ± 6 (1), 105 ± 5 (7.5), 89 ± 9.1 (15), 15 (37.5), 13 ± 4.2 (75), 9.4 ± 8.7(150)	N/A	91 ± 7 (0.02), 91 ± 4 (0.5), 97 ± 4.9 (20), 99 ± 9 (50)	106 ± 1.1 (0.02), 109 ± 0.5 (0.5), 131 ± 11 (20), 135 ± 6 (50)	N/A	N/A	N/A	N/A
C_{max} (μM)		2.56	0.17	0.9	0.22	0.02	0.02	1.42	0.0004	0.0009	0.11

6.4.1.1.1 Chlorpromazine

In a study published by Cikankova *et al.,* activities of the different ETC complexes were evaluated after 30 min incubation with several APs at 50 μM[404]. In this study, both chlorpromazine and haloperidol caused significant inhibitory effects on complex I activity, especially chlorpromazine, which completely blocked the reaction. Additionally, complex IV activity was also significantly inhibited by chlorpromazine[404]. Modica-Napolitano *et al.* found that, in freshly isolated rat liver mitochondria, Chl induced a dose-dependent stimulation of state 2 respiration with both glutamate + malate or succinate as substrates[408]. However, at higher concentrations, such as 200 μM, state 2 respiration was decreased. In state 3 respiration, induced by addition of ADP, Chl induced a dose-dependent decrease in respiration with approximately 90% inhibition achieved at 200 μM using glutamate + malate and succinate as substrates[408]. Then, individual enzymatic assays revealed that both Chl and Hlp induced a dose-dependent inhibition of complex I activity, both with an IC_{50} of 35 μM. Additionally, Chl, but not Hlp, inhibited succinate-cytochrome *c* reductase activity by 50% at 150 μM[408].

In this study, investigations using isolated rat liver mitochondria revealed a dual activity of Chl depending on the state of respiration. In complex II-linked basal respiration, increasing concentrations of Chl (20-100 μM) led to a significant increase in the oxygen consumption rate (Figure 6.9) with a simultaneous dissipation of the MMP, which would suggest an uncoupling activity. However, in complex II-linked uncoupled respiration (induced by addition of CCCP), Chl showed a dose-dependent decrease in OCR (50 - 400 μM) with an IC_{50} of 135 ± 5 μM (Figure 6.10). This is in agreement with SCR enzymatic assays performed in chapter 3, which gave an IC_{50} of 194 ± 67 μM (Figure 5.8). Previous studies have shown inhibition of complex I and IV by Chl and, in fact, docking studies show greatest affinity for complex IV (Figure 6.14). Nevertheless, acute injections of Chl onto HepG2 cells led to a simultaneous reduction in both OCR and ECAR in a dose-dependent manner, a response that categorises Chl primarily as a cytotoxic compound rather than a specific ETC inhibitor. Similarly, in the Glu/Gal assay, Chl equally reduced cell viability in both culture media conditions (AC_{50} Glu > 15.9 μM, AC_{50} Gal > 16.9 μM). Therefore, although Chl seems to exert a dual effect (inhibitor and uncoupler) on mitochondria respiration in isolated mitochondria, cell assays suggest that Chl has a number of off-mitochondrial target effects, which ultimately kill the cells, as seen in Figure 6.13 .

6.4.1.1.2 Haloperidol

As described above, Modica-Napolitano *et al.* showed that Hlp induced a dose-dependent inhibition of complex I activity with an IC_{50} of 35 μM using individual enzymatic assays[408]. Furthermore, Hlp showed a mild effect on NADH-linked state 3 respiration, decreasing it by 50% at 200 μM[408]. A study done on psychotic patients treated with Hlp for a minimum of 28 months found that complex I activity and oxygen consumption rates using pyruvate + malate were significantly reduced in peripheral venous blood cells of patients in comparison with controls[437].

Here, acute injection of up to 100 μM Hlp onto HepG2 cells did not cause any significant response in any of the mitochondrial parameters measured (Table 6.2 and Table 6.3). However, when Glu-grown cells were incubated with 50 μM Hlp for a longer period of time, such as 1 h, OCR was reduced and ECAR was significantly increased, which was accompanied by a dramatic reduction in maximal respiration and complete abolition of spare respiratory capacity, a response that would allow categorisation of Hlp as an ETC inhibitor (Figure 6.6). These results suggest that Hlp might not have an immediate effect on mitochondria, but rather, haloperidol's effect is time-dependent. For instance, 48 h incubation with Hlp led to a higher reduction in cell viability than 24 h incubation, which provides additional evidence that detrimental effects of Hlp on cell function might be time-dependent. Hlp has classically been considered a complex I inhibitor, however, high-resolution respirometry has demonstrated that Hlp can also decrease complex II-linked respiration in a dose-dependent manner in isolated mitochondria, which suggests that Hlp could target other ETC complexes. Docking results showed that Hlp had a great binding affinity for complex IV, followed by complex I (Figure 6.14).

6.4.1.1.3 Trifluoperazine

There is very limited data available in the literature regarding trifluoperazine's effects on mitochondria. In a study published in 1981 by Ruben *et al*. trifluoperazine was found to inhibit rat liver mitochondrial ATPase at 60 μM[417]. In another study published in 1983, trifluoperazine inhibited ADP-stimulated oxidation of succinate of porcine liver and skeletal muscle mitochondria at low concentrations (88 nmol/mg protein). At high concentrations (233 nmol/mg protein), trifluoperazine inhibited electron transport of succinate oxidation of skeletal muscle mitochondria within the cytochrome bc_1 and cytochrome c-aa_3 segments of the respiratory chain system[416]. In 1984, another study

found that trifluoperazine inhibits state 3 respiration of mung bean mitochondria (*Phaseolus aureus*) oxidising either malate, succinate or exogenous NADH (IC_{50} values of 56, 59 and 55 μM, respectively)[443]. Additionally, the same study reported that both membrane-bound and soluble ATPases were equally sensitive to trifluoperazine (IC_{50} of 28 μM for both)[443]. Since then, not many more studies have been published to shed more light on these findings.

In this study **t**he effects of trifluoperazine on mitochondrial function were investigated using HepG2 cells. Acute injection of up to 2 μM (more than 2000-fold its C_{max} value[444]) caused no significant effects on mitochondrial OCR, but it did cause a reduction in reserve capacity (AC_{50} = 0.157 μM) (Table 6.2 and Table 6.3). In the permeabilised assay, none of the concentrations tested (0.002 – 2 μM) caused inhibition of any of the ETC complexes. Previous studies have shown inhibition of complex V[417, 443] and inhibition within the cytochrome *bc₁* and cytochrome *c-aa₃* segments of the respiratory chain system[416], which would be in agreement with docking studies that have shown binding affinity in the ranking order: complex IV > complex V > complex II > complex I > complex II (Figure 6.14). Finally, the Glu/Gal assay revealed that 24 h incubation with 2 μM trifluoperazine leads to complete loss of cell viability in both media conditions.

6.4.1.2. Atypical antipsychotics

More recently, given the vital role that mitochondria play in energy metabolism and homeostasis, the increased risk of metabolic syndrome observed in patients taking atypical APs has also been associated with mitochondrial dysfunction. The strong relationship between mitochondrial function and mitochondrial dynamics has led to explore the hypothesis that the metabolic disturbances caused by atypical APs may be explained by a fusion/fission imbalance of the mitochondrial network, which would result in a reduced capacity to trigger insulin-dependent pathways, necessary to preserve adequate energy production and metabolic homeostasis[445]. For instance, clozapine and olanzapine induced a general downregulation in genes encoding subunits of the ETC complexes, as well as decreased ATP levels and mitochondrial oxygen consumption in peripheral blood cells of patients and controls[374]. Furthermore, medium-risk drug quetiapine decreased oxygen consumption and respiratory control ratio in patients and controls[374]. Olanzapine and aripiprazole, at therapeutic and supra-therapeutic concentrations, respectively, reduced the expression of genes involved in the regulation

of mitochondrial biogenesis and metabolism in human subcutaneous adipose tissue[446]. In a study of cultured myoblasts, adipocytes, hepatocytes and monocytes, clozapine was found to reduce ATP levels and to alter mitochondrial morphology and membrane potential in all cell lines[447]. In another study, a concentration-dependent decrease in the ATP content was observed in rat isolated ovarian theca interstitial cells treated with clozapine and risperidone. At their estimated IC_{50}s (35 µM and 37 µM, respectively) they also significantly decreased OCR (approximately by 50%) and mitochondrial complex I activity (clozapine by 70% clozapine and risperidone by 60% approximately)[375].

Several studies have investigated the effects of atypical APs on the individual activities of the mitochondrial respiratory complexes. For instance, chronic administration for 28 days of clozapine (25 mg/kg), olanzapine (2.5, 5 or 10 mg/kg) and aripiprazole (2, 10 or 20 mg/kg) showed that olanzapine significantly reduced succinate dehydrogenase activity (SDH, complex II) only in the cerebellum, whereas clozapine reduced it in the striatum and aripiprazole increased SDH activity only in the prefrontal cortex[448]. Another study using isolated rat liver mitochondria showed modest effects on state 2 respiration exerted by clozapine, olanzapine and quetiapine when succinate was used as the respiratory substrate, but only at concentrations above 100 µM. In addition, NADH-linked state 3 respiratory rates were affected by risperidone (IC_{50} = 100 µM) and quetiapine (IC_{50} > 200 µM, reduction of approx. 80% at 100 µM). Clozapine produced a modest effect on state 3 respiration when either glutamate + malate or succinate were used as respiratory substrates (IC_{50} > 200 µM). The same study also investigated the effects of APs on individual enzymatic activities: complex I was inhibited by risperidone and quetiapine (IC_{50} = 65 µM and 125 µM, respectively) and at 200 µM clozapine and olanzapine caused 30% and 12% inhibition, respectively. Clozapine caused 25% inhibition of complex II+III at 200 µM[408].

Clozapine and risperidone inhibited complex I activity and oxygen consumption rates using pyruvate + malate as substrates in peripheral venous blood cells of patients treated for a minimum of 28 months in comparison with controls[437]. Ovaries of rats treated with clozapine (20 mg/kg/day) for 28 days showed a reduction in complex I activity (approx. 90% of control), but not complex III[449]. Finally, spectrophotometric measurements of mitochondrial respiratory complexes from pig brain mitochondria showed that 30 min incubation with 50 µM aripiprazole, quetiapine, risperidone and clozapine decreased complex I activity (by 50%, 60%, 65% and 85%, respectively). 50 µM olanzapine caused

no significant effects. Complex II+III activity was inhibited only by aripiprazole (75%), quetiapine (90%) and risperidone (90%). Complex IV was not inhibited by any of the drugs tested. Mitochondrial respiratory rates were inhibited by all tested APs, except for olanzapine. Complex I-linked respiration was strongly inhibited by aripiprazole (IC_{50} = 13.1 µM), risperidone (IC_{50} = 263 µM), quetiapine (IC_{50} = 424 µM), while clozapine and ziprasidone were only partial inhibitors of complex I-linked respiration. Complex II-linked respiration was inhibited by quetiapine and clozapine (IC_{50} = 491 and 650 µM, respectively)[404].

In the present study, the effects of the atypical APs amisulpride, aripiprazole, clozapine, olanzapine, quetiapine, reserpine and ziprasidone were investigated using HepG2 cells. Firstly, HepG2 cells were acutely treated with different concentrations of compounds based on their C_{max} values and solubility limitations (Table 6.2). This assay identified aripiprazole as a mitochondrial inhibitor, however, the permeabilised cell assay did not shed light on the mechanism of action. Docking scores showed that aripiprazole has high affinity for complex IV, complex I and complex V (Figure 6.14). The acute assay identified quetiapine as a substrate inhibitor (Table 6.2) and further studies revealed inhibition of complex I-linked respiration as the most sensitive mechanism, indicating inhibition of complex I or complex I substrates (Figure 6.4). Amisulpride showed no response in any of the assays and, to the best of my knowledge, there are no reported effects on mitochondrial function in the literature to date (Table 6.2). A substantial number of publications have studied the effects of clozapine on mitochondrial function, and the majority reported effects on complex I activity at concentrations greater than 200 µM, as discussed above. This could explain why at 100 µM top concentration clozapine showed no effects on mitochondrial respiration (Table 6.2). Olanzapine's effects were investigated more in depth. Firstly, acute treatment with olanzapine (up to 50 µM) did not lead to any response in any of the mitochondrial parameters measured (Table 6.2). However, 1 h incubation treatment with 50 µM olanzapine caused a significant decrease in ECAR (Figure 6.6). Further investigations will be required to unravel the molecular mechanisms involved in this response. What seems clear, based on previous studies and findings obtained here, is that the relative potency of olanzapine as inhibitor of mitochondrial function is in accordance with the known risk of adverse effects. Hence, data seems to agree with reports indicating that olanzapine is probably a safer drug than the typical antipsychotics chlorpromazine and haloperidol.

6.4.2. Anticonvulsants

6.4.2.1.1 Carbamazepine

Carbamazepine, trade as Tegretol, is an anticonvulsant primarily used in the treatment of epilepsy and neuropathic pain, but it is also increasingly prescribed as a mood stabiliser[450]. Carbamazepine is a sodium channel blocker, hence the anticonvulsant properties appear to act by reducing polysynaptic responses and blocking the post-tetanic potentiation, while the mechanism to control the pain of trigeminal neuralgia remains unknown[451]. Carbamazepine is highly bound to plasma proteins (75-80%)[452] and has significant adverse effects. Some of the adverse reactions most commonly associated to its use include effects in the hemopoietic system (aplastic anaemia, agranulocytosis, pancytopenia, leukopenia and more), effects in the skin (toxic epidermal necrolysis, Stevens-Johnson syndrome and more), effects in the cardiovascular system (congestive heart failure, edema, syncope and collapse and more), effects in the nervous system (nausea, vomiting, abdominal pain), abnormalities in liver function tests, hepatitis and pancreatitis[451].

A study performed on children treated with carbamazepine for 8 months revealed significantly reduced ATP production in lymphocytes with respect to the untreated controls[405]. However, enzymatic activities of the mitochondrial ETC complexes II, II+III and IV were not affected[405]. A study done by Santos *et al*., investigated the effects of the parent drug and the metabolites of carbamazepine (bioactivated by hepatic enzymes present in murine microsomes) and found that only the bioactivated carbamazepine, and not the parent drug (at 500 µM), decreased RCR, ATP synthesis and the mitochondrial membrane potential[397]. Finally, a recent study done on pig brain mitochondria found that 30 min incubation with 50 µM led to a significant inhibition of the enzymatic activity of complex I and a mild inhibition of complex IV, while complex II+III activity was not affected. The same study also found that carbamazepine was a partial inhibitor of complex-I linked respiration at >100 µM (IC_{50}= 353 ± 87 µM) and complex II-linked respiration (182 ± 90 µM) in isolated mitochondria[400].

In this research, carbamazepine decreased ATP production (AC_{50} = 363 µM) and OCR (AC_{50} > 600 µM) in whole cells, while ECAR remained unaffected (Table 6.6). The permeabilized assay did not reveal further information with regards to the mechanism of action, therefore, with the information obtained so far it can only be concluded that

carbamazepine most likely acts as a substrate inhibitor, and based on the literature data, complex I-linked respiration substrates are most likely its primary target.

6.4.2.1.2 Lamotrigine

Lamotrigine is a dual sodium channel blocker and glutamate release inhibitor. It was initially launched by GlaxoSmithKline (GSK) in 1990 for the treatment of epilepsy, but in 2003 it was commercialized as maintenance treatment of bipolar disorder and in 2010 GSK launched the product in the UK for the prevention of depressive episodes in bipolar disorder[453].

A study done on lymphocytes of children treated for 24 months with lamotrigine found significantly increased ATP production in comparison to untreated controls[405]. Additionally, the enzymatic activities of complex II, II+III or IV were not significantly affected after 24 months treatment with lamotrigine[405]. Another study assessed the preventive effect of lamotrigine against the toxicity of rotenone and MPP+ in relation to the mitochondria-mediated cell death signalling events and role of oxidative stress. This study found that lamotrigine exerted a protective effect against neuronal cell injury due to mitochondrial complex I inhibition caused by rotenone or MPP+ by attenuating the formation of ROS and depletion of GSH, but the mechanism of action is not clear yet[412]. Finally, another study found that lamotrigine was a partial inhibitor of complex I-linked (IC_{50}= 332 ± 87 µM) and complex II-lined respiration (IC_{50} = 381 ± 120 µM) in isolated pig brain mitochondria, however lamotrigine did not inhibit individual enzymatic activities of complex I, II+II or IV[400].

In this research lamotrigine did not inhibit OCR upon acute injection (0.03 – 100 µM) in HepG2 cells, but it did decrease production of mitochondrial ATP (AC_{50} = 75.7 µM) (Table 6.6). The Glu/Gal assay revealed that HepG2 cells remained viable after 24 h incubation treatment with up to 100 µM in both media conditions, suggesting no mitochondrial toxicity (Table 6.8).

6.4.2.1.3 Phenobarbital

Phenobarbital has been showen to cause a mild stimulatory effect in ATP production in lymphocytes of children treated for 14 months[405]. The same study also showed that phenobarbital did not inhibit the enzymatic activities of complex II-IV[405]. In a murine hepatic microsomal system, phenobarbital decreased state 3 respiration at 500 µM (with

glutamate + malate, succinate + rotenone, and ascorbate/TMPD as substrates) and ATP synthesis at 500 µM and 1 mM [397]. The potential to induce mitochondrial dysfunction was higher compared to carbamazepine but lower compared to phenytoin[397]. The hepatotoxic effect of phenobarbital was explained by oxidative stress induced by metabolites of these drugs[454].

The present study showed that acute injection of phenobarbital (0.1 – 100 µM) on HepG2 cells did not cause any response in any of the mitochondrial parameters measured (Figure 6.7), therefore it was not investigated in further studies using the permeabilised assay. In the Glu/Gal assay (0.1 – 100 µM), phenobarbital also did not show any response in either of the media conditions. It should be noted that C_{max} value of phenobarbital is 89 µM, therefore it seems reasonable that 100 µM would not have a significant effect in mitochondrial function. Testing higher concentrations than 100 µM was not possible due to solubility limitations.

6.4.2.1.4 Phenytoin

Phenytoin administration has been associated with hepatotoxic reactions in some patients, but mechanisms are not completely clear yet[455]. A study done in rat hepatocytes found that phenytoin increased ROS formation, reduced intracellular reduced glutathione, enhanced lipid peroxidation and mitochondrial damage and increased intracellular oxidised glutathione[456]. In a murine hepatic microsomal system, phenytoin decreased state 3 respiration and ATP synthesis. The effects caused by phenytoin were higher than the ones caused by phenobarbital and carbamazepine[397].

In this research phenytoin decreased OCR (AC_{50} > 200 µM), reserve capacity (AC_{50} = 26.6 µM) and ATP production (AC_{50} > 200 µM), while it increased ECAR (AC_{50} > 200 µM), therefore, it was categorized as an ETC inhibitor (Table 6.6). Phenytoin's response in the cell permeabilised assay did not significantly cross the vehicle control threshold, however, there was a small decrease in complex I-linked and complex IV-linked respiration only at 200 µM. It should be noted that C_{max} value of phenytoin is 180 µM (Figure 6.17)[427]. Finally, phenytoin's response in the Glu/Gal assay did not cross the vehicle control threshold, but there was only a very small decrease in viability at 200 µM in both media (Figure 6.18).

6.4.2.1.5 Primidone

Literature data about the effect of primidone on mitochondria is very limited[457]. In an animal model of epilepsy, intraperitoneal injection of primidone resulted in enhanced SOD activity and decrease of mitochondrial activity of monoamine oxidases A and B[413]. Here, a C_{max} value for primidone could not be retrieved from the literature, therefore the top concentration was arbitrarily set at 100 µM. Acute injection of 100 µM primidone on HepG2 cells did not cause any effects in any of the mitochondrial parameters measured and it did not cause any response in the Glu/Gal assay in any of the media conditions (Table 6.6 and Table 6.8).

6.4.2.1.6 Valproic acid

Valproic acid (VPA) is a widely used antiepileptic drug in various types of epileptic seizures[458]. After acetaminophen and troglitazone, valproic acid has been considered to as the third most common drug suspected of causing death because of hepatotoxicity[459]. In clinical practice, the therapeutic range of VPA is narrow (300-700 µm/L)[460] and mitochondrial toxicity of VPA has been extensively documented particularly in patients with mitochondrial disorders. In a newborn with mitochondrial encephalomyopathy due to complex IV deficiency, VPA treatment was associated with severe liver failure and cortical blindness[461]. A fatal hepatic failure was also observed in a 3-year-old female with complex IV deficiency after 3 months VPA administration[462]. A 39-year-old female with chronic progressive external ophthalmoplegia (the most common manifestation of mitochondrial myopathy) who received VPA for status epilepticus died five months after starting the treatment from fatal liver failure[463]. An 11-year-old boy with Alpers-Huttenlocher syndrome (AHS, a rare form of mitochondrial DNA depletion syndrome) with slight developmental delay and epilepsy, developed hepatic failure and increasing neurologic symptoms and died after being treated with VPA[464]. VPA treatment caused liver injury in several other patients with AHS[465-468]. Therefore, on a clinical level, mitochondrial diseases seem to represent an important risk factor for VPA-induced fatal hepatic failure.

The exact mechanisms leading to VPA-induced liver injury are still unclear. In a study published by Komulainen *et al.*[419], the effects of VPA on mitochondrial respiration in HepG2 cells cultured either in glucose or galactose media were investigated. Results showed that 24 h incubation with 1 mM and 2 mM VPA in glucose media and 0.5-2 mM

VPA in galactose media significantly decreased OCR. Similarly, MMP decreased following 24 h and 48 h 1 mM and 2 mM VPA exposure. No statistically significant differences were found in ROS production after 24 h or 48 h VPA incubation at 0.5-2 mM, but 2 mM VPA over 72 h caused a significant increase in ROS production in both glucose and galactose media. Finally, this study found that VPA treatments for 48 and 72 h (0.5-2 mM) led to a significant decrease in ATP levels only in galactose media[419]. Another study found a statistically significant decrease of complex I and complex IV activity in isolated pig brain mitochondria after 30 min incubation with 5 mM VPA [406]. Liver mitochondria from rats fed with 1% (w/w) VPA for 75 days displayed a 30% decrease of the respiration rate with substrates feeding complex I and II. The inhibition was found to be located at the site of the proton-pumping activity of complex IV[469]. Additionally, it has been reported to inhibit mitochondrial fatty acid β-oxidation (FAO)[418] and to induce the MPTP opening[470].

In this research, the effects of VPA (10-10000 µM) were investigated using HepG2 cells. On the one hand, acute injection of VPA caused a dose-dependent decrease in OCR (AC_{50} = 10000 µM), reserve capacity (AC_{50} = 10000 µM), ATP production (AC_{50} = 10000 µM) and ECAR (AC_{50} = 10000 µM) (Table 6.6). On the other hand, it caused a dose-dependent increase in proton leak (AC_{50} = 9180 µM) (Table 6.6). The minimum effective concentrations (MEC) that significantly crossed vehicle control threshold were 520 µM for OCR, 3090 µM for reserve capacity, 5200 µM for ATP production, 1140 µM for proton leak and 2600 µM for ECAR (Table 6.7). From this, it can be concluded that concentrations that are relevant in the clinical use of VPA could potentially cause mitochondrial dysfunction (VPA C_{max} = 364 µM, see Table 6.6). Nevertheless, given the reduction in both OCR and ECAR, VPA was categorized as “cytotoxic”, meaning that there are probably other mechanisms apart from mitochondrial dysfunction by which VPA exerts its toxic effects in hepatocytes. In HepG2 cells permeabilized with rPFO, the most sensitive mechanism of VPA was inhibition of pyruvate respiration (MEC = 6730 µM) (Figure 6.17), which is in agreement with previous studies[406].

6.4.2.1.7 Vigabatrin

Vigabatrin is an inhibitor of γ-aminobutyric acid aminotransferase (GABA-AT), an enzyme responsible for the catabolism of GABA. Through this mechanism, vigabatrin increases GABA concentrations and inhibits excitatory processes that could lead to seizures[471]. Literature data regarding the effects of vigabatrin on mitochondrial function is very limited. Vigabatrin has been shown to have some beneficial effects on mitochondria, for instance, it has been shown to increase the number and area of mitochondria in parietal cortex, hippocampus, retina and liver in wild-type mice[472]. Additionally, vigabatrin seemed to help with infantile spasms and hypsarrhythmia in infants carrying the T8993G mtDNA mutation[473]. In this study, concentrations that ranged from 1-1000 µM (C_{max} value for vigabatrin is 4 µM)[431] had no significant effects on HepG2 cell viability or on any of the mitochondrial parameters that were measured in the AEFA (Table 6.6, Table 6.7, Table 6.8).

Table 6.15. Summary of *in vitro* assays performed to investigate the mitochondrial effects of the ACs. Direction of change in basal OCR, reserve capacity, basal ECAR, ATP production and proton leak, where: ↑ = increase compared to vehicle control, ↓ = decrease compared to vehicle control, NR = no response compared to vehicle control. N/A = not available.

Assays		Carbamazepine	Lamotrigene	Phenobarbital	Phenytoin	Primidone	Valproic acid	Vigabatrin
Acute HepG2 Extracellular Flux Assay (AEFA)	OCR (AC_{50} μM)	>600↓	NR	NR	>200↓	NR	>10000↓	NR
	Reserve capacity (AC_{50} μM)	>190↓	NR	NR	26.6↓	NR	>10000↓	NR
	ECAR (AC_{50} μM)	NR	NR	NR	>200↑	NR	>10000↓	NR
	ATP production (AC_{50} μM)	363↓	75.7↓	NR	>200↓	NR	>10000↓	NR
	Proton leak (AC_{50} μM)	>600↓	NR	NR	NR	NR	9180↑	NR
	Summary mechanism	Substrate inhibitor	NR	NR	ETC inhibitor	NR	Cytotoxicity	NR
Permeabilised HepG2 Extracellular Flux Assay (OCR)	Most sensitive mechanism (AC_{50} μM)	NR	N/A	N/A	NR	N/A	pyruvate respiration↓ >10000	N/A
Glu/Gal assay (cell viability reduction)	Glucose (AC_{50} μM)	>600↓	NR	NR	NR	NR	NR	NR
	Galactose (AC_{50} μM)	>600↓	NR	NR	NR	NR	NR	NR
	Fold Change	UD	NR	NR	NR	NR	NR	NR
C_{max} (μM)		6	4	89	180	N/A	364	4

6.4.3. Antidepressants and anxiolytic drugs

6.4.3.1.1 Buspirone

Buspirone, sold under the name of Buspar, is a medication used to treat anxiety disorders. It is a 5-HT1A receptor partial agonist, and it also has moderate affinity for brain D2-dopamine receptors. It has a unique structure and it belongs to the azaspirodecanedione drug class, it is not chemically or pharmacologically related to the benzodiazepines or barbiturates[474]. The mechanism of action of buspirone is not fully understood, but it differs from typical benzodiazepine anxiolytics in that it does not exert anticonvulsant or muscle relaxant effects[475]. Relative to other anxiolytics, buspirone has low toxicity[476].

There is very limited data available in the literature regarding the effect of buspirone on mitochondrial function. A study published by Dykens *et al*. is one of the few available to date, where the effects of buspirone on HepG2 cells and bovine heart mitochondria were investigated[60]. First, they incubated HepG2 cells grown in glucose or galactose-containing media with 200 µM buspirone and found that, in galactose containing media, buspirone exerted moderate toxicity (60%), while in glucose-grown cells no toxicity was observed. Then, the use of the XF24 Seahorse analyzer to investigate the effects of acute injection of 25 µM buspirone on OCR and ECAR in HepG2 cells revealed OCR inhibition and an increase in ECAR[60]. Further investigations using bovine heart mitochondria revealed that buspirone inhibited complex I activity (IC_{50} = 48 µM), but no complex II/III, IV or V inhibition was observed at 150 µM[60].

The results obtained in this research agree with the data published by Dykens *et al*. Here, while cytotoxicity exerted by buspirone in glucose media did not exceed the control threshold, buspirone showed a significant cytotoxicity in galactose-grown cells (MEC = 41 µM, IC_{50} = 99 µM) (Table 6.12). Dykens *et al*. identified buspirone as an ETC inhibitor given the decrease in OCR and increase in the ECAR signal. Here, an increase in ECAR was not observed, therefore buspirone was categorised as a substrate inhibitor. Clarification of this will require further investigations. Finally, Dykens *et al.* observed inhibition of complex I activity but no inhibition of other ETC complexes, a response that is in agreement with inhibition of pyruvate respiration observed in the HepG2 cell permeabilised assay (MEC = 44.5 µM, AC_{50} >100 µM) (Figure 6.22).

6.4.3.1.2 Lorazepam

Lorazepam is a benzodiazepine commonly used as a sedative and anxiolytic. It is a gamma-aminobutyric acid (GABA-A) receptor agonist, therefore, after binding to the receptor, a conformational change occurs which allows the GABA neurotransmitter to bind with much higher affinity. GABA is the major inhibitory neurotransmitter in the brain and spinal cord, while GABA-A receptors are widely distributed throughout the central nervous system (CNS). Hence, lorazepam exerts its anxiolytic, sedative and muscle relaxant effects on the CNS by enhancing GABA-mediated inhibition of synaptic transmission[477]. Lorazepam is very rarely associated with liver injury, in fact there have been no case reports of symptomatic, acute liver injury from lorazepam. It is considered the benzodiazepine best tolerated by patients with advanced liver disease[432]. Nevertheless, the potential effects of lorazepam on mitochondrial function have not been investigated so far to the best of my knowledge. In this study, lorazepam caused a significant decrease in OCR (MEC = 63.7 µM, AC_{50} >100 µM) and ATP production (MEC = 3.2 µM, AC_{50} >100 µM), while ECAR remained unaffected (Table 6.10). 100 µM lorazepam did not significantly inhibit any of the OXPHOS complexes when evaluated individually (Figure 6.22). Likewise, lorazepam did not exhibit toxicity neither in glucose nor in galactose-grown cells after 24 h incubation (0.03 – 100 µM) (Table 6.12).

6.4.3.1.3 Citalopram

Citalopram, sold under the brand name Celexa, is one of the most widely prescribed antidepressants[478]. It acts as a potent inhibitor of the serotonin reuptake transporter (SSRI), resulting in increased neuronal accumulation of serotonin. Long-term trials have demonstrated an overall safety/side effect profile consistent with other SSRIs. The most frequent adverse effects (nausea, somnolence, dry mouth, increased sweating) are mainly transient, mostly mild to moderate in severity[479]. Liver injury has been reported to occur in less than 1% of patients on citalopram and test abnormalities are usually modest and rarely require dose modification or discontinuation. The mechanism by which citalopram can cause liver injury is unknown. However, citalopram is extensively metabolized by the liver, mainly via the cytochrome P450 system, therefore it has been proposed that hepatotoxicity may be mediated by toxic intermediates[432, 480]. A study by Ahmadian *et al*. investigated the mechanisms of citalopram-induced hepatotoxicity *in vitro* and *in vivo*. *In vitro*, 500 µM citalopram exposure caused cell death, a marked increase in ROS

formation, mitochondrial potential collapse, glutathione depletion and lipid peroxidation in freshly isolated rat hepatocytes. In an i*n vivo* rat model, biochemistry assays for liver enzymes function and histological examination confirmed citalopram-induced damage (20 mg/kg)[478]. In a study published by Xia *et al*., done in human acute myeloid leukemia HL-60 cells, showed that 24 h treatment with 220 µM citalopram caused increased generation of ROS, loss of mitochondrial membrane potential and loss in cell viability by the activation of the apoptotic process[407]. Hroudova and Fisar found that complex I and II, but not complex IV, were significantly inhibited by 500 µM citalopram after 30 min incubation using pig brain mitochondria[406]. The same authors found in another study that the activities of the mitochondrial monoamine oxidases (MAO) A and B were acutely affected by several antidepressants, among which was citalopram, with an IC_{50} of 55 ± 5.4 µM for MAO-A and 110 ± 11 µM for MAO-B[481]. In the present study, the effects of citalopram were investigated at a top concentration (10 µM) that was more than 30,000-fold its C_{max} value (0.0003 µM, see Table 6.10[482]). The concentrations investigated here did not report any significant effect in any of the mitochondrial parameters measured, except for proton leak, which was reduced (MEC = 7.17 µM) (Table 6.10 and Table 6.11). Since citalopram did not report any effect in the AEFA, it was not further investigated for its effect on individual OXPHOS complexes in the permeabilised assay. The Glu/Gal assay reported a reduction in cell viability (around 40%) at 10 µM in both media conditions, which may suggests the existence of other mechanisms of toxicity other than mitochondrial toxicity (Table 6.12 and Figure 6.23).

6.4.3.1.4 Fluoxetine

Fluoxetine is an antidepressant commonly known as Prozac that belongs to the selective serotonin reuptake inhibitor (SSRI) class. It modulates the concentrations of serotonin in the synaptic cleft due to its high selectivity for the 5-hydroxytryptamine (5-HT) transporters[483]. Its side effects are less pronounced than other antidepressants, however, it has been reported to cause undesirable side effects such as sexual dysfunction or gastrointestinal adverse reactions, which often require additional pharmacology[440, 484].

The first study to prove that fluoxetine affects mitochondrial function was published by Souza *et al*[409]. In that study, in rat liver mitochondria fluoxetine inhibited state 3 respiration by 50% at 250 µM using α-ketoglutarate as substrate and at 350 µM using succinate as substrate. The same study also found that fluoxetine inhibited the ATP

synthase non-competitively *in vitro* through direct binding with the membrane F_0 component, with 50% of the effect at 60 µM in pH 7.4. Curti *et al.* also published that fluoxetine (50-250 µM) decreased state 3 respiration supported by pyruvate + malate (IC_{50} = 150 µM), succinate or ascorbate + TMPD in isolated rat brain mitochondria. Additionally, they found that fluoxetine decreased the activity of F_1F_0-ATPase in submitochondrial particles (IC_{50} = 80 µM)[105]. Hroudova and Fisar published a study done on pig brain mitochondria were fluoxetine inhibited respiration with higher potency when respiration was supported by pyruvate + malate (IC_{50} = 86.2 ± 9.5 µM) than when respiration was supported through complex II using succinate as substrate (IC_{50} = 266.2 ± 8.9 µM)[440]. Nahon *et al.* found that, at 50 µM, fluoxetine inhibited the opening of the mitochondrial permeability transition pore (MPTP) and release of cytochrome *c* by decreasing channel conductance of the voltage-dependent anion-selective channel protein (VDAC) in mitochondria isolated from rat liver[410]. Another study found that norfluoxetine, the active metabolite of fluoxetine, significantly inhibited the activities of mitochondrial complexes I, II+III and IV in rat heart mitochondria at concentrations greater than 20 µM[402]. It is evident that the effect of fluoxetine on the mitochondria has sparked significant interest, which is reflected by the numerous studies recently published.

In this study, fluoxetine responded as an ETC inhibitor in the AEFA, as it simultaneously decreased OCR (IC_{50} > 100 µM) and increased ECAR (IC_{50} > 100 µM). Furthermore, fluoxetine decreased other mitochondrial parameters such as reserve capacity (IC_{50} = 70.4 µM) and ATP production (IC_{50} > 100 µM). Given the response obtained in the AEFA, fluoxetine was selected for further investigations using the HepG2-permeabilised assay, which showed that fluoxetine's most sensitive mechanism was inhibition of pyruvate respiration (IC_{50} > 100 µM). Nevertheless, fluoxetine exerted similar HepG2 toxicity in both glucose and galactose containing media (fold change = 0.76), which may suggest the existence of other cytotoxic mechanisms apart from mitochondrial toxicity (Figure 6.23).

6.4.3.1.5 Tianeptine

Tianeptine is a unique tricyclic antidepressant, mainly prescribed for major depressive disorder, but also used to treat anxiety, asthma and IBS. In contrast with SSRIs, tianeptine increases the 5-HT-mediated serotonin reuptake in the brain and it may also have

properties related to its effect on the glutamatergic system[485, 486]. It also differs from most antidepressants in that it is not primarily metabolised by the hepatic cytochrome P450 system[485]. Most common adverse effects associated with tianeptine use include gastrointestinal impairments, dizziness, insomnia, asthenia, tremor, sweating, tachycardia and sexual dysfunction[487].

Tianeptine was first found to affect mitochondrial function in a study published by Fromenty *et al*. in 1989, where it was discovered that 0.5 mM tianeptine inhibited β-oxidation and the TCA cycle *in vitro*. Such inhibition also appeared to happen in mitochondria from mice exposed to tianeptine *in vivo* (0.0625 mmol/kg)[415]. In 2010, Fisar *et al*. found that tianeptine inhibited the activity of the mitochondrial monoamine oxidases (MAO) A and B in pig brain mitochondria (MAO-A IC_{50} = 1105 ± 101 µM, MAO-B IC_{50} = 526 ± 34 µM)[481]. In a different study, the same authors reported inhibition of the respiratory chain complex IV by 500 µM tianeptine after 30 min incubation using a pig brain crude mitochondrial fraction (however inhibition of activity of complexes I or II was not observed)[406]. In 2011, a study published by Abdel-Razaq *et al.* also investigated the effects of 18 h incubation with 50 µM tianeptine on mitochondrial function using cell lysates of a Chinese hamster ovary cell line. Spectrophotometric measurements of mitochondrial complex I, II+III and IV activities revealed 50% inhibition of complex I[402]. Additionally, 50 µM tianeptine inhibited OCR by 60% in state 3 respiration fuelled by glutamate and malate in isolated rat liver mitochondria[402]. A year later, another study investigated the the effects of multiple antidepressants on pig brain mitochondrial respiration. In that study, tianeptine showed the highest efficacy of inhibition among all tested antidepressants tested, as it inhibited mitochondrial respiration energized through both complex I (IC_{50} = 88.9 ± 2.6 µM) and complex II (IC_{50} = 67.4 ± 4.9 µM)[411]. Another study done on rats treated with 15 mg/kg tianeptine for 14 days showed that tianeptine inhibited the activity of the mitochondrial complex I in brain tissues[488]. Finally, the most recent study to date investigated the effects of chronic administration of 10 mg/kg tianeptine on the expression of the brain's mitochondrial protein profile in the hippocampus and the frontal cortex of 3-month-old rats following a prenatal stress procedure (animal model of depression). 2D electrophoresis coupled with mass spectrometry revealed mitoproteome changes in the rat brains, including an increase in the expression of glutamate dehydrogenase and cytochrome bc_1 complex subunit 2[489].

In the present work, acute injection of 100 µM tianeptine caused a dose-dependent decrease in OCR (MEC = 5.5 µM, AC_{50} > 100 µM), reserve capacity (MEC = 0.182 µM, AC_{50} = 21.6 µM) and ATP production (MEC = 40.3 µM, AC_{50} > 100 µM) in HepG2 cells (Table 6.10 and Table 6.11). Tianeptine was categorised as a substrate inhibitor due to the lack of increase in ECAR signal. Further investigations revealed that acute injection of 100 µM tianeptine onto permeabilized HepG2 cells did not significantly inhibit any of the individual OXPHOS complexes. Nevertheless, the Glu/Gal assay revealed that glucose-grown cells were resistant to 24 h treatment with 100 µM tianeptine, while galactose-grown cells showed high levels of cytotoxicity, suggesting that mitochondrial toxicity is probably the primary mechanism of toxicity of tianeptine (Figure 6.23).

Table 6.16. Summary of *in vitro* assays performed to investigate the mitochondrial effects of the antidepressants and anxiolytic drus. Direction of change in basal OCR, reserve capacity, basal ECAR, ATP production and proton leak, where: ↑ = increase compared to vehicle control, ↓ = decrease compared to vehicle control, NR = no response compared to vehicle control. N/A = not available.

Assays		Buspirone	Lorazepam	Citalopram	Fluoxetine	Tianeptine
Acute HepG2 Extracellular Flux Assay (AEFA)	OCR (AC_{50} µM)	>100↓	>100↓	NR	>100↓	>100↓
	Reserve capacity (AC_{50} µM)	43.7↓	NR	NR	70.4↓	21.6↓
	ECAR (AC_{50} µM)	NR	NR	NR	>100↑	NR
	ATP production (AC_{50} µM)	>100↓	>100↓	NR	>100↓	>100↓
	Proton leak (AC_{50} µM)	NR	15↑	>10↓	NR	NR
	Summary mechanism	Substrate inhibitor	Other	NR	ETC inhibitor	Substrate inhibitor
Permeabilised HepG2 Extracellular Flux Assay (OCR)	Most sensitive mechanism (AC_{50} µM)	pyruvate respiration↓ >100	NR	N/A	pyruvate respiration↓ >100	NR
Glu/Gal assay (cell viability reduction)	Glucose (AC_{50} µM)	NR	NR	>10↓	13.3↓	NR
	Galactose (AC_{50} µM)	99↓	NR	NR	17.5↓	57.6↓
	Fold Change	UD	NR	UD	0.76	UD
MTT assay (Glu media, 24 h incubation treatment)	% Cell viability (Conc. µM)	N/A	N/A	N/A	N/A	95 ± 2 (0.5), 94 ± 7 (10), 75 ± 8 (50), 60 ± 13 (100)
MTT assay (Gal media, 24 h incubation treatment)	% Cell viability (Conc. µM)	N/A	N/A	N/A	N/A	89 ± 7.7 (0.5), 83 ± 22 (10), 79 ± 19 (50), 51 ± 17 (100)
C_{max} (µM)		0.003	0.1	0.0003	0.0004	0.62

7. QSAR and Molecular Docking Studies on Succinate-Cytochrome *c* Reductase (SCR) Inhibitors

7.1. Introduction

The overall clinical success rate of drugs selected for preclinical testing is only 11%, with failures often being due to toxicity and adverse drug events[490]. As already discussed in previous chapters, increasing evidence links mitochondrial dysfunction with organ toxicity, which demonstrates the need for the development of efficient predictive tools to help us identify drug-induced mitochondrial dysfunction early in the drug discovery process. These tools would allow us to deprioritize drug candidates with potential safety liabilities, allowing resources to be focused on those compounds with the highest chance of success to the market.

Computational methods such as Quantitative Structure Activity Relationships (QSAR) and molecular docking are powerful computer-based tools in the identification of potentially toxic structural and physicochemical features during the initial design of compounds. They can reduce the time and cost required for the development of new drugs. This is also relevant to the non-pharmaceutical sectors, such as the cosmetics industry, due to European Union law aimed at replacing the use of animals in chemical risk assessment[491]. However, there are currently very limited structure-activity models published in the scientific literature for prediction of mitochondrial toxicity, presumably due to limited publicly available data[492]. In fact, an important limitation in the development of QSAR models is the need for extensive experimental data from which a training and test set can be generated for model development and then assessing the reliability of the model[492]. Nevertheless, existing studies that have applied some of these computational techniques have proven to have great value for prediction of mitochondrial toxicants[281, 493]. QSAR is particularly useful, as it can be used to predict whether a toxic event may occur based on the structural and chemical features of a compound[162].

The present chapter was aimed at performing a QSAR study on mitochondrial toxicity, specifically focused on the inhibition of succinate-cytochrome *c* reductase (SCR, a mixture of respiratory complex II and III) using experimental data that was generated in previous chapters. There are very limited structure-activity studies on ETC inhibition in the literature, and those available have mainly focused on uncoupling activity of compounds[281, 494]. Therefore, the ultimate goal of this chapter was to shed light on

structural and physicochemical features associated with inhibition of SCR, given its key role in the ETC and the high number of compounds that have been reported to target complex III. To this end, IC_{50} values of a total of 50 compounds were used as the response variable in the models, 24 of which were tested in our laboratory. The IC_{50} values for the remaining 26 compounds were obtained from the literature, where all had been measured under the same experimental conditions. The literature compounds included a number of complex III Q_o inhibitors, such as ametoctradin and 12 derivatives of the parent compound[211], famoxadone and 11 its derivatives[212] and pyribencarb[213]. Out of the 50 compounds, 40 were fungicides, while the remaining 10 compounds were pharmaceutical drugs. In addition to QSAR, molecular docking was performed on the ubiquinone site of both complex II and III to investigate residues involved in the binding of the compounds.

7.2. Chapter Aims

The aim of this chapter was to develop *in silico* methods, such as QSAR and molecular docking, to enable a mechanistic link between inhibition of the mitochondrial respiratory chain complexes II+III and chemical characteristics of compounds. Specific objectives within this work included:

1. To gather *in vitro* data (IC_{50} values for SCR activity) from the literature and use this along with the SCR IC_{50} values from our laboratory, reported in previous chapters of this thesis.
2. To perform molecular docking experiments to investigate the binding mode and affinities of these compounds to the Q_o and Q_i sites of the cytochrome bc_1 complex, as well as the Q site of complex II.
3. To analyse the docking results and generate a protein-ligand interaction fingerprinting (PLIF) analysis with the purpose of identifying the significant interactions between the ligands and the binding sites in terms of frequency of occurrence and the resulting activity.
4. To develop QSAR models using a regression-based approach to highlight structural and chemical features that might be responsible for complex II and complex III inhibition.

7.3. Results

7.3.1. *In vitro* Inhibition of Succinate-Cytochrome *c* Reductase Activity

The half maximal inhibitory concentrations (IC_{50s}) of a number of pharmaceutical drugs and fungicides for succinate-cytochrome *c* reductase (SCR) activity were obtained in chapters 4 and 5. Figure 7.1 depicts a summary of the IC_{50} values in logarithmic scale (converted to -log IC_{50} or pIC_{50}). Compounds tested in the laboratory included 19 fungicides and 15 medical drugs (Appendix II, Table 2.1), but an exact IC_{50} value for the pharmaceutical drugs acetaminophen (IC_{50} > 5000 µM), colchicine (IC_{50} > 1300 µM), haloperidol (IC_{50} > 660 µM), sulfamethoxazole (IC_{50} >1300 µM) and valproic acid (IC_{50} > 6600 µM) could not be obtained due to solubility limitations, therefore were not included in the QSAR study. To improve the applicability domain of the models, the compounds selected for testing were from a diverse chemical space (Appendix II, Table 2.1) and covered a wide range of potencies (Figure 7.1). Additionally, in order to have enough observations to build a robust QSAR model, IC_{50} values of a series of fungicides obtained under the same experimental conditions were taken from the literature (Appendix II, Table 2.2).

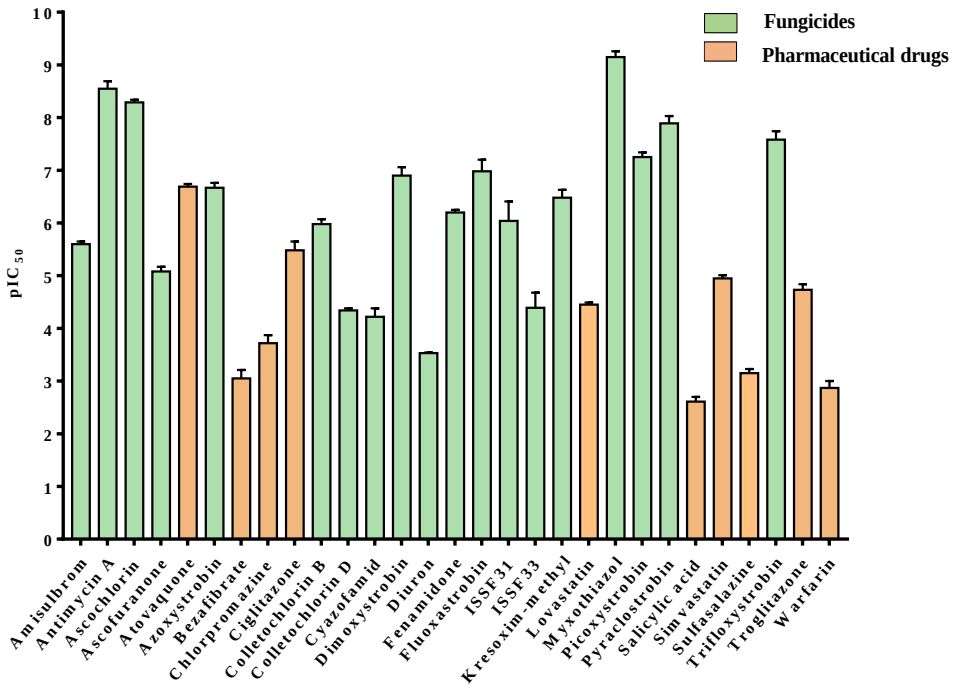

Figure 7.1. Depiction of pIC_{50} values of the compounds tested. Fungicides are represented in green whereas pharmaceutical drugs are represented in orange. Higher values of pIC_{50} indicate exponentially greater potency. Data are mean of triplicates obtained in different biological samples ± standard error.

7.3.2. Molecular Docking Analysis on the cytochrome *bc₁* complex

Molecular docking was performed to investigate the binding affinities of the compounds tested in our laboratory to highlight key residues for ligand-protein interactions and reveal structural features that might lead to the inhibition of the cytochrome *bc₁* complex.

For comparative and consistency purposes, since RLM have been used in the SCR inhibition experiments, it would have been more desirable for molecular docking to use a rat crystallographic structure of *bc₁*. However, at the time of writing, this protein structure was not available, hence other close mammalian structures available on PDB[199] were considered. To this end, a sequence alignment between the human cyt *b* of the cytochrome *bc₁*[27] (PDB entry: 5XTE, resolution of 3.4 Å) and the bovine cyt *b* (PDB entry: 1PPJ, resolution of 2.1 Å)[201] revealed a high homology (78.6%). Eventually, the bovine crystal structure was selected for docking purposes over the human structure because it offered a higher resolution. Furthermore, the bovine crystal structure facilitated the study of both Q_o and Q_i sites, due to the presence of bound ligands at both sites (stigmatellin and antimycin A, respectively) that can be used to define the binding site within a 2.5 Å distance around the co-crystallised ligand atoms.

All Q_o inhibitors and pharmaceutical drugs were docked into the quinol oxidation site, whereas Q_i inhibitors were docked into the quinone reduction site. The docking protocol was validated by re-docking the co-crystallized ligand stigmatellin into the active site, which gave a RMSD of 0.812 Å (ΔG_{bind} = -10.70 kcal/mol), a very satisfactory value considering the size of the molecule and the high presence of rotatable bonds in this ligand (Figure 7.2).

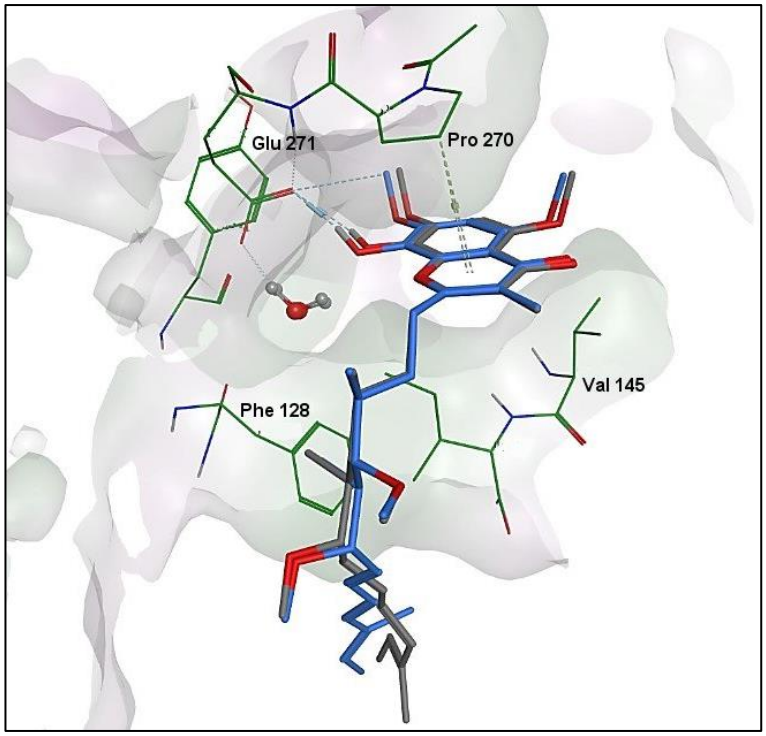

Figure 7.2. Superimposition of the crystallographic stigmatellin (carbon atoms in grey, oxygen in red) and the best ranked pose of the re-docked stigmatellin (carbon atoms in blue, oxygen in red). Hydrogens bonds are represented by light blue dashed lines, whereas arene-H interactions are depicted by green dashed lines.

The top docking scores for the ligands ranged from -4.97 kcal/mol for salicylic acid to -10.06 kcal/mol for myxothiazol. The lowest scores were observed for strong and specific inhibitors such as antimycin A (-9.63 kcal/mol), ascochlorin (-8.79 kcal/mol), azoxystrobin (-8.71 kcal/mol) and pyraclostrobin (-9.46 kcal/mol). Conversely, the highest scores were observed for compounds that, even at the range of millimolar concentration, showed very low or no inhibition at all in the SCR assay, such as acetaminophen (-5.85 kcal/mol), sulfamethoxazole (-6.68 kcal/mol) and valproic acid (-6.30 kcal/mol). In order to assess the accuracy of docking scores for the prediction of inhibitory activity, a simple regression analysis was performed between the top docking scores and the log IC_{50} values. As seen in Figure 7.3, this resulted in a moderate positive linear correlation (R = 0.70). A summary of the docking scores obtained for the pharmaceutical drugs tested is shown in Table 7.1.

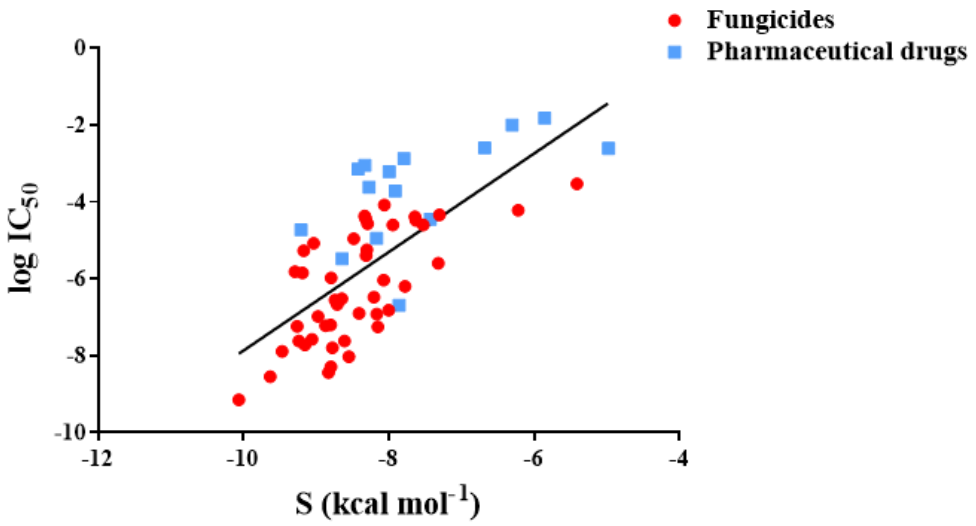

Figure 7.3. Correlation between the top docking scores (kcal/mol) and log IC_{50} values of compounds. Fungicides are depicted in red dots, whereas pharmaceutical drugs are depicted in blue squares. Pearson's R = 0.70, slope significantly non-zero, ****p value < 0.0001.

Table 7.1. Summary of pharmaceutical drugs, their mode of action, docking scores and IC_{50} values against SCR activity.

Compound	Mode of action	ΔG_{bind} (kcal/mol)	SCR IC_{50} (µM)
Acetaminophen	Analgesic	-5.86	>5000
Atovaquone	Anti-infective	-7.86	0.2 ± 0.024
Bezafibrate	Anticholesteremic agent	-8.32	920 ± 304
Chlorpromazine	Antipsychotic	-7.91	194 ± 67
Ciglitazone	Antidiabetic	-8.64	3.4 ± 1
Colchicine	Anti-mitotic	-7.99	>1300
Haloperidol	Antipsychotic	-8.27	>660
Lovastatin	Anticholesteremic agent	-7.43	35 ± 3
Salicylic acid	Anti-inflammatory agent	-4.98	2476 ± 475
Simvastatin	Anticholesteremic agent	-8.17	11 ± 1
Sulfamethoxazole	Antibiotic	-6.68	>1300
Sulfasalazine	Anti-inflammatory agent	-8.42	709 ± 130
Troglitazone	Antidiabetic	-9.21	19 ± 5
Valproic acid	Anti-epileptic	-6.31	>6600
Warfarin	Anticoagulant	-7.80	1359 ± 358

7.3.3. Protein-Ligand Interaction Fingerprinting (PLIF) of the Q_o site of Cytochrome *bc₁* Complex (Complex III)

The results of molecular docking were used for protein–ligand interaction fingerprinting (PLIF) analysis to provide detailed information on the molecular interactions between the ligands and the Q_o site of cytochrome *bc₁* complex. In total, 56 compounds were docked, including 41 fungicides (compounds tested in our laboratory and compounds retrieved from literature) and 15 pharmaceutical drugs. The Q_i inhibitors were not included in the docking analysis (antimycin A, amisulbrom, cyazofamid and diuron). Subsequently, the top five best scoring poses for each compound were retained, resulting in 280 poses to be analysed. To further study the significance of the fingerprints, compounds were classified as active or inactive based on their pIC_{50} values by setting an arbitrary cut-off threshold at $pIC_{50} \geq 6$ classed as active and the remaining compounds as inactive.

Figure 7.4 shows the details of the top ten most abundant interaction fingerprints, their percentage abundance and the extent of contribution to ligands' activity. Nature of these top 10 most abundant interactions were: backbone hydrogen bond acceptors (a) and donors (d), sidechain hydrogen bond acceptors (A) and donors (D), arene interactions (R) and solvent hydrogen bonds (O). Figure 7.4A shows the interaction frequency of the residues with the different docking poses of compounds. Side chain H-bond donors (D) and acceptors (A), along with arene interactions (R) were extensively encoded in the ligand-protein complexes. Upon classification of compounds into active ($pIC_{50} \geq 6$) or inactive ($pIC_{50} < 6$), the frequency bars were annotated with a qualitative indication of the overabundance of active vs. inactive compounds. If the fraction of active compounds containing the fingerprint was greater than the fraction of actives overall, the extent to which it was greater was indicated by a black line above the bar. In the contrary situation, this was similarly indicated by an inverse line below the top of the bar. Often, a combination of height and overabundance is an indication that the interaction is important for activity.

The significance display in Figure 7.4B is related to the population histogram, but in this case the heights of the bars are built in a way that they indicate the extent to which each fingerprint is an important prerequisite for activity. Figure 7.4C shows this information in more detail. It includes the abundance percentage *(% abundance)* of the fingerprints, which is calculated in a way that if the fingerprint occurs in every pose it takes a value of

100. Therefore, among the residues that interact most often with the ligands are proline 270 (R) (21.43%), glutamate 271 (D) (14.29%) and histidine 161 (A) (14.29%). The percentage of activity *(% active)* shows the percentage abundance of the fingerprints within the compounds that are classified as active ($pIC_{50} \geq 6$). The percentage of relative activity *(% relative activity)* shows the percentage abundance of the fingerprint within the compounds which are classified as active, scaled so that the most populous active fingerprint is set to 100%. The percentage of over-activity *(% over-activity)* represents the difference between the activity percentage and the abundance percentage. A positive value means that the fingerprint occurs more often in active compounds than it does in the database overall. Finally, *"% wovact"* multiplies the value of the percentage of over-activity by the abundance percentage, expressed as a percentage. Scaling the over-activity by the overall abundance is an indication of when the fingerprint frequently appears in favour of activity. Fingerprints with higher values are likely to be important for activity. From Figure 7.4 it can be concluded that the most important interactions for inhibition are His 161 sidechain H-acceptor (strong and weak, *% over-activity* of 1.91 and 1.71, respectively) and Pro 270 strong arene interactions (*% over-activity* = 2.271). Conversely, although Glu 271 showed a high frequency of occurrence overall, it contributes to the binding of inactive ligands (strong and weak, *% over-activity* of -3.88 and -4.58), as well as Pro 270 weak arene interactions (*% over-activity* = -3.02).

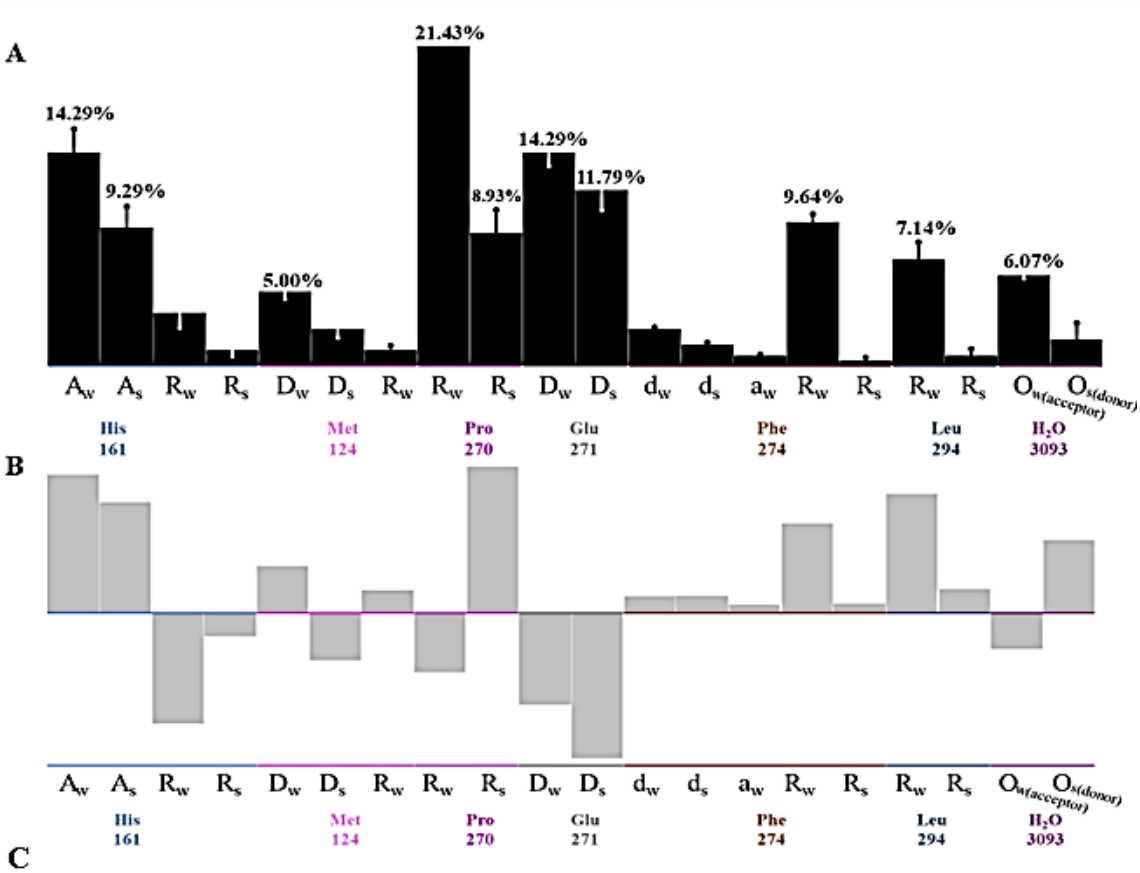

C

Residue	Type of interaction	Abundance (%)	Strength of interaction	Active (%)	Relative activity (%)	Over-activity (%)	Wovact (%)
Pro 270	Arene interaction	21.43	Weak *	18.4	100	-3.02	-0.64
Glu 271	Sidechain H-donor	14.29	Weak	10.4	56.5	-3.88	-0.55
His 161	Sidechain H-acceptor	14.29	Weak	16	86.9	1.71	0.24
Glu 271	Sidechain H-donor	11.79	Strong **	7.2	39.1	-4.58	-0.54
Phe 274	Arene interaction	9.64	Weak	9.6	52.1	-0.04	-0.004
His 161	Sidechain H-acceptor	9.29	Strong	11.2	60.8	1.91	0.17
Pro 270	Arene interaction	8.93	Strong	11.2	60.8	2.27	0.20
Leu 294	Arene interaction	7.14	Weak	8.8	47.8	1.65	0.11
H_2O 3093	Solvent H-bond	6.07	Weak	4.8	26	-1.27	-0.07
Met 124	Sidechain H-donor	5.00	Weak	3.2	17.3	-1.8	-0.09

Figure 7.4. Results of the PLIF analysis for the Q_o site of cytochrome *bc_1* complex. A) Population histogram. It displays the frequency of occurrence of the fingerprints amongst the different poses of all ligands (subscript *w* denotes weak interactions, while subscript *s* denotes strong interactions). Percentages above the bars are percentage abundance. The extent to which the fraction of actives containing the bit is higher than the fraction of actives overall is indicated as a black line above the bar. B) Significance display. It shows the extent to which each fingerprint is an important prerequisite for activity. The height of the bars for each fingerprint bit are a product of the frequency of the fingerprint and the normalised probability of a ligand being active if it contains the fingerprint. C) Nature and statistics of the top ten most abundant fingerprints for the Q_o site of complex III. *weak = 0.5 kcal/mol, **strong = 1.5 kcal/mol

7.3.4. Protein-Ligand Interaction Fingerprinting (PLIF) of the Q site of Succinate-Ubiquinone Oxidoreductase (Complex II)

Molecular docking was also performed on succinate-ubiquinone oxidoreductase (mitochondrial SQR, EC 1.3.5.1), also known as complex II, to explore the potential important residues for binding around the ubiquinone binding site or Q site. Complex II is a membrane-anchored protein that consists of four subunits: a flavo protein that catalyses the oxidation of succinate to fumarate (SDH-A), an iron-sulfur protein containing the three iron-sulfur clusters responsible for the electron transfer from succinate to ubiquinone (SDH-B), and two membrane anchor subunits (SDH-C and SDH-D) (Figure 7.6)[495]. The Q site is a hydrophobic pocket formed by residues of the subunits B, C and D and is highly conserved throughout a range of organisms[496].

All 60 compounds listed in this chapter (Appendix II, Table 2.1 and 2.2) were docked into the Q site of complex II. It should be noted that most compounds used in this study were well-known specific complex III inhibitors and, additionally, it has been reported that none of the compounds taken from the literature showed an inhibitory effect on complex II[211, 212]. For this reason, molecular docking and subsequent PLIF analysis was limited to the investigation of the residues that interacted most frequently with compounds, without further studying the significance of the fingerprints based on their pIC_{50} values.

There are several crystal structures of complex II available on PDB[199], out of which some have a ligand bound to the Q site that facilitate defining the binding pocket for docking studies. An initial candidate for these studies was the E. *coli* complex II crystal structure with a resolution of 2.6 Å (PDB entry: 1NEK), which contains the endogenous ligand ubiquinone co-crystallised at the Q site. However, protein alignment with a mammalian (porcine) structure (PDB entry: 3SFD) revealed a very poor homology (45.73%). Therefore, the mammalian structure (PDB: 3SFD, which had a resolution of 2.6 Å and the ligand pentachlorophenol bound to the Q site was selected for docking studies. For validation of the methodology, the co-crystallised ligand pentachlorophenol was re-docked into the Q site and a RMSD of 0.375 Å was obtained, which is a satisfactory value (ΔG_{bind} was -5.52 kcal/mol) (Figure 7.5).

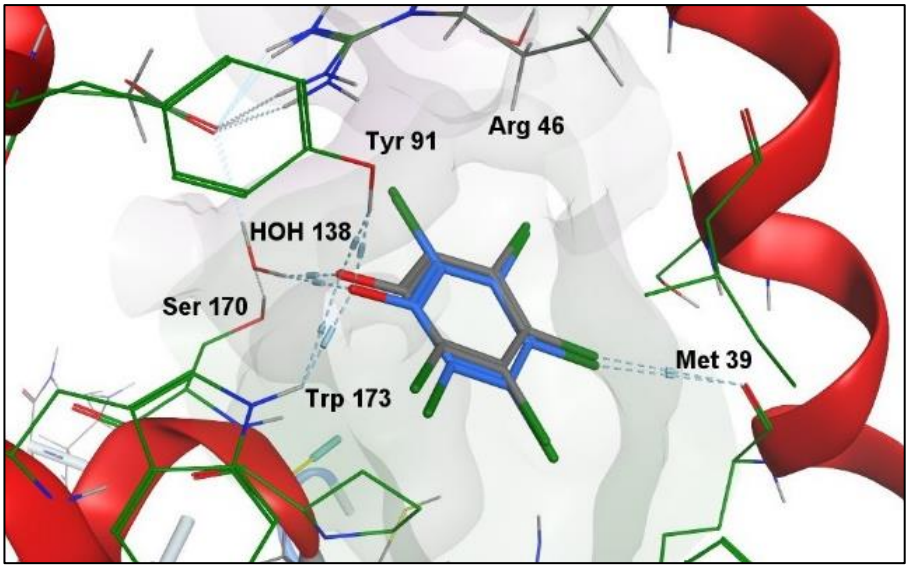

Figure 7.5. Superimposition of the crystallographic pentachlorophenol (carbon atoms in grey) and the best ranked pose of the re-docked pentachlorophenol (carbon atoms in blue). Hydrogens bonds are represented by light blue dashed lines.

As expected, docking scores obtained for complex II were significantly more positive (less favourable) than those obtained for complex III. For instance, within the top poses for each compound, the best score obtained was -7.80 kcal/mol (colchicine), whereas the worst score obtained was -4.87 kcal/mol (salicylic acid). Additionally, a linear regression applied to the top docking scores of each compound and log IC_{50} values showed a very weak correlation (Pearson's R = 0.4).

Molecular docking studies retained the top 5 best scoring poses for each compound, which resulted in a total of 300 poses that were subsequently used as the input in the PLIF analysis. PLIF analysis revealed six types of fingerprints involved in the protein-ligand interactions, including backbone hydrogen bond acceptors (a) and donors (d), sidechain hydrogen bond acceptors (A) and donors (D), arene interactions (R) and solvent hydrogen bonds (O). Details of the top ten most abundant fingerprints are shown in Figure 7.7. Among the residues in the Q site of complex II that interacted most frequently with the compounds were Trp 173 (chain B), Tyr 91 (chain D), Arg 46 (chain C), Ile 43 (chain C) and Met 39 (chain C). Additionally, a water molecule located in the Q site (H_2O 138) was also found to be involved in ligand-binding through hydrogen bonds (Figure 7.7).

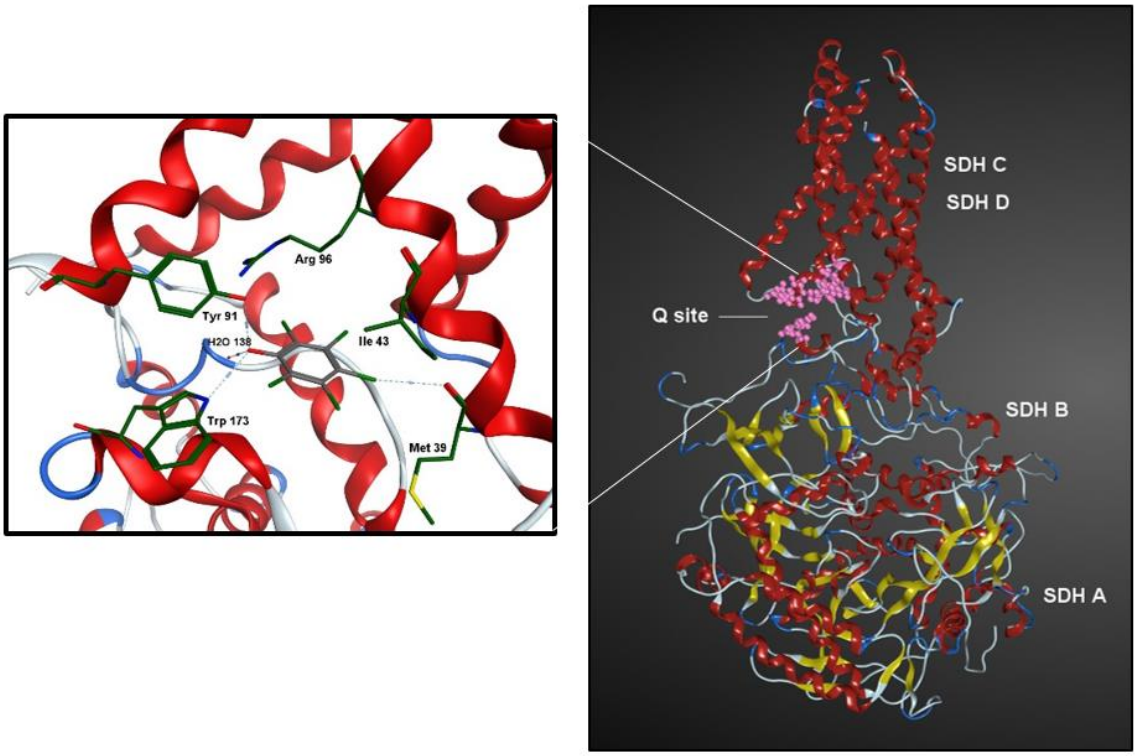

Figure 7.6. Crystal structure of porcine complex II (PDB entry: 3SFD) and indication of the location of Q site within the structure. A zoomed in depiction of the Q site (with re-docked pentachlorophenol) shows the location within the pocket of the residues that interacted most frequently with the compounds.

A

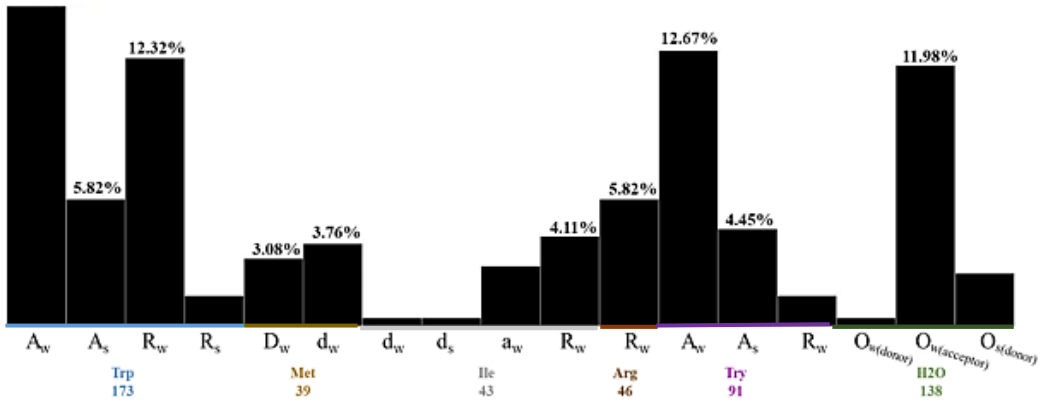

B

Residue	Type of interaction	Abundance (%)	Strength of interaction
Trp 173	Sidechain H-acceptor	14.72	Weak *
Tyr 91	Sidechain H-acceptor	12.67	Weak
Trp 173	Arene interaction	12.32	Weak
H_2O 138	Solvent H-bond	11.98	Weak
Arg 46	Arene interaction	5.82	Weak
Trp 173	Sidechain H-acceptor	5.82	Strong**
Tyr 91	Sidechain H-acceptor	4.45	Strong
Ile 43	Arene interaction	4.11	Weak
Met 39	Backbone H-donor	3.76	Weak
Met 39	Sidechain H-donor	3.08	Weak

Figure 7.7. A) Population histogram that shows the abundance percentage of the fingerprints (subscript *w* denotes weak interactions, while subscript *s* denotes strong interactions). B) Nature and statistics of the top ten most abundant fingerprints in the analysis for complex II. *weak = 0.5 kcal/mol, **strong = 1.5 kcal/mol.

7.3.5. QSAR Models

In vitro assays performed in previous chapters showed inhibition of complex II+III by a wide range of chemicals. Some of these chemicals were widely prescribed pharmaceutical drugs whose ability to induce mitochondrial dysfunction could be related to organ toxicities. In this chapter, QSAR models were developed to correlate chemistry of compounds with their biological behaviour. This information is of great value, given that there are very limited QSAR models available in the published literature for the prediction of mitochondrial toxicity, despite the fact they would be an important breakthrough in the drug discovery and the cosmetics industry[492].

The purpose of QSAR is to use chemical information and correlate it with a behaviour of the compound employing mathematical algorithms to eventually predict the response value of unknown chemicals. Here, the potency of the chemicals in inhibiting complex II+III measured as pIC_{50} values was the response variable modelled. The independent variables were computationally derived molecular properties known as "molecular descriptors". Ultimately, since a QSAR model could potentially predict mitochondrial toxicity caused by new drug candidates, it provides a rational strategy towards the design of new molecules and could help reduce practical experimentation burden as well as time.

The initial step of the QSAR workflow was to obtain the molecular descriptors. A total of 325 molecular descriptors for the 50 compounds included within this study were calculated using both ACD percepta[206] and MOE software packages[204]. These included 2D and 3D molecular descriptors, docking scores and fingerprints. Subsequently, the data set of 50 compounds was divided into a training set (32 compounds) and a test set (18 compounds). The method of data allocation into training set and test set was manually, considering the structural diversity and a wide range of activity in the data set from a Principal Component Analysis (PCA) as can be seen in Figure 7.8. PCA is a powerful technique used for data exploration that involves a linear transformation of a set of correlated variables to an alternative representation of orthogonal variables (a.k.a Principle Components), which emphasizes the variance among observations. This simplifies the complexity in high-dimensional data while bringing out strong patterns and trends, making data easier to explore and visualise[214]. Figure 7.8 shows the scores plot between the first two principle components. Compounds were allocated to test set by

picking compounds manually from this plot, so they cover the same chemical space as the training set.

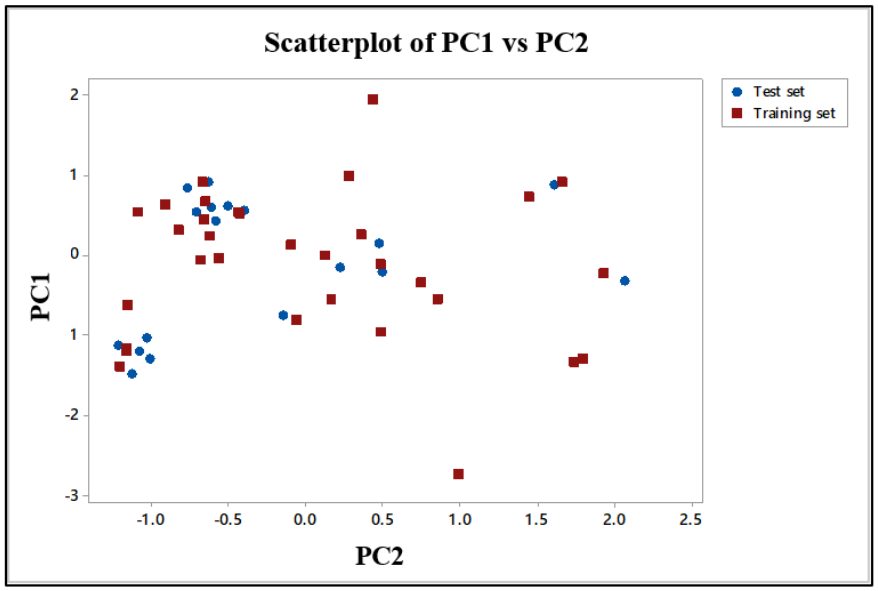

Figure 7.8. Principle Component Analysis (PCA) indicating the spread of training and test set compounds in a PC1 vs. PC2 plot.

In order to prune the initial molecular descriptors and pre-select the ones with better correlation with the pIC_{50} values, 200 different random samples of 24 compounds were picked from the total set of 32 compounds to be used as the "training set". A stepwise regression analysis was carried out for these 200 data samples and a histogram plot was generated with the frequencies of each molecular descriptor, as it can be seen in Figure 7.9. Only those descriptors with frequencies greater than 10 were selected and used in the final stepwise regression analysis using all the training set compounds (49 descriptors in total). A ratio of at least 10:1 between the number of compounds and the number of descriptors was maintained in the final models in order to avoid model overfitting. When overfitting occurs, a model can fit to an acceptable level the activities of the compounds included in the training set, but it fails when applied to an external set of compounds.

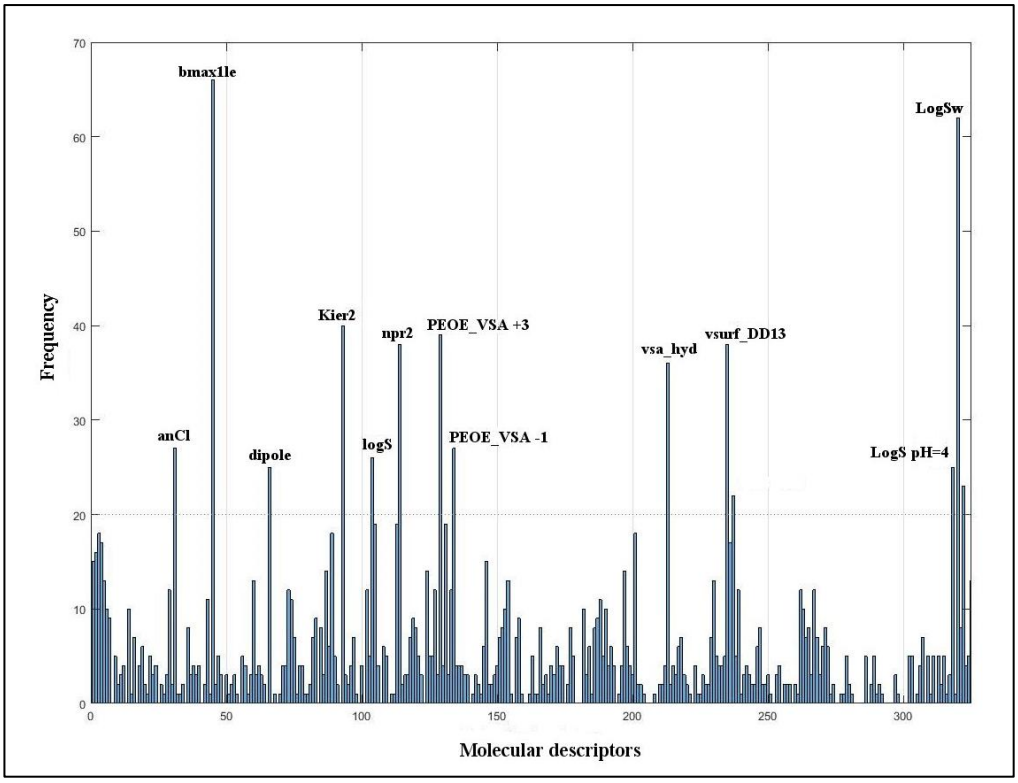

Figure 7.9. Histogram of frequencies of the 325 molecular descriptors used to generate the QSAR model. The molecular descriptors with highest frequencies are labelled.

Hence, two final QSAR models were obtained in a final stepwise regression analysis, which included no more than four molecular descriptors. The final QSAR models obtained are discussed below:

QSAR models A and B:

A) **pIC_{50}** = 2.384 (± 0.605) + 2.119 (± 0.311) *Neutral form (pH = 7.4)* - 0.679 (± 0.109) *Log S* - 0.495 (± 0.171) *Number of rings (size 6)*

N = 32, R = 0.87, R^2 = 0.76, SE = 0.82, F = 31.1 (df3,28), p = 0.000

B) **pIC_{50}** = 2.826 (± 0.561) + 1.680 (± 0.317) *Neutral form (pH = 7.4)* - 0.943 (± 0.134) *Log S* - 0.741 (± 0.175) *Number of rings (size 6)* - 0.274 (± 0.096) *b_max1le*

N = 32, R = 0.90, R^2 = 0.82, SE = 0.73, F = 31.3 (df4,27), p = 0.000

Here, n is the number of compounds used in the development of the QSAR model; R and R^2 are the correlation coefficient and the squared correlation coefficient, respectively; SE

is the standard error of the estimate, F is the Fischer ratio value and p is the statistical confidence level. All regression coefficients are significant at $p<0.05$.

Neutral form (pH=7.4) is the first molecular descriptor in these equations. This is the fraction of compounds that is unionised (not dissociated) at pH 7.4, calculated by the classic ACD Percepta method from pKa values using the Henderson–Hasselbalch equation. Given that there are both acidic and basic compounds in the dataset, the positive sign of the *Neutral form* term indicates that less acidic and less basic compounds are better inhibitors. In this dataset, the basic compounds with high ionisation (unfavourable for inhibition potency) are drugs such as chlorpromazine and ametoctradin analogues (aminotriazolopyrimidine compounds 4a-4z), while acidic ionisation (unfavourable for inhibition) are AOX inhibitors such as ascofuranone and colletochlorin D, and pharmaceutical drugs such as salicylic acid and sulfasalazine. On the other hand, mainly neutral compounds include fungicides such as famoxadone, azoxystrobin and other oxazolidinedione derivatives (compounds 8a-8k).

The second most important descriptor in the equations is *Log S*, which is the aqueous solubility. This property is calculated from a linear atom contribution model based on 2D-molecular topology developed by Hou *et al*[497]. The negative sign in the equation indicates that molecules with greater aqueous solubility will show lower inhibitory activity. This may be due to the lipophilic nature of the mitochondrial enzymes allowing better diffusion of more lipophilic (less water soluble) compounds to diffuse into the site of action of the mitochondrial enzymes. As such, this property could be even more important for the prediction of cell-based or tissue-based activity measures.

The third most important descriptor is *Number of rings (size 6).* The negative coefficient of this parameter indicates that presence of fewer 6-membered rings may increase inhibitory potency. This could be due to reduced steric hindrance, the phenomenon by which chemical interactions are reduced due to steric bulk. Often, bulky substituents can interfere with the intermolecular interactions leading to a reduction in the drug's biological activity. However, it must also be noted that the correlation does not necessarily imply causation. It was also noted here that the most potent compound in the training set (myxothiazol) lacked 6-membered rings, while fluoxastrobin and atovaquone have 4, ametoctradin and its derivatives have 2, famoxadone derivatives have 3, and pharmaceutical drugs and other fungicides have between 0-3 6-membered rings.

Model B included a fourth molecular descriptor. This final descriptor is *b_max1len*, which represents the length of the longest single bond chain within the molecular structure (excluding conjugated bonds and any rings). With a negative coefficient, the relationship indicates negative impact of long hydrocarbon chains such as those seen in some ametoctradin derivatives (compounds 4a, 4b and 4c), some pharmaceutical drugs such as chlorpromazine and warfarin, and ascofuranone. It must also be noted that this relationship does not penalise presence of long molecules such as those having long conjugated chains (e.g. myxothiazol) or long chains of rings such as famoxadone derivatives.

Regression of predicted pIC_{50} values in QSAR models A and B vs. experimental ones are characterised by slopes close to 1 (0.77 and 0.82, respectively) (Figure 7.10). Model B gives the best QSAR model in terms of the best fit accuracy of the pIC_{50} values of the training set, as it has the highest Pearson's R (R = 0.90) and the lowest standard error (SE = 0.73).

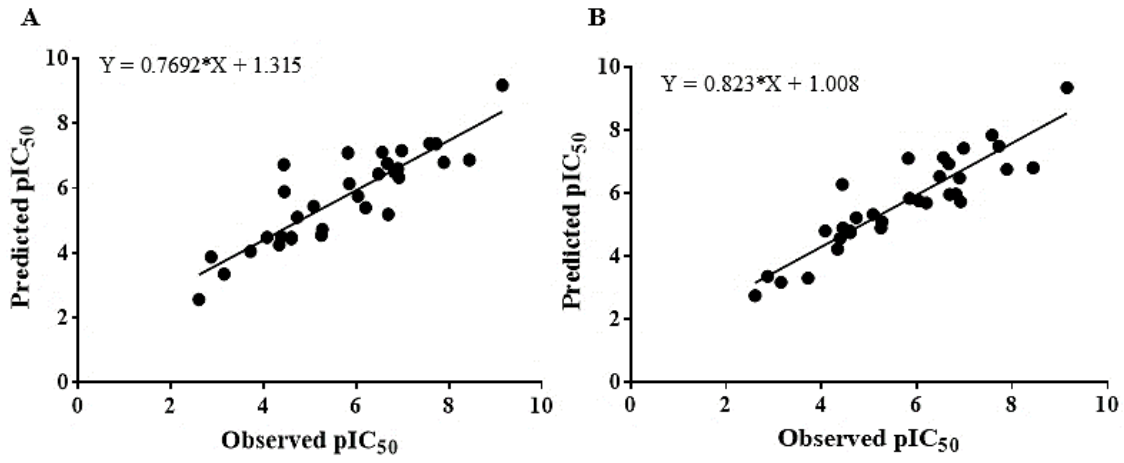

Figure 7.10. Predicted pIC_{50} values with QSAR model A and B vs. experimentally obtained ones (training set). Model A: Pearson's R = 0.88; R^2 = 0.77, $p < 0.0001$ (95% confidence interval). Model B: Pearson's R = 0.90; R^2 = 0.82, $p < 0.0001$ (95% confidence interval).

7.3.5.1. Validation of the QSAR Models

The molecules involved in the QSAR model development (training set) were subject to internal validation in order to judge the quality and goodness-of-fit of the models. The internal validation method was leave-one-out (LOO) cross-validation, where each compound of the training data is removed one at a time, and then the QSAR model is

built based on the remaining molecules. The activities of the deleted compounds are then predicted by the QSAR equations where they have not been involved in the model training. The predicted pIC_{50} values and LOO cross-validation predicted pIC_{50} values by both models, along with absolute error values and Z-scores are shown in Appendix II, Table 2.3 (model A) and Appendix II, Table 2.4 (model B).

Predictability of the models was judged using the square of cross-validation coefficient (Q^2) (explained in Equation 2.3, Materials and Methods section 2.12.1.3). The values of Q^2 for models A and B were 0.684 and 0.738, respectively, which exceeded the threshold value of 0.5 suggested by Tropsha[227]. According to Tropsha, a QSAR model is considered acceptable if the value of Q^2 exceeds the predetermined value of 0.5[227]. However, Q^2 alone is not sufficient to evaluate the predictive power of a QSAR model[166]. Frequently, if there is a high structural redundancy of the training set, models developed using the LOO cross-validation technique undergo the problem of overfitting and therefore overestimate the value of Q^2. If that is the case, the developed model will be unsuccessful in the prediction of the activity of a completely new set of compounds. For this reason, Q^2 often serves as a basic, but insufficient criterion to judge the predictive capability of the models, making necessary an external validation to ensure the applicability of the models for the prediction of untested molecules[166].

Therefore, external validation was performed using a new set of compounds that were not used in the development of the model, i.e. the test set. The predicted pIC_{50} values for the test set along with the absolute error values are shown in Appendix II, Table 2.5 (model A) and Appendix II, Table 2.6 (model B). Among these, compound 8a was found to be an outlier in both models, as the absolute error was greater than 2 for this compound. MAE of the predicted pIC_{50} values for the test set of compounds was also calculated to assess the predictability of the models, yielding a value of 0.68 in the case of model A and 0.63 in the case of model B. However, if compound 8a was excluded from the calculations, MAE values would reduce to 0.55 and 0.52 for models A and B respectively.

Based on Golbraikh and Tropsha's criteria for an acceptable QSAR model, a linear regression through the origin between observed against predicted pIC_{50} values, or between predicted against observed pIC_{50} values, should be characterised by regression lines slopes close to 1 (i.e. should be close to 1 in $Y_{obs}^{r0} = k\,Y_{pred}$ and $Y_{pred}^{r0} = k'Y_{obs}$). Additionally, the value of correlation coefficient (R) should also be close to 1[167]. An

additional more strict condition they proposed for a QSAR model to have a high predictive ability is that either R_0^2 or $R_0'^2$ (the squared correlation coefficients of the regression lines without intercept) must have similar values to R^2.[167] Overall, the criteria proposed by Golbraikh and Tropsha for models to be considered acceptable are as follows:

i. $Q^2 > 0.5$
ii. $R^2 > 0.6$
iii. $R^2 – R_0^2 / R^2 < 0.1$ and $0.85 \leq k \leq 1.15$ or $R^2 – R'_0{}^2 / R^2 < 0.1$ and $0.85 \leq k' \leq 1.15$
iv. $| R_0^2 - R'_0{}^2 | < 0.3$
v. R_0^2 or $R'_0{}^2$ close to R^2

For both models, a linear regression between observed vs. predicted and predicted vs. observed was performed and parameters such as R^2, R_0^2, $R_0'^2$, *k* and *k'* were calculated (Figure 7.11 and Figure 7.12). The validity of the models was supported by R^2 values of 0.62 in model A and 0.61 in model B, which fulfilled the condition ii above. Both values improved if compound 8a was not considered in the calculations ($R^2 = 0.79$ in model A and $R^2 = 0.74$ in model B). Also, it is important to note that R_0^2 and $R_0'^2$ were not substantially very different from each other, and they were both close to R^2. Both models were truly predictive, as all criteria proposed by Golbraikh and Tropsha[167] was satisfied even if the outlier 8a was kept in the calculations. In both models, *k* and *k'* were close to 1 (1.04 and 0.93 in model A, and 1.03 and 0.94 in model B, respectively), but again these values improved when compound 8a was not considered. Finally, the R_m^2 metrics for external validation proposed by Roy *et al*[215] were calculated: $\Delta R_m^2 = 0.009$ (model A) and $\Delta R_m^2 = 0.01$ (model B) and $\overline{R_m^2} = 0.50$ (model A) and R_m^2 0.50 (model B), which satisfied the criteria for an acceptable prediction. A summary of all statistical parameters can be found in Table 7.2. Based on a statistical significance, model B gives the best QSAR model, as it has the highest R^2 and Q^2 and the lowest MAE values. Correlation plots between the experimental pIC_{50} values and predicted pIC_{50} values of both the training set and test set based on models A and B are shown in Figure 7.13.

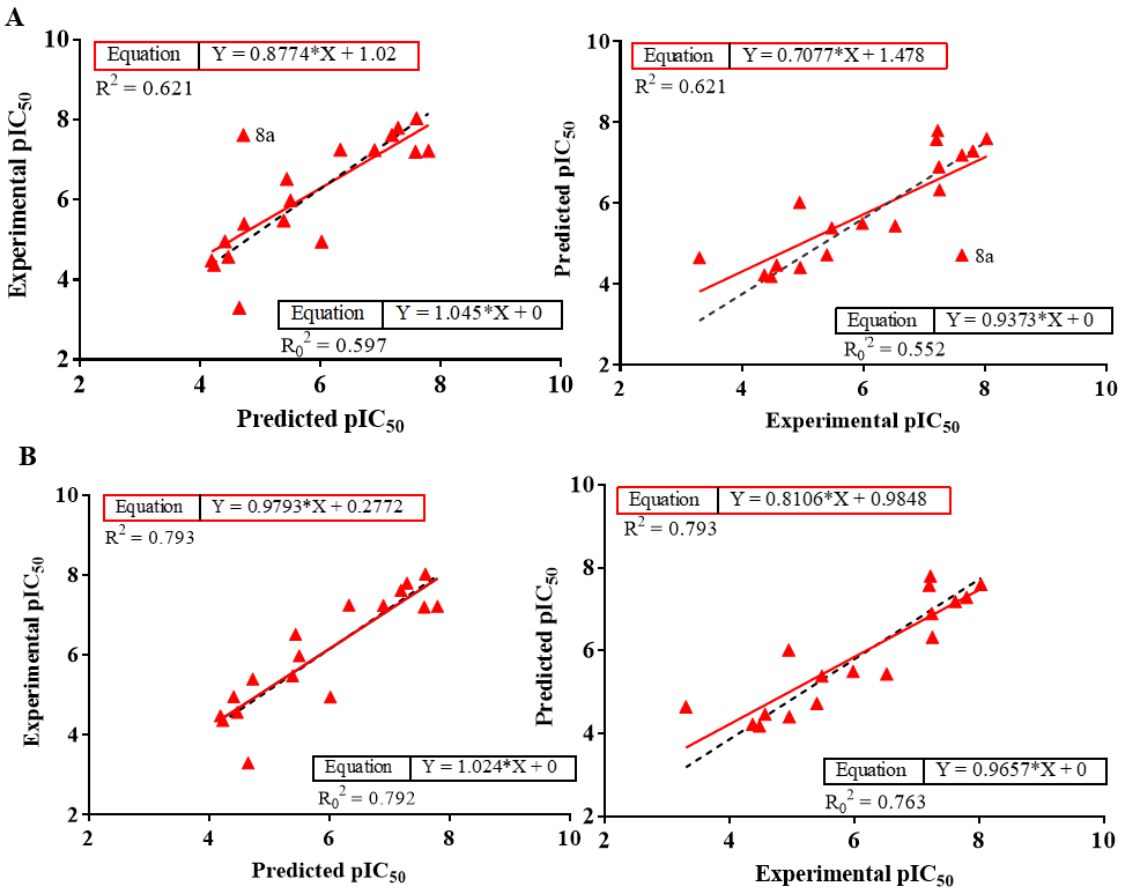

Figure 7.11. Regression between observed vs. predicted and predicted vs. observed activities for the external set of compounds based on model A including (A) and excluding (B) the outlier (compound 8a). Each graph contains a regression plot with and without intercept, depicted by red and black dotted lines, respectively.

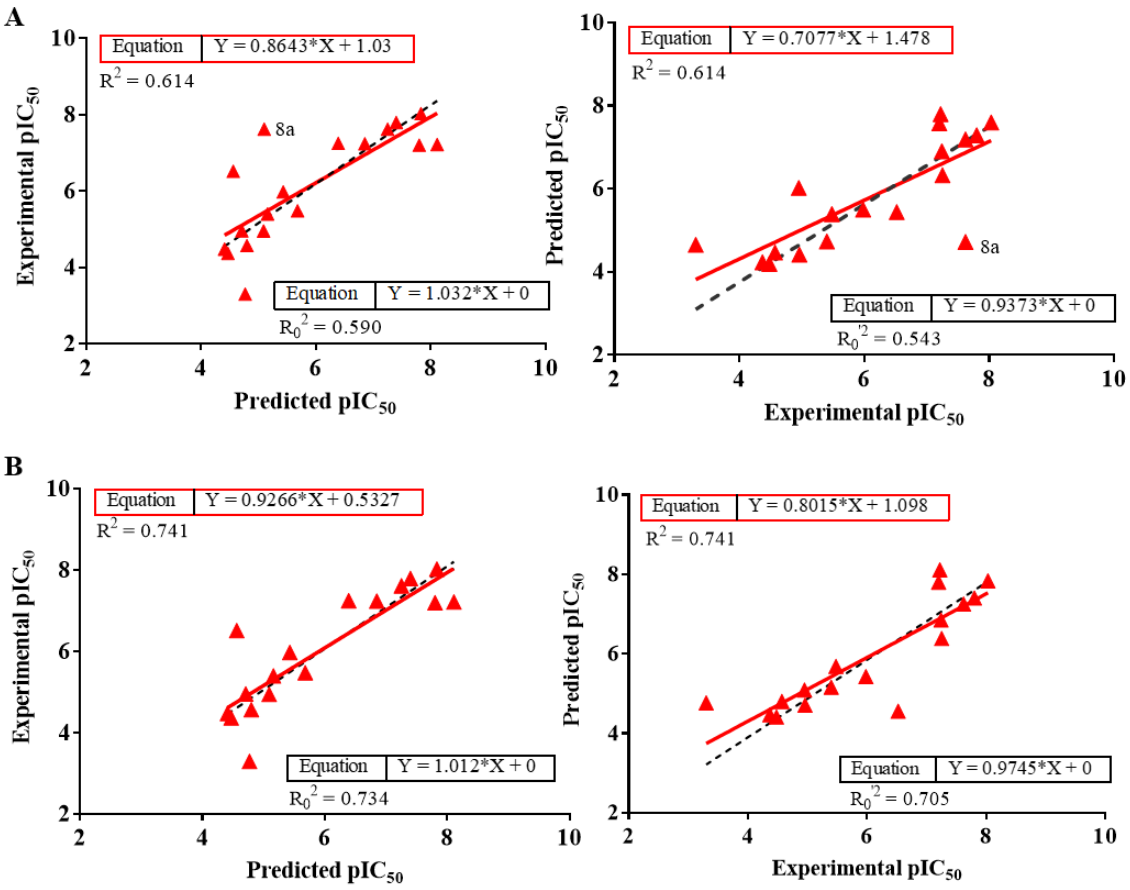

Figure 7.12. Regression between observed vs. predicted and predicted vs. observed activities for the external set of compounds based on model B including (A) and excluding (B) the outlier (compound 8a). Each graph contains a regression plot with and without intercept, depicted by red and black dotted lines, respectively.

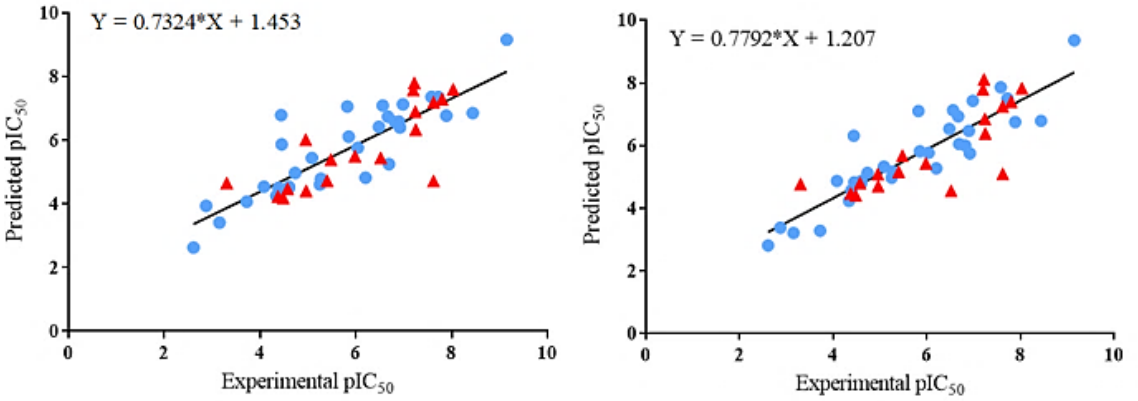

Figure 7.13. Correlation plot of experimental pIC_{50} values and predicted pIC_{50} values based on equations of QSAR models A (left) and B (right). Training set is depicted in blue dots, while test set is depicted in red triangles. Model A: Pearson's R = 0.84, R^2 = 0.70, p value < 0.0001. Model B: Pearson's R = 0.86, R^2 = 0.75, p value < 0.0001.

Table 7.2. Summary of statistical parameters for evaluating the predictive abilities of QSAR models A and B reported in this study.

		Model A		Model B	
Training set	**N**	32		32	
	R^2	**0.77**		**0.82**	
	F	31.1		31.4	
	SE	0.82		0.73	
	MAE (100 % data)	**0.55**		**0.50**	
	LOO Q^2	**0.68**		**0.73**	
Test set	**N**	18		18	
		with outlier	without outlier	with outlier	without outlier
	MAE (100% data)	0.683	**0.553**	0.635	**0.524**
	R^2	0.621	**0.793**	0.614	**0.741**
	R_0^2	0.597	0.792	0.590	0.734
	$R'_0{}^2$	0.552	0.763	0.543	0.705
	k	1.045	1.024	1.031	1.012
	k'	0.937	0.965	0.949	0.974
	$(R^2 - R'_0{}^2 / R^2)$	0.110	0.038	0.116	0.049
	$(R^2 - R_0^2 / R^2)$	0.038	0.002	0.040	0.009
	$\overline{R_m^2}$	0.503	0.716	0.50	0.649
	ΔR_m^2	0.009	0.050	0.01	0.046

7.4. Discussion

Computational toxicology is an active area of research and it has proven to be very useful during the initial design of compounds as drug candidates[492]. Recent changes in the European legislation regarding chemical risk assessment, particularly in the cosmetic sector, has shifted the attention towards *in silico* approaches for safety testing purposes, which have the potential to reduce the cost and time required for the development of new drugs, as well as *in vivo* experimentation[498]. For instance, techniques like QSAR, molecular docking and toxicophore models have been successfully used to predict cytotoxicity and specific organ toxicities[499-502]. Increasingly, these methods have become a key part of the adverse outcome pathway (AOP) approach, which emerged in an attempt to establish a mechanistic link between an upstream molecular initiating event (MIE) and a downstream adverse effect through a series of events[503-505]. Elucidation of the mechanistic information relating to a given MIE is of particular importance and allows identification of chemical characteristics of compounds that are responsible for interaction with a certain biological macromolecule and consequent progression of an AOP[492].

Despite their great predictive value to identify potential problematic chemicals, very few QSAR models for mitochondrial toxicity have been developed so far. As mentioned earlier in this chapter, this could be due to the lack of consistent experimental data, which is critical for the development of computational tools. It could also be due to the number of mechanisms by which toxicity can occur in mitochondria or that a single chemical might have the ability to induce several mechanisms of toxicity[494]. Nevertheless, relevance of mitochondria in cell metabolism, awareness of drug off-target mitochondrial effects, and the emerging link with several organ toxicities have increased interest in mitochondrial toxicity over the past few decades and there is now an increasing interest in the development of computational techniques[492]. As an example of the importance of mitochondrial toxicity, to date approximately 35% of more than 500 pharmaceutically relevant chemicals have been shown to impair mitochondrial function either by inhibition of the ETC and/or by uncoupling of OXPHOS[69].

Naven *et al.* developed one of the very few existing QSAR studies done on mitochondrial toxicity to date[281]. Their study aimed to identify structural and physicochemical features associated with an uncoupling activity of the OXPHOS by looking at the effects of over

2000 compounds in oxygen consumption using isolated rat liver mitochondria[281]. In their study, the authors outlined 11 "toxicophores" or "structural alerts" in a structural-alert model and were able to identify 68% of the chemicals in the data set with potent uncoupling activity[281]. Another study published by Nelms *et al.* developed structural alerts for mitochondrial toxicity analysing a set of chemical structures typically used in hair dye products[506]. The outcome of this study was 4 structural alerts related to both uncoupling and ETC inhibition[506]. In another study by Nelms *et al*., 288 drug-like chemicals published by Zhang *et al*.[507] were analysed, which allowed the identification of eight structural alerts related to several key mechanisms of mitochondrial toxicity[494]. Within all the structural alerts identified in those previous studies (22 in total), 14 were associated with protonophoric mechanisms, whereas only 6 alerts related to redox cycling and 2 alerts related to the inhibition of complexes I-IV[281, 492, 494, 506].

Therefore, given the clear need for additional structure-activity studies to define the chemical space for ETC inhibition, the availability of *in vitro* inhibition data on succinate-cytochrome *c* reductase was valuable for the development of the QSAR models presented in this chapter. Investigating the inhibition of these complexes is important for several reasons. First of all, a high number of compounds have been reported to target complex III (EC 1.10.2.2)[69]. Secondly, although the number of compounds reported to target complex II is significantly lower than the complex III inhibitors, complex II or succinate dehydrogenase (EC 1.3.5.1) is an enzyme with multiple unique characteristics and crucial roles, constituting an attractive research target[508]. For instance, it is the only ETC complex fully encoded by the nDNA, it doesn't pump protons across the IMM unlike other ETC complexes, it comprises only four subunits and, located on the matrix side of the IMM, it also constitutes a component of the Krebs cycle[22, 23]. Additionally, multiple roles beyond metabolism have been attributed to complex II, such as succinate signalling, ROS generation or ischemic preconditioning[508].

Here, prior to the development of QSAR models, a molecular docking study was performed on the ubiquinone site of both complex II and complex III. First, molecular docking of compounds into the Q_o site of the cytochrome bc_1 complex and subsequent PLIF analysis was performed to gain more insight into the nature of the ligand-protein interactions in that particular site. A considerable number of crystal structures for complex III from a wide range of organisms and resolutions are available on PDB[29, 34, 201, 509], however for this study a mammalian structure with high resolution (2.1 Å) and a

ligand bound to the Q_o site (used to define the binding site) was selected (PDB entry: 1PPJ)[201]. PLIF analysis highlighted the high participation in the ligand-protein interactions of a number of residues (Figure 7.4), with His 161 as H-bond acceptor and Pro 270 for arene interaction with an aromatic system in the compounds being key residues for inhibitor activity.

Next, this study also investigated the binding of compounds into the Q site of complex II. Despite the low sequence homology between the protein structures of E. *coli* and mammalian complex II (45%), molecular docking and PLIF analysis revealed a highly conserved ubiquinone binding site. This site was mainly formed of residues that belonged to the subunits B, C and D such as a tryptophan residue (porcine Trp B-173, E. *coli* Trp B-164), a tyrosine residue (porcine Tyr D-91, E. *coli* Tyr D-83), an arginine residue (porcine Arg C-46, E. *coli* Arg C-31) and an isoleucine residue (porcine Ile C-43, E. *coli* Arg C-28). Additionally, results revealed the participation of a water molecule (H_2O 138) and a methionine residue (Met C-39) in the binding pocket of the mammalian structure (Figure 7.7). Other computational studies in the literature have also highlighted the involvement of these residues in the binding of ubiquinone and complex II inhibitors used as fungicides[496, 510-512].

The success of any QSAR model depends on the accuracy of the input data. Therefore, it was important that all IC_{50} values were obtained under the same experimental conditions and, additionally, standard error for each data point was carefully verified. Consequently, all IC_{50} values, including those obtained from the literature, were obtained using mammalian mitochondria by monitoring the increase in absorbance of cytochrome *c* at 550 nm using sodium succinate as substrate. Then, to avoid model overfitting, all models kept a ratio of at least 10:1 between the number of compounds and the number of molecular descriptors.

The QSAR models generated in this research showed good correlation and prediction accuracy for the external test set compounds. The QSAR highlighted the importance of several physicochemical (*Log S, Neutral form pH=7.4*) and topological descriptors (*b_max1le* and *Number of rings size 6*). Accordingly, low aqueous solubility and low ionisation (low acidity or basicity) of compounds lead to more potent inhibitors. These may indicate the requirement for the inhibitors to be hydrophobic/non-polar enough so they can diffuse into the hydrophobic enzymes' binding sites. The topological parameters

indicate fewer 6-membered rings and shorter hydrocarbon alkane chains (but not alkene chains) are preferable for better inhibition of SCR. Interestingly, some of these features are present in phenothiazines, a structural alert identified by Nelms *et al.* for the inhibition of complexes I-IV[494].

QSAR models developed in this chapter were successful in internal and external validation, but QSAR model B showed the best statistical quality and predictive abilities (R^2 = 0.82, Q^2 = 0.73). External validation identified compound 8a as an outlier in both models, where a much lower pIC_{50} value (lower potency) was predicted for this compound every time. The fact that compound 8a came up as an outlier in the models could be explained by the high similarity in structure with compound 8k (with an IC_{50} value more than 200 times higher than that of 8a), where the only difference between the two compounds was the position of the carboxyl group in the phenylamino (3-COOH in 8a and 4-COOH in 8k). This structural difference is not contemplated in the models as the molecular descriptors were identical/very similar between the two compounds (i.e. number of 6-membered rings, length of single bonds, unionised fraction and solubility). In their study, Wang *et al.* found through X-ray diffraction analysis that hydrophobic groups on the phenylamino group (such as 4-Br, 4-Cl and 4-CH_3) were favourable for a deeper binding inside the Q_o pocket, whereas electron-withdrawing groups (4-COOH, 4-CN and 4-CF_3) were unfavourable[212]. Despite this, compound 8a showed a remarkably low IC_{50} value of 24 nM, probably due to diminished resonance electron withdrawing effect of COOH when in the meta position[212]. Molecular docking studies performed on complex III did not shed much light on this matter, as similar orientation and docking poses within the Q_o pocket for both compounds 8a and 8k were observed (data not shown), although the arene interaction with Pro 270 will be greatly reduced with COOH on position 4 (compound 8k) due to reduced electron distribution on the aromatic ring when compared with 3-COOH analogue (8a), which will have a stronger arene interaction.

In summary, the ability to predict toxicities *in silico* will become increasingly important to the long-term goal of replacing animal use. This study shows that it is possible to incorporate molecular docking and QSAR to achieve these local models for individual mechanisms like SCR inhibition. This also shows the importance of availability of more *in vitro* data for the developments of such models. As more functional screens are performed, computational techniques like QSAR and molecular docking can help us

identify chemical features associated with mitochondrial toxicity. In terms of future work, it is essential that we also consider the different mechanisms of mitochondrial toxicity, for instance, currently there are no structural alerts generated for chemicals that inhibit specific ETC substrates/transporters or those that inhibit mtDNA synthesis[492].

8. Final Discussion

Drug therapies provide beneficial effects by helping in the management of symptoms and even by driving many diseases into remission. However, in some cases, the success of a particular drug is limited due to adverse off-target effects or toxicity-induced effects[513]. Mitochondrial dysfunction plays a key role in the mechanisms whereby drugs can damage different tissues and organs, because mitochondria are mandatory for adequate energy output and the metabolism of several key endogenous substrates[514]. Hence, drug-induced mitochondrial toxicity (DIMT) represents an important phenomenon by which different drug classes can induce adverse effects leading to liver, muscle, kidney, heart and central nervous system injury.[515] In the most severe cases, DIMT can lead to death of the patient[516].

There is a need for increased preclinical testing for mitochondrial toxicity significantly earlier in the drug discovery process than is currently done. A number of drugs have made it to market (e.g. ciglitazone and troglitazone), only to discover that they are mitochondrial toxicants and needed to be withdrawn. This is of particular concern for the pharmaceutical industry, as safety-related clinical attrition associated with late-stage failures represents a big economic burden. Therefore, better understanding of the different mechanisms whereby drugs can impair mitochondrial function and development of reliable screening methods of DIMT prediction is imperative to better inform early decision making, reduce safety-related compound attrition, and ultimately improve the safety profile of medicines by preventing future cases of DIMT. In order to avoid late-stage failures, the industry has started to make considerable efforts to shift towards *in vitro* toxicology, particularly during the early stages of drug discovery[517]. This has been highly motivated by the observation that several off-target human organ toxicities are sometimes poorly predicted by conventional animal models[518].

Overall, the aim of this research project was two-fold: 1) to compare multiple *in vitro* assays to generate relevant information to aid the identification/elucidation and prediction of mechanisms of DIMT (particularly those affecting the mitochondrial ETC), and 2) to identify the structural and physicochemical features associated with ETC toxicity using two *in silico* approaches: QSAR and molecular docking studies.

Before looking into the more complicated mammalian mitochondrial toxicity, first the established methods at the University of Sussex were applied to the AOX enzyme, due to its relative structural simplicity that would allow better development of assays and laboratory skills. The AOX is a ubiquinol oxidoreductase present in the ETC of numerous pathogens, which makes it a desirable target for the development of novel antimicrobial agents. *In vitro* inhibition studies were carried on this enzyme, followed by QSAR and molecular docking studies. Development of these *in silico* methods was possible due to the availability of data obtained in our laboratory, as well as the literature data regarding inhibitory activities towards AOX activity of a series of compounds reported by Saimoto *et al.*[52].

Molecular docking studies revealed the importance of the residues Leu 122, Arg 118 and Thr 219 within the hydrophobic cavity of AOX for inhibitor binding. Two of those residues, Arg 118 and Thr 219, were key in establishing a strong interaction between the compounds and the enzyme by acting as hydrogen bond donors in interaction with the hydrogen binding acceptor groups on the meta position of the aromatic ring of the inhibitors. An example of these groups is the benzaldehyde group in ascofuranone structure. Furthermore, a similar conclusion was made from QSAR analysis, where a multiple linear regression model with a good prediction accuracy was obtained using pIC_{50} values of AOX inhibitors. The model highlighted the importance of the presence of hydrogen bond acceptor groups on the aromatic ring of compounds, acidity of compounds (ortho-phenolic groups), and a linear (non-bulky) shape of the compounds for the inhibitory potency of the AOX enzyme. Despite their great predictive value, no QSAR models on the AOX have been developed to date, hence the model obtained in this study could aid with the design of better and more specific AOX inhibitors. This is important because the AOX represents a promising target to address the threat posed by multiple human pathogenic organisms and numerous fungi of agronomic importance[53, 232]. Finally, the QSAR methodology developed for the AOX was successfully used in chapter 7 for investigations on the cytochrome bc_1 complex, which is another respiratory protein structurally more complex.

The multiple *in vitro* assays used in this research for drug-induced mitochondrial toxicity investigations incorporated two main model systems: isolated rat liver mitochondria and the human hepatoblastoma cell line HepG2. Therefore, it was important to develop

reproducible methods for obtaining good quality mitochondrial preparations that could be employed in the experiments, as well as to examine the validity of the methodology using control compounds. This objective was achieved as shown by the ADP/O and RCR ratios and congruous fluctuations observed in the OCR, ROS and MMP measurements using high-resolution respirometry upon addition of various mitochondrial stressors to the media. Subsequently, this methodology was successfully employed in chapter 5 and chapter 6 (section 6.3.2.4) in the study of the effects of a number of pharmaceutical drugs on mitochondrial function.

Rat liver isolated mitochondria were used in enzymatic assays to assess the inhibitory activities of several well-known complex III and AOX inhibitors against succinate-cytochrome *c* reductase (SCR), a mixture of respiratory complex II and III. This assay allowed the generation of a consistent set of experimental results in the form of pIC_{50} values, which, along with SCR pIC_{50} values obtained for other pharmaceutical drugs (chapters 5 and 6), were used for the QSAR studies performed in chapter 7. In addition, the results of this investigation on AOX inhibitors were particularly valuable, since these compounds, synthesised in-house as chemotherapeutic agents against trypanasomiasis, lacked mitochondrial toxicity data required as part of drug-safety investigations. This information is of great value in order to avoid mammalian toxicities through complex III inhibition, given the resemblance of complex III and AOX in terms of the use of the same substrate (ubiquinol). These AOX inhibitors are quinol mimetics (i.e. they all have a hexa-substituted head group with an isoprene tail) and consequently could potentially inhibit complex III as an off-target effect. Results suggested that colletochlorin D and compounds ISSF33 may be the most promising candidates for the treatment of human pathogens, as they show the lowest inhibitory potency against the mammalian cytochrome bc_1 complex.

Furthermore, the SCR inhibition data was compared with results obtained from other tests and assays of mitochondrial function, including mitochondrial respiration assays from acute injection of compounds on both intact and permeabilised HepG2 cells. IC_{50} values obtained in HepG2 cells, both permeabilised and intact, were significantly higher than those obtained in isolated mitochondria, which could be attributed to the nature of the endpoint measured in each of the experiments (i.e. enzyme inhibition vs. the oxygen consumption rate), but also to the fact that the absence of a cell membrane in isolated

mitochondria may give compounds a more unrestricted access to the ETC. When comparing the methods, it was also noted that OCR IC_{50} values obtained in both acute and permeabilised cells were comparable, which indicates that both assays may be complementary and may be used together for a better assessment of mitochondrial dysfunction and elucidation of mechanisms of action.

Drug-induced mitochondrial dysfunction can result from different drug types through a variety of mechanisms (see Introduction section 1.4), but this research has focused on mechanisms involving binding of drugs to specific mitochondrial targets located in the ETC, i.e. direct inhibition or uncoupling of the ETC. ETC inhibition is an issue that deserves special attention because of the variety of drugs that can cause it, and its impact on mitochondrial function. ETC inhibition can lead to ATP depletion, ROS overproduction and secondary impairment of other key processes such as mitochondrial β-oxidation and the TCA cycle[519, 520]. Mitochondrial dysfunction can eventually lead to microvesicular steatosis (which involves the accumulation of small intracytoplasmic fat vacuoles), hypoglycemia, and, in some tissues, such as lung and liver, ROS overproduction and oxidative stress can trigger inflammation processes that can cause damage, coma and death[519, 520].

Investigating the different toxicological mechanisms of a drug can be a challenging task, but it is of paramount importance. As mentioned before, in many cases long-term pharmacological treatment is essential for the patients' well-being, therefore, using the medication with the best safety profile is an important issue for public health. Avoiding the usage of medications with mitochondrial liabilities, especially in patients with an already compromised mitochondrial function, is critical in both short and long term therapies, as otherwise it could lead to fatalities as described in several case reports[461-465].

In chapter 5 and 6, Acute Extracellular Flux Assays (AEFA) using intact HepG2 cells were carried out, and changes in respiration parameters as a result of the injection of various concentrations of compounds were recorded. This test could identify the concentration-dependent effect of compounds on bioenergetic parameters such as OCR, reserve capacity, ECAR, proton leak and ATP production. When these effects were statistically significant, 50% effective concentrations (AC_{50}) were determined. Also, in these two chapters, permeabilised HepG2 cells along with various substrates/inhibitors were used to assess the real-time effects of compounds on mitochondrial respiration and

evaluate the respiration mechanisms that are most susceptible to the drugs. Additionally, DIMT was assessed in HepG2 cells cultured in galactose or glucose containing media (Glu/Gal assay), an *in vitro* assay developed to increase the detection of deleterious mitochondrial effects of drugs that are often missed using glycolytic cells.

Chapter 5 focused on the effects on mitochondrial function of some antidiabetic, antihyperlipidemic and anti-inflammatory drugs, as well as a selection of drugs ranked as "essential medicines" by the WHO[247]. Here, the effects of a total of 16 pharmaceutical drugs on mitochondrial function were investigated in detail using different cell-based *in vitro* assays, rat liver isolated mitochondria and molecular docking. Of the 16 compounds tested in the AEFA using intact HepG2 cells, 10 were identified as potential mitochondrial toxicants; of those, ciglitazone, lovastatin, rosiglitazone and troglitazone were classified as ETC inhibitors, while acetaminophen was identified as a substrate inhibitor (Table 5.2). The remaining five compounds (bezafibrate, pioglitazone, salicylic acid and warfarin) were causing their mitochondrial effect through "other" mechanisms that could not be confirmed using this assay system and the strict definitions used for ETC inhibitors/uncouplers. Experiments performed using permeabilised cells identified pyruvate respiration as the most sensitive mechanism in most of the cases. This means that complex I-linked respiration may be the primary target of the drugs identified as ETC inhibitors. The Glu/Gal assay was also employed in the study of DIMT; however, this test could not identify many compounds as mitochondrial toxicants, which could be due to the low sensitivity of this assay. Although the Glu/Gal assay has been suggested to have a high specificity of almost 100% (meaning that a positive response will almost always be a true positive), its sensitivity has been shown to be low, which means it will often report false negatives[136]. There are at least two explanations for this, one being cytotoxicity of compounds and another being reduction of availability of highly protein-bound compounds due to the presence of FCS in the growth media.

Studies performed using isolated mitochondria revealed that, in some cases, pharmaceutical drugs can have multiple mechanisms of activity by acting both as respiration inhibitors (sometimes affecting multiple ETC targets) and uncouplers, which can be dependent on the drug concentration and the mitochondrial state. Examples of drugs that displayed this dual behaviour include ciglitazone, troglitazone, lovastatin, salicylic acid and warfarin. Finally, *in silico* studies such as molecular docking, reported better scores (i.e. higher binding affinities) for those compounds that showed

mitochondrial toxicity in the AEFA, which highlights the importance of *in vitro* testing. Finally, experimental results obtained for all 16 drugs were compared with available information in the literature regarding reported possible mechanisms, including those from *in vitro*, *in vivo* or clinical studies. In some cases the effects reported in the literature varied greatly depending on the model system of choice, incubation time or drug concentration, which confirms the challenges in fully understanding the off-target effects of drugs and suggests that analysis of toxicity should integrate different approaches to provide a better understanding of the underlying mechanisms.

Chapter 6 presents studies pertaining to the effects on mitochondrial function of 22 psychotropic drugs belonging to different drug classes (10 antipsychotics, 7 anticonvulsants, 3 antidepressants and 2 anxiolytic drugs) with the AEFA using both intact and permeabilised cells, the Glu/Gal assay and molecular docking. Furthermore, the typical antipsychotics (APs) chlorpromazine and haloperidol and the atypical antipsychotic olanzapine were investigated more in depth using freshly isolated rat liver mitochondria and high-resolution respirometry (Oroboros® Oxygraph-2K).

Since their emergence in the 1950s, APs have been used in the treatment of schizophrenia and mood disorders, but several adverse effects have been associated to their use, including metabolic disturbances and extrapyramidal symptoms[367]. Of the 10 APs that were tested in the AEFA using intact HepG2 cells, aripiprazole was identified as an ETC inhibitor, reserpine was identified as an uncoupler and quetiapine was identified as a substrate inhibitor (Table 6.2). Then, the AEFA using permeabilised HepG2 cells did not show an effect by reserpine or aripiprazole, but indicated that quetiapine may act as a complex I inhibitor or an inhibitor of substrates linked to complex I respiration (IC_{50} > 150 µM) (Figure 6.4). In regard to this, other studies have reported direct inhibition of complex I activity by quetiapine through enzymatic assays, so it remains unclear whether quetiapine inhibits complex I directly or instead it hampers the oxidation of complex I substrates[404, 521]. The reason for classification of this drug as substrate inhibitor, and not ETC inhibitor, was a lack of statistically significant ECAR increase in HepG2 cells.

The incubated extracellular flux assay (1 h incubation, intact HepG2 cells) further explored the toxicities of three AP compounds: haloperidol, chlorpromazine and olanzapine. The typical AP haloperidol behaved as an ETC inhibitor (IC_{50} > 50 µM), while chlorpromazine behaved as a cytotoxic compound (Figure 6.6). In addition, the

atypical AP olanzapine decreased ECAR (IC_{50} > 50 µM), a possible indication of decreased glycolysis, which must be confirmed through techniques that directly monitor glycolysis, such as tests that quantify glucose and lactate levels within cell culture media[522]. If this is confirmed, it would be in agreement with side effects reported by long term use of olanzapine, which include hyperglycaemia and weight gain[422].

With regards to these three APs, additional experiments using freshly isolated rat liver mitochondria on succinate respiration and the Oroboros® Oxygraph-2K revealed that haloperidol decreased complex II-linked basal respiration, while olanzapine showed no effects on respiration in this system and chlorpromazine had a mitochondrial-state dependent effect (Figure 6.9). Although haloperidol has been classically considered a complex I inhibitor, these results indicate that it may also target other ETC complexes. On the other hand, chlorpromazine behaved as an uncoupler in basal respiration, while it inhibited uncoupled respiration (CCCP stimulated) with an IC_{50} = 135 ± 5 µM (Figure 6.9 and Figure 6.10). Although chlorpromazine has an effect on mitochondrial respiration in isolated mitochondria, cell assays suggest that it may have a number of other off-mitochondrial effects, which ultimately kill the cells at lower concentrations, making it a cytotoxic compound as seen in Figure 6.13. In fact, from these results and the dose-response curves of cell viability (Figure 6.11), it can be concluded that chlorpromazine most likely poses a higher toxicity risk than haloperidol and olanzapine.

There is a large body of evidence in the literature proving that mitochondria are a common off-target of several anticonvulsant drugs (ACs), particularly valproic acid[405]. However, information regarding the detailed mechanisms of toxicity of these drugs is scarce and sometimes contradictory. In this research the effects of 7 ACs on mitochondrial function were investigated to evaluate toxicological risks posed by some members of this drug class. Of the 7 compounds tested with AEFA using intact cells, phenytoin was identified as an ETC inhibitor, carbamazepine was identified as a substrate inhibitor and valproic acid was identified as a cytotoxic compound (Table 6.6). Valproic acid also showed an effect on complex I-linked respiration in acute treatment of permeabilised cells, while the ETC inhibitor phenytoin did not show a statistically significant effect (Figure 6.17) .

Of the 3 antidepressants (citalopram, fluoxetine and tianeptine) and the 2 anxiolytic drugs (buspirone and lorazepam) studied here, the AEFA assay using intact cells revealed that fluoxetine acts as an ETC inhibitor, both buspirone and tianeptine act as substrate inhibitors, while the mechanisms of lorazepam were inconclusive (Table 6.10). Then, acute injection of compounds to permeabilised cells revealed inhibition of complex I-linked respiration was the most sensitive mechanisms for both buspirone and fluoxetine (MEC = 44.5 μM and 72.1 μM, respectively) (Figure 6.22).

Finally, chapter 7 focused on the development of *in silico* methods such as molecular docking and QSAR studies for the prediction of SCR inhibition. As already outlined throughout the thesis, these predictive computer-assisted tools are of great value to potentially reduce the number of animal studies needed for the identification of potentially toxic compounds, something that is particularly useful in light of the most recent regulations[491]. *In silico* models use computer technology to connect and integrate existing experimental data and can be used to assess thousands of chemicals, however in practice there are still several limitations to their use. Lack of consistent experimental data for developing new models for particular endpoints is one of the most significant limitations for *in silico* studies[523].

In vitro assays performed in this thesis allowed the generation of sufficient experimental data for QSAR studies. The QSAR used the IC_{50} values obtained in the SCR assays (complex II+III inhibition) as the response variable. QSAR models for inhibition of the ETC are practically non-existent in the scientific literature to the best of my knowledge, while more information regarding structural and physicochemical features associated with inhibition of the mitochondrial ETC could be achieved using QSAR studies. The Q_o site of complex III in particular has been reported in the literature to be a common off-target of several pharmaceutical drugs that are currently in the market[192]. Therefore, a detailed understanding of the protein-ligand interactions could facilitate the design of drugs with low affinity for the Q_o site of complex III. To investigate such interactions, molecular docking studies were performed on the Q_o site of complex III, which revealed that the residues His 161 and Pro 270 in the bovine cytochrome bc_1 complex are key for inhibitors' activity. Although residue Glu 271 showed a high frequency of occurrence overall, it did not show a high frequency in active compounds, suggesting that Glu 271 contributes to the binding of inactive compounds.

QSAR analysis using stepwise regression analysis resulted in multiple regression equations with good prediction accuracy. The QSAR highlighted the impact of certain physicochemical and topological features on inhibitory potency of compounds. These were the impact of acid/base dissociation and polarity of compounds (as indicated by aqueous solubilty) in reducing the complex II+III inhibition, as well as topological properties of large number of 6-membered rings and longer hydrocarbon alkane chains (but not alkene chains) that also reduce inhibition of SCR. These properties may be considered early stages of discovery and design of new drugs to reduce the incidence of ETC inhibition by new drug candidates.

This research has demonstrated the challenges associated with trying to understand why and how DIMT occurs. It also highlights complexities of the design of high-throughput *in vitro* screening methods for the estimation of DIMT with a reasonable accuracy. Parameters such as permeabilised vs intact cells, acute treatment vs incubation, and the length of incubation, mitochondrial substrates and mitochondrial state are of paramount importance when trying to capture any drug toxicities that may be relevant to clinical situations. Nevertheless, incorporation of *in silico* methods can add to the body of evidence when trying to make decisions on the likelihood of mitochondrial toxicity of compounds. Therefore, it is imperative to obtain complete understanding of protein-ligand interactions to improve the safety of pharmaceutical drugs and treatment success. To achieve this, a true picture of drug interactions and toxic effects will only be obtained through the combination of multiple approaches (*in vitro*, *in vivo* and *in silico*), different model systems and measurement of multiple mitochondrial endpoints. This is a growing area with high potential to affect the healthcare system, which could lead to personalised medicine in the future. Personalised medicine would involve understanding that there is great patient-to-patient variation due to factors such as age, gender, pre-existing conditions, co-medications, state of the immune system and genetic variants that may play crucial roles in determining susceptibility to DIMT. For instance, mitochondrial quality and function declines with age and certain mtDNA haplogroups (distinct patterns in single-nucleotide polymorphisms) are associated with increased individual susceptibility to DIMT[524-527]. In those cases, prescription of certain pharmaceutical drugs with known mitochondrial liabilities should be avoided and alternative safer options should be considered.

With respect to exploring the positive opportunities of off-target effects of pharmaceutical drugs, there is an emerging research showing that such drugs can be repurposed as research tools or in the clinic to treat cancer[528-530], neurodegenerative disorders or to clear chronic viral infections by upregulating the immune system[513]. For instance, recent research is exploring the use of drugs that inhibit mitochondrial OXPHOS in clinical trials across a wide range of tumour types[531-533] and also exploring the idea of manipulating mtROS production to drive an increased immune response through both innate immune signalling and increased release of mtDNA for pattern recognition receptors (PRR) stimulation[534-536]. Undoubtedly, advancements in this direction will require detailed understanding of the mechanisms of action of the drugs in question, hence, there is still considerable work to be done in this field.

8.1. Future Work

The objectives established at the start of this research project have been achieved through determination of the mechanisms of DIMT of some clinically used pharmaceutical drugs of a diverse group of pharmacological classes. However, there is still substantial work to be done in this field. For instance, unravelling the detailed biochemical pathways and metabolic effects of the drugs that showed mitochondrial impairment will require further investigations.

Additionally, this research has focused on just a number of drug classes, however, there are many other drug classes in the market that have not been evaluated with respect to mitochondrial toxicity, especially those reported to cause DILI, such as the antivirals like the nucleoside/nucleotide reverse transcriptase inhibitors (NRTIs), antibiotics and anesthetics[537, 538].

Pharmaceutical drugs are not the only compounds that should be subjected to mitochondrial injury studies; many common environmental pollutants, cosmetics and hygienic products are also recognised as potential mitochondrial toxicants and, as such, deserve to be fully investigated. Suspected environmental chemicals that act as mitochondrial toxicants include polycyclic aromatic hydrocarbons and organohalogens[539]. Moreover, a number of naturally occurring compounds such as the anthocyanins, isothiocyanates and polyphenols, have been reported to cause alterations in mitochondrial function[540, 541], in some cases acting as mitochondrial protectors or even antiaging compounds, but further studies need to be done to completely unravel

mechanisms of action. With regards to this, during this research project investigations have been initiated to address the effects of resveratrol and some resveratrol derivatives synthesised by our external collaborators from the University of Brighton Dr Lizzy Ostler and Prof Richard Faragher, in conjunction with our collaborators at Cyprotex. Preliminary studies have shown that these compounds ought to be investigated further and this will be done in the future.

Finally, future work needs to be done to obtain more experimental data for the development of new QSAR models. Ideally, experimental data should be obtained through high-throughput screening (HTS), which has the potential of screening large compound libraries for activity against different biological targets via the use of large-scale data analysis. New QSAR models of mitochondrial toxicity may focus on different mechanisms of mitochondrial toxicity, such as inhibition of mtDNA replication, transcription and translation, inhibition of the transport or oxidation of substrates or opening of the MPTP.

References

1. Ernster, L. and G. Schatz, *Mitochondria: A historical review.* The Journal of Cell Biology, 1981. **91**(3): p. 227-255.
2. Lazarow, A. and S.J. Cooperstein, *Studies on the enzymatic basis for the janus green b staining reaction.* Journal of Histochemistry & Cytochemistry, 1953. **1**(4): p. 234-241.
3. Palade, G.E., *The fine structure of mitochondria.* The Anatomical Record, 1952. **114**(3): p. 427-451.
4. Mitchell, P., *Chemiosmotic coupling in oxidative and photosynthetic phosphorylation.* Biological Reviews, 1966. **41**(3): p. 445-501.
5. Berman, S.B., F.J. Pineda, and J.M. Hardwick, *Mitochondrial fission and fusion dynamics: The long and short of it.* Cell Death Differ, 2008. **15**(7): p. 1147-52.
6. McCarron, J.G., et al., *From structure to function: Mitochondrial morphology, motion and shaping in vascular smooth muscle.* Journal of vascular research, 2013. **50**(5): p. 357-371.
7. Kühlbrandt, W., *Structure and function of mitochondrial membrane protein complexes.* BMC biology, 2015. **13**: p. 89-89.
8. Giles, R.E., et al., *Maternal inheritance of human mitochondrial DNA.* Proc Natl Acad Sci USA, 1980. **77**(11): p. 6715-9.
9. Chinnery, P.F. and G. Hudson, *Mitochondrial genetics.* British Medical Bulletin, 2013. **106**(1): p. 135-159.
10. Wei, Y.H., *Oxidative stress and mitochondrial DNA mutations in human aging.* Proc Soc Exp Biol Med, 1998. **217**(1): p. 53-63.
11. Brandon, M., P. Baldi, and D.C. Wallace, *Mitochondrial mutations in cancer.* Oncogene, 2006. **25**: p. 4647.
12. Hegde, M.L., et al., *Oxidative genome damage and its repair: Implications in aging and neurodegenerative diseases.* Mechanisms of Ageing and Development, 2012. **133**(4): p. 157-168.
13. Wallace, D.C., et al., *Mitochondrial DNA mutation associated with leber's hereditary optic neuropathy.* Science, 1988. **242**(4884): p. 1427-30.
14. Pavlakis, S.G., et al., *Mitochondrial myopathy, encephalopathy, lactic acidosis, and strokelike episodes: A distinctive clinical syndrome.* Ann Neurol, 1984. **16**(4): p. 481-8.
15. Shoffner, J.M., et al., *Myoclonic epilepsy and ragged-red fiber disease (merrf) is associated with a mitochondrial DNA trna(lys) mutation.* Cell, 1990. **61**(6): p. 931-7.
16. Zeviani, M., et al., *Deletions of mitochondrial DNA in kearns-sayre syndrome.* Neurology, 1988. **38**(9): p. 1339-46.
17. Rotig, A., et al., *Pearson's marrow-pancreas syndrome. A multisystem mitochondrial disorder in infancy.* J Clin Invest, 1990. **86**(5): p. 1601-8.
18. Ott, M., et al., *Mitochondria, oxidative stress and cell death.* Apoptosis, 2007. **12**(5): p. 913-922.
19. Rich, P.R. and A. Marechal, *The mitochondrial respiratory chain.* Essays Biochem, 2010. **47**: p. 1-23.
20. Vakifahmetoglu-Norberg, H., A.T. Ouchida, and E. Norberg, *The role of mitochondria in metabolism and cell death.* Biochem Biophys Res Commun, 2017. **482**(3): p. 426-431.
21. Berg JM, T.J., Stryer L., *The regulation of cellular respiration is governed primarily by the need for atp,* in *Biochemistry*, N.Y.W.H. Freeman, Editor. 2002.
22. Sun, F., et al., *Crystal structure of mitochondrial respiratory membrane protein complex ii.* Cell, 2005. **121**(7): p. 1043-57.
23. Hägerhäll, C., *Succinate: Quinone oxidoreductases: Variations on a conserved theme.* Biochimica et Biophysica Acta (BBA) - Bioenergetics, 1997. **1320**(2): p. 107-141.
24. Nicholls, D.G. and S.J. Ferguson, *4 - the chemiosmotic proton circuit,* in *Bioenergetics (third edition)*, D.G. Nicholls and S.J. Ferguson, Editors. 2003, Academic Press: London. p. 57-88.
25. Hatefi, Y., A.G. Haavik, and D.E. Griffiths, *Studies on the electron transfer system. Xli. Reduced coenzyme q (qh2)-cytochrome c reductase.* J Biol Chem, 1962. **237**: p. 1681-5.

26. Xia, D., et al., *Crystal structure of the cytochrome bc_1 complex from bovine heart mitochondria.* Science, 1997. **277**(5322): p. 60.
27. Guo, R., et al., *Architecture of human mitochondrial respiratory megacomplex i2iii2iv2.* Cell, 2017. **170**(6): p. 1247-1257.e12.
28. Yu, C.-A., et al., *Structural basis of functions of the mitochondrial cytochrome bc1 complex.* Biochimica et Biophysica Acta (BBA) - Bioenergetics, 1998. **1365**(1): p. 151-158.
29. Esser, L., et al., *Crystallographic studies of quinol oxidation site inhibitors: A modified classification of inhibitors for the cytochrome bc(1) complex.* J Mol Biol, 2004. **341**(1): p. 281-302.
30. Mitchell, P., *Possible molecular mechanisms of the protonmotive function of cytochrome systems.* Journal of Theoretical Biology, 1976. **62**(2): p. 327-367.
31. Xia, D., et al., *Structural analysis of cytochrome bc1 complexes: Implications to the mechanism of function.* Biochim Biophys Acta, 2013. **1827**(11-12): p. 1278-94.
32. Crofts, A.R., et al., *The q-cycle reviewed: How well does a monomeric mechanism of the bc1 complex account for the function of a dimeric complex?* Biochimica et Biophysica Acta (BBA) - Bioenergetics, 2008. **1777**(7): p. 1001-1019.
33. Li, H., et al., *Comparative kinetics of qi site inhibitors of cytochrome bc1 complex: Picomolar antimycin and micromolar cyazofamid.* Chem Biol Drug Des, 2014. **83**(1): p. 71-80.
34. Berry, E.A., et al., *Ascochlorin is a novel, specific inhibitor of the mitochondrial cytochrome bc1 complex.* Biochim Biophys Acta, 2010. **1797**(3): p. 360-70.
35. Moore, A.L. and M.S. Albury, *Further insights into the structure of the alternative oxidase: From plants to parasites.* Biochem Soc Trans, 2008. **36**(Pt 5): p. 1022-6.
36. Moore, A.L., et al., *Unraveling the heater: New insights into the structure of the alternative oxidase.* Annual Review of Plant Biology, 2013. **64**(1): p. 637-663.
37. Martin E. Andersson, P.N., *A revised model of the active site of alternative oxidase.* FEBS Lett, 1999. **449**(1): p. 17-22.
38. McDonald, A., *Alternative oxidase: An inter-kingdom perspective on the function and regulation of this broadly distributed 'cyanide-resistant' terminal oxidase*. Vol. 35. 2008.
39. McDonald, A.E. and G.C. Vanlerberghe, *Origins, evolutionary history, and taxonomic distribution of alternative oxidase and plastoquinol terminal oxidase.* Comp Biochem Physiol Part D Genomics Proteomics, 2006. **1**(3): p. 357-64.
40. Zhu, Y., et al., *Regulation of thermogenesis in plants: The interaction of alternative oxidase and plant uncoupling mitochondrial protein.* J Integr Plant Biol, 2011. **53**(1): p. 7-13.
41. Tsaousis, A.D., et al., *The human gut colonizer blastocystis respires using complex ii and alternative oxidase to buffer transient oxygen fluctuations in the gut.* Frontiers in cellular and infection microbiology, 2018. **8**: p. 371-371.
42. Martins, V.P., et al., *Involvement of an alternative oxidase in oxidative stress and mycelium-to-yeast differentiation in paracoccidioides brasiliensis.* Eukaryot Cell, 2011. **10**(2): p. 237-48.
43. Yan, L., et al., *The alternative oxidase of candida albicans causes reduced fluconazole susceptibility*. J Antimicrob Chemother, 2009. **64**(4): p. 764-73.
44. Suzuki, T., et al., *Direct evidence for cyanide-insensitive quinol oxidase (alternative oxidase) in apicomplexan parasite cryptosporidium parvum: Phylogenetic and therapeutic implications.* Biochem Biophys Res Commun, 2004. **313**(4): p. 1044-52.
45. Hunter, P.R. and G. Nichols, *Epidemiology and clinical features of cryptosporidium infection in immunocompromised patients.* Clinical Microbiology Reviews, 2002. **15**(1): p. 145.
46. Ebiloma, G.U., et al., *Alternative oxidase inhibitors: Mitochondrion-targeting as a strategy for new drugs against pathogenic parasites and fungi.* Medicinal Research Reviews, 2019. **39**(5): p. 1553-1602.
47. WHO. *Trypanosomiasis, human african (sleeping sickness)*. 2016; Available from: https://www.who.int/trypanosomiasis_african/en/.

48. Menzies, S.K., et al., *The trypanosome alternative oxidase: A potential drug target?* Parasitology, 2016. **145**(2): p. 175-183.
49. Nihei, C., Y. Fukai, and K. Kita, *Trypanosome alternative oxidase as a target of chemotherapy.* Biochimica et Biophysica Acta (BBA) - Molecular Basis of Disease, 2002. **1587**(2): p. 234-239.
50. Balogun, E.O., et al., *Discovery of trypanocidal coumarins with dual inhibition of both the glycerol kinase and alternative oxidase of trypanosoma brucei brucei.* Faseb j, 2019: p. fj201901342R.
51. Shiba, T., et al., *Structure of the trypanosome cyanide-insensitive alternative oxidase.* Proc Natl Acad Sci U S A, 2013. **110**(12): p. 4580-5.
52. Saimoto, H., et al., *Pharmacophore identification of ascofuranone, potent inhibitor of cyanide-insensitive alternative oxidase of trypanosoma brucei.* J Biochem, 2013. **153**(3): p. 267-73.
53. May, B., L. Young, and A.L. Moore, *Structural insights into the alternative oxidases: Are all oxidases made equal?* Biochem Soc Trans, 2017. **45**(3): p. 731-740.
54. Chappell, J.B. and G.D. Greville, *Effects of oligomycin on respiration and swelling of isolated liver mitochondria.* Nature, 1961. **190**(4775): p. 502-504.
55. Katyare, S.S., P. Fatterpaker, and A. Sreenivasan, *Effect of 2, 4-dinitrophenol (dnp) on oxidative phosphorylation in rat liver mitochondria.* Arch Biochem Biophys, 1971. **144**(1): p. 209-15.
56. Villa, T., L. Andri, and F. Brasca, *Enzymatic research at the mitochondrial level in experimental carbon monoxide poisoning. Behavior of the cytochrome oxidases, aldolases and glutamic-oxalacetic and glutamic-pyruvic transaminases in the hepatic and renal mitochondria.* Folia Med (Napoli), 1961. **44**: p. 486-95.
57. Dykens, J.A. and Y. Will, *The significance of mitochondrial toxicity testing in drug development.* Drug Discov Today, 2007. **12**(17-18): p. 777-85.
58. Marroquin, L.D., et al., *Circumventing the crabtree effect: Replacing media glucose with galactose increases susceptibility of hepg2 cells to mitochondrial toxicants.* Toxicological Sciences, 2007. **97**(2): p. 539-547.
59. Dykens, J.A., L.D. Marroquin, and Y. Will, *Strategies to reduce late-stage drug attrition due to mitochondrial toxicity.* Expert Rev Mol Diagn, 2007. **7**(2): p. 161-75.
60. Dykens, J.A., et al., *In vitro assessment of mitochondrial dysfunction and cytotoxicity of nefazodone, trazodone, and buspirone.* Toxicological Sciences, 2008. **103**(2): p. 335-345.
61. Pereira, C.V., et al., *Investigating drug-induced mitochondrial toxicity: A biosensor to increase drug safety?* Curr Drug Saf, 2009. **4**(1): p. 34-54.
62. FDA. *The drug development process*. 2018; Available from: https://www.fda.gov/forpatients/approvals/drugs/
63. Koczor, C.A. and W. Lewis, *Nucleoside reverse transcriptase inhibitor toxicity and mitochondrial DNA.* Expert Opin Drug Metab Toxicol, 2010. **6**(12): p. 1493-504.
64. Arnaudo, E., et al., *Depletion of muscle mitochondrial DNA in aids patients with zidovudine-induced myopathy.* The Lancet, 1991. **337**(8740): p. 508-510.
65. Joly, V., et al., *Increased risk of lipoatrophy under stavudine in hiv-1-infected patients: Results of a substudy from a comparative trial.* AIDS, 2002. **16**(18).
66. Gerber, N., et al., *Reye-like syndrome associated with valproic acid therapy.* The Journal of Pediatrics, 1979. **95**(1): p. 142-144.
67. Draye, J.P. and J. Vamecq, *The inhibition by valproic acid of the mitochondrial oxidation of monocarboxylic and omega-hydroxymonocarboxylic acids: Possible implications for the metabolism of gamma-aminobutyric acid.* J Biochem, 1987. **102**(1): p. 235-42.
68. Begriche, K., et al., *Drug-induced toxicity on mitochondria and lipid metabolism: Mechanistic diversity and deleterious consequences for the liver.* J Hepatol, 2011. **54**(4): p. 773-94.
69. Dykens, J.A. and Y. Will, *Drug-induced mitochondrial dysfunction*. 2008: John Wiley & Sons, Inc. 1-616.

70. McStay, G.P., *Contributions of plasma protein binding and membrane transporters to drug-induced mitochondrial toxicity,* in *Mitochondrial dysfunction caused by drugs and environmental toxicants*. 2018. p. 1-14.
71. Smith, R., *Mitochondria-targeted small molecule therapeutics and probes.* Antioxidants & Redox Signaling, 2011. **15**(12): p. 3021-3038.
72. Wallace, K.B., *Mitochondrial off targets of drug therapy.* Trends Pharmacol Sci, 2008. **29**(7): p. 361-6.
73. Borgne-Sanchez, A., *Mitochondrial dysfunction in drug-induced liver injury,* in *Mitochondrial dysfunction caused by drugs and environmental toxicants*. 2018. p. 47-72.
74. Ulrich, R.G., *Idiosyncratic toxicity: A convergence of risk factors.* Annual Review of Medicine, 2007. **58**(1): p. 17-34.
75. Simoes, R., *In vitro methodologies to investigate drug-induced toxicities*, in *Mitochondrial dysfunction caused by drugs and environmental toxicants*. 2018. p. 229-247.
76. Wallace, K.B. and A.A. Starkov, *Mitochondrial targets of drug toxicity.* Annual Review of Pharmacology and Toxicology, 2000. **40**(1): p. 353-388.
77. Goncharov, N., R. O Jenkins, and A. S Radilov, *Toxicology of fluoroacetate: A review, with possible directions for therapy research*. Vol. 26. 2006. 148-61.
78. Degli Esposti, M., *Inhibitors of nadh–ubiquinone reductase: An overview.* Biochimica et Biophysica Acta (BBA) - Bioenergetics, 1998. **1364**(2): p. 222-235.
79. Miyoshi, H., *Structure–activity relationships of some complex i inhibitors.* Biochimica et Biophysica Acta (BBA) - Bioenergetics, 1998. **1364**(2): p. 236-244.
80. Caterina, M.J. and D. Julius, *The vanilloid receptor: A molecular gateway to the pain pathway.* Annu Rev Neurosci, 2001. **24**: p. 487-517.
81. Burkhardt, C., et al., *Neuroleptic medications inhibit complex i of the electron transport chain.* Ann Neurol, 1993. **33**(5): p. 512-7.
82. Sztark, F., et al., *Absence of stereospecific effects of bupivacaine isomers on heart mitochondrial bioenergetics.* Anesthesiology, 2000. **93**(2): p. 456-62.
83. Johnson, M.E., et al., *Mitochondrial injury and caspase activation by the local anesthetic lidocaine.* Anesthesiology, 2004. **101**(5): p. 1184-94.
84. Hanley, P.J., et al., *Halothane, isoflurane and sevoflurane inhibit nadh:Ubiquinone oxidoreductase (complex i) of cardiac mitochondria.* J Physiol, 2002. **544**(3): p. 687-93.
85. Nadanaciva, S., et al., *Mitochondrial impairment by ppar agonists and statins identified via immunocaptured oxphos complex activities and respiration.* Toxicol Appl Pharmacol, 2007. **223**(3): p. 277-87.
86. Wojtczak, L., A.B. Wojtczak, and L. Ernster, *The inhibition of succinate dehydrogenase by oxaloacetate.* Biochimica et Biophysica Acta (BBA) - Enzymology, 1969. **191**(1): p. 10-21.
87. Rodriguez, R.J. and D. Acosta, Jr., *Inhibition of mitochondrial function in isolated rate liver mitochondria by azole antifungals.* J Biochem Toxicol, 1996. **11**(3): p. 127-31.
88. Miyadera, H., et al., *Atpenins, potent and specific inhibitors of mitochondrial complex ii (succinate-ubiquinone oxidoreductase).* Proc Natl Acad Sci U S A, 2003. **100**(2): p. 473-7.
89. von Jagow, G. and T.A. Link, *Use of specific inhibitors on the mitochondrial bc1 complex.* Methods Enzymol, 1986. **126**: p. 253-71.
90. Ramsay, R.R., M.S. Rashed, and S.D. Nelson, *In vitro effects of acetaminophen metabolites and analogs on the respiration of mouse liver mitochondria.* Archives of Biochemistry and Biophysics, 1989. **273**(2): p. 449-457.
91. Ludwig, L.M., et al., *Preconditioning by isoflurane is mediated by reactive oxygen species generated from mitochondrial electron transport chain complex iii.* Anesth Analg, 2004. **99**(5): p. 1308-15; table of contents.
92. Riess, M.L., et al., *Anesthetic preconditioning: The role of free radicals in sevoflurane-induced attenuation of mitochondrial electron transport in guinea pig isolated hearts.* Anesth Analg, 2005. **100**(1): p. 46-53.

93. Erecińska, M. and D.F. Wilson, *Inhibitors of cytochrome c oxidase.* Pharmacology & Therapeutics, 1980. **8**(1): p. 1-20.
94. Khan, A.A., et al., *Effects of hydrogen sulfide exposure on lung mitochondrial respiratory chain enzymes in rats.* Toxicol Appl Pharmacol, 1990. **103**(3): p. 482-90.
95. Stringer, B.K. and H.J. Harmon, *Inhibition of cytochrome oxidase by dibucaine.* Biochem Pharmacol, 1990. **40**(5): p. 1077-81.
96. Tuquet, C., et al., *Effects of tamoxifen on the electron transport chain of isolated rat liver mitochondria.* Cell Biol Toxicol, 2000. **16**(4): p. 207-19.
97. Dabbeni-Sala, F., G. Schiavo, and P. Palatini, *Mechanism of local anesthetic effect on mitochondrial atp synthase as deduced from photolabelling and inhibition studies with phenothiazine derivatives.* Biochimica et Biophysica Acta (BBA) - Biomembranes, 1990. **1026**(1): p. 117-125.
98. Palmeira, C.M., A.J. Moreno, and V.M. Madeira, *Mitochondrial bioenergetics is affected by the herbicide paraquat.* Biochim Biophys Acta, 1995. **1229**(2): p. 187-92.
99. Wei, Y.H., et al., *Inhibition of the mitochondrial mg2+-atpase by propranolol.* Biochem Pharmacol, 1985. **34**(7): p. 911-7.
100. Rao, K.S.P., C.S. Chetty, and D. Desaiah, *In vitro effects of pyrethroids on rat brain and liver atpase activities.* Journal of Toxicology and Environmental Health, 1984. **14**(2-3): p. 257-265.
101. McEnery, M.W. and P.L. Pedersen, *Diethylstilbestrol. A novel f0-directed probe of the mitochondrial proton atpase.* J Biol Chem, 1986. **261**(4): p. 1745-52.
102. Terada, H., *The interaction of highly active uncouplers with mitochondria.* Biochimica et Biophysica Acta (BBA) - Reviews on Bioenergetics, 1981. **639**(3): p. 225-242.
103. Moreno-Sánchez, R., et al., *Inhibition and uncoupling of oxidative phosphorylation by nonsteroidal anti-inflammatory drugs: Study in mitochondria, submitochondrial particles, cells, and whole heart.* Biochem Pharmacol, 1999. **57**(7): p. 743-752.
104. Souza, M.E.J., et al., *Effect of fluoxetine on rat liver mitochondria.* Biochem Pharmacol, 1994. **48**(3): p. 535-541.
105. Curti, C., et al., *Fluoxetine interacts with the lipid bilayer of the inner membrane in isolated rat brain mitochondria, inhibiting electron transport and f1f0-atpase activity.* Mol Cell Biochem, 1999. **199**(1): p. 103-109.
106. Burbenskaya, N.M., et al., *The uncoupling effect of some psychotropic drugs on oxidative phosphorylation in rat liver mitochondria.* Biochem Mol Biol Int, 1998. **45**(2): p. 261-8.
107. Sun, X. and K.D. Garlid, *On the mechanism by which bupivacaine conducts protons across the membranes of mitochondria and liposomes.* J Biol Chem, 1992. **267**(27): p. 19147-54.
108. Sztark, F., et al., *Comparison of the effects of bupivacaine and ropivacaine on heart cell mitochondrial bioenergetics.* Anesthesiology, 1998. **88**(5): p. 1340-9.
109. Floridi, A., et al., *Effect of local anesthetic ropivacaine on isolated rat liver mitochondria.* Biochem Pharmacol, 1999. **58**(6): p. 1009-16.
110. Acco, A., J.F. Comar, and A. Bracht, *Metabolic effects of propofol in the isolated perfused rat liver.* Basic Clin Pharmacol Toxicol, 2004. **95**(4): p. 166-74.
111. Borges, N., *Tolcapone-related liver dysfunction: Implications for use in parkinson's disease therapy.* Drug Saf, 2003. **26**(11): p. 743-7.
112. Nissinen, E., et al., *Entacapone, a novel catechol-o-methyltransferase inhibitor for parkinson's disease, does not impair mitochondrial energy production.* Eur J Pharmacol, 1997. **340**(2-3): p. 287-94.
113. Haasio, K., et al., *Effects of entacapone and tolcapone on mitochondrial membrane potential.* Eur J Pharmacol, 2002. **453**(1): p. 21-6.
114. Parascandola, J., *Dinitrophenol and bioenergetics: An historical perspective.* Mol Cell Biochem, 1974. **5**(1): p. 69-77.
115. Miranda, E.J., et al., *Two deaths attributed to the use of 2,4-dinitrophenol.* J Anal Toxicol, 2006. **30**(3): p. 219-22.

116. Brand, M.D., *Mitochondrial generation of superoxide and hydrogen peroxide as the source of mitochondrial redox signaling.* Free Radical Biology and Medicine, 2016. **100**: p. 14-31.
117. Chance, B. and G. Hollunger, *The interaction of energy and electron transfer reactions in mitochondria. I. General properties and nature of the products of succinate-linked reduction of pyridine nucleotide.* J Biol Chem, 1961. **236**: p. 1534-43.
118. Robb, E.L., et al., *Control of mitochondrial superoxide production by reverse electron transport at complex i.* J Biol Chem, 2018. **293**(25): p. 9869-9879.
119. Holmström, K.M. and T. Finkel, *Cellular mechanisms and physiological consequences of redox-dependent signalling.* Nature Reviews Molecular Cell Biology, 2014. **15**: p. 411.
120. Hamanaka, R.B. and N.S. Chandel, *Mitochondrial reactive oxygen species regulate cellular signaling and dictate biological outcomes.* Trends in Biochemical Sciences, 2010. **35**(9): p. 505-513.
121. Klimova, T. and N.S. Chandel, *Mitochondrial complex iii regulates hypoxic activation of hif.* Cell Death Differ, 2008. **15**: p. 660.
122. Lim, C.B., et al., *Mitochondria-derived reactive oxygen species drive gant61-induced mesothelioma cell apoptosis.* Oncotarget, 2015. **6**(3): p. 1519-1530.
123. Tormos, Kathryn V., et al., *Mitochondrial complex iii ros regulate adipocyte differentiation.* Cell Metabolism, 2011. **14**(4): p. 537-544.
124. Lenaz, G., *The mitochondrial production of reactive oxygen species: Mechanisms and implications in human pathology.* IUBMB Life, 2001. **52**(3-5): p. 159-64.
125. Nicholls, D.G., *Mitochondrial membrane potential and aging.* Aging Cell, 2004. **3**(1): p. 35-40.
126. Chouchani, Edward T., et al., *A unifying mechanism for mitochondrial superoxide production during ischemia-reperfusion injury.* Cell Metabolism, 2016. **23**(2): p. 254-263.
127. Loor, G., et al., *Mitochondrial oxidant stress triggers cell death in simulated ischemia-reperfusion.* Biochim Biophys Acta, 2011. **1813**(7): p. 1382-94.
128. Arslan, F., D.P. de Kleijn, and G. Pasterkamp, *Innate immune signaling in cardiac ischemia.* Nature Reviews Cardiology, 2011. **8**: p. 292.
129. Deavall, D.G., et al., *Drug-induced oxidative stress and toxicity.* J Toxicol, 2012. **2012**: p. 645460.
130. Kohen, R. and A. Nyska, *Invited review: Oxidation of biological systems: Oxidative stress phenomena, antioxidants, redox reactions, and methods for their quantification.* Toxicologic Pathology, 2002. **30**(6): p. 620-650.
131. Bestman, J.E., et al., *The cellular and molecular progression of mitochondrial dysfunction induced by 2,4-dinitrophenol in developing zebrafish embryos.* Differentiation, 2015. **89**(3-4): p. 51-69.
132. Jayasundara, N., et al., *High-throughput tissue bioenergetics analysis reveals identical metabolic allometric scaling for teleost hearts and whole organisms.* PLoS One, 2015. **10**(9): p. e0137710.
133. Luz, A.L., et al., *Seahorse xfe 24 extracellular flux analyzer-based analysis of cellular respiration in caenorhabditis elegans.* Curr Protoc Toxicol, 2015. **66**: p. 25.7.1-15.
134. Andreux, P.A., et al., *A method to identify and validate mitochondrial modulators using mammalian cells and the worm c. Elegans.* Sci Rep, 2014. **4**: p. 5285.
135. Wills, L.P., et al., *Assessment of toxcast phase ii for mitochondrial liabilities using a high-throughput respirometric assay.* Toxicol Sci, 2015. **146**(2): p. 226-34.
136. Eakins, J., et al., *A combined in vitro approach to improve the prediction of mitochondrial toxicants.* Toxicology in Vitro, 2016. **34**: p. 161-170.
137. Kuznetsov, A.V., et al., *Analysis of mitochondrial function in situ in permeabilized muscle fibers, tissues and cells.* Nat Protoc, 2008. **3**(6): p. 965-76.
138. Picard, M., et al., *Mitochondria: Isolation, structure and function.* J Physiol, 2011. **589**(Pt 18): p. 4413-21.
139. Brand, M.D. and D.G. Nicholls, *Assessing mitochondrial dysfunction in cells.* The Biochemical journal, 2011. **435**(2): p. 297-312.

140. Ball, A., *Evaluating mitotoxicity as either a single or multi-mechanistic insult in the context of hepatotoxicity*, in *Mitochondrial dysfunction caused by drugs and environmental toxicants*. 2018. p. 73-92.
141. Rossjohn, J., et al., *Structures of perfringolysin o suggest a pathway for activation of cholesterol-dependent cytolysins.* J Mol Biol, 2007. **367**(5): p. 1227-36.
142. Moe, P.C. and A.P. Heuck, *Phospholipid hydrolysis caused by clostridium perfringens alpha-toxin facilitates the targeting of perfringolysin o to membrane bilayers.* Biochemistry, 2010. **49**(44): p. 9498-507.
143. Ramachandran, R., et al., *Structural insights into the membrane-anchoring mechanism of a cholesterol-dependent cytolysin.* Nat Struct Biol, 2002. **9**(11): p. 823-7.
144. Heuck, A.P., P.C. Moe, and B.B. Johnson, *The cholesterol-dependent cytolysin family of gram-positive bacterial toxins.* Subcell Biochem, 2010. **51**: p. 551-77.
145. Divakaruni, A.S., et al., *Thiazolidinediones are acute, specific inhibitors of the mitochondrial pyruvate carrier.* Proc Natl Acad Sci U S A, 2013. **110**(14): p. 5422-7.
146. Kim, C., et al., *Comparative analysis of the mitochondrial physiology of pancreatic β cells.* Bioenergetics : open access, 2014. **3**(1): p. 110-110.
147. Hamilton, B.F., et al., *In vivo assessment of mitochondrial toxicity.* Drug Discovery Today, 2008. **13**(17): p. 785-790.
148. Robinson, B.H., *Lactic acidemia and mitochondrial disease.* Molecular Genetics and Metabolism, 2006. **89**(1): p. 3-13.
149. Shaughnessy, D.T., et al., *Meeting report: Identification of biomarkers for early detection of mitochondrial dysfunction.* Mitochondrion, 2010. **10**(5): p. 579-581.
150. Whitaker, R.M., et al., *Urinary atp synthase subunit β is a novel biomarker of renal mitochondrial dysfunction in acute kidney injury.* Toxicol Sci, 2015. **145**(1): p. 108-117.
151. Whitaker, R.M., et al., *Urinary mitochondrial DNA is a biomarker of mitochondrial disruption and renal dysfunction in acute kidney injury.* Kidney Int, 2015. **88**(6): p. 1336-1344.
152. McGill, M.R., et al., *Argininosuccinate synthetase as a plasma biomarker of liver injury after acetaminophen overdose in rodents and humans.* Biomarkers, 2014. **19**(3): p. 222-30.
153. Wills, L.P., *The use of high-throughput screening techniques to evaluate mitochondrial toxicity.* Toxicology, 2017. **391**: p. 34-41.
154. Pereira, C., et al., *Investigating drug-induced mitochondrial toxicity: A biosensor to increase drug safety?* Vol. 4. 2009. 34-54.
155. Hynes, J., et al., *Investigation of drug-induced mitochondrial toxicity using fluorescence-based oxygen-sensitive probes.* Toxicological Sciences, 2006. **92**(1): p. 186-200.
156. Will, Y. and J. Dykens, *Mitochondrial toxicity assessment in industry--a decade of technology development and insight.* Expert Opin Drug Metab Toxicol, 2014. **10**(8): p. 1061-7.
157. Frezza, C., S. Cipolat, and L. Scorrano, *Organelle isolation: Functional mitochondria from mouse liver, muscle and cultured fibroblasts.* Nat Protoc, 2007. **2**(2): p. 287-95.
158. Ong, M.M.K., C. Latchoumycandane, and U.A. Boelsterli, *Troglitazone-induced hepatic necrosis in an animal model of silent genetic mitochondrial abnormalities.* Toxicological Sciences, 2006. **97**(1): p. 205-213.
159. CORDIS. *Mechanism-based integrated systems for the prediction of drug-induced liver injury*. 2017; Available from: https://cordis.europa.eu/project/id/115336.
160. Roy, K., S. Kar, and R.N. Das, *Chapter 1 - background of qsar and historical developments*, in *Understanding the basics of qsar for applications in pharmaceutical sciences and risk assessment*, K. Roy, S. Kar, and R.N. Das, Editors. 2015, Academic Press: Boston. p. 1-46.
161. Todeschini, R., V. Consonni, and P. Gramatica, *4.05 - chemometrics in qsar*, in *Comprehensive chemometrics*, S.D. Brown, R. Tauler, and B. Walczak, Editors. 2009, Elsevier: Oxford. p. 129-172.
162. Cherkasov, A., et al., *Qsar modeling: Where have you been? Where are you going to?* J Med Chem, 2014. **57**(12): p. 4977-5010.

163. Cronin, M.T.D., *Quantitative structure–activity relationships (qsars) – applications and methodology,* in *Recent advances in qsar studies: Methods and applications*, T. Puzyn, J. Leszczynski, and M.T. Cronin, Editors. 2010, Springer Netherlands: Dordrecht. p. 3-11.
164. Roy, K., S. Kar, and R.N. Das, *Chapter 6 - selected statistical methods in qsar*, in *Understanding the basics of qsar for applications in pharmaceutical sciences and risk assessment*, K. Roy, S. Kar, and R.N. Das, Editors. 2015, Academic Press: Boston. p. 191-229.
165. Roy, K., S. Kar, and R.N. Das, *Chapter 2 - chemical information and descriptors*, in *Understanding the basics of qsar for applications in pharmaceutical sciences and risk assessment*, K. Roy, S. Kar, and R.N. Das, Editors. 2015, Academic Press: Boston. p. 47-80.
166. Roy, K., S. Kar, and R.N. Das, *Chapter 7 - validation of qsar models*, in *Understanding the basics of qsar for applications in pharmaceutical sciences and risk assessment*, K. Roy, S. Kar, and R.N. Das, Editors. 2015, Academic Press: Boston. p. 231-289.
167. Golbraikh, A. and A. Tropsha, *Beware of q2!* Journal of Molecular Graphics and Modelling, 2002. **20**(4): p. 269-276.
168. Roy, K. and S. Kar, *The rm2 metrics and regression through origin approach: Reliable and useful validation tools for predictive qsar models (commentary on 'is regression through origin useful in external validation of qsar models?').* European Journal of Pharmaceutical Sciences, 2014. **62**: p. 111-114.
169. Topliss, J.G. and R.J. Costello, *Change correlations in structure-activity studies using multiple regression analysis.* J Med Chem, 1972. **15**(10): p. 1066-8.
170. Martin, T.M., et al., *Does rational selection of training and test sets improve the outcome of qsar modeling?* Journal of Chemical Information and Modeling, 2012. **52**(10): p. 2570-2578.
171. Morris, G.M. and M. Lim-Wilby, *Molecular docking.* Methods Mol Biol, 2008. **443**: p. 365-82.
172. Gupta, M., R. Sharma, and A. Kumar, *Docking techniques in pharmacology: How much promising?* Computational Biology and Chemistry, 2018. **76**: p. 210-217.
173. Morris, G.M., et al., *Autodock4 and autodocktools4: Automated docking with selective receptor flexibility.* J Comput Chem, 2009. **30**(16): p. 2785-91.
174. Verdonk, M.L., et al., *Improved protein-ligand docking using gold.* Proteins, 2003. **52**(4): p. 609-23.
175. Ewing, T.J., et al., *Dock 4.0: Search strategies for automated molecular docking of flexible molecule databases.* J Comput Aided Mol Des, 2001. **15**(5): p. 411-28.
176. Rarey, M., et al., *A fast flexible docking method using an incremental construction algorithm.* J Mol Biol, 1996. **261**(3): p. 470-89.
177. Xie, L., L. Xie, and P.E. Bourne, *Structure-based systems biology for analyzing off-target binding.* Curr Opin Struct Biol, 2011. **21**(2): p. 189-99.
178. Campillos, M., et al., *Drug target identification using side-effect similarity.* Science, 2008. **321**(5886): p. 263-6.
179. Du, X., et al., *Insights into protein-ligand interactions: Mechanisms, models, and methods.* Int J Mol Sci, 2016. **17**(2).
180. Sousa, S.F., P.A. Fernandes, and M.J. Ramos, *Protein-ligand docking: Current status and future challenges.* Proteins, 2006. **65**(1): p. 15-26.
181. Ferreira, L.G., et al., *Molecular docking and structure-based drug design strategies.* Molecules, 2015. **20**(7): p. 13384-421.
182. Forli, S., et al., *Computational protein-ligand docking and virtual drug screening with the autodock suite.* Nat Protoc, 2016. **11**(5): p. 905-19.
183. Matsuzaki, Y., et al., *Rigid-docking approaches to explore protein-protein interaction space.* Adv Biochem Eng Biotechnol, 2017. **160**: p. 33-55.
184. Totrov, M. and R. Abagyan, *Flexible ligand docking to multiple receptor conformations: A practical alternative.* Curr Opin Struct Biol, 2008. **18**(2): p. 178-184.
185. Weiland, G.A. and P.B. Molinoff, *Quantitative analysis of drug-receptor interactions: I. Determination of kinetic and equilibrium properties.* Life Sci, 1981. **29**(4): p. 313-30.

186. Eftink, M.R., A.C. Anusiem, and R.L. Biltonen, *Enthalpy-entropy compensation and heat capacity changes for protein-ligand interactions: General thermodynamic models and data for the binding of nucleotides to ribonuclease a.* Biochemistry, 1983. **22**(16): p. 3884-96.
187. Sharp, K., *Entropy-enthalpy compensation: Fact or artifact?* Protein Sci, 2001. **10**(3): p. 661-7.
188. Leffler, J.E., *The enthalpy-entropy relationship and its implications for organic chemistry.* The Journal of Organic Chemistry, 1955. **20**(9): p. 1202-1231.
189. Li, J., A. Fu, and L. Zhang, *An overview of scoring functions used for protein-ligand interactions in molecular docking.* Interdiscip Sci, 2019. **11**(2): p. 320-328.
190. Kitchen, D.B., et al., *Docking and scoring in virtual screening for drug discovery: Methods and applications.* Nat Rev Drug Discov, 2004. **3**(11): p. 935-49.
191. Plewczynski, D., et al., *Can we trust docking results? Evaluation of seven commonly used programs on pdbbind database.* J Comput Chem, 2011. **32**(4): p. 742-55.
192. Schirris, T.J., et al., *Statin-induced myopathy is associated with mitochondrial complex iii inhibition.* Cell Metab, 2015. **22**(3): p. 399-407.
193. Elliott, C., et al., *Purification and characterisation of recombinant DNA encoding the alternative oxidase from sauromatum guttatum.* Mitochondrion, 2014. **19**: p. 261-268.
194. Bradford, M.M., *A rapid and sensitive method for the quantitation of microgram quantities of protein utilizing the principle of protein-dye binding.* Anal Biochem, 1976. **72**: p. 248-54.
195. Gnaiger, E., *Polarographic oxygen sensors, the oxygraph and high-resolution respirometry to assess mitochondrial function.* Mitochondrial Dysfunction in Drug-Induced Toxicity, 2008: p. 327-352.
196. Krumschnabel, G., et al., *Chapter nine - use of safranin for the assessment of mitochondrial membrane potential by high-resolution respirometry and fluorometry*, in *Methods enzymol*, L. Galluzzi and G. Kroemer, Editors. 2014, Academic Press. p. 163-181.
197. Au - Nicholls, D.G., et al., *Bioenergetic profile experiment using c2c12 myoblast cells.* JoVE, 2010(46): p. e2511.
198. Salabei, J.K., A.A. Gibb, and B.G. Hill, *Comprehensive measurement of respiratory activity in permeabilized cells using extracellular flux analysis.* Nat Protoc, 2014. **9**(2): p. 421-38.
199. PDB, R. *The rcsb protein data bank*. 2020; Available from: www.rcsb.org.
200. Yankovskaya, V., et al., *Architecture of succinate dehydrogenase and reactive oxygen species generation.* Science, 2003. **299**(5607): p. 700.
201. Huang, L.S., et al., *Binding of the respiratory chain inhibitor antimycin to the mitochondrial bc1 complex: A new crystal structure reveals an altered intramolecular hydrogen-bonding pattern.* J Mol Biol, 2005. **351**(3): p. 573-97.
202. Shimada, A., et al., *X-ray structural analyses of azide-bound cytochrome c oxidases reveal that the h-pathway is critically important for the proton-pumping activity.* J Biol Chem, 2018. **293**(38): p. 14868-14879.
203. Gledhill, J.R., et al., *Mechanism of inhibition of bovine f1-atpase by resveratrol and related polyphenols.* Proc Natl Acad Sci U S A, 2007. **104**(34): p. 13632-7.
204. MOE, *Integrated computer-aided molecular design platform*. 2020.
205. Fedor, J.G., et al., *Correlating kinetic and structural data on ubiquinone binding and reduction by respiratory complex i.* Proceedings of the National Academy of Sciences, 2017. **114**(48): p. 12737.
206. ACD. *Physchem, adme & toxicity calculations with percepta software*. 2020 [cited 2020; Available from: https://www.acdlabs.com/products/percepta/.
207. Aliferis, K.A. and S. Jabaji, *Metabolomics – a robust bioanalytical approach for the discovery of the modes-of-action of pesticides: A review.* Pesticide Biochemistry and Physiology, 2011. **100**(2): p. 105-117.

208. Mitani, S., et al., *Biological properties of the novel fungicide cyazofamid against phytophthora infestans on tomato and pseudoperonospora cubensis on cucumber.* Pest Manag Sci, 2002. **58**(2): p. 139-45.
209. Convent, B. and M. Briquet, *Properties of 3-(3, 4-dichlorophenyl)-1, 1-dimethylurea and other inhibitors of the cytochrome bc1 segment of the mitochondrial respiratory chain in saccharomyces cerevisiae.* Eur J Biochem, 1978. **82**(2): p. 473-81.
210. Fisher, N. and B. Meunier, *Molecular basis of resistance to cytochrome bc1 inhibitors.* FEMS Yeast Res, 2008. **8**(2): p. 183-92.
211. Zhu, X., et al., *Ametoctradin is a potent qo site inhibitor of the mitochondrial respiration complex iii.* J Agric Food Chem, 2015. **63**(13): p. 3377-86.
212. Wang, F., et al., *Design, syntheses, and kinetic evaluation of 3-(phenylamino)oxazolidine-2,4-diones as potent cytochrome bc(1) complex inhibitors.* Bioorg Med Chem, 2011. **19**(15): p. 4608-15.
213. Kataoka, S., et al., *Mechanism of action and selectivity of a novel fungicide, pyribencarb.* Journal of Pesticide Science, 2010. **advpub**: p. 1001080106-1001080106.
214. Lever, J., M. Krzywinski, and N. Altman, *Principal component analysis.* Nature Methods, 2017. **14**: p. 641.
215. Roy, K., et al., *Comparative studies on some metrics for external validation of qspr models.* Journal of Chemical Information and Modeling, 2012. **52**(2): p. 396-408.
216. Siedow, J.N. and M.E. Girvin, *Alternative respiratory pathway: It's role in seed respiration and its inhibition by propyl gallate.* Plant Physiol, 1980. **65**(4): p. 669-74.
217. Lambowitz, A.M. and C.W. Slayman, *Cyanide-resistant respiration in neurospora crassa.* Journal of Bacteriology, 1971. **108**(3): p. 1087-1096.
218. van der Meer, C., et al., *Pitfalls of salicylhydroxamic acid plus glycerol treatment of t. Vivax infected goats.* Tropenmed Parasitol, 1980. **31**(3): p. 275-82.
219. Minagawa, N., et al., *An antibiotic, ascofuranone, specifically inhibits respiration and in vitro growth of long slender bloodstream forms of trypanosoma brucei brucei.* Mol Biochem Parasitol, 1997. **84**(2): p. 271-80.
220. Yabu, Y., et al., *Chemotherapeutic efficacy of ascofuranone in trypanosoma vivax-infected mice without glycerol.* Parasitology International, 2006. **55**(1): p. 39-43.
221. Shiba, T., et al., *Structure of the trypanosome cyanide-insensitive alternative oxidase.* Proceedings of the National Academy of Sciences, 2013. **110**(12): p. 4580.
222. West, R.A., et al., *Toward more drug like inhibitors of trypanosome alternative oxidase.* ACS Infect Dis, 2018. **4**(4): p. 592-604.
223. Young, L., et al., *Structure and mechanism of action of the alternative quinol oxidases*, in *Cytochrome complexes: Evolution, structures, energy transduction, and signaling*, W.A. Cramer and T. Kallas, Editors. 2016, Springer Netherlands: Dordrecht. p. 375-394.
224. Young, L., et al., *Probing the ubiquinol-binding site of recombinant sauromatum guttatum alternative oxidase expressed in e. Coli membranes through site-directed mutagenesis.* Biochimica et Biophysica Acta (BBA) - Bioenergetics, 2014. **1837**(7): p. 1219-1225.
225. Gasteiger, J. and M. Marsili, *Iterative partial equalization of orbital electronegativity—a rapid access to atomic charges.* Tetrahedron, 1980. **36**(22): p. 3219-3228.
226. Petitjean, M., *Applications of the radius-diameter diagram to the classification of topological and geometrical shapes of chemical compounds.* Journal of Chemical Information and Computer Sciences, 1992. **32**(4): p. 331-337.
227. Tropsha, A., P. Gramatica, and K. Gombar Vijay *The importance of being earnest: Validation is the absolute essential for successful application and interpretation of qspr models.* QSAR & Combinatorial Science, 2003. **22**(1): p. 69-77.
228. Roy, K., *On some aspects of validation of predictive quantitative structure–activity relationship models.* Expert Opinion on Drug Discovery, 2007. **2**(12): p. 1567-1577.
229. Saimoto, H., et al., *Pharmacophore identification of ascofuranone, potent inhibitor of cyanide-insensitive alternative oxidase of trypanosoma brucei.* Journal of Biochemistry, 2013. **153**(3): p. 267-273.

230. Mogi, T., et al., *Antibiotics ll-z1272 identified as novel inhibitors discriminating bacterial and mitochondrial quinol oxidases.* Biochim Biophys Acta, 2009. **1787**(2): p. 129-33.
231. Rich, P.R., et al., *Studies on mechanism of inhibition of redox enzymes by substituted hydroxamic acids.* Biochimica Et Biophysica Acta, 1978. **525**(2): p. 325-337.
232. Fisher, M.C., et al., *Emerging fungal threats to animal, plant and ecosystem health.* Nature, 2012. **484**(7393): p. 186-194.
233. Zorova, L.D., et al., *Mitochondrial membrane potential.* Analytical Biochemistry, 2018. **552**: p. 50-59.
234. Murphy, M.P., *How mitochondria produce reactive oxygen species.* The Biochemical journal, 2009. **417**(1): p. 1-13.
235. Liguori, I., et al., *Oxidative stress, aging, and diseases.* Clinical interventions in aging, 2018. **13**: p. 757-772.
236. Perry, S.W., et al., *Mitochondrial membrane potential probes and the proton gradient: A practical usage guide.* BioTechniques, 2011. **50**(2): p. 98-115.
237. Nixon, G.L., et al., *Antimalarial pharmacology and therapeutics of atovaquone.* J Antimicrob Chemother, 2013. **68**(5): p. 977-985.
238. Hinkle, P.C., *P/o ratios of mitochondrial oxidative phosphorylation.* Biochimica et Biophysica Acta (BBA) - Bioenergetics, 2005. **1706**(1): p. 1-11.
239. Berry, B.J., et al., *Use the protonmotive force: Mitochondrial uncoupling and reactive oxygen species.* Journal of Molecular Biology, 2018. **430**(21): p. 3873-3891.
240. Panduri, V., et al., *Mitochondrial-derived free radicals mediate asbestos-induced alveolar epithelial cell apoptosis.* Am J Physiol Lung Cell Mol Physiol, 2004. **286**(6): p. L1220-7.
241. Taylor, R.W., et al., *Succinate-cytochrome c reductase: Assessment of its value in the investigation of defects of the respiratory chain.* Biochimica et Biophysica Acta (BBA) - Molecular Basis of Disease, 1993. **1181**(3): p. 261-265.
242. FRAC. *Fungicide resistance action commitee. Qoi fungicides*. 2020; Available from: https://www.frac.info/frac-teams/working-groups/qol-fungicides/information.
243. Makrecka-Kuka, M., G. Krumschnabel, and E. Gnaiger, *High-resolution respirometry for simultaneous measurement of oxygen and hydrogen peroxide fluxes in permeabilized cells, tissue homogenate and isolated mitochondria.* Biomolecules, 2015. **5**(3): p. 1319-1338.
244. Acin-Perez, R., et al., *A novel approach to measure mitochondrial respiration in frozen biological samples.* The EMBO journal, 2020. **39**(13): p. e104073-e104073.
245. Scialo, F., D.J. Fernandez-Ayala, and A. Sanz, *Role of mitochondrial reverse electron transport in ros signaling: Potential roles in health and disease.* Front Physiol, 2017. **8**: p. 428.
246. Mitani, S., et al., *The biochemical mode of action of the novel selective fungicide cyazofamid: Specific inhibition of mitochondrial complex iii in phythium spinosum.* Pesticide Biochemistry and Physiology, 2001. **71**(2): p. 107-115.
247. WHO. *Who model list of essential medicines*. 2019; Available from: https://www.who.int/medicines/publications/essentialmedicines/en/.
248. WHO. *The top 10 causes of death*. 2018; Available from: https://www.who.int/news-room/fact-sheets/detail/the-top-10-causes-of-death.
249. Ramachandran, R. and A.S. Wierzbicki, *Statins, muscle disease and mitochondria.* Journal of clinical medicine, 2017. **6**(8): p. 75.
250. du Souich, P., G. Roederer, and R. Dufour, *Myotoxicity of statins: Mechanism of action.* Pharmacol Ther, 2017. **175**: p. 1-16.
251. Federation, I.D., *Idf diabetes atlas*. 8th ed, ed. B.I.D. Federation. 2017.
252. Dykens, J.A., et al., *Biguanide-induced mitochondrial dysfunction yields increased lactate production and cytotoxicity of aerobically-poised hepg2 cells and human hepatocytes in vitro.* Toxicol Appl Pharmacol, 2008. **233**(2): p. 203-10.
253. Brunmair, B., et al., *Thiazolidinediones, like metformin, inhibit respiratory complex i.* A Common Mechanism Contributing to Their Antidiabetic Actions?, 2004. **53**(4): p. 1052-1059.

254. Aithal, G.P. and C.P. Day, *Nonsteroidal anti-inflammatory drug–induced hepatotoxicity.* Clinics in Liver Disease, 2007. **11**(3): p. 563-575.
255. Nadanaciva, S., et al., *Toxicity assessments of nonsteroidal anti-inflammatory drugs in isolated mitochondria, rat hepatocytes, and zebrafish show good concordance across chemical classes.* Toxicology and Applied Pharmacology, 2013. **272**(2): p. 272-280.
256. Xu, J.J., D. Diaz, and P.J. O'Brien, *Applications of cytotoxicity assays and pre-lethal mechanistic assays for assessment of human hepatotoxicity potential.* Chemico-Biological Interactions, 2004. **150**(1): p. 115-128.
257. Labbe, G., D. Pessayre, and B. Fromenty, *Drug-induced liver injury through mitochondrial dysfunction: Mechanisms and detection during preclinical safety studies.* Fundam Clin Pharmacol, 2008. **22**(4): p. 335-53.
258. Schumacher, J.D. and G.L. Guo, *Mechanistic review of drug-induced steatohepatitis.* Toxicol Appl Pharmacol, 2015. **289**(1): p. 40-7.
259. Warburg, O., *On the origin of cancer cells.* Science, 1956. **123**(3191): p. 309-14.
260. Sassa, S., et al., *Drug metabolism by the human hepatoma cell, hep g2.* Biochem Biophys Res Commun, 1987. **143**(1): p. 52-7.
261. Levy, G., et al., *Long-term culture and expansion of primary human hepatocytes.* Nat Biotechnol, 2015. **33**(12): p. 1264-1271.
262. Dott, W., et al., *Modulation of mitochondrial bioenergetics in a skeletal muscle cell line model of mitochondrial toxicity.* Redox Biology, 2014. **2**: p. 224-233.
263. Xu, Q., et al., *Can galactose be converted to glucose in hepg2 cells? Improving the in vitro mitochondrial toxicity assay for the assessment of drug induced liver injury.* Chemical Research in Toxicology, 2019.
264. Frey, P.A., *The leloir pathway: A mechanistic imperative for three enzymes to change the stereochemical configuration of a single carbon in galactose.* Faseb j, 1996. **10**(4): p. 461-70.
265. Swiss, R., et al., *Validation of a hts-amenable assay to detect drug-induced mitochondrial toxicity in the absence and presence of cell death.* Toxicology in Vitro, 2013. **27**(6): p. 1789-1797.
266. DrugBank. 2020; Available from: https://www.drugbank.ca/.
267. Fuentes, A.V., M.D. Pineda, and K.C.N. Venkata, *Comprehension of top 200 prescribed drugs in the us as a resource for pharmacy teaching, training and practice.* Pharmacy (Basel, Switzerland), 2018. **6**(2): p. 43.
268. Jaeschke, H., *Troglitazone hepatotoxicity: Are we getting closer to understanding idiosyncratic liver injury?* Toxicological Sciences, 2007. **97**(1): p. 1-3.
269. Fiorillo, M., et al., *Repurposing atovaquone: Targeting mitochondrial complex iii and oxphos to eradicate cancer stem cells.* Oncotarget, 2016. **7**(23): p. 34084-34099.
270. Liu, R., et al., *Sa inhibits complex iii activity to generate reactive oxygen species and thereby induces ga overproduction in ganoderma lucidum.* Redox Biology, 2018. **16**: p. 388-400.
271. Long, J., et al., *Comparison of two methods for assaying complex i activity in mitochondria isolated from rat liver, brain and heart.* Life Sci, 2009. **85**(7-8): p. 276-80.
272. Lenaz, G., et al., *Mitochondrial quinone reductases: Complex i*, in *Methods enzymol.* 2004, Academic Press. p. 3-20.
273. Shimada, H., et al., *Mitochondrial nadh-quinone oxidoreductase of the outer membrane is responsible for paraquat cytotoxicity in rat livers.* Arch Biochem Biophys, 1998. **351**(1): p. 75-81.
274. Tolosa, L., et al., *High-content screening of drug-induced mitochondrial impairment in hepatic cells: Effects of statins.* Arch Toxicol, 2015. **89**(10): p. 1847-60.
275. Berson, A., et al., *Mechanisms for experimental buprenorphine hepatotoxicity: Major role of mitochondrial dysfunction versus metabolic activation.* J Hepatol, 2001. **34**(2): p. 261-9.
276. Card, J.W., et al., *Amiodarone-induced disruption of hamster lung and liver mitochondrial function: Lack of association with thiobarbituric acid-reactive substance production.* Toxicology Letters, 1998. **98**(1): p. 41-50.

277. Deschamps, D., et al., *Inhibition by perhexiline of oxidative phosphorylation and the β-oxidation of fatty acids: Possible role in pseudoalcoholic liver lesions.* Hepatology, 1994. **19**(4): p. 948-961.
278. Larosche, I., et al., *Tamoxifen inhibits topoisomerases, depletes mitochondrial DNA, and triggers steatosis in mouse liver.* J Pharmacol Exp Ther, 2007. **321**(2): p. 526-35.
279. Doi, H. and T. Horie, *Salicylic acid-induced hepatotoxicity triggered by oxidative stress.* Chemico-Biological Interactions, 2010. **183**(3): p. 363-368.
280. Norman, C., et al., *Salicylic acid is an uncoupler and inhibitor of mitochondrial electron transport.* Plant Physiol, 2004. **134**(1): p. 492-501.
281. Naven, R.T., et al., *The development of structure-activity relationships for mitochondrial dysfunction: Uncoupling of oxidative phosphorylation.* Toxicological Sciences, 2012. **131**(1): p. 271-278.
282. Stock, U., et al., *Measuring interference of drug-like molecules with the respiratory chain: Toward the early identification of mitochondrial uncouplers in lead finding.* Assay and drug development technologies, 2013. **11**(7): p. 408-422.
283. Massart, J., et al., *Drug-induced inhibition of mitochondrial fatty acid oxidation and steatosis.* Current Pathobiology Reports, 2013. **1**(3): p. 147-157.
284. Margolis, A.M., et al., *A review of the toxicity of hiv medications.* J Med Toxicol, 2014. **10**(1): p. 26-39.
285. Anissa, I., et al., *Mitochondrial, metabolic and genotoxic effects of antiretroviral nucleoside reverse-transcriptase inhibitors.* Anti-Infective Agents in Medicinal Chemistry, 2006. **5**(3): p. 273-292.
286. Maruthur, N.M., et al., *Diabetes medications as monotherapy or metformin-based combination therapy for type 2 diabetes: A systematic review and meta-analysis.* Annals of internal medicine, 2016. **164**(11): p. 740-751.
287. Owen, M.R., E. Doran, and A.P. Halestrap, *Evidence that metformin exerts its anti-diabetic effects through inhibition of complex 1 of the mitochondrial respiratory chain.* Biochem J, 2000. **348 Pt 3**: p. 607-14.
288. El-Mir, M.Y., et al., *Dimethylbiguanide inhibits cell respiration via an indirect effect targeted on the respiratory chain complex i.* J Biol Chem, 2000. **275**(1): p. 223-8.
289. Davis, T.M., et al., *The relationship between metformin therapy and the fasting plasma lactate in type 2 diabetes: The fremantle diabetes study.* British journal of clinical pharmacology, 2001. **52**(2): p. 137-44.
290. Isley, W.L., *Hepatotoxicity of thiazolidinediones.* Expert Opinion on Drug Safety, 2003. **2**(6): p. 581-586.
291. Smith, M.T., *Mechanisms of troglitazone hepatotoxicity.* Chemical Research in Toxicology, 2003. **16**(6): p. 679-687.
292. Masubuchi, Y., S. Kano, and T. Horie, *Mitochondrial permeability transition as a potential determinant of hepatotoxicity of antidiabetic thiazolidinediones.* Toxicology, 2006. **222**(3): p. 233-239.
293. Aleo, M.D., C.M. Doshna, and K.A. Navetta, *Ciglitazone-induced lenticular opacities in rats: In vivo and whole lens explant culture evaluation.* J Pharmacol Exp Ther, 2005. **312**(3): p. 1027-33.
294. Budde, K., et al., *The pharmacokinetics of pioglitazone in patients with impaired renal function.* British journal of clinical pharmacology, 2003. **55**(4): p. 368-374.
295. Buhaescu, I. and H. Izzedine, *Mevalonate pathway: A review of clinical and therapeutical implications.* Clin Biochem, 2007. **40**(9-10): p. 575-84.
296. Russo, M.W., M. Scobey, and H.L. Bonkovsky, *Drug-induced liver injury associated with statins.* Semin Liver Dis, 2009. **29**(4): p. 412-22.
297. Davidson, M.H., *Safety profiles for the hmg-coa reductase inhibitors: Treatment and trust.* Drugs, 2001. **61**(2): p. 197-206.
298. Furberg, C.D. and B. Pitt, *Withdrawal of cerivastatin from the world market.* Curr Control Trials Cardiovasc Med, 2001. **2**(5): p. 205-207.
299. Abdoli, N., et al., *Mechanisms of the statins cytotoxicity in freshly isolated rat hepatocytes.* J Biochem Mol Toxicol, 2013. **27**(6): p. 287-94.

300. Sirvent, P., et al., *Simvastatin induces impairment in skeletal muscle while heart is protected.* Biochem Biophys Res Commun, 2005. **338**(3): p. 1426-34.
301. Sirvent, P., et al., *Simvastatin triggers mitochondria-induced ca2+ signaling alteration in skeletal muscle.* Biochem Biophys Res Commun, 2005. **329**(3): p. 1067-75.
302. Nadanaciva, S., et al., *Target identification of drug induced mitochondrial toxicity using immunocapture based oxphos activity assays.* Toxicol In Vitro, 2007. **21**(5): p. 902-11.
303. Schirris, Tom J.J., et al., *Statin-induced myopathy is associated with mitochondrial complex iii inhibition.* Cell Metabolism, 2015. **22**(3): p. 399-407.
304. Dohlmann, T.L., *The acute effects of therapeutic concentrations of simvastatin lactone on mitochondrial respiratory capacity in human skeletal muscle: The lifestat study.* Clin Pharmacol Toxicol Res, 2018. **1**(1): p. 4-7.
305. Kikutani, Y., et al., *Involvement of monocarboxylate transporter 4 expression in statin-induced cytotoxicity.* Journal of Pharmaceutical Sciences, 2016. **105**(4): p. 1544-1549.
306. Vladutiu, G.D., et al., *Genetic risk factors associated with lipid-lowering drug-induced myopathies.* Muscle Nerve, 2006. **34**(2): p. 153-62.
307. Fujino, H., et al., *Metabolic properties of the acid and lactone forms of hmg-coa reductase inhibitors.* Xenobiotica, 2004. **34**(11-12): p. 961-71.
308. Kaufmann, P., et al., *Toxicity of statins on rat skeletal muscle mitochondria.* Cell Mol Life Sci, 2006. **63**(19-20): p. 2415-25.
309. Neuvonen, P.J., T. Kantola, and K.T. Kivisto, *Simvastatin but not pravastatin is very susceptible to interaction with the cyp3a4 inhibitor itraconazole.* Clin Pharmacol Ther, 1998. **63**(3): p. 332-41.
310. Deichmann, R., C. Lavie, and S. Andrews, *Coenzyme q10 and statin-induced mitochondrial dysfunction.* Ochsner J, 2010. **10**(1): p. 16-21.
311. Larsen, S., et al., *Simvastatin effects on skeletal muscle: Relation to decreased mitochondrial function and glucose intolerance.* J Am Coll Cardiol, 2013. **61**(1): p. 44-53.
312. Paiva, H., et al., *High-dose statins and skeletal muscle metabolism in humans: A randomized, controlled trial.* Clin Pharmacol Ther, 2005. **78**(1): p. 60-8.
313. Rundek, T., et al., *Atorvastatin decreases the coenzyme q10 level in the blood of patients at risk for cardiovascular disease and stroke.* Arch Neurol, 2004. **61**(6): p. 889-92.
314. Manoukian, A.A., et al., *Rhabdomyolysis secondary to lovastatin therapy.* Clin Chem, 1990. **36**(12): p. 2145-7.
315. Banach, M., et al., *Statin therapy and plasma coenzyme q10 concentrations--a systematic review and meta-analysis of placebo-controlled trials.* Pharmacol Res, 2015. **99**: p. 329-36.
316. Hargreaves, I.P., et al., *The effect of hmg-coa reductase inhibitors on coenzyme q10: Possible biochemical/clinical implications.* Drug Saf, 2005. **28**(8): p. 659-76.
317. Lee, S.S., et al., *Targeted disruption of the alpha isoform of the peroxisome proliferator-activated receptor gene in mice results in abolishment of the pleiotropic effects of peroxisome proliferators.* Mol Cell Biol, 1995. **15**(6): p. 3012-22.
318. Hodel, C., *Myopathy and rhabdomyolysis with lipid-lowering drugs.* Toxicol Lett, 2002. **128**(1-3): p. 159-68.
319. Bhardwaj, S.S. and N. Chalasani, *Lipid-lowering agents that cause drug-induced hepatotoxicity.* Clin Liver Dis, 2007. **11**(3): p. 597-613, vii.
320. Zhou, S. and K.B. Wallace, *The effect of peroxisome proliferators on mitochondrial bioenergetics.* Toxicol Sci, 1999. **48**(1): p. 82-9.
321. Scatena, R., et al., *Bezafibrate induces a mitochondrial derangement in human cell lines: A ppar-independent mechanism for a peroxisome proliferator.* Chem Res Toxicol, 2003. **16**(11): p. 1440-7.
322. Yamada, K., et al., *Mitochondria toxicity of antihyperlipidemic agents bezafibrate and fenofibrate.* Diabetology International, 2013. **4**(2): p. 126-131.
323. Yang, K.-C., et al., *Treatment of fibrate-induced rhabdomyolysis with plasma exchange in esrd.* American Journal of Kidney Diseases, 2005. **45**(3): p. e57-e60.

324. Brunton, L., *Goodman & gilman's pharmacological basis of therapeutics.* 12th ed. 2011: New York: McGraw-Hill.
325. Davison, C., *Salicylate metabolism in man.* Ann N Y Acad Sci, 1971. **179**: p. 249-68.
326. Liu, R., et al., *Sa inhibits complex iii activity to generate reactive oxygen species and thereby induces ga overproduction in ganoderma lucidum.* Redox Biol, 2018. **16**: p. 388-400.
327. Nie, S., et al., *Mitochondrial-derived reactive oxygen species play a vital role in the salicylic acid signaling pathway in arabidopsis thaliana.* PLoS One, 2015. **10**(3): p. e0119853.
328. Mahmud, T., et al., *Nonsteroidal antiinflammatory drugs and uncoupling of mitochondrial oxidative phosphorylation.* Arthritis Rheum, 1996. **39**(12): p. 1998-2003.
329. Masubuchi, Y., S. Yamada, and T. Horie, *Diphenylamine as an important structure of nonsteroidal anti-inflammatory drugs to uncouple mitochondrial oxidative phosphorylation††abbreviations: Nsaids, nonsteroidal anti-inflammatory drugs; and mpt, mitochondrial permeability transition.* Biochem Pharmacol, 1999. **58**(5): p. 861-865.
330. Couto, D., et al., *Scavenging of reactive oxygen and nitrogen species by the prodrug sulfasalazine and its metabolites 5-aminosalicylic acid and sulfapyridine.* Redox Rep, 2010. **15**(6): p. 259-67.
331. Rains, C.P., S. Noble, and D. Faulds, *Sulfasalazine. A review of its pharmacological properties and therapeutic efficacy in the treatment of rheumatoid arthritis.* Drugs, 1995. **50**(1): p. 137-56.
332. Azad Khan, A.K., J. Piris, and S.C. Truelove, *An experiment to determine the active therapeutic moiety of sulphasalazine.* Lancet, 1977. **2**(8044): p. 892-5.
333. van Hees, P.A., J.H. Bakker, and J.H. van Tongeren, *Effect of sulphapyridine, 5-aminosalicylic acid, and placebo in patients with idiopathic proctitis: A study to determine the active therapeutic moiety of sulphasalazine.* Gut, 1980. **21**(7): p. 632-5.
334. Sharon, P., et al., *Role of prostaglandins in ulcerative colitis. Enhanced production during active disease and inhibition by sulfasalazine.* Gastroenterology, 1978. **75**(4): p. 638-40.
335. Rodenburg, R.J., et al., *The antiinflammatory drug sulfasalazine inhibits tumor necrosis factor alpha expression in macrophages by inducing apoptosis.* Arthritis Rheum, 2000. **43**(9): p. 1941-50.
336. Gan, H.-T., Y.-Q. Chen, and Q.I.N. Ouyang, *Sulfasalazine inhibits activation of nuclear factor-κb in patients with ulcerative colitis.* Journal of Gastroenterology and Hepatology, 2005. **20**(7): p. 1016-1024.
337. Linares, V., V. Alonso, and J.L. Domingo, *Oxidative stress as a mechanism underlying sulfasalazine-induced toxicity.* Expert Opinion on Drug Safety, 2011. **10**(2): p. 253-263.
338. Neumann, V.C., et al., *A study to determine the active moiety of sulphasalazine in rheumatoid arthritis.* J Rheumatol, 1986. **13**(2): p. 285-7.
339. Niknahad, H., et al., *Sulfasalazine induces mitochondrial dysfunction and renal injury.* Ren Fail, 2017. **39**(1): p. 745-753.
340. Snow, W., et al., *Investigating a role for nfkb in cellular bioenergetics in normal and amyloid-exposed neurons in vitro.* Alzheimer's & Dementia, 2016. **12**: p. P650.
341. Couto, D., et al., *Scavenging of reactive oxygen and nitrogen species by the prodrug sulfasalazine and its metabolites 5-aminosalicylic acid and sulfapyridine.* Redox Report, 2010. **15**(6): p. 259-267.
342. Ennis, Z.N., et al., *Acetaminophen for chronic pain: A systematic review on efficacy.* Basic Clin Pharmacol Toxicol, 2016. **118**(3): p. 184-189.
343. Smith, H.S., *Potential analgesic mechanisms of acetaminophen.* Pain Physician, 2009. **12**(1): p. 269-80.
344. Ghanem, C.I., et al., *Acetaminophen from liver to brain: New insights into drug pharmacological action and toxicity.* Pharmacol Res, 2016. **109**: p. 119-31.
345. Ostapowicz, G., et al., *Results of a prospective study of acute liver failure at 17 tertiary care centers in the united states.* Annals of internal medicine, 2002. **137**(12): p. 947-954.

346. Masubuchi, Y., C. Suda, and T. Horie, *Involvement of mitochondrial permeability transition in acetaminophen-induced liver injury in mice.* J Hepatol, 2005. **42**(1): p. 110-6.
347. Meyers, L.L., et al., *Acetaminophen-induced inhibition of hepatic mitochondrial respiration in mice.* Toxicology and Applied Pharmacology, 1988. **93**(3): p. 378-387.
348. Burcham, P.C. and A.W. Harman, *Acetaminophen toxicity results in site-specific mitochondrial damage in isolated mouse hepatocytes.* Journal of Biological Chemistry, 1991. **266**(8): p. 5049-5054.
349. Chrois, K.M., et al., *Acetaminophen toxicity induces mitochondrial complex i inhibition in human liver tissue.* Basic Clin Pharmacol Toxicol, 2019.
350. Satoh, D., et al., *Establishment of a novel hepatocyte model that expresses four cytochrome p450 genes stably via mammalian-derived artificial chromosome for pharmacokinetics and toxicity studies.* PLoS One, 2017. **12**(10): p. e0187072.
351. Gerets, H.H., et al., *Characterization of primary human hepatocytes, hepg2 cells, and heparg cells at the mrna level and cyp activity in response to inducers and their predictivity for the detection of human hepatotoxins.* Cell Biol Toxicol, 2012. **28**(2): p. 69-87.
352. Guillouzo, A., et al., *The human hepatoma heparg cells: A highly differentiated model for studies of liver metabolism and toxicity of xenobiotics.* Chem Biol Interact, 2007. **168**(1): p. 66-73.
353. Robinson, D.M. and G.M. Keating, *Memantine: A review of its use in alzheimer's disease.* Drugs, 2006. **66**(11): p. 1515-34.
354. Creeley, C., et al., *Low doses of memantine disrupt memory in adult rats.* J Neurosci, 2006. **26**(15): p. 3923-32.
355. McAllister, J., et al., *Effects of memantine on mitochondrial function.* Biochem Pharmacol, 2008. **75**(4): p. 956-64.
356. Reus, G.Z., et al., *Administration of memantine and imipramine alters mitochondrial respiratory chain and creatine kinase activities in rat brain.* J Neural Transm (Vienna), 2012. **119**(4): p. 481-91.
357. Fan, D. and T.J. Fan, *Clonidine induces apoptosis of human corneal epithelial cells through death receptors-mediated, mitochondria-dependent signaling pathway.* Toxicological Sciences, 2017. **156**(1): p. 252-260.
358. Chang, E., et al., *A review of spasticity treatments: Pharmacological and interventional approaches.* Critical reviews in physical and rehabilitation medicine, 2013. **25**(1-2): p. 11-22.
359. Chen, X.-m., et al., *Colchicine-induced apoptosis in human normal liver l-02 cells by mitochondrial mediated pathways.* Toxicology in Vitro, 2012. **26**(5): p. 649-655.
360. Li, T., et al., *Identification of the gene for vitamin k epoxide reductase.* Nature, 2004. **427**(6974): p. 541-544.
361. Mullokandov, E., *Protein binding drug-drug interaction between warfarin and tizoxanide in human plasma.* Austin Journal of Pharmacology and Therapeutics, 2014. **2**.
362. Teresa Jde, P., et al., *Complex acetylenes from the roots of ferula communis.* Planta Med, 1986(6): p. 458-62.
363. Shiba, T., et al., *Insights into the ubiquinol/dioxygen binding and proton relay pathways of the alternative oxidase.* Biochim Biophys Acta Bioenerg, 2019. **1860**(5): p. 375-382.
364. Hartuti, E.D., et al., *Biochemical studies of membrane bound plasmodium falciparum mitochondrial l-malate:Quinone oxidoreductase, a potential drug target.* Biochimica et Biophysica Acta (BBA) - Bioenergetics, 2018. **1859**(3): p. 191-200.
365. Lahouel, M., et al., *Ferulenol specifically inhibits succinate ubiquinone reductase at the level of the ubiquinone cycle.* Biochem Biophys Res Commun, 2007. **355**(1): p. 252-257.
366. Carlsson, A., *Antipsychotic drugs, neurotransmitters, and schizophrenia.* Am J Psychiatry, 1978. **135**(2): p. 165-73.
367. Dazzan, P. and R.M. Murray, *Neurological soft signs in first-episode psychosis: A systematic review.* Br J Psychiatry Suppl, 2002. **43**: p. s50-7.

368. Meltzer, H.Y., S. Matsubara, and J.C. Lee, *Classification of typical and atypical antipsychotic drugs on the basis of dopamine d-1, d-2 and serotonin2 pki values.* J Pharmacol Exp Ther, 1989. **251**(1): p. 238-46.
369. Geddes, J., et al., *Atypical antipsychotics in the treatment of schizophrenia: Systematic overview and meta-regression analysis.* BMJ (Clinical research ed.), 2000. **321**(7273): p. 1371-1376.
370. Jones, P.B., et al., *Randomized controlled trial of the effect on quality of life of second- vs first-generation antipsychotic drugs in schizophrenia: Cost utility of the latest antipsychotic drugs in schizophrenia study (cutlass 1).* Arch Gen Psychiatry, 2006. **63**(10): p. 1079-87.
371. Lieberman, J.A., et al., *Effectiveness of antipsychotic drugs in patients with chronic schizophrenia.* N Engl J Med, 2005. **353**(12): p. 1209-23.
372. Allison, D.B., et al., *Antipsychotic-induced weight gain: A comprehensive research synthesis.* Am J Psychiatry, 1999. **156**(11): p. 1686-96.
373. Mittal, K., et al., *A comprehensive analysis of mitochondrial genes variants and their association with antipsychotic-induced weight gain.* Schizophr Res, 2017. **187**: p. 67-73.
374. Scaini, G., et al., *Second generation antipsychotic-induced mitochondrial alterations: Implications for increased risk of metabolic syndrome in patients with schizophrenia.* Eur Neuropsychopharmacol, 2018. **28**(3): p. 369-380.
375. Elmorsy, E., et al., *Effect of antipsychotics on mitochondrial bioenergetics of rat ovarian theca cells.* Toxicology Letters, 2017. **272**: p. 94-100.
376. Serretti, A. and A. Chiesa, *A meta-analysis of sexual dysfunction in psychiatric patients taking antipsychotics.* Int Clin Psychopharmacol, 2011. **26**(3): p. 130-40.
377. Casey, D.E., et al., *Antipsychotic-induced weight gain and metabolic abnormalities: Implications for increased mortality in patients with schizophrenia.* J Clin Psychiatry, 2004. **65 Suppl 7**: p. 4-18; quiz 19-20.
378. Muench, J. and A.M. Hamer, *Adverse effects of antipsychotic medications.* Am Fam Physician, 2010. **81**(5): p. 617-22.
379. Leslie, D.L. and R.A. Rosenheck, *Incidence of newly diagnosed diabetes attributable to atypical antipsychotic medications.* Am J Psychiatry, 2004. **161**(9): p. 1709-11.
380. Paredes, R.M., et al., *Metabolomic profiling of schizophrenia patients at risk for metabolic syndrome.* Int J Neuropsychopharmacol, 2014. **17**(8): p. 1139-48.
381. Newcomer, J.W., *Metabolic considerations in the use of antipsychotic medications: A review of recent evidence.* J Clin Psychiatry, 2007. **68 Suppl 1**: p. 20-7.
382. Tschoner, A., et al., *Effects of six second generation antipsychotics on body weight and metabolism - risk assessment and results from a prospective study.* Pharmacopsychiatry, 2009. **42**(1): p. 29-34.
383. Rummel-Kluge, C., et al., *Second-generation antipsychotic drugs and extrapyramidal side effects: A systematic review and meta-analysis of head-to-head comparisons.* Schizophr Bull, 2012. **38**(1): p. 167-77.
384. Carbon, M., et al., *Tardive dyskinesia prevalence in the period of second-generation antipsychotic use: A meta-analysis.* J Clin Psychiatry, 2017. **78**(3): p. e264-e278.
385. Pierre, J.M., *Extrapyramidal symptoms with atypical antipsychotics : Incidence, prevention and management.* Drug Saf, 2005. **28**(3): p. 191-208.
386. Roberts, R.C., *Postmortem studies on mitochondria in schizophrenia.* Schizophr Res, 2017. **187**: p. 17-25.
387. Chan, S.T., M.J. McCarthy, and M.P. Vawter, *Psychiatric drugs impact mitochondrial function in brain and other tissues.* Schizophr Res, 2019.
388. WHO. *Epilepsy*. 2019; Available from: https://www.who.int/news-room/fact-sheets/detail/epilepsy.
389. Ahmed, S.N. and Z.A. Siddiqi, *Antiepileptic drugs and liver disease.* Seizure, 2006. **15**(3): p. 156-64.
390. Zhou, M., et al., *Oxcarbazepine for neuropathic pain.* Cochrane Database Syst Rev, 2017. **12**: p. Cd007963.

391. Eisenberg, E., et al., *Antiepileptic drugs in the treatment of neuropathic pain.* Drugs, 2007. **67**(9): p. 1265-89.
392. Subbarao, B. *Seizure medications*. StatPearls 2020; Available from: https://www.ncbi.nlm.nih.gov/books/NBK482269/.
393. Hanada, T., *The ampa receptor as a therapeutic target in epilepsy: Preclinical and clinical evidence.* Journal of Receptor, Ligand and Channel Research, 2014. **7**: p. 39-50.
394. Finsterer, J. and S. Zarrouk Mahjoub, *Mitochondrial toxicity of antiepileptic drugs and their tolerability in mitochondrial disorders.* Expert Opin Drug Metab Toxicol, 2012. **8**(1): p. 71-9.
395. Finsterer, J. and F.A. Scorza, *Effects of antiepileptic drugs on mitochondrial functions, morphology, kinetics, biogenesis, and survival.* Epilepsy Res, 2017. **136**: p. 5-11.
396. Kudin, A.P., et al., *Mitochondrial liver toxicity of valproic acid and its acid derivatives is related to inhibition of α-lipoamide dehydrogenase.* Int J Mol Sci, 2017. **18**(9): p. 1912.
397. Santos, N.A.G., et al., *Aromatic antiepileptic drugs and mitochondrial toxicity: Effects on mitochondria isolated from rat liver.* Toxicology in Vitro, 2008. **22**(5): p. 1143-1152.
398. Boelsterli, U.A. and P.L. Lim, *Mitochondrial abnormalities--a link to idiosyncratic drug hepatotoxicity?* Toxicol Appl Pharmacol, 2007. **220**(1): p. 92-107.
399. Castrén, E., *Neurotrophic effects of antidepressant drugs.* Current Opinion in Pharmacology, 2004. **4**(1): p. 58-64.
400. Cikánková, T., Z. Fišar, and J. Hroudová, *In vitro effects of antidepressants and mood-stabilizing drugs on cell energy metabolism.* Naunyn Schmiedebergs Arch Pharmacol, 2019.
401. Li, Y., et al., *Mitochondrial dysfunction induced by sertraline, an antidepressant agent.* Toxicological Sciences, 2012. **127**(2): p. 582-591.
402. Abdel-Razaq, W., D.A. Kendall, and T.E. Bates, *The effects of antidepressants on mitochondrial function in a model cell system and isolated mitochondria.* Neurochemical Research, 2011. **36**(2): p. 327-338.
403. de Oliveira, M.R., *Fluoxetine and the mitochondria: A review of the toxicological aspects.* Toxicology Letters, 2016. **258**: p. 185-191.
404. Cikankova, T., et al., *In vitro effects of antipsychotics on mitochondrial respiration.* Naunyn Schmiedebergs Arch Pharmacol, 2019. **392**(10): p. 1209-1223.
405. Berger, I., et al., *The effect of antiepileptic drugs on mitochondrial activity: A pilot study.* J Child Neurol, 2010. **25**(5): p. 541-5.
406. Hroudova, J. and Z. Fisar, *Activities of respiratory chain complexes and citrate synthase influenced by pharmacologically different antidepressants and mood stabilizers.* Neuro Endocrinol Lett, 2010. **31**(3): p. 336-42.
407. Xia, Z., et al., *Changes in the generation of reactive oxygen species and in mitochondrial membrane potential during apoptosis induced by the antidepressants imipramine, clomipramine, and citalopram and the effects on these changes by bcl-2 and bcl-x(l).* Biochem Pharmacol, 1999. **57**(10): p. 1199-208.
408. Modica-Napolitano, J.S., et al., *Differential effects of typical and atypical neuroleptics on mitochondrial function in vitro.* Arch Pharm Res, 2003. **26**(11): p. 951-9.
409. Souza, M.E., et al., *Effect of fluoxetine on rat liver mitochondria.* Biochem Pharmacol, 1994. **48**(3): p. 535-41.
410. Nahon, E., et al., *Fluoxetine (prozac) interaction with the mitochondrial voltage-dependent anion channel and protection against apoptotic cell death.* FEBS Letters, 2005. **579**(22): p. 5105-5110.
411. Hroudova, J. and Z. Fisar, *In vitro inhibition of mitochondrial respiratory rate by antidepressants.* Toxicol Lett, 2012. **213**(3): p. 345-52.
412. Kim, Y.J., et al., *Lamotrigine inhibition of rotenone- or 1-methyl-4-phenylpyridinium-induced mitochondrial damage and cell death.* Brain Research Bulletin, 2007. **71**(6): p. 633-640.
413. Bogdanov, G.N., et al., *Anticonvulsants as bioantioxidants under stress conditions.* Biomed Khim, 2009. **55**(4): p. 519-24.

414. Maina, G., *Reserpine as an uncoupling agent.* Biochimica et Biophysica Acta (BBA) - Bioenergetics, 1974. **333**(3): p. 481-486.
415. Fromenty, B., et al., *Tianeptine, a new tricyclic antidepressant metabolized by β-oxidation of its heptanoic side chain, inhibits the mitochondrial oxidation of medium and short chain fatty acids in mice.* Biochem Pharmacol, 1989. **38**(21): p. 3743-3751.
416. Cheah, K.S. and J.C. Waring, *Effect of trifluoperazine on skeletal muscle mitochondrial respiration.* Biochim Biophys Acta, 1983. **723**(1): p. 45-51.
417. Ruben, L. and H. Rasmussen, *Phenothiazines and related compounds disrupt mitochondrial energy production by a calmodulin-independent reaction.* Biochimica et Biophysica Acta (BBA) - Bioenergetics, 1981. **637**(3): p. 415-422.
418. Silva, M.F., et al., *Differential effect of valproate and its delta2- and delta4-unsaturated metabolites, on the beta-oxidation rate of long-chain and medium-chain fatty acids.* Chem Biol Interact, 2001. **137**(3): p. 203-12.
419. Komulainen, T., et al., *Sodium valproate induces mitochondrial respiration dysfunction in hepg2 in vitro cell model.* Toxicology, 2015. **331**: p. 47-56.
420. Beedham, C., J.J. Miceli, and R.S. Obach, *Ziprasidone metabolism, aldehyde oxidase, and clinical implications.* J Clin Psychopharmacol, 2003. **23**(3): p. 229-32.
421. Nicholls, D.G., et al., *Bioenergetic profile experiment using c2c12 myoblast cells.* JoVE, 2010(46): p. e2511.
422. Salviato Balbão, M., et al., *Olanzapine, weight change and metabolic effects: A naturalistic 12-month follow up.* Therapeutic advances in psychopharmacology, 2014. **4**(1): p. 30-36.
423. Nadanaciva, S., et al., *Target identification of drug induced mitochondrial toxicity using immunocapture based oxphos activity assays.* Toxicology in Vitro, 2007. **21**(5): p. 902-911.
424. Gupta, S.K., et al., *Effect of alosetron (a new 5-ht3 receptor antagonist) on the pharmacokinetics of haloperidol in schizophrenic patients.* J Clin Pharmacol, 1995. **35**(2): p. 202-7.
425. Gossen, D., et al., *Influence of fluoxetine on olanzapine pharmacokinetics.* AAPS PharmSci, 2002. **4**(2): p. E11.
426. Grossmann, J., et al., *Apoptotic signaling during initiation of detachment-induced apoptosis ("anoikis") of primary human intestinal epithelial cells.* Cell Growth Differ, 2001. **12**(3): p. 147-55.
427. Inoue, Y., et al., *Bioavailability of intravenous fosphenytoin sodium in healthy japanese volunteers.* Eur J Drug Metab Pharmacokinet, 2013. **38**(2): p. 139-48.
428. Darwish, M., et al., *Evaluation of the potential for pharmacokinetic drug-drug interaction between armodafinil and carbamazepine in healthy adults.* Clin Ther, 2015. **37**(2): p. 325-37.
429. Burger, D.M., et al., *The effect of atazanavir and atazanavir/ritonavir on udp-glucuronosyltransferase using lamotrigine as a phenotypic probe.* Clin Pharmacol Ther, 2008. **84**(6): p. 698-703.
430. Lee, S.-Y., et al., *Effects of amoxicillin/clavulanic acid on the pharmacokinetics of valproic acid.* Drug design, development and therapy, 2015. **9**: p. 4559-4563.
431. He, Y.L., et al., *Lack of pharmacokinetic interaction between vildagliptin and amlodipine in healthy volunteers*. 2005. 1084-1084.
432. NIDDK. *Livertox: Clinical and research information on drug-induced liver injury*. 2017; Available from: https://www.ncbi.nlm.nih.gov/books/NBK548793/.
433. Björnsson, E.S., *Hepatotoxicity by drugs: The most common implicated agents.* Int J Mol Sci, 2016. **17**(2): p. 224-224.
434. Sundaram, V. and E.S. Björnsson, *Drug-induced cholestasis.* Hepatology communications, 2017. **1**(8): p. 726-735.
435. Dold, M., et al., *Haloperidol versus first-generation antipsychotics for the treatment of schizophrenia and other psychotic disorders.* Cochrane Database Syst Rev, 2015. **1**: p. Cd009831.

436. Holper, L., D. Ben-Shachar, and J.J. Mann, *Psychotropic and neurological medication effects on mitochondrial complex i and iv in rodent models.* European Neuropsychopharmacology, 2019. **29**(9): p. 986-1002.
437. Casademont, J., et al., *Neuroleptic treatment effect on mitochondrial electron transport chain: Peripheral blood mononuclear cells analysis in psychotic patients.* J Clin Psychopharmacol, 2007. **27**(3): p. 284-8.
438. Balijepalli, S., M.R. Boyd, and V. Ravindranath, *Inhibition of mitochondrial complex i by haloperidol: The role of thiol oxidation.* Neuropharmacology, 1999. **38**(4): p. 567-577.
439. Maurer, I. and H.J. Moller, *Inhibition of complex i by neuroleptics in normal human brain cortex parallels the extrapyramidal toxicity of neuroleptics.* Mol Cell Biochem, 1997. **174**(1-2): p. 255-9.
440. Hroudová, J. and Z. Fišar, *In vitro inhibition of mitochondrial respiratory rate by antidepressants.* Toxicology Letters, 2012. **213**(3): p. 345-352.
441. Shinoda, Y., et al., *Haloperidol aggravates transverse aortic constriction-induced heart failure via mitochondrial dysfunction.* J Pharmacol Sci, 2016. **131**(3): p. 172-83.
442. Babich, L.G., et al., *Ca(2+)-dependent regulation of the ca(2+) concentration in the myometrium mitochondria. I. Trifluoperazine effects on mitochondria membranes polarization and [ca(2+)](m).* Ukr Biochem J, 2016. **88**(4): p. 5-11.
443. Dunn, P.P., et al., *Trifluoperazine inhibition of electron transport and adenosine triphosphatase in plant mitochondria.* Arch Biochem Biophys, 1984. **229**(1): p. 287-94.
444. Iyama, Y., et al., *Photochemical and pharmacokinetic characterization of orally administered chemicals to evaluate phototoxic risk.* J Pharm Sci, 2019. **108**(3): p. 1303-1308.
445. Del Campo, A., et al., *Metabolic syndrome and antipsychotics: The role of mitochondrial fission/fusion imbalance.* Front Endocrinol (Lausanne), 2018. **9**: p. 144.
446. Sarsenbayeva, A., et al., *Effects of second-generation antipsychotics on human subcutaneous adipose tissue metabolism.* Psychoneuroendocrinology, 2019. **110**: p. 104445.
447. Contreras-Shannon, V., et al., *Clozapine-induced mitochondria alterations and inflammation in brain and insulin-responsive cells.* PLoS One, 2013. **8**(3): p. e59012.
448. Streck, E.L., et al., *Effect of antipsychotics on succinate dehydrogenase and cytochrome oxidase activities in rat brain.* Naunyn Schmiedebergs Arch Pharmacol, 2007. **376**(1-2): p. 127-33.
449. Khalaf, H.A., et al., *The role of oxidative stress in ovarian toxicity induced by haloperidol and clozapine-a histological and biochemical study in albino rats.* Cell Tissue Res, 2019. **378**(2): p. 371-383.
450. Soderstrom, J., et al., *Toxicology case of the month: Carbamazepine overdose.* Emergency medicine journal : EMJ, 2006. **23**(11): p. 869-871.
451. Novartis, *Tegretol (carbamazepine) chewable tablets, tablets and suspension and tegretol xr extended-release tablets prescribing information*, 2018.
452. Tolou-Ghamari, Z., et al., *A quick review of carbamazepine pharmacokinetics in epilepsy from 1953 to 2012.* Journal of research in medical sciences : the official journal of Isfahan University of Medical Sciences, 2013. **18**(Suppl 1): p. S81-S85.
453. Tränkner, A., C. Sander, and P. Schönknecht, *A critical review of the recent literature and selected therapy guidelines since 2006 on the use of lamotrigine in bipolar disorder.* Neuropsychiatric disease and treatment, 2013. **9**: p. 101-111.
454. Santos, N.A., et al., *Involvement of oxidative stress in the hepatotoxicity induced by aromatic antiepileptic drugs.* Toxicol In Vitro, 2008. **22**(8): p. 1820-4.
455. Parker, W.A. and C.A. Shearer, *Phenytoin hepatotoxicity: A case report and review.* Neurology, 1979. **29**(2): p. 175-8.
456. Eghbal, M.A., S. Taziki, and M.R. Sattari, *Mechanisms of phenytoin-induced toxicity in freshly isolated rat hepatocytes and the protective effects of taurine and/or melatonin.* J Biochem Mol Toxicol, 2014. **28**(3): p. 111-8.

457. Finsterer, J., *Toxicity of antiepileptic drugs to mitochondria*, in *Pharmacology of mitochondria*. 2016, Springer, Cham.
458. Perucca, E., *Pharmacological and therapeutic properties of valproate.* CNS Drugs, 2002. **16**(10): p. 695-714.
459. Björnsson, E. and R. Olsson, *Suspected drug-induced liver fatalities reported to the who database.* Digestive and Liver Disease, 2006. **38**(1): p. 33-38.
460. Silva, M.F.B., et al., *Valproic acid metabolism and its effects on mitochondrial fatty acid oxidation: A review.* Journal of Inherited Metabolic Disease, 2008. **31**(2): p. 205-216.
461. Castro-Gago, M., et al., *Early mitochondrial encephalomyopathy due to complex iv deficiency consistent with alpers-huttenlocher syndrome: Report of two cases.* Rev Neurol, 1999. **29**(10): p. 912-7.
462. Chabrol, B., et al., *Valproate-induced hepatic failure in a case of cytochrome c oxidase deficiency.* Eur J Pediatr, 1994. **153**(2): p. 133-5.
463. Krähenbühl, S., et al., *Mitochondrial diseases represent a risk factor for valproate-induced fulminant liver failure.* Liver, 2000. **20**(4): p. 346-348.
464. Rasmussen, M., et al., *Evidence that alpers-huttenlocher syndrome could be a mitochondrial disease.* J Child Neurol, 2000. **15**(7): p. 473-7.
465. Pronicka, E., et al., *Drug-resistant epilepsia and fulminant valproate liver toxicity. Alpers-huttenlocher syndrome in two children confirmed post mortem by identification of p.W748s mutation in polg gene.* Med Sci Monit, 2011. **17**(4): p. Cr203-9.
466. Saneto, R.P., et al., *Polg DNA testing as an emerging standard of care before instituting valproic acid therapy for pediatric seizure disorders.* Seizure, 2010. **19**(3): p. 140-6.
467. Schaller, A., et al., *Molecular and biochemical characterisation of a novel mutation in polg associated with alpers syndrome.* BMC Neurol, 2011. **11**: p. 4.
468. Wolf, N.I., et al., *Status epilepticus in children with alpers' disease caused by polg1 mutations: Eeg and mri features.* Epilepsia, 2009. **50**(6): p. 1596-607.
469. Ponchaut, S., F. van Hoof, and K. Veitch, *Cytochrome aa3 depletion is the cause of the deficient mitochondrial respiration induced by chronic valproate administration.* Biochem Pharmacol, 1992. **43**(3): p. 644-7.
470. Begriche, K., et al., *Drug-induced toxicity on mitochondria and lipid metabolism: Mechanistic diversity and deleterious consequences for the liver.* Journal of Hepatology, 2011. **54**(4): p. 773-794.
471. Jackson, M.C., et al., *Effect of vigabatrin on seizure control and safety profile in different subgroups of children with epilepsy.* Epilepsia, 2017. **58**(9): p. 1575-1585.
472. Vogel, K.R., et al., *Torin 1 partially corrects vigabatrin-induced mitochondrial increase in mouse.* Ann Clin Transl Neurol, 2015. **2**(6): p. 699-706.
473. Desguerre, I., et al., *Infantile spasms with basal ganglia mri hypersignal may reveal mitochondrial disorder due to t8993g mt DNA mutation.* Neuropediatrics, 2003. **34**(5): p. 265-9.
474. Loane, C. and M. Politis, *Buspirone: What is it all about?* Brain Research, 2012. **1461**: p. 111-118.
475. Jann, M.W., *Buspirone: An update on a unique anxiolytic agent.* Pharmacotherapy, 1988. **8**(2): p. 100-16.
476. Wilson, T.K. and J. Tripp, *Buspirone*, in *Statpearls*. 2020: Treasure Island (FL).
477. Ghiasi, N., R.K. Bhansali, and R. Marwaha, *Lorazepam*, in *Statpearls*. 2020: Treasure Island (FL).
478. Ahmadian, E., et al., *In vitro and in vivo evaluation of the mechanisms of citalopram-induced hepatotoxicity.* Arch Pharm Res, 2017. **40**(11): p. 1296-1313.
479. Nemeroff, C.B., *Overview of the safety of citalopram.* Psychopharmacol Bull, 2003. **37**(1): p. 96-121.
480. Milkiewicz, P., et al., *Antidepressant induced cholestasis: Hepatocellular redistribution of multidrug resistant protein (mrp2).* Gut, 2003. **52**(2): p. 300-3.
481. Fisar, Z., J. Hroudova, and J. Raboch, *Inhibition of monoamine oxidase activity by antidepressants and mood stabilizers.* Neuro Endocrinol Lett, 2010. **31**(5): p. 645-56.

482. Baumann, P., *Pharmacology and pharmacokinetics of citalopram and other ssris.* Int Clin Psychopharmacol, 1996. **11 Suppl 1**: p. 5-11.
483. Fuller, R.W., D.T. Wong, and D.W. Robertson, *Fluoxetine, a selective inhibitor of serotonin uptake.* Medicinal Research Reviews, 1991. **11**(1): p. 17-34.
484. Brambilla, P., et al., *Side-effect profile of fluoxetine in comparison with other ssris, tricyclic and newer antidepressants: A meta-analysis of clinical trial data.* Pharmacopsychiatry, 2005. **38**(2): p. 69-77.
485. Wagstaff, A.J., D. Ormrod, and C.M. Spencer, *Tianeptine: A review of its use in depressive disorders.* CNS Drugs, 2001. **15**(3): p. 231-59.
486. McEwen, B.S., et al., *The neurobiological properties of tianeptine (stablon): From monoamine hypothesis to glutamatergic modulation.* Molecular psychiatry, 2010. **15**(3): p. 237-249.
487. Sharma, B., *Antidepressants: Mechanism of action, toxicity and possible amelioration.* Journal of Applied Biotechnology & Bioengineering, 2017. **3**.
488. Della, F.P., et al., *Treatment with tianeptine induces antidepressive-like effects and alters the neurotrophin levels, mitochondrial respiratory chain and cycle krebs enzymes in the brain of maternally deprived adult rats.* Metabolic Brain Disease, 2013. **28**(1): p. 93-105.
489. Głombik, K., et al., *The effect of chronic tianeptine administration on the brain mitochondria: Direct links with an animal model of depression.* Molecular Neurobiology, 2016. **53**(10): p. 7351-7362.
490. Kola, I. and J. Landis, *Can the pharmaceutical industry reduce attrition rates?* Nat Rev Drug Discov, 2004. **3**(8): p. 711-5.
491. Commision, E. *Reach legislation*. 2007; Available from: https://echa.europa.eu/regulations/reach/legislation.
492. Enoch, S., *Structure–activity modeling of mitochondrial dysfunction*, in *Mitochondrial dysfunction caused by drugs and environmental toxicants*. 2018. p. 25-34.
493. Wills, L.P., et al., *High-throughput respirometric assay identifies predictive toxicophore of mitochondrial injury.* Toxicol Appl Pharmacol, 2013. **272**(2): p. 490-502.
494. Nelms, M.D., et al., *Development of an in silico profiler for mitochondrial toxicity.* Chemical Research in Toxicology, 2015. **28**(10): p. 1891-1902.
495. Stammler G., W.A., Glaettli A., Klappach K, *Respiration inhibitors: Complex ii, fungicide resistance in plant pathogens*, ed. Springer. 2015.
496. Horsefield, R., et al., *Structural and computational analysis of the quinone-binding site of complex ii (succinate-ubiquinone oxidoreductase): A mechanism of electron transfer and proton conduction during ubiquinone reduction.* J Biol Chem, 2006. **281**(11): p. 7309-16.
497. Hou, T.J., et al., *Adme evaluation in drug discovery. 4. Prediction of aqueous solubility based on atom contribution approach.* Journal of Chemical Information and Computer Sciences, 2004. **44**(1): p. 266-275.
498. Cameron, R., *Biological and computational techniques to identify mitochondrial toxicants*, in *Mitochondrial dysfunction caused by drugs and environmental toxicants*. 2018. p. 205-215.
499. Ford, K.A., et al., *Comparative evaluation of 11 in silico models for the prediction of small molecule mutagenicity: Role of steric hindrance and electron-withdrawing groups.* Toxicol Mech Methods, 2017. **27**(1): p. 24-35.
500. Singh, P.K., et al., *Toxicophore exploration as a screening technology for drug design and discovery: Techniques, scope and limitations.* Arch Toxicol, 2016. **90**(8): p. 1785-802.
501. Frid, A.A. and E.J. Matthews, *Prediction of drug-related cardiac adverse effects in humans--b: Use of qsar programs for early detection of drug-induced cardiac toxicities.* Regul Toxicol Pharmacol, 2010. **56**(3): p. 276-89.
502. Beck, D.E., et al., *Discovery of potent indenoisoquinoline topoisomerase i poisons lacking the 3-nitro toxicophore.* J Med Chem, 2015. **58**(9): p. 3997-4015.

503. Ankley, G.T., et al., *Adverse outcome pathways: A conceptual framework to support ecotoxicology research and risk assessment.* Environ Toxicol Chem, 2010. **29**(3): p. 730-41.
504. Vinken, M., *The adverse outcome pathway concept: A pragmatic tool in toxicology.* Toxicology, 2013. **312**: p. 158-165.
505. Landesmann, B., et al., *Adverse outcome pathway-based screening strategies for an animal-free safety assessment of chemicals.* Alternatives to Laboratory Animals, 2013. **41**(6): p. 461-471.
506. Nelms, M.D., et al., *Proposal of an in silico profiler for categorisation of repeat dose toxicity data of hair dyes.* Arch Toxicol, 2015. **89**(5): p. 733-41.
507. Zhang, H., et al., *In silico prediction of mitochondrial toxicity by using ga-cg-svm approach.* Toxicol In Vitro, 2009. **23**(1): p. 134-40.
508. Wojtovich, A.P., et al., *Physiological consequences of complex ii inhibition for aging, disease, and the mkatp channel.* Biochim Biophys Acta, 2013. **1827**(5): p. 598-611.
509. Gao, X., et al., *Structural basis for the quinone reduction in the bc1 complex: A comparative analysis of crystal structures of mitochondrial cytochrome bc1 with bound substrate and inhibitors at the qi site.* Biochemistry, 2003. **42**(30): p. 9067-9080.
510. Xiong, L., et al., *Structure-based discovery of potential fungicides as succinate ubiquinone oxidoreductase inhibitors.* Journal of Agricultural and Food Chemistry, 2017. **65**(5): p. 1021-1029.
511. Zhu, X.L., et al., *Computational and experimental insight into the molecular mechanism of carboxamide inhibitors of succinate-ubquinone oxidoreductase.* ChemMedChem, 2014. **9**(7): p. 1512-21.
512. Zhou, Q., et al., *Thiabendazole inhibits ubiquinone reduction activity of mitochondrial respiratory complex ii via a water molecule mediated binding feature.* Protein Cell, 2011. **2**(7): p. 531-42.
513. Stoker, M.L., et al., *Impact of pharmacological agents on mitochondrial function: A growing opportunity?* Biochem Soc Trans, 2019. **47**(6): p. 1757-1772.
514. Massart, J., A. Borgne-Sanchez, and B. Fromenty, *Drug-induced mitochondrial toxicity*, in *Mitochondrial biology and experimental therapeutics*, P.J. Oliveira, Editor. 2018, Springer International Publishing: Cham. p. 269-295.
515. Oliveira, P.J., *Mitochondrial biology and experimental therapeutics*. Mitochondrial biology and experimental therapeutics. 2018. 1-708.
516. Will, Y., J.E. Shields, and K.B. Wallace, *Drug-induced mitochondrial toxicity in the geriatric population: Challenges and future directions.* Biology, 2019. **8**(2): p. 32.
517. Hynes, J. and Y. Will, *The evolution of mitochondrial toxicity assessment in industry*, in *Mitochondrial biology and experimental therapeutics*, P.J. Oliveira, Editor. 2018, Springer International Publishing: Cham. p. 319-332.
518. Olson, H., et al., *Concordance of the toxicity of pharmaceuticals in humans and in animals.* Regul Toxicol Pharmacol, 2000. **32**(1): p. 56-67.
519. Pessayre, D., et al., *Mitochondrial involvement in drug-induced liver injury*, in *Adverse drug reactions*, J. Uetrecht, Editor. 2010, Springer Berlin Heidelberg: Berlin, Heidelberg. p. 311-365.
520. Begriche, K., et al., *Mitochondrial adaptations and dysfunctions in nonalcoholic fatty liver disease.* Hepatology, 2013. **58**(4): p. 1497-507.
521. Ignacio, Z.M., et al., *Acute and chronic treatments with quetiapine increase mitochondrial respiratory chain complex activity in the rat brain.* Curr Neurovasc Res, 2015. **12**(3): p. 283-92.
522. TeSlaa, T. and M.A. Teitell, *Techniques to monitor glycolysis.* Methods Enzymol, 2014. **542**: p. 91-114.
523. Benfenati, E., et al., *The acceptance of in silico models for reach: Requirements, barriers, and perspectives.* Chemistry Central journal, 2011. **5**: p. 58-58.
524. Canter, J.A., et al., *The mitochondrial pharmacogenomics of haplogroup t: Mtnd2*lhon4917g and antiretroviral therapy-associated peripheral neuropathy.* Pharmacogenomics J, 2008. **8**(1): p. 71-7.

525. Kampira, E., et al., *Mitochondrial DNA subhaplogroups l0a2 and l2a modify susceptibility to peripheral neuropathy in malawian adults on stavudine containing highly active antiretroviral therapy.* J Acquir Immune Defic Syndr, 2013. **63**(5): p. 647-52.
526. Garrabou, G., et al., *Influence of mitochondrial genetics on the mitochondrial toxicity of linezolid in blood cells and skin nerve fibers.* Antimicrob Agents Chemother, 2017. **61**(9).
527. Pacheu-Grau, D., et al., *Mitochondrial antibiograms in personalized medicine.* Human Molecular Genetics, 2012. **22**(6): p. 1132-1139.
528. Kelley, L.C., et al., *Adaptive f-actin polymerization and localized atp production drive basement membrane invasion in the absence of mmps.* Dev Cell, 2019. **48**(3): p. 313-328.e8.
529. Hirpara, J., et al., *Metabolic reprogramming of oncogene-addicted cancer cells to oxphos as a mechanism of drug resistance.* Redox Biol, 2019. **25**: p. 101076.
530. Tan, A.S., et al., *Mitochondrial genome acquisition restores respiratory function and tumorigenic potential of cancer cells without mitochondrial DNA.* Cell Metab, 2015. **21**(1): p. 81-94.
531. Shi, Y., et al., *Gboxin is an oxidative phosphorylation inhibitor that targets glioblastoma.* Nature, 2019. **567**(7748): p. 341-346.
532. Molina, J.R., et al., *An inhibitor of oxidative phosphorylation exploits cancer vulnerability.* Nature Medicine, 2018. **24**(7): p. 1036-1046.
533. Zhang, L., et al., *Metabolic reprogramming toward oxidative phosphorylation identifies a therapeutic target for mantle cell lymphoma.* Sci Transl Med, 2019. **11**(491).
534. Fang, C., X. Wei, and Y. Wei, *Mitochondrial DNA in the regulation of innate immune responses.* Protein Cell, 2016. **7**(1): p. 11-16.
535. Walker, M.A., et al., *Powering the immune system: Mitochondria in immune function and deficiency.* Journal of immunology research, 2014. **2014**: p. 164309-164309.
536. Mohanty, A., R. Tiwari-Pandey, and N.R. Pandey, *Mitochondria: The indispensable players in innate immunity and guardians of the inflammatory response.* J Cell Commun Signal, 2019. **13**(3): p. 303-318.
537. Kohler, J.J. and W. Lewis, *A brief overview of mechanisms of mitochondrial toxicity from nrtis.* Environ Mol Mutagen, 2007. **48**(3-4): p. 166-72.
538. Björnsson, E.S., *Drug-induced liver injury: An overview over the most critical compounds.* Arch Toxicol, 2015. **89**(3): p. 327-334.
539. Walker, D., *The mitochondrial exposome*, in *Mitochondrial dysfunction caused by drugs and environmental toxicants*. p. 613-637.
540. Madreiter-Sokolowski, C.T., et al., *Targeting mitochondria to counteract age-related cellular dysfunction.* Genes, 2018. **9**(3): p. 165.
541. Arauna, D., et al., *Natural bioactive compounds as protectors of mitochondrial dysfunction in cardiovascular diseases and aging.* Molecules, 2019. **24**(23): p. 4259.

APPENDIX I - QSAR AND MOLECULAR DOCKING STUDIES FOR THE SEARCH OF AOX INHIBITORS

Table I.1. Compounds used to develop the QSAR model, selected descriptors, experimental pIC_{50} values, predicted pIC_{50} values and absolute error. *LOO cross-validation absolute error values, **LSO cross-validation absolute error values.

Compounds	H-bond donor	Neutral form	PEOE_VSA_FP POS	Petit jean	pIC_{50} Exp.	pIC_{50} Pred.	Abs. error	Abs. error *	Abs. error **
1	1	0.07	0.076	0.500	9.398	9.338	0.060	0.065	0.250
2	1	0.07	0.087	0.462	8.921	8.471	0.450	0.479	0.398
3	1	0.07	0.085	0.467	8.854	8.603	0.251	0.264	0.058
4	1	0.1	0.048	0.467	9.523	9.196	0.327	0.359	0.647
5	1	0.04	0.052	0.467	9.000	9.264	0.264	0.288	0.042
6	1	0.1	0.052	0.467	9.301	9.116	0.185	0.201	0.985
7a	1	0.05	0.091	0.429	7.000	7.869	0.869	1.122	0.066
7b	1	0.04	0.079	0.444	8.420	8.390	0.030	0.034	0.265
7c	1	0.04	0.070	0.455	9.155	8.733	0.422	0.457	0.690
7d	1	0.04	0.063	0.462	9.420	8.988	0.433	0.464	0.318
7e	1	0.04	0.060	0.500	9.420	9.718	0.298	0.332	1.908
7f	1	0.04	0.054	0.500	9.347	9.815	0.468	0.529	1.359
8	1	0.1	0.071	0.474	9.301	8.894	0.407	0.422	1.122
9	1	0.1	0.075	0.500	9.523	9.292	0.231	0.250	0.508
10	1	0.1	0.127	0.500	9.495	8.350	1.145	1.535	0.065
11	1	0.1	0.096	0.462	8.222	8.242	0.020	0.022	0.184
12	1	0	0.139	0.462	7.398	7.713	0.316	0.442	0.029
13	1	0	0.115	0.471	8.377	8.306	0.071	0.081	0.299
14	1	0.17	0.046	0.467	8.602	9.042	0.440	0.483	1.137
15	1	0.17	0.074	0.500	9.155	9.135	0.020	0.022	0.078
16	1	0.17	0.057	0.500	9.824	9.436	0.388	0.422	0.401
17	1	0.83	0.070	0.500	7.553	7.540	0.013	0.019	0.393
18	1	0.24	0.094	0.462	7.347	7.924	0.578	0.637	0.307
19	0	0.77	0.063	0.462	5.000	4.881	0.119	0.301	0.393
20	1	0.01	0.081	0.462	9.347	8.731	0.616	0.654	0.164
21	1	0.07	0.082	0.500	8.222	9.243	1.021	1.116	0.726
22	1	0.23	0.079	0.500	7.000	8.890	1.890	2.033	0.050
23	0	0.01	0.062	0.462	6.699	6.818	0.119	0.301	0.460
24	1	0.07	0.063	0.500	10.222	9.586	0.636	0.699	0.332
25	1	0.06	0.050	0.467	9.347	9.250	0.097	0.106	1.568
26	1	0.06	0.063	0.500	9.638	9.606	0.032	0.035	0.160
27	1	0.63	0.063	0.500	9.301	8.165	1.136	1.385	0.697
28	1	0.58	0.067	0.500	7.420	8.228	0.808	0.956	0.018
29	1	0.6	0.023	0.467	8.398	8.378	0.020	0.029	0.422

Table I.2. Structures and 50% inhibitory concentrations (nM) of a series of AF derivatives obtained by Saimoto *et al.*, 2012[52]

1 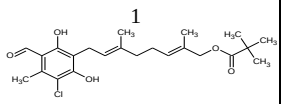 **IC_{50} = 0.40**	2 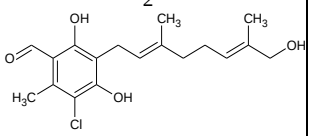 **IC_{50} = 1.2**	3 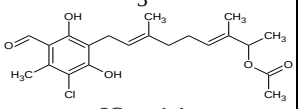 **IC_{50} = 1.4**	4 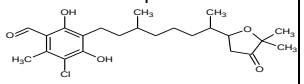 **IC_{50} = 0.3**	5 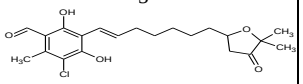 **IC_{50} = 1.0**	6 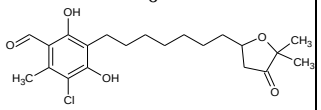 **IC_{50} = 0.5**
7a **IC_{50}=100** 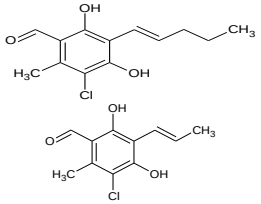 7b **IC_{50} = 3.8**	7c **IC_{50} = 0.70** 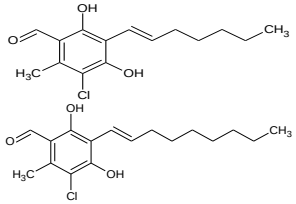 7d **IC_{50} = 0.38**	7e **IC_{50} = 0.38** 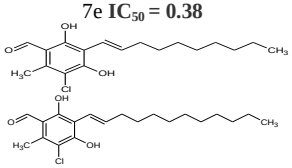 7f **IC_{50} = 0.45**	8 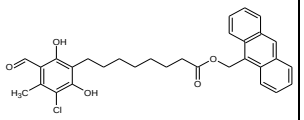 **IC_{50} = 0.50**	9 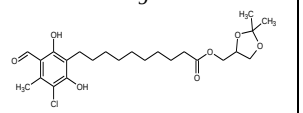 **IC_{50} = 0.30**	10 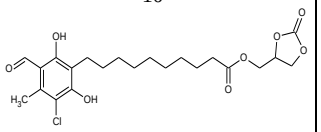 **IC_{50} = 0.32**
11 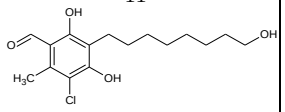 **IC_{50} = 6.0**	12 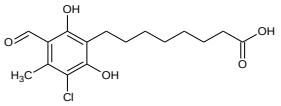 **IC_{50} = 40**	13 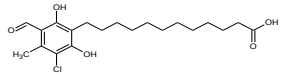 **IC_{50} = 4.2**	14 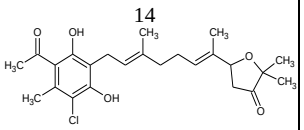 **IC_{50} = 2.5**	15 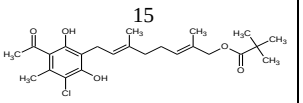 **IC_{50} = 0.70**	16 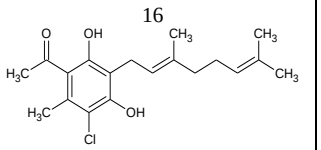 **IC_{50} = 0.15**
17 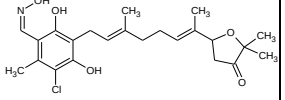 **IC_{50} = 28**	18 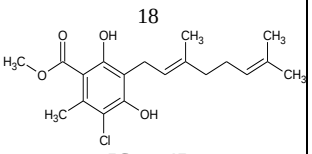 **IC_{50} = 45**	19 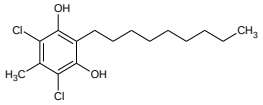 **IC_{50} = 10000**	20 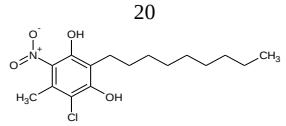 **IC_{50} = 0.45**	21 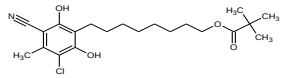 **IC_{50} = 6.0**	22 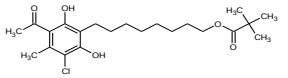 **IC_{50} = 100**
23 **IC_{50} = 200** 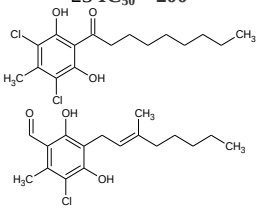 24 **IC_{50} = 0.06**	25 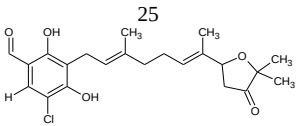 **IC_{50} = 0.45**	26 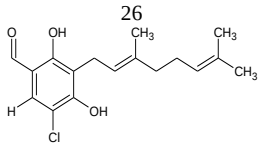 **IC_{50}=0.23**	27 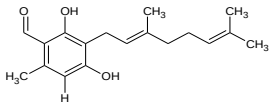 **IC_{50} = 0.50**	28 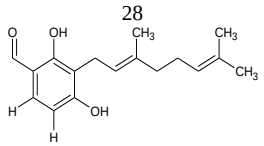 **IC_{50} = 38**	29 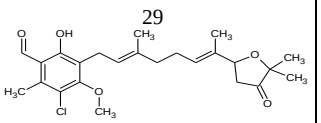 **IC_{50} = 4.0**

APPENDIX II - QSAR AND MOLECULAR DOCKING STUDIES FOR THE SEARCH OF COMPLEX II AND COMPLEX III INHIBITORS

Table II.1. Structures and inhibitory activities towards SCR of the compounds tested in the laboratory. Values are average ± standard deviation for triplicate measurements using different biological samples. a = test set, b = training set.

Compound	Chemical structure	Drug class	pIC_{50}
Acetaminophen	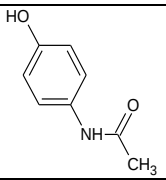	Analgesic	<1.82
Amisulbrom	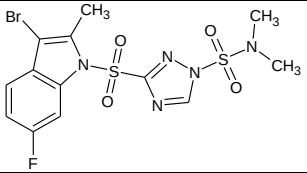	Fungicide	5.60 ± 0.05
Antimycin A	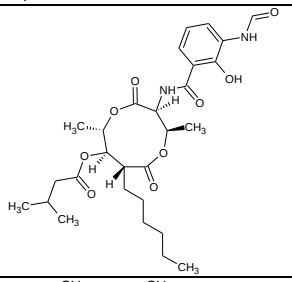	Antifungal, macrolide antibiotic	8.55 ± 0.14
Ascochlorin	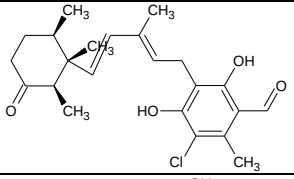	Fungicide	8.29 ± 0.05
[b]Ascofuranone	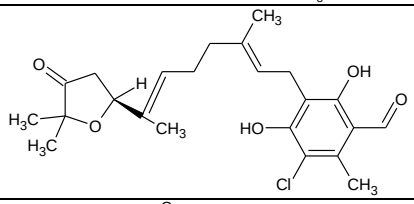	Fungicide	5.08 ± 0.09
[b]Atovaquone	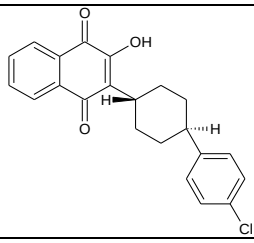	Anti-infective (antimalarial)	6.69 ± 0.05
[b]Azoxystrobin	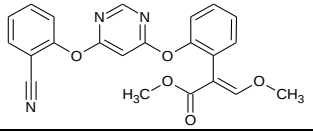	Fungicide	6.67 ± 0.09

Compound	Chemical structure	Drug class	pIC_{50}
[a]**Bezafibrate**	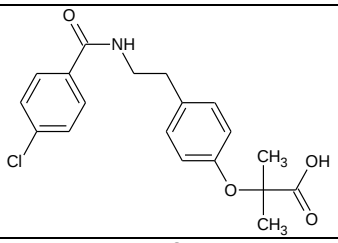	Lipid lowering agent	<3.30
[b]**Chlorpromazine**	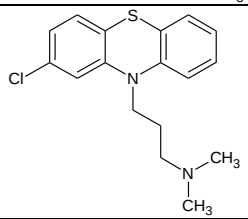	Antipsychotic	3.72 ± 0.15
[a]**Ciglitazone**	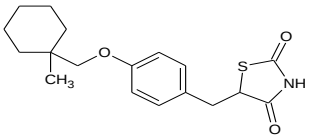	Blood glucose lowering agent	5.48 ± 0.17
Colchicine	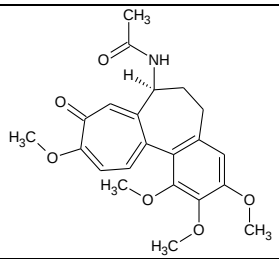	Antimitotic agent	<3.22
[a]**Colletochlorin B**	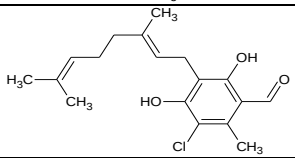	Fungicide	5.98 ± 0.09
[b]**Colletochlorin D**	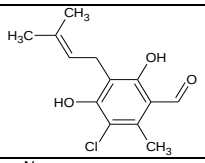	Fungicide	4.34 ± 0.04
Cyazofamid	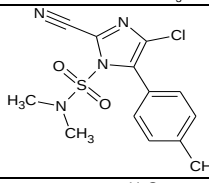	Fungicide	4.22 ± 0.16
[b]**Dimoxystrobin**	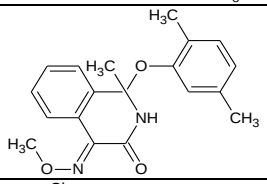	Fungicide	6.90 ± 0.16
Diuron	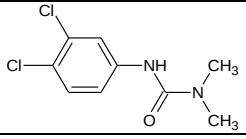	Herbicide	3.53 ± 0.01

Compound	Chemical structure	Drug class	pIC_{50}
[b]**Fenamidone**	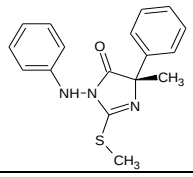	Fungicide	6.20 ± 0.05
[b]**Fluoxastrobin**	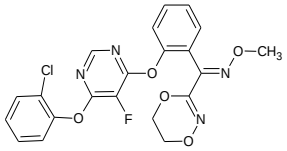	Fungicide	6.98 ± 0.22
Haloperidol	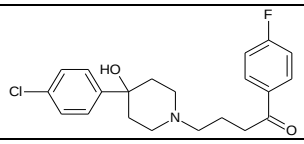	Antipsychotic	<3.62
[b]**ISSF31**	Structure cannot be disclosed due to patent restrictions	Fungicide	6.04 ± 0.37
[b]**ISSF33**	Structure cannot be disclosed due to patent restrictions	Fungicide	4.39 ± 0.29
[b]**Kresoxim-methyl**	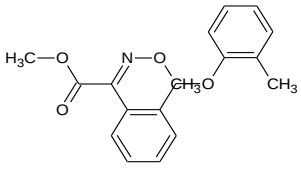	Fungicide	6.48 ± 0.15
[b]**Lovastatin**	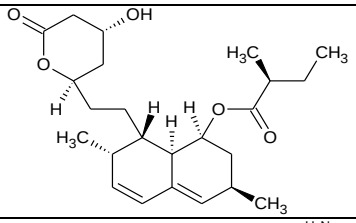	Lipid lowering agent	4.45 ± 0.04
[b]**Myxothiazol**	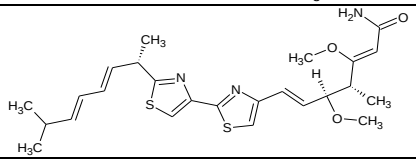	Fungicide	9.15 ± 0.11
[a]**Picoxystrobin**	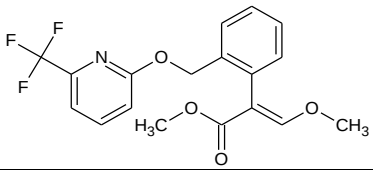	Fungicide	7.25 ± 0.09
[b]**Pyraclostrobin**	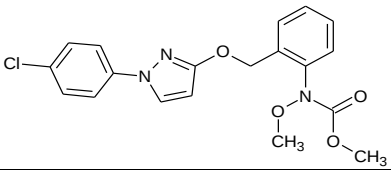	Fungicide	7.89 ± 0.14
[b]**Salicylic acid**	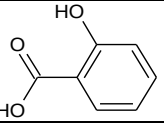	Anti-inflammatory agent	2.61 ± 0.09

Compound	Chemical structure	Drug class	pIC_{50}
[a]**Simvastatin**	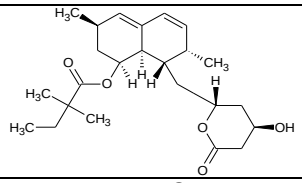	Lipid-lowering agent	4.95 ± 0.06
Sulfamethoxazole	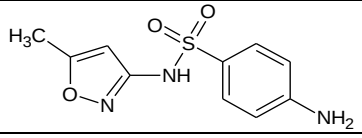	Antibiotic	<2.60
[b]**Sulfasalazine**	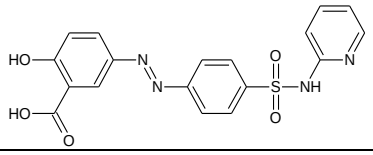	Anti-inflammatory agent	3.15 ± 0.08
[b]**Trifloxystrobin**	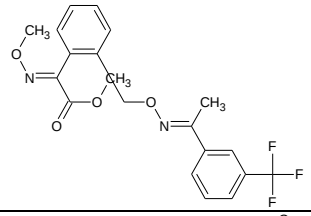	Fungicide	7.58 ± 0.16
[b]**Troglitazone**	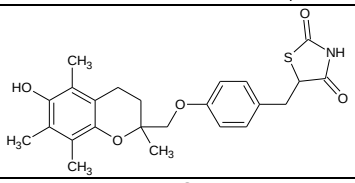	Blood glucose lowering agent	4.73 ± 0.11
Valproic acid	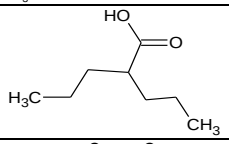	Anticonvulsant, antiepileptic	<2.00
[b]**Warfarin**	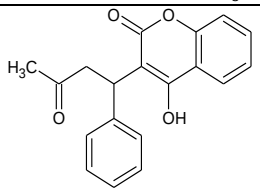	Anticoagulant	2.87 ± 0.13

Table II.2. Structures and inhibitory activities towards SCR of the compounds retrieved from the literature. a = test set, b = training set.

Compound	Chemical structure	pIC_{50}	Reference
[b]**Famoxadone**	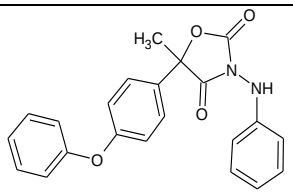	8.44	Wang F. *et al*., 2011[212]
[a]**8a**	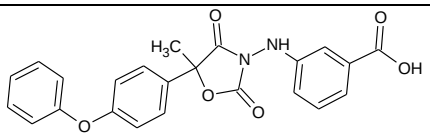	7.62	Wang F. *et al*., 2011
[a]**8b**	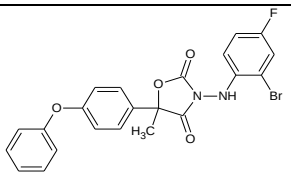	7.22	Wang F. *et al*., 2011
[b]**8c**	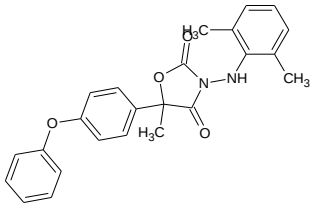	5.82	Wang F. *et al*., 2011
[a]**8d**	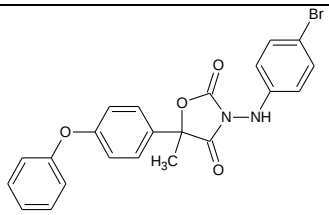	8.03	Wang F. *et al*., 2011
[a]**8e**	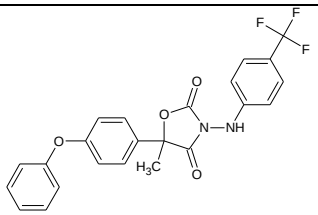	7.20	Wang F. *et al*., 2011
[b]**8f**	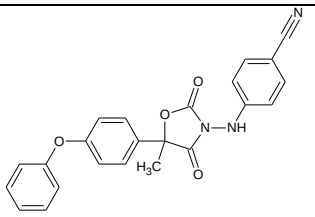	6.56	Wang F. *et al*., 2011
[a]**8g**	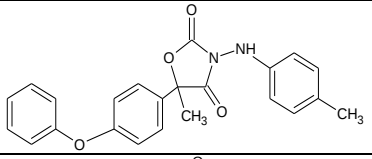	7.62	Wang F. *et al*., 2011
[b]**8h**	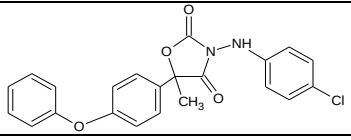	7.72	Wang F. *et al*., 2011

Compound	Chemical structure	pIC_{50}	Reference
[a]**8i**	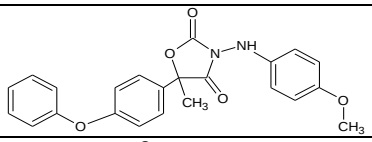	7.24	Wang F. *et al*., 2011
[a]**8j**	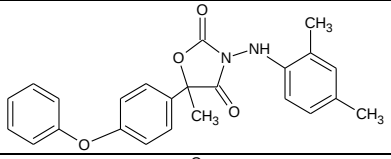	7.80	Wang F. *et al*., 2011
[b]**8k**	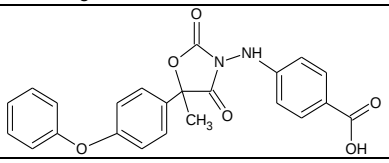	5.27	Wang F. *et al*., 2011
[a]**Ametoctradin**	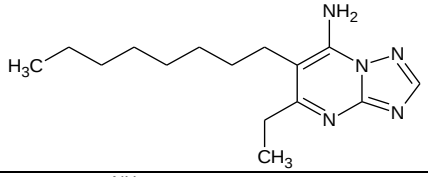	6.52	Zhu X. *et al*., 2015[211]
[b]**4a**	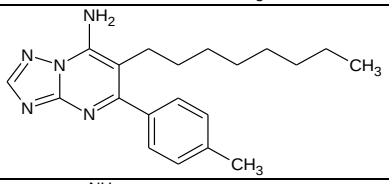	6.92	Zhu X. *et al*., 2015
[b]**4b**	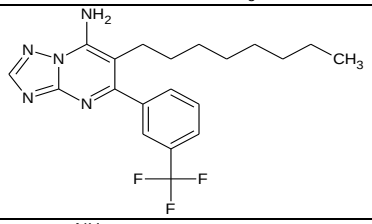	4.44	Zhu X. *et al*., 2015
[b]**4c**	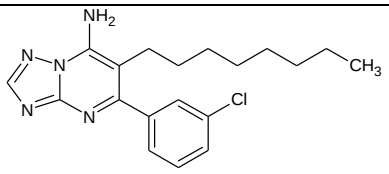	6.82	Zhu X. *et al*., 2015
[b]**4g**	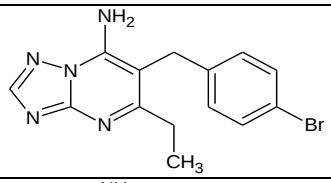	4.60	Zhu X. *et al*., 2015
[a]**4i**	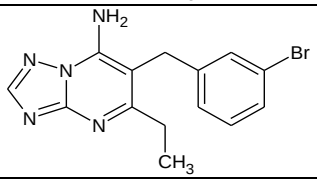	4.57	Zhu X. *et al*., 2015
[b]**4k**	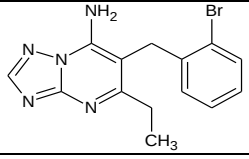	4.08	Zhu X. *et al*., 2015

Compound	Chemical structure	pIC_{50}	Reference
[a]**4m**	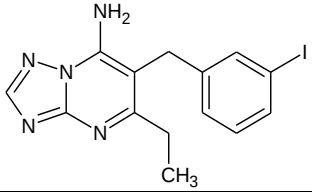	4.96	Zhu X. *et al*., 2015
[b]**4o**	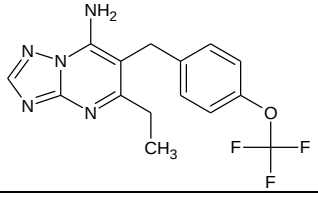	5.25	Zhu X. *et al*., 2015
[a]**4p**	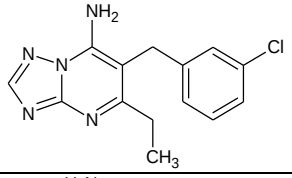	4.37	Zhu X. *et al*., 2015
[a]**4q**	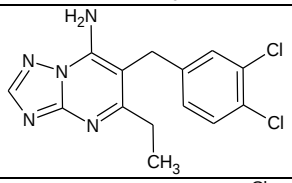	5.40	Zhu X. *et al*., 2015
[a]**4x**	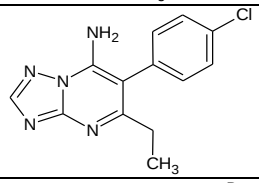	4.48	Zhu X. *et al*., 2015
[b]**4y**	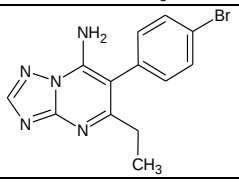	4.60	Zhu X. *et al*., 2015
[b]**Pyribencarb**	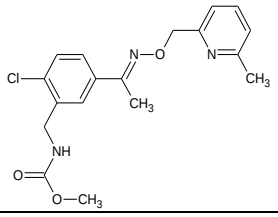	5.85	Kataoka S. *et al*., 2010

Table II.3. Training set of compounds. Selected descriptors, experimental pIC_{50} values and predicted pIC_{50} values, absolute error values and Z-scores of QSAR model A. Absolute error represents the difference between the predicted and experimental pIC_{50} values. Z-scores represent the absolute difference between the predicted and experimental pIC_{50} values, divided by the square root of the mean square error of the data set. All molecules with a Z-score of 2.5 or more were considered outliers.

Compounds	Log S	Neutral form (pH = 7.4)	Number of Rings (size 6)	pIC_{50} Exp.	pIC_{50} Pred.	Abs. error	pIC_{50} Pred.*	Abs. error*	Z-score*
4a	-7.27	0	2	6.92	6.40	0.52	6.31	0.61	0.76
[a]4b	-7.85	0	2	4.44	6.79	2.35	7.37	2.93	4.45
4c	-7.53	0	2	6.82	6.57	0.24	6.53	0.30	0.37
4g	-4.54	0	2	4.60	4.54	0.05	4.54	0.06	0.07
4k	-4.54	0	2	4.08	4.54	0.46	4.57	0.49	0.61
4o	-4.64	0	2	5.25	4.61	0.63	4.57	0.68	0.84
4y	-4.48	0	2	4.60	4.50	0.09	4.50	0.10	0.13
8c	-5.99	1	3	5.82	7.06	1.24	7.19	1.37	1.77
8f	-6.02	1	3	6.56	7.09	0.52	7.14	0.58	0.72
8h	-6.40	1	3	7.72	7.35	0.37	7.31	0.42	0.52
8k	-5.64	0	3	5.27	4.79	0.47	4.75	0.52	0.65
Ascofuranone	-5.13	0	1	5.08	5.44	0.36	5.49	0.41	0.51
Atovaquone	-7.05	0	4	6.69	5.25	1.43	4.84	1.85	2.45
Azoxystrobin	-5.51	1	3	6.67	6.74	0.06	6.75	0.08	0.09
Chlorpromazine	-4.57	0	3	3.72	4.07	0.34	4.11	0.39	0.48
Colletochlorin D	-3.38	0	1	4.34	4.25	0.08	4.24	0.10	0.12
Dimoxystrobin	-4.54	1	2	6.90	6.58	0.32	6.55	0.35	0.44
Famoxadone	-5.67	1	3	8.44	6.85	1.59	6.69	1.75	2.33
Fenamidone	-4.95	0	2	6.20	4.82	1.37	4.75	1.45	1.89
Fluoxastrobin	-6.82	1	4	6.98	7.13	0.15	7.17	0.19	0.23
ISSF31	-5.59	0	1	6.04	5.76	0.28	5.72	0.32	0.40
ISSF33	-3.74	0	1	4.39	4.50	0.10	4.51	0.12	0.15
Kresoxim-methyl	-4.30	1	2	6.48	6.42	0.06	6.41	0.07	0.09
Lovastatin	-4.23	1	3	4.45	5.87	1.41	6.07	1.62	2.12
Myxothiazol	-6.88	1	0	9.15	9.16	0.01	9.18	0.03	0.03
Pyraclostrobin	-4.83	1	2	7.89	6.77	1.11	6.67	1.22	1.57
Pyribencarb	-3.86	1	2	5.85	6.11	0.26	6.15	0.30	0.37
Salicylic acid	-0.99	0	1	2.61	2.63	0.02	2.64	0.03	0.04
Sulfasalazine	-3.60	0	3	3.15	3.41	0.25	3.45	0.30	0.37
Trifloxystrobin	-5.69	1	2	7.58	7.36	0.22	7.34	0.24	0.30
Troglitazone	-5.90	0	3	4.73	4.97	0.24	5.00	0.27	0.33
Warfarin	-4.38	0	3	2.87	3.94	1.06	4.06	1.19	1.52

* LOO-cross validation predicted activity values, [a] Outliers

Table II.4. Training set of compounds. Selected descriptors, experimental pIC_{50} values and predicted pIC_{50} values, absolute error values and Z-scores of QSAR model B Absolute error represents the difference between the predicted and experimental pIC_{50} values. Z-scores represent the absolute difference between the predicted and experimental pIC_{50} values, divided by the square root of the mean square error of the data set. All molecules with a Z-score of 2.5 or more were considered outliers.

Compounds	Log S	b_max1len	Neutral form (pH = 7.4)	Number of Rings (size 6)	pIC_{50} Exp.	pIC_{50} Pred.	Abs. error	pIC_{50} Pred.*	Abs. error*	Z-score*
4a	-7.27	9	0	2	6.92	5.75	1.17	5.41	1.51	2.29
[a]4b	-7.85	9	0	2	4.44	6.31	1.87	6.91	2.47	4.21
4c	-7.53	9	0	2	6.82	6.00	0.82	5.76	1.07	1.56
4g	-4.54	3	0	2	4.60	4.87	0.27	4.90	0.30	0.42
4k	-4.54	3	0	2	4.08	4.87	0.79	4.94	0.86	1.26
4o	-4.64	3	0	2	5.25	4.97	0.28	4.94	0.31	0.44
4y	-4.48	3	0	2	4.60	4.81	0.22	4.83	0.23	0.33
8c	-5.99	3	1	3	5.82	7.10	1.28	7.23	1.41	2.14
8f	-6.02	3	1	3	6.56	7.13	0.57	7.19	0.63	0.90
8h	-6.40	3	1	3	7.72	7.50	0.22	7.47	0.25	0.36
8k	-5.64	3	0	3	5.27	5.17	0.10	5.15	0.12	0.17
Ascofuranone	-5.13	6	0	1	5.08	5.33	0.25	5.36	0.28	0.40
Atovaquone	-7.05	2	0	4	6.69	6.05	0.64	5.71	0.98	1.43
Azoxystrobin	-5.51	2	1	3	6.67	6.93	0.26	6.96	0.29	0.41
Chlorpromazine	-4.57	6	0	3	3.72	3.28	0.44	3.16	0.56	0.81
Colletochlorin D	-3.38	4	0	1	4.34	4.23	0.11	4.22	0.13	0.18
Dimoxystrobin	-4.54	3	1	2	6.90	6.47	0.43	6.43	0.48	0.68
[a]Famoxadone	-5.67	3	1	3	8.44	6.79	1.65	6.63	1.81	2.88
Fenamidone	-4.95	3	0	2	6.20	5.27	0.93	5.17	1.03	1.51
Fluoxastrobin	-6.82	2	1	4	6.98	7.43	0.45	7.54	0.56	0.80
ISSF31	-5.59	6	0	1	6.04	5.77	0.27	5.73	0.31	0.44
ISSF33	-3.74	4	0	1	4.39	4.57	0.18	4.60	0.21	0.29
Kresoxim-methyl	-4.30	2	1	2	6.48	6.53	0.05	6.54	0.06	0.08
Lovastatin	-4.23	5	1	3	4.45	4.83	0.38	5.03	0.58	0.83
Myxothiazol	-6.88	6	1	0	9.15	9.36	0.21	9.52	0.37	0.53
Pyraclostrobin	-4.83	3	1	2	7.89	6.75	1.14	6.64	1.26	1.88
Pyribencarb	-3.86	3	1	2	5.85	5.82	0.04	5.81	0.04	0.06
Salicylic acid	-0.99	1	0	1	2.61	2.81	0.20	2.91	0.30	0.43
Sulfasalazine	-3.60	3	0	3	3.15	3.21	0.06	3.23	0.08	0.11
Trifloxystrobin	-5.69	2	1	2	7.58	7.86	0.28	7.90	0.32	0.46
Troglitazone	-5.90	4	0	3	4.73	5.13	0.40	5.17	0.44	0.64
Warfarin	-4.38	5	0	3	2.87	3.38	0.51	3.48	0.61	0.88

* LOO-cross validation predicted activity values, [a] Outliers

Table II.5. Test set of compounds. Selected descriptors, experimental pIC_{50}, predicted pIC_{50} and absolute error values for QSAR model A.

Compounds	Log S	Number of Rings (size 6)	Neutral form (pH = 7.4)	pIC_{50} Exp.	pIC_{50} Pred.	Abs. error
4i	-4.54	2	0	4.57	4.47	0.10
4m	-4.44	2	0	4.96	4.41	0.55
4p	-4.18	2	0	4.37	4.23	0.14
4q	-4.92	2	0	5.4	4.73	0.67
4x	-4.12	2	0	4.48	4.19	0.29
[a]8a	-5.64	3	0	7.62	4.72	2.90
8b	-7.05	3	1	7.22	7.80	0.58
8d	-6.76	3	1	8.03	7.60	0.43
8e	-6.73	3	1	7.2	7.58	0.38
8g	-6.14	3	1	7.62	7.19	0.44
8i	-5.72	3	1	7.24	6.90	0.34
8j	-6.30	3	1	7.8	7.29	0.51
Ametoctradin	-5.23	1	0	6.52	5.44	1.08
Bezafibrate	-4.80	2	0	3.3	4.65	1.35
Ciglitazone	-5.60	2	0.09	5.48	5.39	0.09
Colletochlorin B	-5.23	1	0.03	5.98	5.50	0.48
Picoxystrobin	-4.15	2	1	7.25	6.33	0.92
Simvastatin	-4.43	3	1	4.95	6.02	1.07

[a] outliers

Table II.6. Test set of compounds. Selected descriptors, experimental pIC_{50}, predicted pIC_{50} and absolute error values for QSAR model B.

Compounds	b_max1len	Log S	Number of Rings (size 6)	Neutral form (pH = 7.4)	pIC_{50} Exp.	pIC_{50} Pred.	Abs. error
4i	3	-4.54	2	0	4.57	4.80	0.23
4m	3	-4.44	2	0	4.96	4.71	0.25
4p	3	-4.18	2	0	4.37	4.47	0.10
4q	3	-4.92	2	0	5.4	5.16	0.24
4x	3	-4.12	2	0	4.48	4.41	0.07
[a]8a	3	-5.64	3	0	7.62	5.10	2.52
8b	3	-7.05	3	1	7.22	8.11	0.89
8d	3	-6.76	3	1	8.03	7.83	0.20
8e	3	-6.73	3	1	7.2	7.80	0.60
8g	3	-6.14	3	1	7.62	7.25	0.37
8i	3	-5.72	3	1	7.24	6.85	0.39
8j	3	-6.30	3	1	7.8	7.40	0.40
Ametoctradin	9	-5.23	1	0	6.52	4.56	1.96
Bezafibrate	4	-4.80	2	0	3.3	4.77	1.47
Ciglitazone	4	-5.60	2	0.09	5.48	5.68	0.20
Colletochlorin B	6	-5.23	1	0.03	5.98	5.43	0.55
Picoxystrobin	2	-4.15	2	1	7.25	6.39	0.86
Simvastatin	5	-4.43	3	1	4.95	5.09	0.14

[a] outlier